

Sheffield Hallam University

Developing models of the small intestine

DOSH, Rasha

Available from the Sheffield Hallam University Research Archive (SHURA) at:

<http://shura.shu.ac.uk/24027/>

A Sheffield Hallam University thesis

This thesis is protected by copyright which belongs to the author.

The content must not be changed in any way or sold commercially in any format or medium without the formal permission of the author.

When referring to this work, full bibliographic details including the author, title, awarding institution and date of the thesis must be given.

Please visit <http://shura.shu.ac.uk/24027/> and <http://shura.shu.ac.uk/information.html> for further details about copyright and re-use permissions.

Developing Models of the Small Intestine

Rasha Hatem Dosh

**A Thesis submitted in partial fulfillment of the requirements of
Sheffield Hallam University for the degree of Doctor of
Philosophy**



August 2018

Dedication

My Mum and Dad,

Thank you for all of your prayers, love and support throughout my entire life.

Thank you for teaching me to work hard and to be independent.

My brothers and sister,

Hassanien, Abbas, and Haneen

for being there all the time.

My beloved deceased brother: Dirgham,

You gave no one a last farewell, nor did you ever say goodbye.

I miss you a million times; in my heart you hold a place.

It broke my heart to lose you; I will meet you again someday in a better place,

I thank God he made you my brother.

A huge thanks to my wonderful husband: Firas,

Without you and your support, I could never have finished this thesis.

You have been there for me every step of the way during my Ph.D., listening

to me, supporting me, and encouraging me. Thank you for your patience,

love, and support.

And finally to my amazing daughter and sons,

Fatimah, Ahmed and Hussein for your patience during these years, it was not easy to have a mum who was always busy studying, but you understood and gave me strength.

Acknowledgements

This thesis is a result of a quest for knowledge that started from the first day in the BMRC, and I would like to thank each and every person who guided, encouraged and inspired me during these years.

Firstly, I would like to give a special thanks and appreciation to my director of study **Professor Christine Le Maitre**. I admire your knowledge, enthusiasm and I am grateful for your assistance, suggestions, scientific comments, and guidance. Thank you for your never-ending support. You encouraged and motivated me to complete the journey.

I would like to deliver my special thanks to my co-supervisor **Dr. Nicola Jordan-Mahy**, for your help, scientific comments, and support during these years, you are always listening to me and I am so grateful for your moral support.

I would also like to thank my co-supervisor **Professor Chris Sammon**, for your help, support, and advice throughout my Ph.D.

A big thanks to all the past and present members of CBRM research group: **Abbie, Abbey, Joseph, Paul, Louise, Essa, Guma and Jordan** for your help and support, you have all provided a great and friendly atmosphere and it has been a pleasure working with all of you, particularly **Abbey**, who kindly helped me when I started my Ph.D.

I would like to express my personal gratitude to all the staff and colleagues in the BMRC for all of your support, friendship and making my Ph.D so enjoyable.

Finally, I give my gratitude and appreciation to **the Ministry of Higher Education and Scientific Research of Iraq** for funding this project and for **the Iraqi cultural Attache** for all the facilities.

Abstract

Inflammatory bowel disease (IBD) is a chronic autoimmune disease characterised by inflammation of the gastrointestinal tract. The pathogenesis of IBD is not fully understood and curative therapies are lacking. Consequently, development of robust intestine models, representative of the pathogenesis of IBD remains an unmet need. Thus, the overall aims of the studies presented in this thesis were to develop a number of models of small intestine including: genetically engineered murine model, epithelial cell culture models, and an intestinal stem cell organoid model which could reflect or be used to study the pathogenesis of IBD.

Interleukin 1 (IL-1) is an important mediator of inflammation and tissue damage in IBD. The balance between IL-1 and IL-1Ra as a natural inhibitor plays a vital role in a variety of diseases. Here, this thesis investigated whether changes seen during IBD could be induced spontaneously by the removal of IL-1Ra in mice that lack a functional *IL-1rn* gene. Data presented from this thesis highlighted the importance of IL-1 in the pathogenesis of inflammatory bowel disease.

In addition, the potential of L-pNIPAM hydrogel scaffolds, which were developed by the research team at Sheffield Hallam University, was utilised to develop long-term 3D co-cultures of layered Caco-2 and HT29-MTX cells under conditions representative of inflammation by treatment with IL-1 β , TNF α , and hypoxia (1% O₂) for 1 week was investigated. *In vitro* cell culture studies in this thesis have demonstrated that L-pNIPAM hydrogel supported long-term 3D co-culture model and stimulation with factors seen during inflammation recapitulated features of IBD.

Finally, the potential of L-pNIPAM hydrogel scaffolds to develop 3D intestinal stem cell organoid model was investigated. The *in vitro* study demonstrated the ability of L-pNIPAM hydrogel as scaffold to support organoid formation and cell differentiation *in vitro* from small intestinal crypts and Lgr5⁺ stem cells isolated from mice.

Dissemination: Scientific publications

- **Dosh R. H.**, Jordan-Mahy N., Sammon C., and Le Maitre C. L. (2018). Tissue engineering laboratory models of the small intestine. *Tissue Engineering Part B*, 24(2), 98-111. **A schematic diagram illustrating the morphology of the small intestinal layers was chosen as the art cover for the journal.**
- **Dosh R. H.**, Essa A., Jordan-Mahy N., Sammon C., and Le Maitre C. L. (2017). Use of hydrogel scaffolds to develop an *in vitro* 3D culture model of human intestinal epithelium. *Acta Biomaterialia*, 62, 128-143.
- **Dosh R. H.**, Jordan-Mahy N., Sammon C., and Le Maitre C. L. (2018). Long-term *in vitro* 3D hydrogel co-culture model of inflammatory bowel disease. *Scientific Reports*. Manuscript submitted July 2018.
- **Dosh R. H.**, Jordan-Mahy N., Sammon C., and Le Maitre C. L. (2018). Interleukin-1 is a key driver of inflammatory bowel disease - demonstration in a murine IL-1Ra knockout model. *Inflammatory bowel disease*. Manuscript submitted July 2018.
- **Dosh R. H.**, Jordan-Mahy N., Sammon C., and Le Maitre C. L. (2018). Isolation and *in vitro* expansion of murine small intestinal stem cells using hydrogel scaffold. Manuscript to be submitted to the *Journal of stem cells research*.

Published abstracts

- **Dosh R. H.**, Jordan-Mahy N., Sammon C., and Le Maitre C. L. (2017)
The use of pNIPAM-laponite[®] hydrogel in 3D-cell culture of the intestine.
European Cells and Materials. Abstract, 33 Suppl. 2 (P517).

Dissemination: Oral and poster presentations

Oral presentations

- January 2017 - Royal Society of Chemistry Biomaterials, Belfast, UK: Novel *in vitro* three-dimensional culture of human intestinal epithelium. **Dosh R. H.**, Jordan-Mahy N., Sammon C., and Le Maitre C. L.
- October 2016 - 6th Clinical Gastroenterology and Hepatology, Toronto, Canada: Novel *in vitro* three-dimensional culture of human intestinal epithelium. **Dosh R. H.**, Jordan-Mahy N., Sammon C., and Le Maitre C. L.
- October 2016 - 9th Euro - Global Gastroenterology Conference, Valencia, Spain: Novel *in vitro* three-dimensional culture of human intestinal epithelium. **Dosh R.H.**, Jordan-Mahy N., Sammon C., and Le Maitre C. L.

Poster presentations

- September 2017 - 1st Iraqi Society Conference, Sheffield. UK: The use of pNIPAM-laponite[®] hydrogel in 3D cell culture of the intestine. **Dosh R.H.**, Jordan-Mahy N., Sammon C., and Le Maitre C. L. (**3rd Place Poster Prize**).
- July 2017 - TCES, Manchester, UK: Development of a 3D *in vitro* co-culture cells model for studying inflammatory bowel disease. **Dosh R.H.**, Jordan-

Mahy N., Sammon C., and Le Maitre C. L.

- June 2017 - TERMIS, Davos, Switzerland: The use of pNIPAM-laponite[®] hydrogel in 3D cell culture of the intestine. **Dosh R.H.**, Jordan-Mahy N., Sammon C., and Le Maitre C. L.
- December 2016 - BMRC Winter Poster Session, Sheffield, UK: Interleukin-1 receptor antagonist knockout mice as a model of the inflammatory bowel disease. **Dosh R.H.**, Jordan-Mahy N., Sammon C., and Le Maitre C. L.
- October 2016 - 6th Clinical Gastroenterology and Hepatology, Toronto, Canada: Interleukin-1 receptor antagonist knockout mice as a model of the inflammatory bowel disease. **Dosh R.H.**, Jordan-Mahy N., Sammon C., and Le Maitre C. L.
- October 2016 - 9th Euro-Global Gastroenterology Conference, Valencia, Spain: Interleukin-1 receptor antagonist knockout mice as a model of the inflammatory bowel disease. **Dosh R.H.**, Jordan-Mahy N., Sammon C., and Le Maitre C. L.
- July 2016 - Health and Wellbeing Faculty Research Day, Sheffield, UK: Novel *in vitro* three-dimensional culture of human intestinal epithelium. **Dosh R.H.**, Jordan-Mahy N., Sammon C., and Le Maitre C. L.
- January 2016 - Royal Society of Chemistry Biomaterials, Birmingham, UK: *In vitro* three-dimensional hydrogel culture of human intestinal cell lines to develop a 3D model. **Dosh R.H.**, Jordan-Mahy N., Sammon C., and Le Maitre C. L.

- December 2015 - BMRC Winter *Poster* Session, Sheffield, UK: *In vitro* three-dimensional hydrogel culture of human intestinal cell lines to develop a 3D model. **Dosh R.H.**, Jordan-Mahy N., Sammon C, and Le Maitre C. L.

Declaration

I hereby declare that the work presented in the thesis entitled "Developing Models of the Small Intestine" in fulfilment of the requirements for the award of the Degree of Philosophy, Biomolecular Sciences Research Centre, Sheffield Hallam University, is an authentic record of my own work carried out under the supervision of Professor Christine Le Maitre, Dr. Nicola Jordan-Mahy, and Professor Christopher Sammon. The matter embodied in this thesis has not been submitted in part or full to any other university or institute for the award of any degree in the UK or abroad.

Name: Rasha Hatem Dosh

Signed:

Table of contents

Dedication.....	i
Acknowledgements.....	ii
Abstract.....	iii
Dissemination: Scientific publications	iv
Dissemination: Oral and poster presentations	v
Declaration.....	viii
List of figures.....	xvi
List of tables.....	xxiv
List of abbreviations	xxv
Chapter 1: General introduction	1
1.1 The gastrointestinal tract (GIT).....	2
1.1.1 The human small intestine	2
1.1.1.1 Anatomy of the human small intestine.....	2
1.1.1.2 Histology of the small intestine	5
1.1.1.3 Intestinal epithelial cell types	6
1.1.1.3.1 Intestinal stem cells.....	7
1.1.1.3.1.1 Stem cell niche	11
1.1.1.4 Digestion and absorption in the small intestine.....	12
1.2 Inflammatory bowel disease	13
1.3 Models of the small intestine	17
1.3.1 Knockout mice models of inflammatory bowel disease	17
1.3.1.1 Cytokine knockout mice models	17
1.3.1.2 Matrix degrading enzyme knockout mice models	19
1.3.1.3 Mucosal expression knockout mice models.....	19
1.3.2 Cell culture models.....	20

1.3.2.1	The use of cell lines in intestinal engineering	21
1.3.2.1.1	Caco-2 cells	21
1.3.2.1.2	HT29-MTX cells	22
1.3.2.1.3	2D co-culture models of the small intestine.....	25
1.3.2.2	3D cell culture models of the small intestine.....	29
1.3.2.2.1	Biomaterials for tissue engineering of the small intestine.....	29
1.3.2.2.1.1	Natural biomaterials.....	32
1.3.2.2.1.2	Synthetic biomaterials	33
1.3.2.3	Recapitulating the dynamic mechanical microenvironment of the small intestine	36
1.3.2.4	Tissue engineering the small intestine.....	37
1.3.3	Stem cells models	37
1.3.3.1	Isolation of small intestinal stem cells.....	37
1.3.3.2	<i>In vivo</i> implantation of organoid seeded scaffolds	41
1.3.3.3	3D cell culture of pluripotent stem cells	43
1.4	Aims and objectives.....	45
Chapter 2: Interleukin-1 is a key driver of inflammatory bowel disease- demonstration in a murine IL-1Ra knockout model.....		47
2.1	Introduction.....	48
2.2	Materials and methods	50
2.2.1	<i>IL-1rn^{-/-}</i> BALB/c mice	50
2.2.2	Tissue preparation and histological assessment.....	50
2.2.2.1	Crypt-villus axes height and villus width	51
2.2.2.2	Goblet cells per crypt-villus axis	51
2.2.3	Immunohistochemical assessment	51
2.2.3.1	Pro-inflammatory cytokine expression and immune cell infiltration.....	51

2.2.3.2	Matrix-degrading enzyme expression	52
2.2.3.3	Polarity of enterocytes and digestive enzyme expression	52
2.2.4	Statistical analysis	54
2.2.5	Ethical consideration	55
2.3	Results	56
2.3.1	Histological analysis	56
2.3.1.1	Crypt-villus axis height and villus width	56
2.3.1.2	Number of goblet cells per crypt-villus axis	59
2.3.2	Immunohistochemistry staining	61
2.3.2.1	Assessment of pro-inflammatory cytokine expression and localization	61
2.3.2.2	Assessment of degrading enzyme expression and localization	69
2.3.2.3	Assessment of enterocyte polarity and digestive enzyme expression and localization	69
2.4	Discussion	77
Chapter 3: Use of hydrogel scaffolds to develop an <i>in vitro</i> 3D culture model of human intestinal epithelium		83
3.1	Introduction	84
3.2	Materials and methods	88
3.2.1	Hydrogel scaffolds synthesis	88
3.2.1.1	Alginate hydrogel scaffolds	88
3.2.1.2	L-pNIPAM hydrogel scaffolds	88
3.2.1.3	L-pNIPAM-co-DMAc hydrogel scaffolds	89
3.2.2	Material Characterisation	89
3.2.2.1	Scanning electron microscopy (SEM)	89
3.2.2.2	Dynamic mechanical analysis (DMA)	90

3.2.3	Cell lines	90
3.2.3.1	Culture conditions.....	91
3.2.3.2	Cytospins of monolayer control cells	92
3.2.3.3	Metabolic activity of cells	93
3.2.4	Histological assessment.....	93
3.2.5	Immunohistochemical assessment	94
3.2.6	Scanning electron microscopy following cell culture	95
3.2.7	Statistical analysis.....	96
3.3	Results	97
3.3.1	Material properties of alginate, L-pNIPAM and L-pNIPAM-co-DMAc scaffolds.....	97
3.3.2	Metabolic activity of Caco-2 cells in three hydrogel scaffolds	98
3.3.2.1	Alginate hydrogel scaffold.....	98
3.3.2.2	L-pNIPAM hydrogel scaffold	99
3.3.2.3	L-pNIPAM-co-DMAc hydrogel scaffold	99
3.3.2.4	Comparison of metabolic activity between three hydrogel systems..	100
3.3.3	Morphological and phenotypic assessment of Caco-2 cells cultured in hydrogel systems	102
3.3.4	Scanning electron microscopy of Caco-2 cells.....	109
3.3.5	Metabolic activity of HT29-MTX cells in three hydrogel scaffolds	112
3.3.5.1	Alginate hydrogel scaffold.....	112
3.3.5.2	L-pNIPAM hydrogel scaffold	112
3.3.5.3	L-pNIPAM-co-DMAc hydrogel scaffold	113
3.3.6	Comparison of cell metabolic activity in three hydrogel systems.	113
3.3.7	Morphological and phenotypic assessment of HT29-MTX cells cultured in hydrogel systems	116

3.3.8	Scanning electron microscopy of HT29-MTX cells.....	123
3.4	Discussion	125
Chapter 4: Long-term in vitro 3D hydrogel co-culture model of inflammatory		
	bowel disease.	134
4.1	Introduction.....	135
4.2	Materials and Methods	140
4.2.1	L-pNIPAM hydrogel scaffolds synthesis.....	140
4.2.2	Monocultures and co-cultures of Caco-2 and HT29-MTX layered on L- pNIPAM hydrogel scaffolds.....	140
4.2.3	Long-term co-cultures	141
4.2.4	Alamar blue assessment of metabolic activity.....	141
4.2.5	Histological assessment.....	142
4.2.6	Immunohistochemical assessment	142
4.2.7	Scanning electron microscopy for monocultures and co-cultures	143
4.2.8	Statistical analysis.....	143
4.3	Results	144
4.3.1	Metabolic activity of monocultures and co-cultures of Caco-2 and HT29- MTX cells layered on L-pNIPAM hydrogel scaffolds under dynamic culture conditions	144
4.3.2	Morphological and phenotypic assessment of monocultures and co- cultures of Caco-2 and HT29-MTX cells layered on L-pNIPAM hydrogel scaffolds under dynamic culture conditions.....	146
4.3.3	Scanning electron microscopy of monocultures and co-cultures following 7 weeks.....	149
4.3.4	Treatment monocultures and co-cultures with pro-inflammatory cytokines or cultured under hypoxic conditions.....	149

4.3.5	Scanning electron microscopy of long-term co-cultures following 12 weeks.....	159
4.4	Discussion	162
Chapter 5: Isolation and <i>in vitro</i> expansion of small intestinal stem cells from mice using L-pNIPAM hydrogel.....		170
5.1	Introduction.....	171
5.2	Materials and methods	175
5.2.1	Mice	175
5.2.2	Culture media.....	175
5.2.3	Small intestinal crypt extraction.....	175
5.2.4	Suspension of small intestinal crypts within Matrigel.....	177
5.2.5	Suspension of small intestinal crypts within L-pNIPAM hydrogel	177
5.2.6	Layering of small intestinal crypts on L-pNIPAM hydrogel	178
5.2.7	Suspension of small intestinal crypts within Matrigel followed by suspension within or layered on L-pNIPAM hydrogel.....	178
5.2.8	Isolation of small intestinal stem cells	179
5.2.9	Magnetic Activated Cell Sorting (MACS) separation	179
5.2.10	Cytospin of Lgr5 ⁺ sorted cells.....	180
5.2.11	Suspension of Lgr5 ⁺ stem cells within Matrigel	181
5.2.12	Suspension of Lgr5 ⁺ stem cells within L-pNIPAM hydrogel.....	181
5.2.13	Layering of Lgr5 ⁺ stem cells on L-pNIPAM hydrogel	182
5.2.14	Suspension of Lgr5 ⁺ stem cells within Matrigel followed by resuspension within or layered on L-pNIPAM hydrogel.....	182
5.2.15	Characterisation of crypts and Lgr5 ⁺ stem cells	183
5.2.15.1	Abright field images of the crypts and Lgr5 ⁺ stem cells.....	183
5.2.15.2	Histological assessment.....	183

5.2.15.3 Immunohistochemical Assessment	183
5.3 Results	185
5.3.1 Morphological assessment of crypts isolated from the small intestine suspended within Matrigel, L-pNIPAM hydrogel or layered on L-pNIPAM hydrogel	185
5.3.2 Morphological assessment of the organoids when released from Matrigel, dissociated and suspended within or layered on L-pNIPAM hydrogel.	185
5.3.3 Phenotypical assessment of the organoids derived from crypts suspended directly in L-pNIPAM hydrogel or in Matrigel for 7 days then dissociated and re-suspended in L-pNIPAM for 10 days	190
5.3.4 Morphological assessment of the isolated Lgr5 ⁺ small intestinal stem cells suspended within Matrigel, L-pNIPAM hydrogel, or layered on L- pNIPAM hydrogel	192
5.4 Discussion	202
Chapter 6: General discussion.....	208
6.1 Future directions.....	214
6.1.1 Genetically engineered animal model	214
6.1.2 Epithelial cell culture model.....	214
6.1.3 Intestinal stem cell organoid model	215
References.....	217

List of figures

Figure 1.1: Blood supply to the small intestine: (A) Schematic representation of arterial supply to the small intestine. (B) Schematic representation of veins supply to the small intestine.....	4
Figure 1.2: (A) Schematic diagram illustrating morphology of the small intestinal layers containing crypt–villus units together with the main intestinal cells of the epithelial layer, crypt intestinal stem cells, and their niche. (B) Histology of the crypt–villus axis represents intestinal cells (C) Enterocytes, (D) Goblet cells, (E) Paneth cells, and (F) Enteroendocrine cells.	9
Figure 1.3: Schematic diagram illustrating the morphology of the microvilli which cover the apical surface of the enterocytes.....	10
Figure 1.4: Schematic diagram illustrating the Lgr5 ⁺ stem cells generating transit amplifying cells which then rapidly proliferated to one of several differentiated lineages: enterocytes, goblet, enteroendocrine and Paneth cells.	10
Figure 1.5: Bright field image of human colon adenocarcinoma cell lines in monolayer (A) Caco-2 cells and (B) HT29-MTX cells.	23
Figure 1.6: Summary of two dimensional monoculture, co-culture, and triple co-culture of Caco-2 and HT29-MTX cells.....	28
Figure 1.7: Summary of three-dimensional monoculture and co-culture of Caco-2 and HT29-MTXcells using collagen gel, collagen scaffolds, and PLGA scaffolds.....	35
Figure 1.8: Schematic diagram illustrating growth of intestinal organoids from isolated crypts and single Lgr5 ⁺ stem cells cultured in Matrigel.	39
Figure 2.1: Histological analysis and morphology of the intact well-oriented crypt-villus axis heights and villus widths of the Jejunum.....	58
Figure 2.2: Histological analysis and morphology of the intact well-oriented	

crypt-villus axis heights and villus widths of the ileum.....	58
Figure 2.3: Histological analysis and morphology of goblet cells per intact well-oriented crypt-villus axis of the A: Jejunum and B: Ileum.	60
Figure 2.4: Immunohistochemistry staining of the expression and localization of pro-inflammatory cytokine A: IL-1 α ; B: IL-1 β ; C: IL-1RI.....	62
Figure 2.5: Immunohistochemistry staining of the expression and localization of pro-inflammatory cytokines: IL-1 α (A and B); IL-1 β (C and D); IL-1RI (E and F) in the ileum.....	63
Figure 2.6: Immunohistochemistry staining of the expression and localization of pro-inflammatory cytokines IL-15 (A); TNF α (B) in the jejunum.	65
Figure 2.7: Immunohistochemistry staining of the expression and localization of pro-inflammatory cytokines: IL-15 (A and B); TNF α (C and D) in the ileum	66
Figure 2.8: Immunohistochemistry staining of the infiltrated cells: Polymorphonuclear cells (PMNs) (A) and Macrophage cells (B) into the lamina propria in the jejunum.	67
Figure 2.9: Immunohistochemistry staining of the infiltrated cells: Polymorphonuclear cells (PMNs) (A) and Macrophage cells (B) into the lamina propria of the intact well oriented crypt-villus axis in the ileum.....	68
Figure 2.10: Immunohistochemistry staining of the expression and localization of degrading enzymes: MMP2 (A); MMP9 (B); ADAMTS1 (C) in the jejunum...	70
Figure 2.11: Immunohistochemistry staining of the expression and localization of degrading enzymes: MMP2 (A); MMP9 (B); ADAMTS1 (C) in the ileum.....	71
Figure 2.12: Immunohistochemistry staining of the expression and localization of junctional proteins: ZO-1 (A); E-cadherin (B) in the jejunum.....	72
Figure 2.13: Immunohistochemistry staining of the expression and localization of junctional proteins: ZO-1 (A and B); E-cadherin (C and D) in the ileum.....	73

Figure 2.14: Immunohistochemistry staining of the expression and localization of digestive enzymes: ALP (A); SI (B); and DPP IV (C) in the jejunum.	75
Figure 2.15: Immunohistochemistry staining of the expression and localization of the digestive enzymes: ALP (A and B); SI (C and D); and DPP IV (E and F) in the ileum.	76
Figure 3.1: Pore size (μm) for acellular alginate, L-pNIPAM, and L-pNIPAM-co-DMAc hydrogels determined using SEM analysis. B: Storage Modulus (G') values for acellular alginate, L-pNIPAM, and L-pNIPAM-co-DMAc hydrogels determined using DMA..	97
Figure 3.2: Viability of Caco-2 cells at a cell density of 2×10^6 cells/ml layered on or suspended within Alginate; L-pNIPAM; L-pNIPAM-co-DMAc.	101
Figure 3.3: Histological analysis of Caco-2 cells layered on or suspended within alginate, L-pNIPAM, and L-pNIPAM-co-DMAc hydrogels under static or dynamic culture conditions 2 days	103
Figure 3.4 Histological analysis of Caco-2 cells layered on or suspended within alginate, L-pNIPAM, and L-pNIPAM-co-DMAc hydrogels under static or dynamic culture conditions following 7 days	103
Figure 3.5: Histological analysis of Caco-2 cells layered on or suspended within alginate, L-pNIPAM, and L-pNIPAM-co-DMAc hydrogels under static or dynamic culture conditions following 14 days.....	105
Figure 3.6: Histological analysis of Caco-2 cells layered on or suspended within alginate, L-pNIPAM, and L-pNIPAM-co-DMAc hydrogels under static or dynamic culture conditions following 21 days	105
Figure 3.7: Immunohistochemistry staining of MUC2 and MUC5AC. A: Caco-2 cells monolayer and layered on or suspended within alginate; B and C: Caco-2 cells layered on L-pNIPAM, and L-pNIPAM-co-DMAc hydrogels, under static or dynamic culture conditions.....	107

Figure 3.8: Immunohistochemistry staining (yellow arrows) for CD10, Zonulin-1 (ZO-1), Alkaline phosphatase (ALP), Dipeptidyl peptidase IV (DPP IV), and Sucrase-isomaltase (SI) of Caco-2 cells in 0 h monolayer and Caco-2 cells layered on L-pNIPAM hydrogel under static or dynamic culture conditions..... 107

Figure 3.9: Scanning electron micrographs of Caco-2 cells layered on A: L-pNIPAM; and B:L-pNIPAM-co-DMAc hydrogels under static or dynamic culture conditions..... 108

Figure 3.10: Scanning electron micrographs of Caco-2 and HT29-MTX cells layered on or suspended within L-pNIPAM hydrogel under static or dynamic culture conditions 110

Figure 3.11: Viability of HT29-MTX cells at a cell density of 2×10^6 cells/ml layered on or suspended within Alginate; L-pNIPAM; L-pNIPAM-co-DMAc following 21 days under static or dynamic culture conditions..... 111

Figure 3.12: Histological analysis of HT29-MTX cells layered on or suspended within alginate, L-pNIPAM, and L-pNIPAM-co-DMAc hydrogels under static or dynamic culture conditions following 2 days 115

Figure 3.13: Histological analysis of HT29-MTX cells layered on or suspended within alginate, L-pNIPAM, and L-pNIPAM-co-DMAc hydrogels under static or dynamic culture conditions following 7 days 117

Figure 3.14: Histological analysis of HT29-MTX cells layered on or suspended within alginate, L-pNIPAM, and L-pNIPAM-co-DMAc hydrogels under static or dynamic culture conditions following 14 days 118

Figure 3.15: Histological analysis of HT29-MTX cells layered on or suspended within alginate, L-pNIPAM, and L-pNIPAM-co-DMAc hydrogels under static or dynamic culture conditions following 21 days 119

Figure 3.16: Immunohistochemistry staining (yellow arrows) of MUC2 and MUC5AC. A: monolayer and IgG negative control. HT29-MTX cells layered on or suspended within B: Alginate, C: L-pNIPAM, and D: L-pNIPAM-co-DMAc hydrogels under static or dynamic culture conditions..... 120

Figure 3.17: Scanning electron micrographs for HT29-MTX cells layered on or suspended within A: L-pNIPAM and B: L-pNIPAM-co-DMAc hydrogels under static or dynamic culture conditions	122
Figure 4.1: Metabolic activity of monocultures and co-cultures of Caco-2 and HT29-MTX cells.	145
Figure 4.2: Morphology of monocultures and co-cultures of Caco-2 and HT29-MTX cells at a total cell density of 2×10^6 cells/ml with different percentages layered on L-pNIPAM hydrogel scaffolds under dynamic culture conditions...	147
Figure 4.3: Mucin expression by monocultures and co-cultures of Caco-2 and HT29-MTX cells at different percentages layered on L-pNIPAM hydrogel scaffolds under dynamic culture conditions	148
Figure 4.4: Scanning electron micrographs of monocultures and co-cultures of Caco-2 and HT29-MTX cells at different percentages layered on L-pNIPAM hydrogel scaffolds under dynamic culture conditions.....	150
Figure 4.5: Morphology of monocultures and co-cultures of Caco-2 and HT29-MTX cells at different percentages layered on L-pNIPAM hydrogel scaffolds under dynamic culture conditions for 6 weeks and then treated with 10ng/ml IL-1 β for 1 week under dynamic culture conditions or hypoxic at 1% O ₂ for 1 week under static culture conditions.....	151
Figure 4.6: Immunopositivity (brown) of co-culture Caco-2 and HT29-MTX cells at percentages 90% Caco-2 / 10% HT29-MTX layered on L-pNIPAM hydrogel scaffolds under dynamic culture conditions following 7 weeks as a control or for 6 weeks and then treated with 10 ng/ml IL-1 β for 1 week under dynamic culture conditions or hypoxic at 1% O ₂ for 1 week under static culture conditions.	153
Figure 4.7: Immunopositivity (brown) of co-culture Caco-2 and HT29-MTX cells at percentages of 75% Caco-2 / 25% HT29-MTX layered on L-pNIPAM hydrogel scaffolds following 7 weeks as a control or for 6 weeks and then treated with 10ng/ml IL-1 β for 1 week under dynamic culture conditions or hypoxic at 1% O ₂ for 1 week under static culture conditions.....	154

Figure 4.8: Morphology of long term co-culture of Caco-2 and HT29-MTX cells at percentages A: 90% Caco-2 / 10% HT29-MTX; B: 75% Caco-2 / 25% HT29-MTX layered on L-pNIPAM hydrogel scaffolds under dynamic culture conditions following 12 weeks as a control or for 11 weeks and then treated with 10 ng/ml IL-1 β or 10 ng/ml TNF α for 1 week under dynamic culture conditions or hypoxic at 1% O₂ for 1 week under static culture conditions..... 157

Figure 4.9: Immunopositivity (brown) of co-culture Caco-2 and HT29-MTX cells at percentages 90 %Caco-2 / 10% HT29-MTX layered on L-pNIPAM hydrogel scaffolds under dynamic culture conditions following 12 weeks as a control or for 11 weeks and then treated with 10 ng/ml IL-1 β or 10 ng/ml TNF α for 1 week under dynamic culture conditions or hypoxic at 1% O₂ for 1 week under static culture conditions. 158

Figure 4.10: Scanning electron micrographs of long-term co-culture Caco-2 and HT29-MTX cells at percentages 90% Caco-2 / 10%HT29-MTX cells layered on L-pNIPAM hydrogel scaffolds under dynamic culture conditions following 12 weeks as a control or for 11 weeks and then treated with 10 ng/ml IL-1 β or 10 ng/ml TNF α for 1 week under dynamic culture conditions or hypoxic at 1% O₂ for 1 week under static culture conditions. 160

Figure 4.11: Scanning electron micrographs of long term co-culture Caco-2 and HT29-MTX cells at percentages 75% Caco-2 / 25% HT29-MTX cells layered on L-pNIPAM hydrogel scaffolds under dynamic culture conditions following 12 weeks as a control or for 11 weeks and then treated with 10ng/ml IL-1 β or 10ng/ml TNF α for 1 week under dynamic culture conditions or hypoxic at 1% O₂ for 1 week under static culture conditions. 161

Figure 5.1: Bright-field morphology of the isolated small intestinal crypts suspended within Matrigel for 0-14 days..... 187

Figure 5.2: Morphology of the isolated small intestinal crypts when suspended directly within or layered on L-pNIPAM hydrogel under dynamic culture conditions for 10 days. 188

Figure 5.3: Morphology of the isolated small intestinal crypts when suspended within Matrigel for 7 days then the derived organoids were released from Matrigel and dissociated into small fragments and then (A) re-suspended within or (B) layered on L-pNIPAM hydrogel under dynamic culture conditions for 10 days.	189
Figure 5.4: Immunohistochemistry staining (black arrows) for Lgr5, E-cadherin, MUC2, Chromogranin-A, and Lysozyme of the isolated small intestinal crypts	191
Figure 5.5: Bright-field morphology of the isolated Lgr5 ⁺ intestinal stem cells suspended within Matrigel from day 0 to 14.....	192
Figure 5.6: Morphology of the isolated Lgr5 ⁺ intestinal stem cells: (A) suspended within L-pNIPAM hydrogel and (B) Layered on L-pNIPAM hydrogel under dynamic culture conditions for 10 to 14 days.	193
Figure 5.7: Morphology of the isolated Lgr5 ⁺ intestinal stem cells suspended within Matrigel for 7 days then the organoids were released from Matrigel and dissociated into single cells and (A) were suspended in L-pNIPAM hydrogel or (B) were layered on L-pNIPAM hydrogel under dynamic culture conditions for 7 to 28 days.	194
Figure 5.8: Immunohistochemistry staining (black arrows) for Lgr5 in: (A) the intact mouse small intestine, (B) cytospin of Lgr5 ⁺ intestinal stem cells, (C) Caco-2 cells and (D) HT29-MTX cell lines..	195
Figure 5.9: Immunohistochemistry staining for (A) E-cadherin; (B) MUC2; (C) Chromogranin-A and (D) Lysozymes in cytospin of the isolated Lgr5 ⁺ intestinal stem cells.	196
Figure 5.10: Immunohistochemistry staining (black arrows) for Lgr5 in isolated Lgr5 ⁺ intestinal stem cells when suspended within Matrigel for 7 days then the organoids were released from Matrigel and dissociated into single cells then (A) suspended within L-pNIPAM hydrogel or (B) layered on L-pNIPAM hydrogel under dynamic culture conditions for 7 to 28 days.	197

Figure 5.11: Immunohistochemistry staining (black arrows) for E-cadherin of the isolated Lgr5⁺ intestinal stem cells suspended within Matrigel for 7 days then the organoids were released from Matrigel and dissociated into single cells and (A) suspended within L-pNIPAM hydrogel; (B) layered on L-pNIPAM hydrogel under dynamic culture conditions for 7 to 28 days. 198

Figure 5.12: Immunohistochemistry staining (black arrows) for MUC2 of the isolated Lgr5⁺ intestinal stem cells suspended within Matrigel for 7 days then the organoids were released from Matrigel and dissociated into single cells and (A) suspended within L-pNIPAM hydrogel; (B) layered on L-pNIPAM hydrogel under dynamic culture conditions for 7 to 28 days. 199

Figure 5.13: Immunohistochemistry staining (black arrows) Chromogranin-A of the isolated Lgr5⁺ intestinal stem cells suspended within Matrigel for 7 days then the organoids were released from Matrigel and dissociated into single cells and (A) suspended within L-pNIPAM hydrogel; (B) layered on L-pNIPAM hydrogel under dynamic culture conditions for 7 to 28 days. 200

Figure 5.14: Immunohistochemistry staining (black arrows) for lysozyme production of the isolated Lgr5⁺ intestinal stem cells suspended within Matrigel for 7 days then the organoids were released from Matrigel and dissociated into single cells and (A) suspended within L-pNIPAM hydrogel; (B) layered on L-pNIPAM hydrogel under dynamic culture conditions for 7 to 28 days. 200

List of tables

Table 1.1: Summary of the major two dimensional cell culture systems of intestinal cell lines.....	24
Table 1.2: Summary of three dimensional cell culture systems of intestinal cell lines.. ..	31
Table 2.1: Target antibodies used in Immunohistochemistry.....	53

List of abbreviations

2D	Two Dimensional
3D	Three Dimensional
ADAMTS	A Disintegrin and Metalloproteinase with Thrombospondin Motifs
ALP	Alkaline Phosphatase
ATCC	American Type Culture Collection
BMP	Bone Morphogenetic Protein
BSA	Bovine Serum Albumin
CCK	Cholecystokinin
CD	Crohn's Disease
Coll	Collagen
DAB	3-3' Diaminobenzidine Tetrahydrochloride
DMAc	N,N'-dimethyl acrylamide
DMEM	Dulbecco's Modified Eagles Media
DPP IV	Dipeptidyl Peptidase 4
ECM	Extracellular Matrix
EDTA	Ethylen Diamine Tetra-acetic Acid
EGF	Epidermal Growth Factor
FBS	Foetal Bovine Serum
GIP	Glucose-dependent Insulin-tropic Peptide
GSK3β	Glycogen Synthase Kinase 3 beta
HATH 1	BHLH transcription factor
H&E	Haematoxylin and Eosin

HEPES	(4-(2-Hydroxyethyl)-1-Piperazineethanesulfonic Acid)
HIF	Hypoxia Induced Factor
HInEpC	Human Intestinal epithelial Cells
HMECs	Human Microvascular Endothelial Cells
HRP	Horseradish Peroxidase
IBD	Inflammatory Bowel Disease
IHC	Immunohistochemistry
IL-1	Interleukin-1
IL-1β	IL-1 beta
IL-1α	IL-1 alpha
IL-1Ra	Interleukin-1 Receptor Antagonist
IL-1RAcP	IL-1 Receptor Accessory Protein
IL-1RI	Interleukin-1 Receptor I
IL-1RII	Interleukin-1 Receptor II
IMS	Industrial Methylated Sprit
iPSC	induced Pluripotent Stem Cells
ISCs	Intestinal Stem Cells
ISEMF	Intestinal Sub-Epithelial Myofibroblasts
JNK	JUN N Terminal kinase
KLF4	Kruppel Like Factor 4
LCST	Lower Critical Solution Temperature
Lgr5	Leucine rich repeat containing G protein-coupled receptor 5
L- pNIPAM	Laponite® Crosslinked pNIPAM
MACS	Magnetic Activated Cell Sorting
MAPK	Mitogen-Activated Protein kinase
MLCK	Myosin L Chain Kinase
MMP	Matrix Metalloproteinases
NF-KB	Nuclear Factor Kappa B

NK	Natural Killer
NOD/SCID	Non-Obese Diabetic/Severe Combined Immune Deficiency
PAS	Periodic Acid Schiff's
PBS	Phosphate Buffer Saline
PDMS	Polydimethylsiloxane
PEG	Poly Ethylene Glycol
PGA	Poly Glycolic Acid
PLA	Poly Lactic Acid
PLGA	Poly-Lactic-Glycolic Acid
PMNs	Polymorphonuclear Cells
pNIPAM	Poly N-isopropylacrylamide
SEM	Scanning Electron Microscope
SI	Sucrase-Isomaltase
TA	Transit-Amplifying Cells
TEER	Trans Epithelial Electrical Resistance
TGF-B	Transforming Growth Factor Beta
Th1	T-helper 1
TNFα	Tumour Necrosis Factor Alpha
UC	Ulcerative Colitis
WT	Wild Type
ZO-1	Zonulin-1

Chapter 1: General introduction

Some of this chapter has been published as a literature review:

Tissue engineering laboratory models of the small intestine.

Rasha H. Dosh, Nicola Jordan-Mahy, Chris Sammon, Christine L. Le Maitre.

Tissue Engineering Part B, Vol. 24, 98-111, 2018.

Author Contributions:

R.H.D. drafted the manuscript. N.J.M., C.S., and C.L.L.M., critically revised the manuscript. All authors read and approved the final manuscript.

1.1 The gastrointestinal tract (GIT)

The gastrointestinal tract (GIT) is a tube which extends from the mouth to the anus and consists of the oral cavity, oesophagus, stomach, small intestine, large intestine, rectum and the anus (McCance & Huether 1998; Tortora & Derrickson 2016).

1.1.1 The human small intestine

The main place for absorption of nutrients from ingested materials is the small intestine. The small intestine is a long, coiled tube that digests and absorbs about 90% of the nutrients and water in the gastrointestinal tract. It is only 2.5 cm in diameter and about 5-6 meters in length. The small intestine starts at the pyloric sphincter of the stomach, winds throughout the abdominal cavity and at the end opens into the large intestine, where the ileum joins the caecum (McCance & Huether 1998; Tortora & Derrickson 2016).

1.1.1.1 Anatomy of the human small intestine

Anatomically, the small intestine includes three regions; the duodenum, jejunum, and ileum. The duodenum is the first, shortest (25 cm) and widest part of the small intestine which is attached to the pyloric sphincter of the stomach at the right side, and ends at the duodenojejunal junction on the left side. The duodenum makes a C-shaped tube around the head of the pancreas and is fixed to the retroperitoneum by suspensory ligament of Treitz (Tortora & Derrickson 2016). The arterial supply of the duodenum is derived from the gastroduodenal artery and inferior pancreaticoduodenal artery which is a branch of the superior mesenteric artery (Figure 1.1 A), the veins drain into the hepatic portal vein (Figure 1.1 B). Lymphatic drainage is to the pancreaticoduodenal and superior mesenteric nodes (McCance & Huether 1998; Tortora &

Derrickson 2016). The Jejunum represents the main site of the nutrient absorption. It is approximately 2.5 metres in length, with a larger diameter, and thicker wall than the most distal end of the small intestine, the ileum. The jejunum has tall and closely packed plica circulars, which are the circular folds that play a crucial role in increasing the surface area for absorption (Tortora & Derrickson 2016). The jejunum is attached to the posterior abdominal wall by mesentery which is a double fold of peritoneum. The final and longest region (approximately 3.5 meters) of the small intestine is the ileum which connects to the large intestine via the ileocecal sphincter. Here there is the completion absorption of nutrients which were neglected in the jejunum (McCance & Huether 1998; Tortora & Derrickson 2016).

The arterial supply to the jejunum and ileum are from branches of the superior mesenteric artery (Tortora & Derrickson 2016) (Figure 1.1 A). The venous drainage passes through the superior mesenteric vein which joins with the splenic vein to form the hepatic portal vein at the neck of the pancreas (Figure 1.1 B). Lymphatic drainage is into the superior mesenteric nodes (McCance & Huether 1998; Tortora & Derrickson 2016).

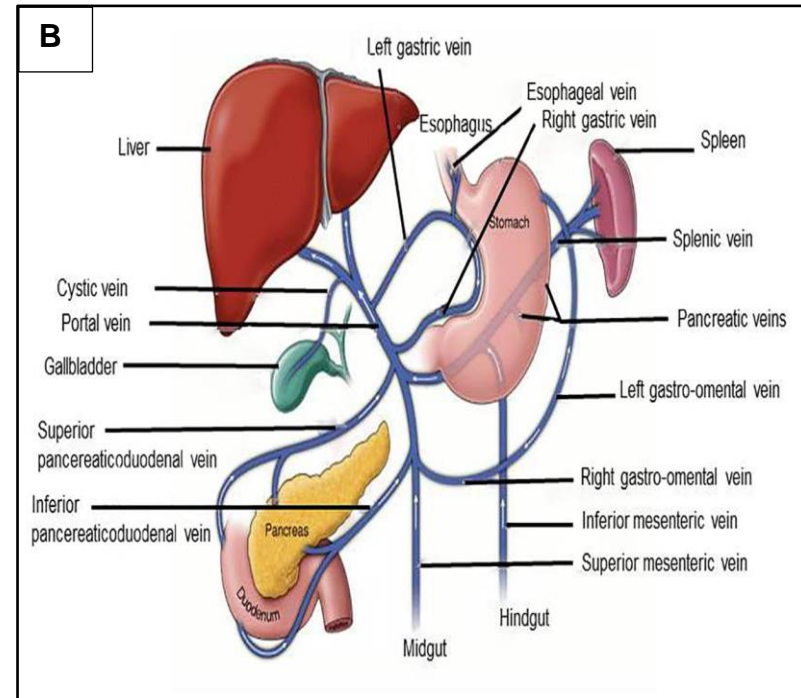
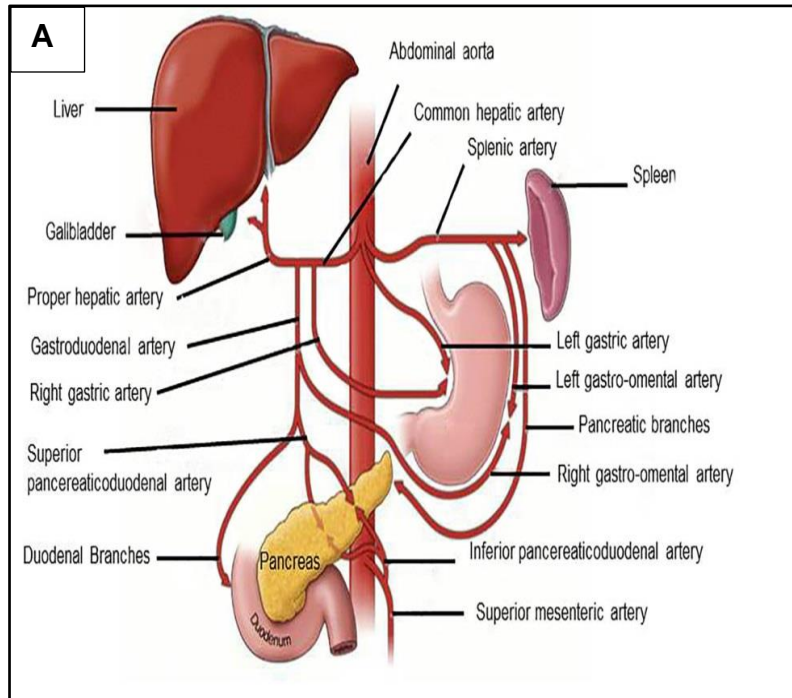


Figure 1.1: Blood supply to the small intestine: (A) Schematic representation of arterial supply to the small intestine. (B) Schematic representation of veins supply to the small intestine. Adapted from (Morton *et al.* 2011).

1.1.1.2 Histology of the small intestine

The small intestinal wall is made up of the same four distinct layers of tissue that comprise the rest of the GIT: mucosa, submucosa, muscularis externa, and adventitia or serosa (McCance & Huether 1998) (Figure 1.2). The mucosa layer lines the lumen of the GIT. It is made up of a simple columnar epithelium. The mucosa surface is folded into projections known as circular folds, which increase their surface area. The surface area is further increased by the formation of finger-like projections called villi. Each the columnar epithelial cell or enterocytes have tiny cylindrical projections called microvilli (1µm long) which further increase the surface area of the small intestine for absorption. Under the light microscope they form fuzzy lines known as the brush border (Figure 1.3). The number and shape of the intestinal villi varies, depending on the position along its length (McCance & Huether 1998), with the highest number of villi seen in the proximal jejunum, decreasing towards the end of the ileum. The morphology of the villi differs through the small intestine, decreasing in size from the proximal to the distal end of the small intestine. In the duodenum, the villi are leaf-like, whilst those of the jejunum and ileum having a tongue-like, and then finger-like appearance, respectively (Tortora & Derrickson 2016). At the base of the villi are crypts of Lieberkuhn (Barker *et al.* 2013), these crypts are tubular glands which descend into the underlying muscularis mucosa (Barker *et al.* 2008) and form the intestinal stem cell niche (Figure 1.2). The mucosa of the ileum has lymphoid follicles called Peyer's patches. The lamina propria is made up of extracellular matrix (including proteoglycan and fibrous proteins such as collagen, elastin, fibronectin, and laminin), containing fibroblasts and leukocytes including: lymphocytes, monocytes/ macrophages, eosinophils, and mast cells (Tortora & Derrickson 2016). The submucosa is rich supply of blood and

lymphatic vessels and is innervated by the ganglionated plexuses of Meissner's nervous plexus; ganglia are composed of enteroglia cells and neurons. Beneath the submucosa is the muscularis externa, composed of an inner circular and outer longitudinal smooth muscle layers separated by a thin layer of connective tissue and innervated by the Auerbach's plexus, which enables the peristaltic movement of food along the intestine (Bitar & Zakhem 2013). This layer is finally supported by a single layer of mesothelium called the serosa (McCance & Huether 1998) (Figure 1.2).

1.1.1.3 Intestinal epithelial cell types

The intestinal mucosa contains six main cell types, each with a specialized function. The most abundant are the absorptive columnar epithelial cells or enterocytes, which are highly polarized cells with their microvilli on their apical surface (Figure 1.2). These enterocytes are responsible for producing digestive enzymes and the absorption of nutrients (McCance & Huether 1998; Barker *et al.* 2010; 2012). The second most abundant cell types are unicellular glandular mucus-secreting goblet cells. Mucins are secreted into the lumen of the intestine, giving rise to an adherent mucus layer which surrounds and coats the intestinal villi. This mucus layer acts as a lubricant and creates a milieu which facilitates digestion and absorption of nutrients (Barker *et al.* 2013). Located at the base of intestinal crypts are Paneth cells, which secrete antimicrobial lysozymes that protect the crypt from pathological microorganisms (Rubin 1971; Barker *et al.* 2010). There are also three types of hormone-secreting enteroendocrine cells: S cells, which secrete secretin; CCK cells, which secrete cholecystinin (CCK) and K cells, which secrete glucose-dependent insulinotropic peptide (GIP). These hormones regulate digestion and absorption in the small intestine (Figure 1.2). A limited number of tuft cells are also located within

the small intestine; their role is to defend against parasites. Finally, microfold or M-cells are located within lymphoid peyer's patches and are responsible for transporting antigens from the lumen to the underlying lymphoid tissues (Barker *et al.* 2010, 2012).

1.1.1.3.1 Intestinal stem cells

Importantly, a small population of stem cells are located at the villus base, within crypts and are responsible for maintaining intestinal epithelial homeostasis (Figure 1.2). These stem cells differentiate as they migrate along the length of the villi, replacing cells which are lost at the villus tip (Clevers 2009; Van Der Flier, & Clevers 2009; Simons & Clevers 2011; Clevers 2013). This process of cell renewal ensures that the functions of the intestinal epithelium are maintained throughout life.

These stem cells generate transit-amplifying cells (TA), which rapidly proliferate to one of several lineages (Cheng & Leblond 1974; Vanuytsel *et al.* 2013; Leushacke & Barker 2014) which terminally differentiate to all intestinal cell types: enterocytes, goblet, enteroendocrine, Paneth cells, tuft, and M cells (Potten 1998; Clatworthy & Subramanian 2001; Montgomery & Breault 2008; Belchior *et al.* 2014) (Figure 1.4). The proliferative capacity of these stem cells ensures there are sufficient cells to regenerate any damaged tissue (Lutolf *et al.* 2009) and continually maintain digestion and absorption processes. Therefore, these cells are ideal candidates for use in tissue engineering and regenerative medicine (Barker *et al.* 2007; Snippert *et al.* 2010; Barker 2014; Leushacke & Barker 2014). The use of stem cell markers is essential for isolation of pure stem cell populations for using in tissue engineering. In the small intestine, there are two stem cell populations within the crypt, classified by location and cycling

dynamics (Barker *et al.* 2008, 2012; Clevers 2013). The first of these stem cells are mitotically active slender cells found at the bottom of the crypt between paneth cells, these are known as crypt base columnar cells. These cells express several stem cell markers including: Lgr5; CD133 (Prom1); Ascl2; Olfm4; Smoc2 and Sox9^{low} (Becker *et al.* 2008; Tian *et al.* 2011; Barker *et al.* 2013; Zhang & Huang 2013; Clevers 2016). The second stem cell populations are quiescent stem cells, which are located in the crypt directly above the terminally differentiated paneth cells (Potten *et al.* 1978). These quiescent stem cells express Bmi-1, Hopx, mTert, and Lrig1, and Sox^{high} (Potten *et al.* 1974; Gracz *et al.* 2010).

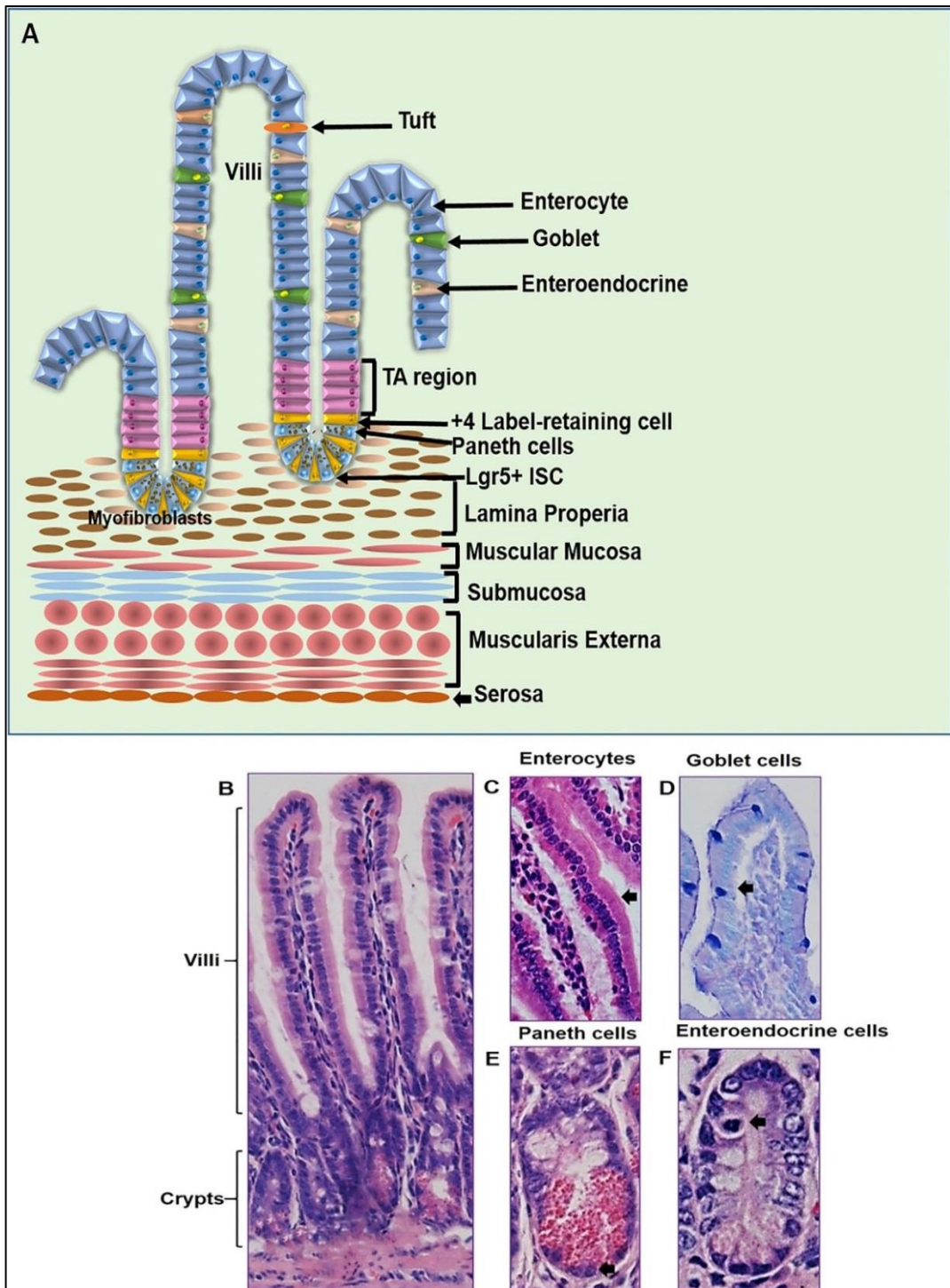


Figure 1.2: (A) Schematic diagram illustrating morphology of the small intestinal layers containing crypt–villus units together with the main intestinal cells of the epithelial layer, crypt intestinal stem cells, and their niche. (B) Histology of the crypt–villus axis represents intestinal cells (C) Enterocytes, (D) Goblet cells, (E) Paneth cells, and (F) Enteroendocrine cells.

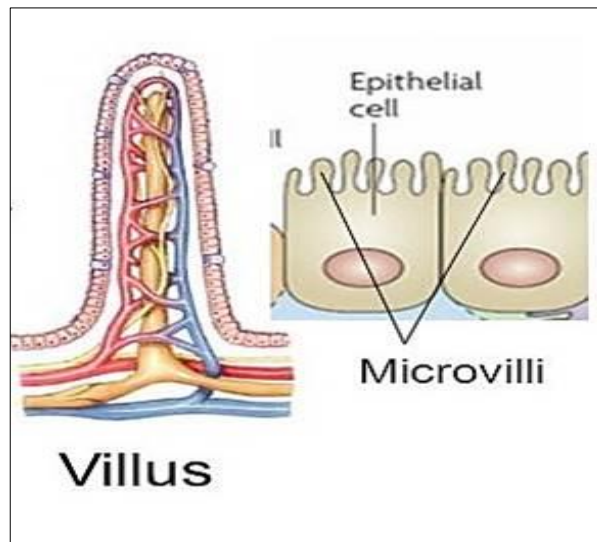


Figure 1.3: Schematic diagram illustrating the morphology of the microvilli which cover the apical surface of the enterocytes (Tortora & Derrickson 2016).

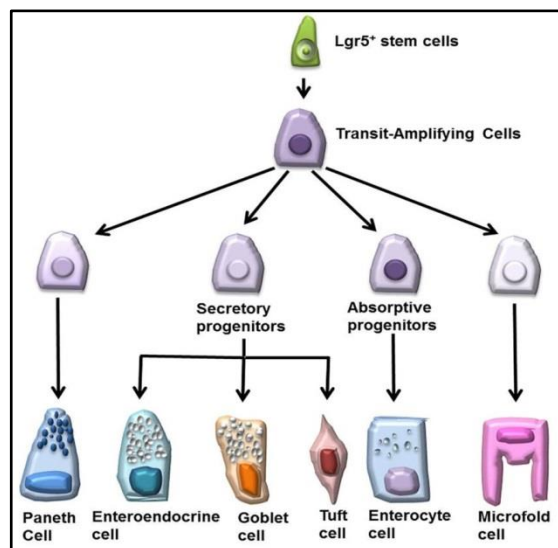


Figure 1.4: Schematic diagram illustrating the $Lgr5^+$ stem cells generating transit amplifying cells which then rapidly proliferated to one of several differentiated lineages.

1.1.1.3.1.1 Stem cell niche

The specific environment where adult stem cells are located in the small intestine is known as the stem cell niche. This provides signals to maintain the undifferentiated state and self-renewal capacity (stemness) (Walker *et al.* 2009). The stem cells niche is composed of cells which together with the basement membrane derived extracellular matrix regulate stem cell differentiation and fate (Walker *et al.* 2009; Henning & Furstenberg 2016; Sailaja *et al.* 2016; Sasaki *et al.* 2017). Due to the location of stem cells in direct contact with Paneth cells at the base of crypts, it seems likely that Paneth cells have important role on the crypt base columnar stem cells niche (Simons & Clevers 2011; Sato *et al.* 2011a; Sasaki *et al.* 2017). Several regulatory pathways have been found to play a role in the maintenance, proliferation and differentiation of stem cells (Barker *et al.* 2008); these include: Wnt; Notch; epidermal growth factor (EGF) and bone morphogenetic protein (BMP) pathways (Yeung *et al.* 2011; Date & Sato 2015; Van Rijn *et al.* 2016). Canonical Wnt signaling is well recognized as the main regulator of epithelial renewal in the small intestine (Clevers 2016). EGF signaling maintains stemness and prompts proliferation (Wong *et al.* 2012; Sato & Clevers 2013; Leushacke & Barker 2014). Whilst Notch signaling controls differentiation to enterocytes, inhibition of Notch signaling leading to the differentiation of stem cell towards secretory lineages, including: goblet, Paneth, enteroendocrine, and tuft cells (VanDussen *et al.* 2012). Bone morphogenetic protein (BMP) signaling negatively regulates stem-cell characteristics and promotes differentiation of progenitor cells in the villus compartment, but has no effect on stem cells located in the crypts (He *et al.* 2004). Thus, the manipulation of these signaling pathways in *in vitro* culture can be used to

maintain stem cell characteristics or drive differentiation of stem cells to appropriate lineages.

1.1.1.4 Digestion and absorption in the small intestine

The main function of the small intestine is digestion of food and absorption of nutrients and water (Clevers 2013). The absorption of the majority of essential nutrients occurs in the proximal jejunum and distal ileum. The pancreas secretes large amounts of digestive enzymes directly to the small intestine via the pancreatic duct. These enzymes include: pancreatic amylase which break down large carbohydrates to simple sugars, and trypsinogen which is converted to trypsin in the presence of the intestinal enzyme enterokinase (enteropeptidase). Trypsin then digests proteins to produce amino acids. Similarly, chymotrypsinogen, elastase, peptidase and carboxypeptidase digest large peptides to smaller peptides and amino acids. Pancreatic lipase acts on fats (triglycerides) that have been emulsified by bile salts and convert them to fatty acids and monoglycerides. Finally nucleases break down RNA and DNA to pentose and nitrogenous bases.

In addition, the intestinal enterocytes synthesize and produce several brush border enzymes: aminopeptidase, peptidase and dipeptidase that digest peptides to give rise to small peptides and amino acids, alongside lactase, sucrase and maltase that digest lactose, sucrose and maltose, respectively to produce simple monosaccharides (Tortora & Derrickson 2016). Absorption of digested nutrients occurs through diffusion, facilitated diffusion, active transport, and osmosis. The mucosal epithelial cells transport nutrients (amino acids derived from proteins, monosaccharides derived from carbohydrate, some vitamins and salts) from the lumen of the small intestine into the network of

capillaries. Whilst fatty acids and monoglycerides derived from lipids (triglycerides) under the action of pancreatic lipases are transported into tiny lymphatic vessels or micelles, and are absorbed into the enterocytes where they are reassembled into triglycerides and coated in a protein to form a chylomicron which is absorbed into lymphatic vessels in the lamina propria of the villi. Lymph drains back into the bloodstream at the subclavian vein by the thoracic duct (Tortora & Derrickson 2016). All the products of digestion and absorption are passed via the blood vessels to different organs of the body while undigested food or unabsorbed materials are moved onwards to the large intestine (Tortora & Derrickson 2016).

1.2 Inflammatory bowel disease

Inflammatory bowel disease (IBD) is a chronic autoimmune disease of the gastrointestinal tract. Clinically, IBD includes Crohn's disease (CD) and ulcerative colitis (UC), which mainly impact on the colon (UC and CD), rectum (UC) or any part of the gastrointestinal tract from the mouth to the anus (CD) (Blumberg *et al.* 1999; Garrett *et al.* 2010; Biasi *et al.* 2013). Inflamed intestinal mucosa is identified by abdominal pain, weight loss, diarrhoea, bloody stools, and infiltration of immune cells such as macrophages and neutrophils. These macrophages and neutrophils secrete cytokines, free radicals, and proteolytic enzymes which cause inflammation (Wong *et al.* 2006). The diagnosis of IBD is depend on clinical, radiologic, endoscopic, and histologic criteria (Seldenrijk *et al.* 1991; Mazzucchelli *et al.* 1994).

The aetiology of IBD is still unknown and the present notion is that a combination of genetic susceptibility, microbiome, environmental factors, and the immune system, (Elson *et al.* 1995; Baumgart & Carding 2007; Landy *et al.*

2016) leading to secretion of pro-inflammatory mediators resulting in loss of homeostasis and epithelial damage (Sartor 2006; Bosca-Watts *et al.* 2015). Several components of the mucosal immune system are involved in the pathogenesis of IBD and consist of intestinal epithelial cells, innate lymphoid cells (natural killer cells (NK)), cells of the innate (macrophages/monocytes, neutrophils, and dendritic cells) and adaptive (T-cells and B-cells) immune system, and their secreted mediators (cytokines and chemokines) (Shih & Targan 2008; Wallace *et al.* 2014). The role of cytokines in mucosal immune system has been investigated intensely. It has been found that increased levels of the pro-inflammatory cytokines interleukin-1 (IL-1), IL-6, IL-8, and tumour necrosis factor α (TNF α) are present in patients with IBD (Isaacs *et al.* 1992; Rogler & Andus 1998). These pro-inflammatory cytokines are expressed by lymphocytes, macrophages, and polymorphonuclear cells (PMNs). Production of these pro-inflammatory cytokines is prompted by the activation of nuclear factor κ B (NF- κ B), mitogen-activated protein kinase (MAPK), and JUN N terminal kinase (JNK) pathways (Elson *et al.* 1995; Beck & Wallace 1997; Rogler & Andus 1998; Williams 2001; Wong *et al.* 2006; Shih & Targan 2008).

It is hypothesised that IBD could be caused by an imbalance between pro- and anti-inflammatory cytokines in local tissues and lead to inflammation and malfunction of the barrier in the intestinal tissue. Interleukin 1 (IL-1) is a key mediator of innate immunity and inflammation which results in tissue damage in IBD. The IL-1 family consists of a number of agonists, antagonists, receptors and accessory proteins. Of which two key agonists: IL-1 α and IL-1 β are key proinflammatory cytokines (Dinarello 2011). These agonists bind to and activate the IL-1 receptor type1 (IL-1RI) in conjugation with the accessory protein (IL-1R AcP), whilst IL-1RII acts as decoy receptor and does not initiate signalling

cascades (Dinarello 2011). In addition, a natural antagonist for IL-1RI exist known as: IL-1 receptor antagonist (IL-1Ra), this binds to IL-1RI but fails to recruit IL-1RAcP and thus does not initiate a signalling cascade (Rider *et al.* 2011).

IL-1 α is synthesized as a precursor protein, which is fully active in pro- and cleaved forms; it is produced by numerous cell types within the body including the epithelia of the gastrointestinal tract, liver, kidney, lung, endothelial cell and astrocytes (Casini-Raggi *et al.* 1995; Ludwiczek *et al.* 2004). Further IL-1 α is released from necrotic cells after cell death by necrosis initiating neutrophil inflammation (Chen *et al.* 2007; Garlanda *et al.* 2013). IL-1 β is also synthesized as a precursor protein but in contrast to IL-1 α precursor, the IL-1 β precursor is not active and requires cleavage by cysteine protease called caspase-1 (also known as IL-1 converting enzyme (ICE)), releasing the active IL-1 β precursor into the extracellular space to be able to bind to IL-1 receptor (Dinarello 2011). IL-1 β is also expressed by a wide number of cells within the body although classically is considered as an inflammatory cytokine synthesised by inflammatory cells (Beck & Wallace 1997; Rogler & Andus 1998; Dinarello 2009).

There is a wide range of negative regulators which tightly regulate the action of pro-inflammatory cytokines IL-1 α and IL-1 β , including IL-1Ra, decoy receptors (IL-1RII), and accessory proteins (IL-1RAcP) by trapping the ligands. IL-1Ra is a member of IL-1 family which is secreted by epithelial cells, immune cells and adipocytes. IL-1Ra act as a natural inhibitor of IL-1 α and IL-1 β and regulates IL-1 pro-inflammatory activity by competing with IL-1 for binding sites of the cell surface IL-1RI preventing IL-1 from sending signal to target cells. IL-1Ra binds

IL-1RI with high affinity, but unable to recruit the IL-1RAcP (Re *et al.* 1996). IL-1RII is found in the cytoplasm and secreted by limited cell types such as monocytes, neutrophils, macrophages, B cells, and T regulatory cells, IL-1RII binds IL-1 both preventing the binding between IL-1 and IL-1RI (Martin *et al.* 2013; Garlanda *et al.* 2013).

The importance of the balance between IL-1 and IL-1Ra in IBD has been demonstrated in experimental animal models and in human tissues. Findings in immune complex induced colitis in rabbits revealed that IL-1 synthesis happened early in the colitis disease and IL-1 levels associated with the state of tissue inflammation (Cominelli *et al.* 1992). High levels of colonic IL-1Ra (10 fold) above those of IL-1 were detected, addressing resolution of the inflammation in rabbit immune complex induced colitis (Ferretti *et al.* 1994). The administration of neutralizing anti-serum against rabbit IL-1Ra resulted in sustained intestinal inflammation and significantly increased mortality, indicating the importance of endogenous IL-1Ra. In contrast, exogenous administration of IL-1Ra blockade in colonic inflammation in this animal model and in acetic acid induced colitis in rats (Thomas *et al.* 1991). Hence, studies of animal models of IBD have demonstrated an important role for IL-1 in inducing inflammation and tissue disruption, with both endogenous and exogenous IL-1Ra reducing severity of disease. In humans suffering with IBD the importance of IL-1 and IL-1Ra has also been demonstrated. Specifically mucosal biopsies from patients with active and inactive Crohn's disease (CD) and active ulcerative colitis (UC) contained mRNA for IL-1 while mRNA for IL-1Ra was decreased in active ulcerative colitis and Crohn's disease (Malyak *et al.* 1998). The intestine IL-1Ra and IL-1 ratio was significantly decreased in CD and UC patients compared to controls. This ratio was negatively related to the degree of the inflammation. IL-

1Ra were produced by normal human intestinal epithelial cells (IEC) while high amounts of IL-1 were produced in inflamed mucosa by lamina propria mononuclear cells in Crohn's disease patients (Daig *et al.* 2000).

1.3 Models of the small intestine

Maintenance of intestinal homeostasis requires interaction between intestinal mucosa, microbiota, and immune components (Garrett *et al.* 2010; Manresa & Taylor 2017). Thus, it is very important to develop experimental models that can reproducibly generate the intestinal microenvironment with three dimensional (3D) architecture.

1.3.1 Knockout mice models of inflammatory bowel disease

Knockout mice are genetically modified mice in which specific genes are deleted, these can either be systemic deletion or targeted promoter controlled deletions (Wirtz & Neurath 2007; Eltzschig *et al.* 2014; Kiesler *et al.* 2015). Knockout mice models are very useful to determine the functions of genes by investigating how the loss of genes can cause or contribute to diseases, from which, the findings are often translated to roles in human diseases (Longenecker & Kulkarni 2009). Although mouse models can not completely mimic human IBD, some of knockout systems have been used to model IBD which have provided substantial insights into the mechanism of diseases and in development of novel therapies for IBD (Mizoguchi *et al.* 2016). A number of different genetically engineered mice models have been utilized for studying IBD.

1.3.1.1 Cytokine knockout mice models

Wolf *et al.* (2000) studied the effect of IL-1 on the cellular homeostasis of small intestinal mucosa, using C57BL6 IL-1R1 knockout mice, demonstrating that

both apoptosis and proliferation increased in intestinal epithelial cells. The importance of IL-1Ra, encoded by the IL-1rn gene, as an endogenous IL-1 inhibitor has been investigated in immune deficient mice (RAG2) (lacking T and B cells) where IL-1Ra knockout mice spontaneously developed colitis (Akitsu *et al.* 2014). Knockout of particular genes including IL-2, IL-10, and transforming growth factor β (TGF- β) also resulted in the development of murine models of spontaneous colitis (Sadlack *et al.* 1993; Kühn *et al.* 1993; Kulkarni *et al.* 1993). IL-2 is a cytokine predominantly secreted by activated T-helper 1 (Th1) cells and promotes proliferation of T cells. Thus, IL-2 levels were increased in inflamed mucosa of patients with Crohn's disease due to the increased activity of Th1 (Sadlack *et al.* 1993). IL-10 is also a regulatory cytokine secreted mainly by T cells and macrophages. IL-10 is an effective inhibitor of macrophages and Th1 cells. IL-10 knockout mice develop spontaneous colitis and show increased levels of IL-1, IL-6, and TNF α . Thus, these observations suggest that IL-10 has the ability to protect the intestinal barrier (Kühn *et al.* 1993). TGF- β is produced by macrophages and induces collagen production by fibroblasts or intestinal smooth muscle cells which lead to rapid healing of injured intestine. TGF- β knockout mouse develops colitis possibly mediated by a defective inhibition of lymphocytes (Kulkarni *et al.* 1993). IL-15 is highly expressed in IBD and regulates the production of pro-inflammatory cytokines from T cells (Liu *et al.* 2000). IL-15 is produced by several cells involving macrophages, dendritic cells and intestinal epithelial cells. IL-15 has a role in intestinal inflammation by recruitment and activation of T cells, activation of neutrophils, natural killer (NK) cell proliferation, and inhibition of apoptosis (Van Heel 2006). In acute colitis, IL-15 knockout mice displayed a reduction in T cells and NK cells and decreased

the level of TNF α . These observations suggest that IL-15 is a potential new therapeutic target in IBD (Yoshihara *et al.* 2006).

1.3.1.2 Matrix degrading enzyme knockout mice models

The gelatinases matrix metalloproteinase MMP2 and MMP9 play a crucial role in inflammatory bowel disease where MMP9 mediated tissue injury in colitis, while MMP2 knockout prevented tissue damage and preserves intestinal barrier function (Garg *et al.* 2009). Induction of colitis in MMP2 and MMP9 knockout mice models by treating with dextran sodium sulfate, *Salmonella typhimurium*, and trinitrobenzene sulfonic acid demonstrated that these knocked out mice were resistant to development of colitis as compared to the induction of colitis to wild type mice which revealed tissue damage due to the upregulated activity of MMP2 and MMP9 (Garg *et al.* 2009).

1.3.1.3 Mucosal expression knockout mice models

The role of the mucus layer in maintaining intestinal epithelial barrier has been displayed in MUC2 knockout mice, which developed spontaneous colon adenocarcinoma at 6 months of age (Velcich *et al.* 2002). Furthermore, colitis with inflammatory cell infiltration was determined mainly in the distal colon of MUC2 knockout mice at 5 weeks of age (Van der Sluis *et al.* 2006). In addition, the role of intestinal alkaline phosphatase (ALP) as a mucosal defence factor essential for maintaining of normal intestinal microbial homeostasis was investigated. ALP knockout mice (C57BL/6) demonstrated increased severity of intestinal inflammation and bacterial growth and translocation into bloodstream as compared to wild type mice (Bilski *et al.* 2017).

Whilst animal models are useful for studying human diseases, there are a number of limitations to their use. In addition to the major ethical concerns,

animal experiments require skilled people, time consuming procedures, and have high cost. Thus, cell culture models were proposed to overcome the drawbacks related to animal experiments and support the 3Rs principle (replacement, reduction, and refinement).

1.3.2 Cell culture models

Until recently, *in vitro* intestinal models have been restricted to simple two-dimensional (2D) cell culture on standard cell-culture plates or transwell culture inserts (Haycock 2011). However, three-dimensional (3D) cell culture models are currently under investigation by groups worldwide to determine if these 3D cell cultures can more closely mimic the *in vivo* environment and support cell differentiation and 3D tissue organization which is not possible in conventional 2D cell culture systems (Cukierman *et al.* 2002; Huh *et al.* 2011; Rimann & Graf-Hausner 2012; Ader & Tanaka 2014; Costello *et al.* 2014a; Pastuła *et al.* 2016).

These 3D cell culture models have been evaluated for use in tissue engineering and drug discovery (Balimane & Chong 2005; Tibbitt & Anseth 2009) and used as an alternative to *in vivo* animal models in drug toxicity studies (Pampaloni *et al.* 2007; Ravi *et al.* 2015). Tissue engineering studies have promised an improved understanding of small intestinal physiology, as well as the response of the small intestine to infection, toxicity and new therapies (Basu & Bertram 2014). Furthermore, using these systems it may be possible to develop personalized intestinal tissue grafts which can be used to repair the intestine, whilst avoiding the risks of immune system rejection (Day 2006).

These 3D scaffolds are often designed to biodegrade after the deposition of extracellular matrix, when the cells become mechanically independent (Day

2006; Bitar & Zakhem 2013) and could potentially be used therapeutically (Sato *et al.* 2009), however matching the degradation rates to synthesis and deposition of new matrix remains a key challenge in tissue engineering (Sung *et al.* 2004; Wu & Ding 2004; Lee & Mooney 2012). The most important element for successful tissue engineering of the small intestine is the use of specialized biomaterial scaffolds providing cells a substrate for the deposition of extracellular matrix and subsequent cell adhesion (Drury & Mooney 2003; Tibbitt & Anseth 2009; Ehrbar *et al.* 2011).

1.3.2.1 The use of cell lines in intestinal engineering

Due to failed attempts to establish long-term primary cell culture of normal small intestine, researchers have successfully utilized cell lines which are derived from gastrointestinal tumours (Pusch *et al.* 2011). The human colonic adenocarcinoma cell lines: Caco-2 and HT29-MTX cells are probably the most frequently used cell lines due to their ability to differentiate into enterocyte-like cells and mucus-producing goblet cells, respectively (Figure 1.5) (Howell *et al.* 1992; Ferraretto *et al.* 2007; Rao & Sankar 2009) whilst these would not be suitable for the tissue engineering applications due to their cancerous nature they are alternative models for *in vitro* cultures.

1.3.2.1.1 Caco-2 cells

Caco-2 cells can spontaneously differentiate into cells with the ability to form tight junctions and produce large amounts of digestive brush border enzymes, similar to small bowel enterocytes (Meunier *et al.* 1995; Yamashita *et al.* 2002; Quante & Wang 2009). Caco-2 cells express a number of digestive enzymes including sucrase-isomaltase, lactase, peptidase, and alkaline phosphatase. The expression of these enzymes are used as markers of intestinal

differentiation and digestive function (Van Beers *et al.* 1995; Basson *et al.* 1996; Olejnik *et al.* 2003; Ferruzza *et al.* 2012; Natoli *et al.* 2012; Lea 2015). However, Caco-2 cells in 2D culture have tight junctions similar to those of the colon, rather than the small intestine. This has led to criticism of their use as a model for the epithelium of the small intestine (Shah *et al.* 2006; Araujo & Sarmiento 2013). Furthermore, Caco-2 cell behaviour can be affected by culture condition (serum supplemented and serum free media), passage number, cell density and incubation times (Ranaldi *et al.* 2003; Sambuy *et al.* 2005) all of which make it difficult to compare research findings between different studies (Nolleaux *et al.* 2006; Natoli *et al.* 2011).

Caco-2 cells are often used to mimic small intestinal enterocytes and have been used extensively in absorption and transport studies of nutrients and drugs (Gamsiz *et al.* 2011; Kauffman *et al.* 2013) (Table 1.1), for example, insulin transport studies (Foss & Peppas 2004; Carr & Peppas 2010). Moreover, Caco-2 cells have been used to investigate the cytotoxicity, for example, that of acrylic-based copolymer protein as an oral insulin delivery system (Foss & Peppas 2004). Caco-2 cells can also be utilized to verify toxicology when exposed to nanoparticles such as polystyrene, which resulted in increased level of iron absorption (Mahler *et al.* 2009).

1.3.2.1.2 HT29-MTX cells

HT29-MTX cells are also a commonly used cell line in intestinal modeling. These cells are derived from human colonic adenocarcinoma cells and are resistant to 10^{-5} mol/L methotrexate (MTX). HT29-MTX cells are composed entirely of differentiated mucus-secreting goblet cells. They maintain this differentiated phenotype in monolayer culture and are used to mimic intestinal

goblet cells, and are commonly co-cultured with Caco-2 cells in 2D culture (Orian-Rousseau *et al.* 1998; Pontier *et al.* 2001; Navabi *et al.* 2013; Martínez-Maqueda *et al.* 2015). HT29-MTX cells have been utilized in studies investigating the diffusion of drugs across the mucus layer (Walter *et al.* 1996; Behrens *et al.* 2001; Chen *et al.* 2010), these have been used to test the mucoadhesive and toxicity of nanoparticles as drug delivery systems (Adamczak *et al.* 2016), and to test adhesion and invasion of Salmonella strains (Gagnon *et al.* 2013) (Table 1.1).

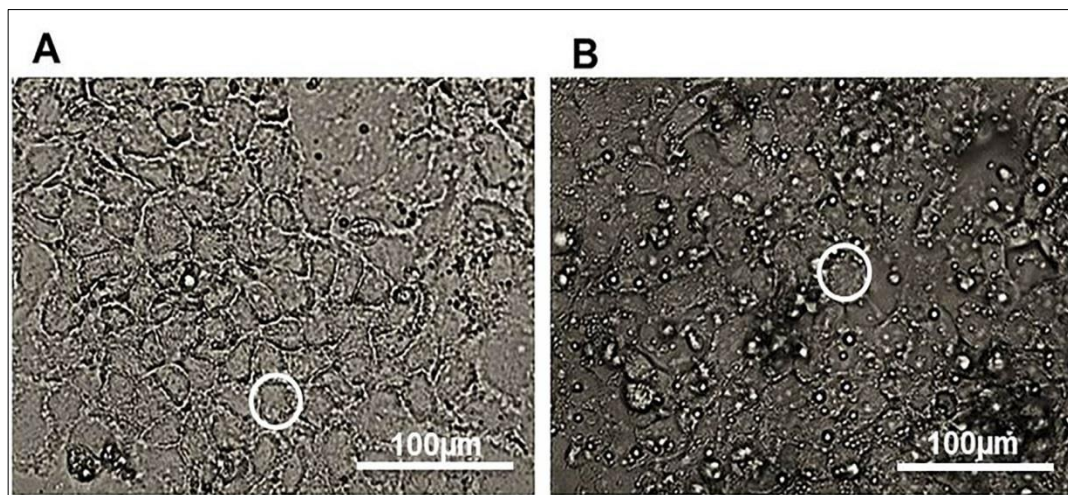


Figure 1.5: Bright field image of human colon adenocarcinoma cell lines in monolayer (A) Caco-2 cells and (B) HT29-MTX cells.

Cell type	Method	Key findings	Ref
Caco-2	Short- term culture (3 days) for absorption.	Barrier formed with high activity transporters.	(Yamashita <i>et al.</i> 2002)
Caco-2	A microchip-based system for intestinal absorption studies.	A high permeability coefficient for cyclophosphamide.	(Imura <i>et al.</i> 2009)
Caco-2	<i>In situ</i> method to measure activities of enzymes.	Increase of alkaline phosphatase and sucrase activity. An absence of aminopeptidase activity.	(Ferruzza <i>et al.</i> 2012)
Caco-2 + HT29-MTX	Permeability study.	Both passive permeability values and diffusion coefficients were same in both cell lines.	(Pontier <i>et al.</i> 2001)
Serum free co-culture Caco-2 and HT29-MTX	Permeability study.	Permeability to macromolecules was decreased. Alkaline phosphatase activity was increased in co-culture compared to Caco-2 monoculture.	(Nolleaux <i>et al.</i> 2006)
Co-culture Caco-2 and HT29-MTX	Iron bioavailability study.	Increasing the ratio of HT29-MTX cells led to decrease the amount of iron bioavailability.	(Mahler <i>et al.</i> 2009)
Co-culture Caco-2 and HT29-MTX	Drug permeability study.	TEER values were decreased and permeability coefficient of drugs were increased following 21day culture time.	(Chen <i>et al.</i> 2010)
Co-culture Caco-2 and HT29-MTX	Permeability study.	TEER value decreased as the proportion of HT29-MTX increased. Significant increase in permeability of intestinal fluoride after remove of mucus.	(Rocha <i>et al.</i> 2012)
Caco-2 + HT29-MTX	Host-pathogen interaction.	Adhesion and invasion of Salmonella strains to HT29-MTX cells were higher than to Caco-2 cells.	(Gagnon <i>et al.</i> 2013)
Caco-2, HInEpC, iPSC	Permeability and drug transport.	HInEpC and iPSC expressed E-cadherin, CDX2, and Villin more than Caco-2.	(Kauffman <i>et al.</i> 2013)

Table 1.1: Summary of the major two dimensional cell culture systems of intestinal cell lines. (Yamashita *et al.* 2002; Imura *et al.* 2009; Ferruzza *et al.* 2012; Pontier *et al.* 2001; Nolleaux *et al.* 2006; Mahler *et al.* 2009; Chen *et al.* 2010; Rocha *et al.* 2012; Gagnon *et al.* 2013; Kauffman *et al.* 2013).

1.3.2.1.3 2D co-culture models of the small intestine

In order to mimic the native small intestinal epithelium which is composed of diverse absorptive and secretory cells a number of studies have co-cultured Caco-2 cells alongside HT29-MTX cells (Walter *et al.* 1996; Nollevaux *et al.* 2006; Mahler *et al.* 2009; Chen *et al.* 2010; Gagnon *et al.* 2013; Béduneau *et al.* 2014) (Table 1.1). These studies have enabled the formation of a Caco-2 derived enterocyte-like layer, which is interspersed with mucus secreting HT29-MTX cells, and avoided the limitations and drawbacks previously seen in mono-cultures (Walter *et al.* 1996).

Walter *et al.* (1996) co-cultured Caco-2 and HT29-MTX cells in cell culture inserts in a transwell format, where they were shown to produce an adherent mucus layer which covered the cell monolayer. The cells were shown to have structures similar to microvilli, although they were of irregular shape and size. The mucus layer which formed by the HT29-MTX cells during co-culture with Caco-2 cells was proposed to play an important role in digestion and bioavailability (Mahler *et al.* 2009) (Figure 1.6). Many studies have exploited *in vitro* co-cultures of Caco-2 and HT29-MTX cells to provide a drug absorption model (Walter *et al.* 1996; Mahler *et al.* 2009), to study drug permeability (Chen *et al.* 2010; Carr & Peppas 2010; Béduneau *et al.* 2014), and to improve alternative *in vitro* systems for the evaluation of cytotoxicity of nanoparticles to replace animal testing (Walczak *et al.* 2015). Furthermore, different co-culture ratios of Caco-2 and HT29-MTX cells have been used to investigate the co-culture ratio most physiologically relevant to *in vivo* situations (Nollevaux *et al.* 2006; Rocha *et al.* 2012; Wan *et al.* 2014).

Another significant aspect of co-culture is the facility to introduce additional cell types to more closely mimic the native multicellular environment seen *in vivo* (Figure 1.6). Antunes *et al.* (2013), developed the triple co-culture model based on the use of Caco-2 and HT29-MTX cells, incorporating Raji B lymphocytes. The Raji B lymphocytes were selected to stimulate differentiation of Caco-2 cells to M-cells (Antunes *et al.* 2013; Araujo & Sarmiento 2013; Lozoya-Agullo *et al.* 2017) (Figure 1.6). This triple co-culture system was used to investigate absorption of insulin, demonstrating insulin permeability was greater in triple co-cultures compared to co-culture of Caco-2 and Raji B cells alone (Antunes *et al.* 2013). Moreover, *in vitro* triple co-culture model has been used for polystyrene nanoparticle permeability studies that demonstrated the strong influence of HT29-MTX cells and M-cells on the nanoparticle permeation. In this study, cellular uptake of polystyrene nanoparticles was affected by the presence of mucus layers. Where, nanoparticle transport was significantly increased in Caco-2/M cells due to a lack of mucus secretion from M cells (Schimpel *et al.* 2014). Most recently, the Caco-2/HT29-MTX co-culture and Caco-2/HT29-MTX/Raji B triple co-culture models have been successfully used to investigate the intestinal permeability of different biopharmaceutical characteristics of drugs. Where it was shown that higher permeability of drugs were observed in more complex models compared with Caco-2 monoculture (Lozoya-Agullo *et al.* 2017). Taken together, these studies demonstrate the importance of cell-cell interactions which can impact on the physiological function in intestinal cells. These models can also be combined with bacterial cells to mimic the microbiota seen within the small intestine (Lievin-Le Moal & Servin 2013; Kang & Kim 2016). Whilst these 2D static culture models of intestinal cells in Transwells display a number of advantages, these models fail to develop villi morphology

(Kim *et al.* 2012). Furthermore, these models fail to undergo cytodifferentiation due to lack of the 3D microenvironment, including luminal flow, and fluid shear stress (Kim *et al.* 2012; Kim & Ingber 2013).

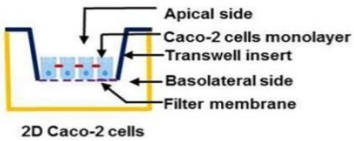
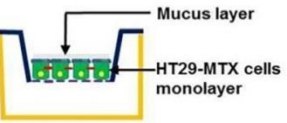
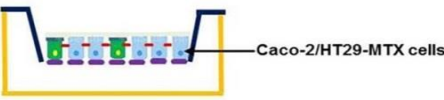
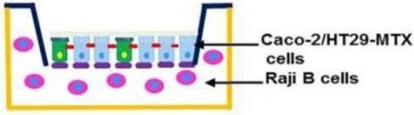
Experimental design	Culture duration	Key findings	Ref
 <p>2D Caco-2 cells</p>	21 days	Caco-2 cells formed monolayers and differentiated into enterocyte-like cells, produced tight junction protein (ZO1). Microvilli were produced, expression of ALP, SI.	(Pinto 1983)
 <p>2D HT29-MTX cells</p>	21 days	HT29-MTX cells formed monolayer and differentiated into goblet cells secreting mucus on the apical side. Sparse and short microvilli were observed.	(Rousset 1986)
 <p>2D co-culture</p>	21 days	Co-cultured Caco-2 and HT29-MTX cells formed monolayer and differentiated into enterocyte and goblet-like cells as above.	(Walter <i>et al.</i> 1996)
 <p>2D triple co-culture</p>	Co-cultured Caco-2 and HT29-MTX cells for 14 days then Raji B cells were added and maintained together for 6-7 days.	HT29-MTX cells maintained their phenotype and produced mucus. Caco-2 cells differentiated into M-cells and cytoskeleton reorganization.	(Araujo & Sarmiento 2013; Lozoya-Agullo <i>et al.</i> 2017)

Figure 1.6: Summary of two dimensional monoculture, co-culture, and triple co-culture of Caco-2 and HT29-MTX cells. (Pinto 1983; Rousset 1986; Walter *et al.* 1996; Araujo & Sarmiento 2013; Lozoya-Agullo *et al.* 2017).

1.3.2.2 3D cell culture models of the small intestine

A major shortcoming of two dimensional studies is that they do not reproduce the villus-crypt architecture of the small intestine. To overcome this shortcoming, Wang *et al.* (2009a) investigated the effect of a biomimetic crypt-like microwell on Caco-2 phenotype. A significant positive correlation between the crypt like topography and Caco-2 metabolic activity and migration with low level of differentiation which mimics cells in crypts of native small intestine was observed. In addition, a number of studies have microfabricated villus-shaped collagen scaffolds into which Caco-2 cells were cultured (Sung *et al.* 2011; Yu *et al.* 2012; Kim *et al.* 2014; Costello *et al.* 2014a) (Figure 1.7). These studies demonstrated that the culture of Caco-2 cells on these prefabricated villi structures led to the formation of villi which were comparable to those of human jejunum after 3 weeks in culture (Sung *et al.* 2011). The transepithelial electrical resistance (TEER) was measured, which is a technique used to assess the barrier tissue integrity and permeability of cell monolayer, it has been observed that TEER of cells in these villus-like structures were lower than those in cells grown on 2D flat substrate.

1.3.2.2.1 Biomaterials for tissue engineering of the small intestine

A major shortcoming of the research utilizing intestinal cells in 2D culture is that it does not mimic the complex architecture of the small intestine and fails to mimic the *in vivo* phenotype. Thus, several biomaterial scaffolds have been investigated for 3D cell culture and tissue engineering of the small intestine (Basson *et al.* 1996; Drury & Mooney 2003; Leonard *et al.* 2010; Sung *et al.* 2011; Costello *et al.* 2014a).

These scaffolds provide a physical structure in which cells migrate and utilize topography to stimulate cell development and formation of tissue networks. Scaffold porosity is a critical factor in directing cell fate within the 3D scaffold architecture. Pore size is essential for the diffusion of cells inside the 3D scaffolds, pores enable cells to penetrate into the matrix and provide a space for cells to reside and synthesize new extracellular matrix (Sung *et al.* 2004; Wu & Ding 2004; Bitar & Zakhem 2013; Costello *et al.* 2014a; Ravi *et al.* 2015). Accordingly, many attempts have been undertaken to develop porous biomaterials such as tubular constructs with mechanical and physical properties well suited to the small intestine (Choi & Vacanti 1997; Grikscheit *et al.* 2004; Huh *et al.* 2011; Totonelli *et al.* 2012; Tabriz *et al.* 2015; Dedhia *et al.* 2016).

The rate of cell growth, however, varies depending on the scaffold used (Cukierman *et al.* 2001, 2002). In 3D cell culture models, the interaction between cells and the scaffold is regulated by the material characteristics of the scaffold. Some materials provide natural adhesion sites for cells whilst others provide a substratum for the deposition of extracellular matrix which subsequently provides adhesion sites for cells (Ehrbar *et al.* 2011). The mechanical characteristics and degradation dynamics of the scaffold are important for specific tissue engineering applications (Kropp & Cheng 2000; Terada *et al.* 2000). The mechanical properties of scaffolds control the shape of cells during tissue reconstruction and provide mechanical cues to cells to tailor differentiation (Bitar & Zakhem 2013; Costello *et al.* 2014a), whilst also providing support for load (Baker *et al.* 2009). Scaffolds investigated to date include natural hydrogels (e.g. collagen gels and Matrigel) and synthetic scaffolds (e.g. poly-lactic-glycolic acid) (PLGA) which have a number of key advantages and disadvantages (Table 1.2) (Figure 1.7).

Cell Types	Scaffolds	Key Findings	Ref
Caco-2	Collagen type I, IV and laminin	Alkaline phosphatase, dipeptidyle peptidase and sucrase-isomaltase activities were higher in Laminin and coll IV compared to coll I	(Basson <i>et al.</i> 1996)
Caco-2	Microfabricated of PDMS coated with fibronectin	Crypt-like topography resulted in higher metabolic activity and lower cell differentiation.	(Wang <i>et al.</i> 2009a)
Caco-2 + Macrophage + Dendritic cells	Collagen	IL-8 and mucus was released after IL-1 β treatment.	(Leonard <i>et al.</i> 2010)
Caco-2	Collagen and PEG	Caco-2 cells proliferated; formed finger-like structures mimicked the human jejunal villi.	(Sung <i>et al.</i> 2011)
Caco-2 + hMECs	Decellularized porcine jejunal segments	Caco-2 cells behaved in a similar fashion to enterocytes, but there was an increased the membranes permeability. p-glycoprotein transporter protein was increased.	(Pusch <i>et al.</i> 2011)
Caco-2	Collagen + Matrigel	Regeneration of basal proliferative crypts and formation of four types of intestinal cells: enterocytes, goblet, enteroendocrine and paneth cell.	(Kim <i>et al.</i> 2012)
Caco-2	PLGA	Determined the location of the 4 strains of bacteria to the Caco-2 monolayers and evaluated the therapeutic ability of probiotic.	(Costello <i>et al.</i> 2014a)
Caco-2 + HT29-MTX	PLGA	Alkaline phosphatase activity was increased. The TEER values were high.	(Costello <i>et al.</i> 2014b)
Caco-2	Fabricated of collagen into 3D villi scaffold	Caco-2 growth was increased. Alkaline phosphatase activity was increased. The TEER values were decreased.	(Yi <i>et al.</i> 2017)

Table 1.2: Summary of three dimensional cell culture systems of intestinal cell lines. (Basson *et al.* 1996; Wang *et al.* 2009; Leonard *et al.* 2010; Sung *et al.* 2011; Pusch *et al.* 2011; Kim *et al.* 2012; Costello *et al.* 2014a; Costello *et al.* 2014b; Yi *et al.* 2017).

1.3.2.2.1.1 Natural biomaterials

Type I collagen gels are commonly used for 3D culture, as they are easy to prepare, inexpensive, can support a range of cell types (Li *et al.* 2013; Lelièvre *et al.* 2017), and enable encapsulation of cells (Chougule *et al.*, 2012) (Table 1.2). Furthermore, pore size, rigidity, and ligand density can be adjusted by changing the collagen concentration or utilizing chemical cross-links (Baker *et al.* 2009). Li *et al.* (2013) used collagen gels to seed fibroblasts, Caco-2 and HT29-MTX cells, which was used to evaluate drug permeability and was shown to have more physiologically relevant drug absorption rates. Pusch *et al.* (2011) performed 3D co-culture of Caco-2 cells and human microvascular endothelial cells (hMECs), created multilayers of enterocyte-like cells which expressed villin, E-cadherin, and the transporter p-glycoprotein at levels that were similar to that of a normal human jejunum. Whilst Viney *et al.* (2009) co-cultured intestinal epithelial cell lines (IEC6: a rat small intestinal epithelial cell line; IPI-21: a small boar ileum epithelial cell line, and CRL-2102: a human epithelial cell line derived from colorectal adenocarcinoma) with Rat-2 (fibroblast-like cells) in collagen gels alone or in combination with Matrigel. After 20 days, optimal epithelial cell growth was seen in collagen gels supplemented with Matrigel, where multi-layered intestinal epithelium were seen, which included clusters of cells similar to the morphology of crypts. This highlighted the importance of the interaction between the cell lines, extracellular matrix and other cell types such as fibroblasts; and how they can impact on cellular proliferation and differentiation (Walker & Stappenbeck 2008). These interactions with localized cells were further demonstrated when rat intestinal sub-epithelial myofibroblasts (ISEMF) were co-cultured with IEC-6 cells on a collagen gel scaffold (Yoshikawa *et al.*

2011), where the myofibroblasts induced differentiation of intestinal epithelial cells into enteroendocrine cells (Table 1.2) (Figure 1.7).

1.3.2.2.1.2 Synthetic biomaterials

Synthetic scaffolds have also been studied for their ability to reconstruct the small intestine. Synthetic biodegradable copolymers: poly lactic acid (PLA) and poly glycolic acid (PGA) have been combined to form poly lactic glycolic acid (PLGA). This polymer has been investigated for scaffold fabrication in tissue engineering of the small intestine (Boomer *et al.* 2014; Ravi *et al.* 2015). The chemical properties of PLGA co-polymer permitted hydrolytic degradation of the ester bond into the acidic, non-toxic monomers (PLA and PGA) which are removed by natural metabolic pathways. Physical properties of PLGA have been found to be related to the molecular weight of the monomers, the hydrophobic PLA/hydrophilic PGA ratio, the storage temperature and the exposure time to water. These studies demonstrated the rate of degradation negatively affected cell proliferation, with the fastest degradation rates displaying the poorest viability (Sung *et al.* 2004; Wu & Ding 2004).

In addition, Costello *et al.* (2014b) used fabricated PLGA as a porous 3D tissue scaffold which mimicked the shape and size of intestinal villi. They showed that co-culture of Caco-2 and HT29-MTX on PLGA resulted in proliferation and differentiation of co-cultured cells. However, these Caco-2 and HT29-MTX cells were differentiated under the stimulation of epidermal growth factor which was added to the basolateral side of scaffolds (Figure 1.7).

Although the latest procedures to engineer the small intestine *in vitro* have been shown to have some positive outcomes, the surface area created is not

adequate for human therapy and the majority of *in vitro* methods created only epithelium and lacked surrounding mesenchymal structures.

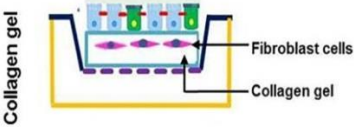
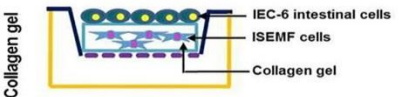
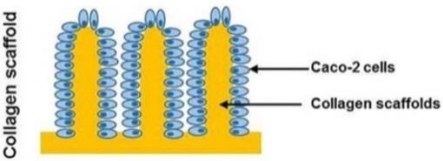
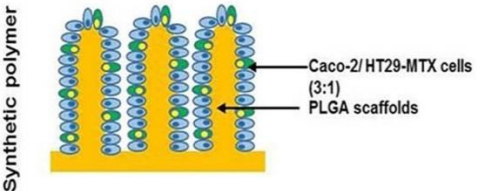
Experimental design	Culture duration	Key findings	Ref
 <p>Collagen gel</p> <p>Fibroblast cells</p> <p>Collagen gel</p>	21 days	Co-cultured cells proliferated for 3 weeks and the cells formed monolayer and secreted mucus. Low level of ZO-1 expression.	(Yoshikawa <i>et al.</i> 2011)
 <p>Collagen gel</p> <p>IEC-6 intestinal cells</p> <p>ISEMF cells</p> <p>Collagen gel</p>	21 days	Decreased TEER value. ISEMF cells well maintained IEC-6 cells. IEC-6 cells proliferated, formed multilayer structures and expressed enteroendocrine markers such as chromogranin A.	(Yu <i>et al.</i> 2012)
 <p>Collagen scaffold</p> <p>Caco-2 cells</p> <p>Collagen scaffolds</p>	21 days	Caco-2 cells proliferated on the surface of fabricated collagen scaffolds and mimicked the intestinal villi. The height of the collagen scaffold condensed to approximately half of the original height and was incapable of withstanding long term culture without loss of villi integrity.	(Sung <i>et al.</i> 2011)
 <p>Synthetic polymer</p> <p>Caco-2/HT29-MTX cells (3:1)</p> <p>PLGA scaffolds</p>	28 days	Co-cultured cells proliferated on the surface of fabricated porous PLGA scaffolds and mimicked the intestinal villi. Caco-2 cells differentiated into enterocyte like cells and HT29-MTX cells differentiated into goblet like cells, this differentiation was stimulated by adding epidermal growth factor to the basolateral side.	(Costello <i>et al.</i> 2014a)

Figure 1.7: Summary of three-dimensional monoculture and co-culture of Caco-2 and HT29-MTX cells using collagen gel, collagen scaffolds, and PLGA scaffolds. (Yoshikawa *et al.* 2011; Yu *et al.* 2012; Sung *et al.* 2011; Costello *et al.* 2014a).

1.3.2.3 Recapitulating the dynamic mechanical microenvironment of the small intestine

Under an *in vitro* static culture microenvironment, cells can be supplied with nutrients by manual medium replacement. Thus, long term culture under static conditions possesses multiple limitations such as poor delivery of nutrients, accumulation of waste and risk of contamination. To overcome these limitations, and for long term maintenance of intestinal cells in a healthy state, many studies have developed dynamic culture microenvironments. An automated perfusion system (Minucells and Minutissue) has been used to study the differentiation and drug transport properties of Caco-2 cells (Masungi *et al.* 2004; Masungi *et al.* 2009). The enzymatic activities and permeability coefficient of drugs in differentiated Caco-2 cells in perfusion systems were increased when compared to Caco-2 cells differentiated in traditional culture using snapwell inserts (Masungi *et al.* 2004; Masungi *et al.* 2009).

Similarly, microfluidic culture methods play an important role in addressing this issue and assist in the development of enhanced barrier function of Caco-2 cells (Imura *et al.* 2009). Several studies have developed gut-on-a-chip microdevices to mimic the dynamic motion seen in the human small intestine (Huh *et al.* 2011; Kim *et al.* 2012; Kim & Ingber 2013; Mochel *et al.* 2017; Bein *et al.* 2018). Microfluidic gut-on-a-chip microdevices are an alternative *in vitro* model, which have the ability to recapitulate the 3D structures of native human intestinal villi. In these models, Caco-2 cells exposed to dynamic fluid flow and peristalsis-like motions resulted in cytodifferentiation of Caco-2 cells into four main types of intestinal epithelial cells and formed proliferative crypts (Huh *et al.* 2011; Kim *et al.* 2012; Kim & Ingber 2013; Bein *et al.* 2018).

1.3.2.4 Tissue engineering the small intestine

The small intestine becomes dysfunctional in a number of diseases including inflammatory driven pathologies (such as ulcerative colitis; Crohn's disease; celiac disease), congenital diseases (such as lactose intolerance and short bowel syndrome) and cancer. These can become extremely debilitating disorders impacting on quality of life or can even become life-threatening (Abadie & Jabri 2014; Belchior *et al.* 2014; Valatas *et al.* 2015).

Thus, the ability to replace damaged and malfunctioning tissues with a tissue-engineered small intestine could be of use in these conditions (Nakamura & Sato 2018). Furthermore, engineered intestinal tissue could be created using patient-specific explants; small samples of healthy tissue could be collected from a patient and expanded within the laboratory. If these cells could then be utilized in the generation of a tissue-engineered small intestine, this could then be returned to the patient to enable intestinal repair or augmentation. Use of self-tissue would avoid the requirement of tissue donors, and the need for lifelong immunosuppression to prevent rejection of tissues (Grant *et al.* 2015).

1.3.3 Stem cell models

1.3.3.1 Isolation of small intestinal stem cells

For the successful isolation of stem cells from intestinal crypts a clear stem cell marker is essential to enable purification of intestinal stem cells, and whilst there are a variety of stem cells markers, a leucine-rich repeat-containing G-protein coupled receptor 5 (Lgr5), also known as GPR49, has been suggested as the most appropriate marker for purification of stem cells (Barker *et al.* 2007, 2008, 2010; Sato *et al.* 2011a; Barker *et al.* 2012, 2013). Lgr5 is expressed in cycling columnar cells in the base of the crypts, but not in the villi (Barker *et al.*

2007; Snippert *et al.* 2010). Lgr5 is a target of Wnt signaling and these cells are capable of generating all epithelial lineages in *in vitro* culture (Barker *et al.* 2007; Sato *et al.* 2009; Tan & Barker 2015). Furthermore, intestinal stem cells are capable of self-organizing into organoid units that recapitulate the intestinal villi and crypt domains and reflect main structural and functional properties of the small intestine (Sato *et al.* 2009, 2011a; Fuller *et al.* 2012; Sato & Clevers 2012, 2013; Wang *et al.* 2013a; Date & Sato 2015; Sato & Clevers 2015; Sasaki *et al.* 2017).

Studies over the past two decades have provided promising results in tissue engineering of small intestine due to the successful isolation of intestinal crypts which could form organoid units (Figure 1.8). It is possible to take complete crypts from intestinal tissues, which contain progenitor cells and expand these crypts *in vitro* to form organoid units and differentiate following transplantation (Mochel *et al.* 2017). Kim *et al.* (2007) harvested intestinal epithelial organoid units from neonatal rats and seeded them on biodegradable polyglycolic acid scaffolds, which were maintained in a perfusion bioreactor for 2 days. The cells were shown to distribute and adhere to the polymer scaffold. Similarly, Sato and colleagues (2009) developed a 3D culture system of mouse intestinal crypts known as 'mini-gut' culture or organoid culture. These 3D cultures in Matrigel supplemented with growth factors (R-spondin-1, epidermal growth factor, and the BMP inhibitor: Noggin). In this system, the crypt-villus organoids developed not only from whole crypts but also from single Lgr5⁺ stem cells. These single intestinal stem cells were shown to form crypt-like structures by day 1-4, and then crypt-buds by day 5.

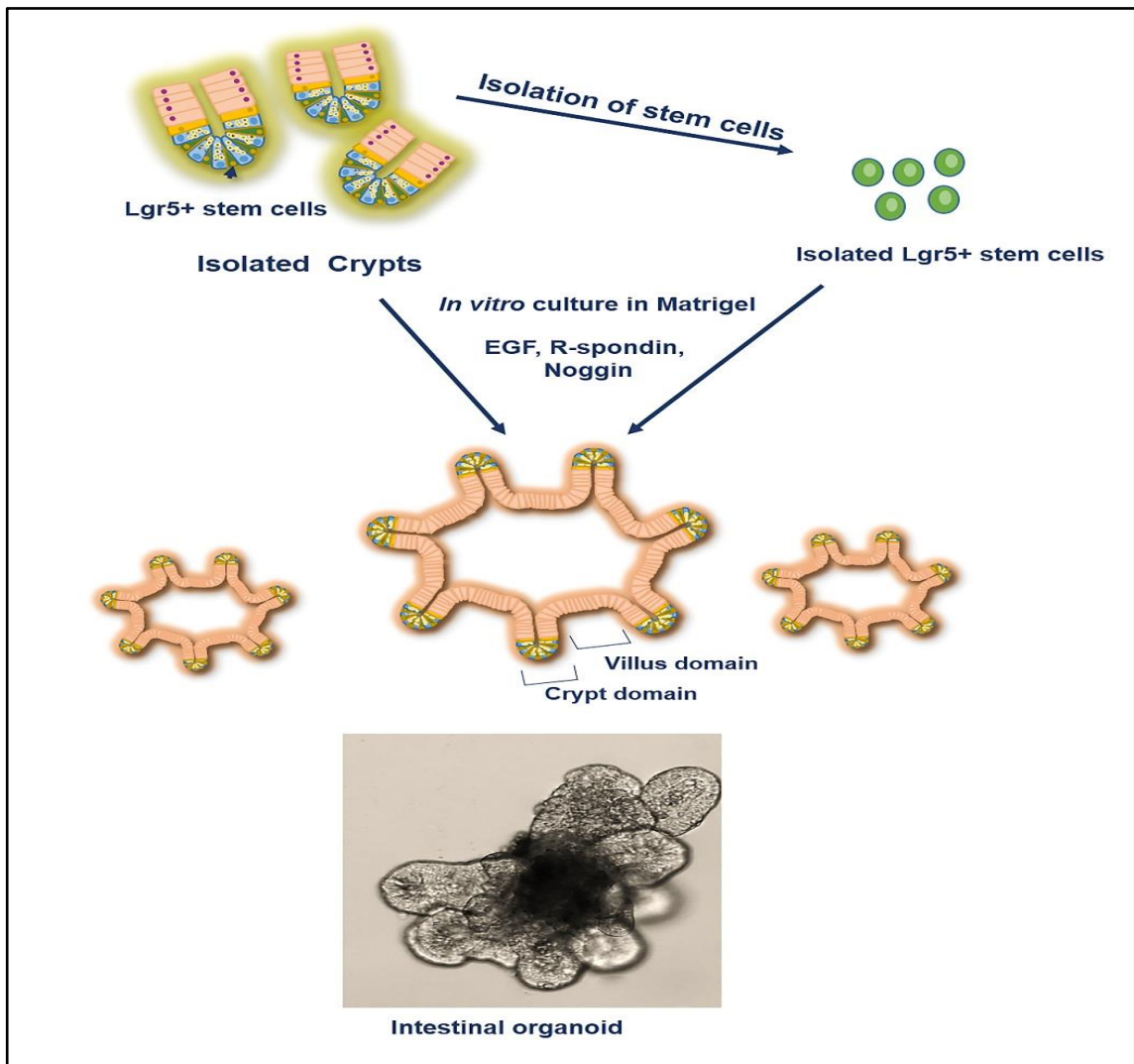


Figure 1.8: Schematic diagram illustrating growth of intestinal organoids from isolated crypts and single Lgr5⁺ stem cells cultured in Matrigel.

In similar studies conducted by Jabaji *et al.*, (2013; 2014) type 1 collagen was compared with Matrigel as an alternative scaffold for growing isolated crypt units. They showed that the intestinal crypts enlarged and formed enteroids *in vitro* when cultured in both scaffolds as monoculture and when cultured with myofibroblasts for 1 week. Khalil *et al.* (2016) developed a long-term culture model of juvenile and adult porcine intestinal crypts to generate budding enteroids. Pastula *et al.* (2016) modified Sato's 3D culture methods using a combination of Matrigel and collagen and co-cultured the epithelial organoid with myofibroblast, and neuronal cells. Where myofibroblasts and neuronal cells supported the growth of epithelial organoids. However, the presence of collagen led to a reduction in the budding of epithelial organoids, potentially due to increased mechanical rigidity.

They concluded that these systems enabled the organoids to align and fuse forming the macroscopic hollow structures. However, in this model although cellular differentiation was observed, villi structures were still missing (Sachs *et al.* 2017). Whilst Wang *et al.* (2017) successfully generated crypt-villus architecture from intestinal stem cells cultured on a fabricated collagen scaffold. Furthermore, application of chemical gradients applied to the scaffold promoted and supported cell migration along the crypt-villus axis. Demonstrating a combined approach of microengineered scaffolds together with biophysical cues and chemical gradients could hold the potential for tissue engineering a small intestinal model *in vitro*. The creation of the 3D organoids provides an ideal culture system to examine how stem cells integrate the multiple signals to maintain stemness, the 3D nature of organoids, however, does not enable the visualisation of the stem cells destiny; which is a great challenge when

investigating the interaction between stem cells and other niche cells (Gjorevski *et al.* 2016).

This work has been progressed by the use of human intestinal stem cells. Scott *et al.* (2016) cultured human small intestinal crypts in 2D monolayers, on a thin layers of bovine type 1 collagen. These human intestinal crypts were expanded in long-term culture, with the ultimate aim being that one day these cultures could be used in clinical cell transplantations. Similarly, Liu *et al.* (2018) successfully established a self-renewing 2D monolayer culture system for investigation of the dynamic of Lgr5⁺ intestinal stem cells. Isolated intestinal crypts from mice were seeded on Matrigel coated glass sheets. Lgr5⁺ intestinal stem cells in monolayer showed stem cell properties, as they efficiently formed 3D organoids in Matrigel.

The use of Matrigel and collagen as cell culture scaffolds suffer the drawbacks of batch to batch variability, high costs, and risk of pathogen contamination. In addition the Matrigel is derived from mouse sarcoma, thus, synthetic scaffolds which are defined physiochemical and mechanical properties were used to overcome these drawbacks (Holmberg *et al.* 2017).

1.3.3.2 *In vivo* implantation of organoid seeded scaffolds

A number of studies have directly seeded the organoid units onto biodegradable scaffolds to test their ability to regenerate the intestine post-implantation in rodents (Choi & Vacanti 1997; Choi *et al.* 1998; Finkbeiner *et al.* 2015) and large animals (Agopian *et al.* 2009). In (1988), Vacanti *et al.*, isolated organoid units from neonatal rat intestine and seeded these onto a tubular scaffold of polyglycolic acid and poly-L-lactic acid prior to implantation into the omentum of the syngeneic adult rat. These organoid units survived, proliferated and had

characteristic villus-crypt structures. Choi & Vacanti (1997), demonstrated that the organoid units isolated from 6-day-old neonatal rat intestines, seeded on PGA and then implanted into adult rats survived, proliferated, and regenerated small intestine-like structures. Similarly, organoid units isolated from 7 week old Yorkshire swine and cultured on tubular biodegradable scaffolds and implanted intraperitoneally in the autologous host, intestinal cells innervated the muscularis mucosa and intestinal sub-epithelial myofibroblasts were identified (Sala *et al.* 2009).

Levin *et al* (2013) seeded multicellular organoid units derived from postnatal human small intestine resections onto a biodegradable PGA / PLA polymer. Following transplantation into NOD/SCID gamma chain-deficient mice, the human tissue formed villus-crypt architecture similar to that of the mature human small intestine, which contained all differentiated epithelial cell types and mesenchymal cells which expressed muscular and neural markers. *In vivo* subcutaneous implantation using PGA scaffolds of one week old collagen based enteroids derived from 3D co-cultures of small intestinal crypts and myofibroblasts resulted in sustainable re-formed intestinal organoids with differentiated lineages after 5 weeks (Jabaji *et al.* 2013). Cromeens *et al.* (2016) produced neomucosa by seeding enteroids derived from LGR5-EGF transgenic mice on Matrigel for 10-14 day and then these enteroids were released from Matrigel and seeded onto PGA scaffolds and implanted into the peritoneal cavity of immunocompromised NOD/SCID mice. After 4 weeks, neomucosa was produced with clear crypt domains and blunted villi. The shortcoming of this study was that villi were blunted and did not extend to the length of native small intestinal villi. The main limitations of these attempts to generate small intestinal tissue are the high number of cells required for engineering functional tissue

and the absence of scaffolds which mimic the native intestine and those capable of generating an intestinal stem cell niche.

1.3.3.3 3D cell culture of pluripotent stem cells

Multipotent stem cells can generate numerous tissues in the body and have high proliferative capacity, making them attractive for use in regenerative medicine (Wang & Sander 2012). Mesenchymal stem cells have been investigated as a promising source of smooth muscle layer for small intestinal tissue engineering. Hori *et al.* (2002) investigated mesenchymal stem cells to study the feasibility of muscle regeneration, the limitations considered the lack of ability to regenerate smooth muscle layer.

Over recent years, several studies have provided evidence that human induced pluripotent stem cells (iPSCs) can be used to generate intestinal tissue (Spence *et al.* 2011; Watson *et al.* 2014; Finkbeiner *et al.* 2015; Mahe *et al.* 2017). A study published in 2011 aimed to direct the differentiation of human pluripotent stem cells to generate fetal intestinal-like immature properties using manipulation of growth factors (Spence *et al.* 2011). Similarly, Yoshida *et al.* (2012) demonstrated that pluripotent stem cells from mice were successfully differentiated into smooth muscle *in vitro*. Watson *et al.* (2014) generated human intestinal organoids from human iPSCs and embedded these in collagen type I scaffolds prior to transplantation into immunocompromised mice for a period of 6 weeks. Following transplantation, iPSCs fully differentiated into all types of small intestinal cells and smooth muscle layers when compared with *in vitro* human intestinal organoids. A study conducted by Finkbeiner *et al.* (2015) also showed that human intestinal organoids derived from iPSCs generated a tissue that resemble the native human intestinal tissue when seeded onto

PGA/PLA scaffolds and implanted into immunocompromised mice for 12 weeks. While these are promising findings, tissue engineered intestines were supplemented with further neuronal cell types to generate physiologically functional tissue-engineered intestine.

1.3.4 Conclusions

Taken together, several effective models for the small intestine exist, whilst they have their advantages they also have a number of limitations. Namely none to date have been able to identify causative factors of inflammatory bowel disease. Furthermore *in vitro* culture models fail to recapitulate the natural villi structure of the small intestine spontaneously. The use of natural biomaterials is hindered by batch to batch variation, contamination and reproducibility, of particular note is the dependence of organoid cultures on Matrigel and collagen gels which hamper their development. Thus, the design of experimental models that can reproducibly generate the intestinal microenvironment which closely mimic the native healthy and diseased small intestine are essential to investigate the pathogenesis of intestinal diseases and further therapeutics development.

1.4 Aims and objectives

Development of a robust intestine model which reflects the pathogenesis of IBD remains a considerable unmet need. Thus, this thesis aimed to develop several models of the small intestine including: genetically engineered murine model, epithelial cell culture models, and an intestinal stem cell organoid model which could be used to study the pathogenesis of IBD and define new therapeutics.

Specific objectives

- 1.** The majority of current animal models of IBD focused on the large intestine where an imbalance between IL-1 and IL-1Ra has been thought to contribute to the pathogenesis of IBD. However, whether this is a causative factor in small intestine is unclear. Thus, this study utilised a murine IL-1Ra knockout mice model to investigate whether features of inflammatory bowel disease would develop spontaneously (Chapter 2).
- 2.** To date, no realistic 3D models which form intestinal villi without prefabrication of structures prior to culture have been achieved. Hence, this study to investigate the potential hydrogel systems which could be utilised to determine their use as scaffolds to support formation of the villi architecture (Chapter 3).
- 3.** The current cell culture studies did not consider the effect of inflammatory conditions in a 3D co-culture model to develop model of the IBD. Thus, the potential of L-pNIPAM hydrogel scaffolds to develop a long-term 3D co-culture model of Caco-2 and HT29-MTX cells under conditions representative of inflammation was investigated to determine its potential use in studying IBD (Chapter 4).

4. Current organoid culture systems are dependent on animal-derived hydrogels with many limitations which make them inappropriate for organoid expansion with clinical applications. Thus, the potential of L-pNIPAM hydrogel scaffold to support proliferation and differentiation of small intestinal crypts and stem cells isolated from mice was investigated (Chapter 5).

Chapter 2

**Interleukin-1 is a key driver of inflammatory bowel disease-
demonstration in a murine IL-1Ra knockout model.**

2.1 Introduction

Inflammatory bowel disease (IBD) is a chronic autoimmune disease characterised by inflammation of the gastrointestinal tract and can be divided into two main types Crohn's disease (CD) which affects any part of the gastrointestinal tract mainly in the terminal ileum and colon; and ulcerative colitis (UC) which affects the rectum and colon (Ludwiczek *et al.* 2004). Although the pathogenesis of IBD is not fully understood, IBD could be caused by an imbalance between pro and anti-inflammatory cytokines in local tissues and lead to inflammation and malfunction of the barrier in the intestinal tissue. Interleukin 1 (IL-1) is a key mediator of innate immunity and inflammation which results in tissue damage in IBD.

An imbalance between IL-1 and IL-1Ra has been shown in the inflamed mucosa of patients with IBD where the levels of IL-1 and IL-1Ra were increased, but importantly the ratio of IL-1Ra to IL-1 was significantly decreased compared with controls (Casini-Raggi *et al.* 1995; Ludwiczek *et al.* 2004). In patients with IBD, IL-1 is generally produced by intestinal macrophages, whilst IL-1Ra is secreted by intestinal epithelial cells (Daig *et al.* 2000). During Crohn's disease, IL-1 β is significantly raised and there is a positive correlation between the severity of mucosal inflammation and the levels of IL-1 β (Al-Sadi *et al.* 2008). IL-1 stimulates recruitment and activation of polymorphonuclear cells (Coccia *et al.* 2012). It can also result in apoptosis of epithelial cells causing tissue damage and barrier dysfunction. Subsequently, the role of IL-1Ra in disease progression has been studied in various experimental animal models of IBD (Cominelli *et al.* 1990; Ferretti *et al.* 1994; McCall *et al.* 1994).

In the SAMP/YiT experimental mice model, which has an increase in Th-1 activity which mediates intestinal inflammation, there was a spontaneous appearance of chronic ileitis which was similar in appearance to Crohn's disease due to increased intestinal paracellular permeability (Olson *et al.* 2006; Kiesler *et al.* 2015). This chronic ileitis is characterised by intestinal inflammation, mononuclear and polymorphonuclear infiltrates of the lamina propria; plus hyperplasia of paneth and goblet cells (Kosiewicz *et al.* 2001).

Although studies have reported that an imbalance between IL-1 and IL-1Ra contributes to inflammation in the large intestine in patients of IBD and in experimental animal models (Hirsch *et al.* 1996; Arend 2002; Ludwiczek *et al.* 2004) whether this is a causative factor is unclear. Here, the histological changes in the small intestine of IL-1Ra knockout mice were investigated to assess the expression of pro-inflammatory cytokines, infiltration of immune cells, matrix-degrading enzymes, junctional proteins, and digestive enzymes in the small intestine of IL-1Ra knockout mice compared to wild-type mice in two age groups in order to determine whether features associated with IBD could be induced spontaneously in the small intestine by the removal of IL-1Ra in mice.

2.2 Materials and methods

2.2.1 *IL-1rn*^{-/-} BALB/c mice

IL-1rn^{tm1Nick} deficient mice (*IL-1rn*^{-/-}) have been described previously (Nicklin *et al.* 2000). All mice were housed behind positive pressure barriers and were reared under UK Home Office licenses. All materials were supplied sterile and certified pathogen free. This work was approved by the University of Sheffield ethical review panel. Formalin-fixed mice were a kind gift from Dr. Martin Nicklin, University of Sheffield.

2.2.2 Tissue preparation and histological assessment

The entire jejunum and ileum portions of small intestine were dissected from BALB/c *IL-1rn*^{-/-} knockout mice aged 50-55 days (n=4) and 155-185 day old (n=4), together with age-matched BALB/c wild-type (WT) controls (n=4 at each age). Following dissection, tissues were rinsed in PBS and fixed in 10% v/v formalin for 24 h and then transferred to 70% v/v ethanol. Tissues were processed and embedded in paraffin wax. Five-micron sections were cut and mounted onto positively charged slides (Leica Microsystem Milton Keynes, UK). Sections were deparaffinised in Sub-X and rehydrated in industrial methylated spirits (IMS) prior to rehydration in distilled water. Sections were then stained with either: Haematoxylin and Eosin; Mayer's Haematoxylin (Leica Microsystem, Milton Keynes, UK) for 2 min rinsed in water for 5 min and immersed in Eosin (Leica Microsystem, Milton Keynes, UK) for 1 min; or Alcian Blue/Periodic acid Schiff's (PAS): 1% w/v Alcian Blue (PH 2.5) (Sigma-Aldrich, Poole, UK) in 3% (v/v) acetic acid (Sigma-Aldrich, Poole, UK) for 30 min and immersed in 0.5% (w/v) Periodic acid for 10 min and rinsed three times in deionised water. Slides were then immersed in Schiff reagent (Merck KGaA, Germany) for 10 min, and then rinsed three times with deionised water. Following staining, sections were

dehydrated in IMS, cleared with Sub-X and mounted in Pertex (Leica Microsystem, Milton Keynes, UK). The slides were examined with an Olympus BX 51 microscope and images captured by the digital camera and Capture Pro OEM V8.0 software (Media Cybernetics, Buckinghamshire, UK).

The tissue morphology was assessed using the Capture Pro OEM V8.0 software measurement tools as follows:

2.2.2.1 Crypt-villus axes height and villus width

Twenty well oriented crypt-villus axes height and villus width at half-axis height in longitudinal tissue sections were measured in the jejunum and ileum of all mice, from each age range and genotype.

2.2.2.2 Goblet cells per crypt-villus axis

The numbers of goblet cells within twenty well oriented crypt-villus axes were counted in the jejunum and ileum of all mice from each age range and genotype.

2.2.3 Immunohistochemical assessment

2.2.3.1 Pro-inflammatory cytokine expression and immune cell infiltration

The expression of pro-inflammatory cytokines IL-1 α , IL-1 β , and their receptor: IL-1RI; IL-15, and TNF α were investigated by immunohistochemistry. In addition, the number of immune cells which infiltrated into lamina propria of crypt-villus axis was determined using immunohistochemistry of polymorphonuclear cell marker: CD11b and macrophage marker CD68, in the jejunum and ileum of three randomly selected mice, from each age range and genotype.

2.2.3.2 Matrix-degrading enzyme expression

The expression of matrix-degrading enzymes: MMP2, MMP9, and ADAMTS1 were assessed in the jejunum and ileum of three randomly selected mice, from each age range and genotype using immunohistochemistry.

2.2.3.3 Polarity of enterocytes and digestive enzyme expression

The expression of tight junction proteins Zonulin 1 (ZO-1) and adherent junction protein E-cadherin, were assessed alongside digestive enzymes: alkaline phosphatase (ALP), sucrase-isomaltase (SI), and dipeptidyl peptidase IV (DPP IV) in the jejunum and ileum of three randomly selected mice, from each age range and genotype.

Immunohistochemistry was performed as described previously (Le Maitre *et al.* 2005). Briefly, 5 µm sections were de-waxed, rehydrated, and endogenous peroxidase blocked using hydrogen peroxide (Sigma-Aldrich, Poole UK). After washing in Tris-buffered saline (TBS) (20mM Tris, 150mM sodium chloride, pH 7.5), tissue sections were subjected to antigen retrieval sections were subjected to an appropriate antigen retrieval method, specific to the antibodies investigated (Table 2.1). Following this sections were washed in TBS. Following TBS washing, nonspecific binding sites were blocked at room temperature for 90 min with 25% (w/v) serum (Abcam, Cambridge, UK) in 1% (w/v) bovine serum albumin in TBS. Sections were incubated overnight at 4°C with appropriate primary antibody (Table 2.1).

Antibody	Clonality	Dilution	Antigen retrieval	Supplier	Catalogue No.
IL-1 α	Rabbit polyclonal	1:100	Heat	Abcam	ab7632
IL-1 β	Rabbit polyclonal	1:100	Heat	Abcam	ab9722
IL-1R1	Rabbit polyclonal	1:100	Enzyme	Abcam	ab106278
IL-15	Rabbit polyclonal	1:50	Enzyme	Abcam	ab7213
TNF α	Rabbit polyclonal	1:50	Enzyme	Abcam	ab6671
CD11b	Goat polyclonal	1:600	None	Abcam	ab62817
CD68	Mouse monoclonal	1:200	Enzyme	Abcam	ab955
MMP2	Rabbit polyclonal	1:800	Enzyme	Abcam	ab37150
MMP9	Rabbit polyclonal	1:25	Heat	Abcam	ab38898
ADAMTS1	Rabbit polyclonal	1:200	Enzyme	Abcam	ab39194
ZO-1	Rabbit polyclonal	1:50	Enzyme	Abcam	ab217334
E-cadherin	Mouse monoclonal	1:200	Heat	Abcam	ab76055
ALP	Rabbit monoclonal	1:200	Heat	Abcam	ab108337
SI	Mouse monoclonal	1:50	Heat	Santa Cruz	sc-393470
DPP I	Mouse monoclonal	1:50	Enzyme	Abcam	ab119346

Table 2.1: Target antibodies used in Immunohistochemistry.

For each immunohistochemistry method, a negative control was performed, replacing the primary antibody with either rabbit or mouse IgG (Abcam, Cambridge, UK) as appropriate, at a concentration equal to that of the primary antibody. Sections were washed in TBS and then incubated in 1:500 dilution of an appropriate biotinylated secondary antibody for 30 min at room temperature. Binding of the secondary antibody was visualised after exposure to horseradish peroxidase (HRP) streptavidin-biotin complex (Vector Laboratories, Peterborough, UK) for 30 min. Sections were washed in TBS, and treated with 0.08% (v/v) hydrogen peroxide in 0.65mg/ml 3, 3'-diaminobenzidine tetrahydrochloride (Sigma-Aldrich, Poole, UK) in TBS for 20 min. Sections were counterstained with Mayer's haematoxylin, dehydrated, cleared and mounted in Pertex. Immunohistochemical staining were examined with an Olympus BX51 microscope and images captured by digital camera and Capture Pro OEM v8.0 software (Media Cybernetics, Buckinghamshire, UK). Immunopositive intensity across the small intestine architecture was independently quantified by two assessors (CLM and NJM), blinded to animal genotype and age. A scale of 0 to 6 was utilised where 0 was no immunopositivity and 6 signifies maximum immunopositivity. The number of immunopositive (CD11b and CD68) immune cells were counted within twenty well oriented crypt-villus axes of each of three randomly selected mice, from each age range and genotype.

2.2.4 Statistical analysis

Data was plotted using GraphPad Prism V6.0. Crypt-villus axes height and villus width were assessed for normality using Stats Direct program and found to be non-parametric and therefore statistical comparisons were performed by Kruskal-Wallis with a pairwise comparison (Conover-Inman) between ages and genotypes. Statistical significance was set at $P \leq 0.05$, for statistical analysis the

mean villi height, width and goblet cells per villi per mouse were utilised for statistical analysis. All replicates are shown with the median values for each mouse to demonstrate clearly the spread of replicates.

2.2.5 Ethical consideration

To ensure that experimental procedures aligned with the 3Rs principle, initial work was completed on n=4 and statistical analysis performed, as statistically significant differences were seen in n=4 it was not deemed ethically appropriate nor necessary to increase the number of animals utilised.

2.3 Results

2.3.1 Histological analysis

2.3.1.1 Crypt-villus axis height and villus width

In the jejunum, there was a significant decrease in height of crypt-villus axis of the 155-185 day old *IL-1rn^{-/-}* mice compared with age-matched WT mice ($P \leq 0.05$) (Figure 2.1). However, the crypt-villus height of the jejunum was significantly greater in the 155-185 day compared to the 55-day in WT groups ($P \leq 0.05$). The width of the villus at half crypt-villus axis was unchanged in all groups (Figure 2.1). Morphology of jejunal villi of 155-185 day old *IL-1rn^{-/-}* mice revealed moderate epithelial damage with separation of the columnar epithelia from the lamina propria within the villi and the formation of large spaces between the crypt base and the muscularis mucosa in the 55-day old *IL-1rn^{-/-}* mice (Figure 2.1).

In the ileum, there was a significant decrease in the crypt-villus axis height of both the 55-day old and 155-185 day old *IL-1rn^{-/-}* mice compared with WT mice ($P \leq 0.05$) and a significant decrease in 155-185 day old *IL-1rn^{-/-}* mice compared with 55-day *IL-1rn^{-/-}* mice ($P \leq 0.05$). In contrast, the crypt-villus axis height was significantly increased in 155-185 day old *IL-1rn^{+/+}* mice compared with 55-day *IL-1rn^{+/+}* mice. A significant decrease was seen in villus width in 155-185 day old *IL-1rn^{-/-}* mice compared with 155-185 day old WT mice and 55-day *IL-1rn^{-/-}* mice ($P \leq 0.05$). While villus width in the ileum was significantly increased in 155-185 day WT mice compared with 55-day old WT mice ($P \leq 0.05$) (Figure 2.2). Once again there was a separation of the columnar epithelium from the lamina propria within the villi and the formation of large spaces between the crypt base and the muscularis mucosa in the 155-185 day old *IL-1rn^{-/-}* mice (Figure 2.2).

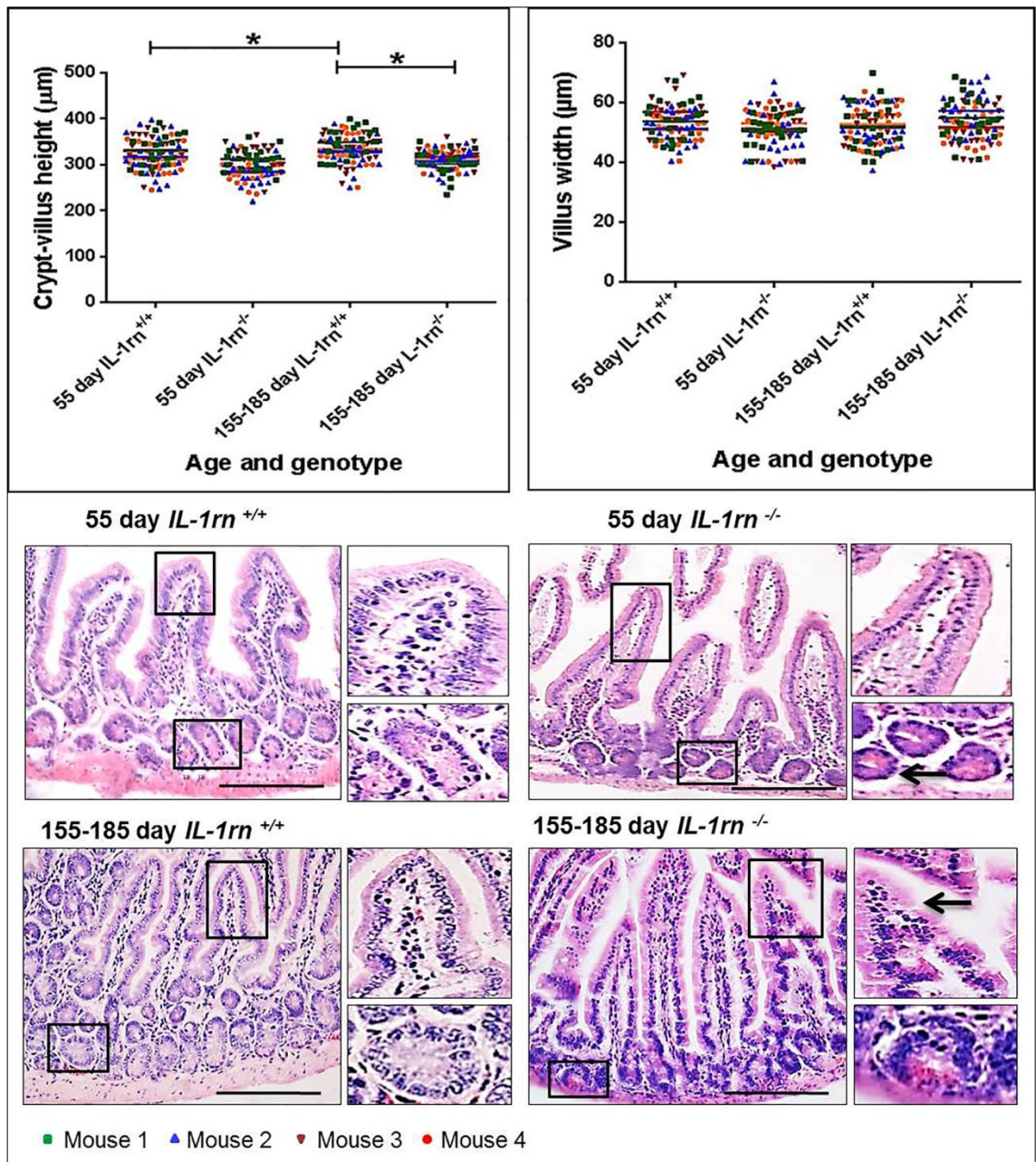


Figure 2.1: Histological analysis and morphology of the intact well-oriented crypt-villus axis heights and villus widths of Jejunum in the 55 day old *IL-1rn*^{-/-} mice and 155-185 day old *IL-1rn*^{-/-} mice compared to age-matched wild-type mice. Stained with H&E. Black arrows indicate moderate epithelial damage in 155-185 day old *IL-1rn*^{-/-} mice, enlarged space between the crypt base and the muscularis mucosa. * $P \leq 0.05$. Scale bar = 100 μm .

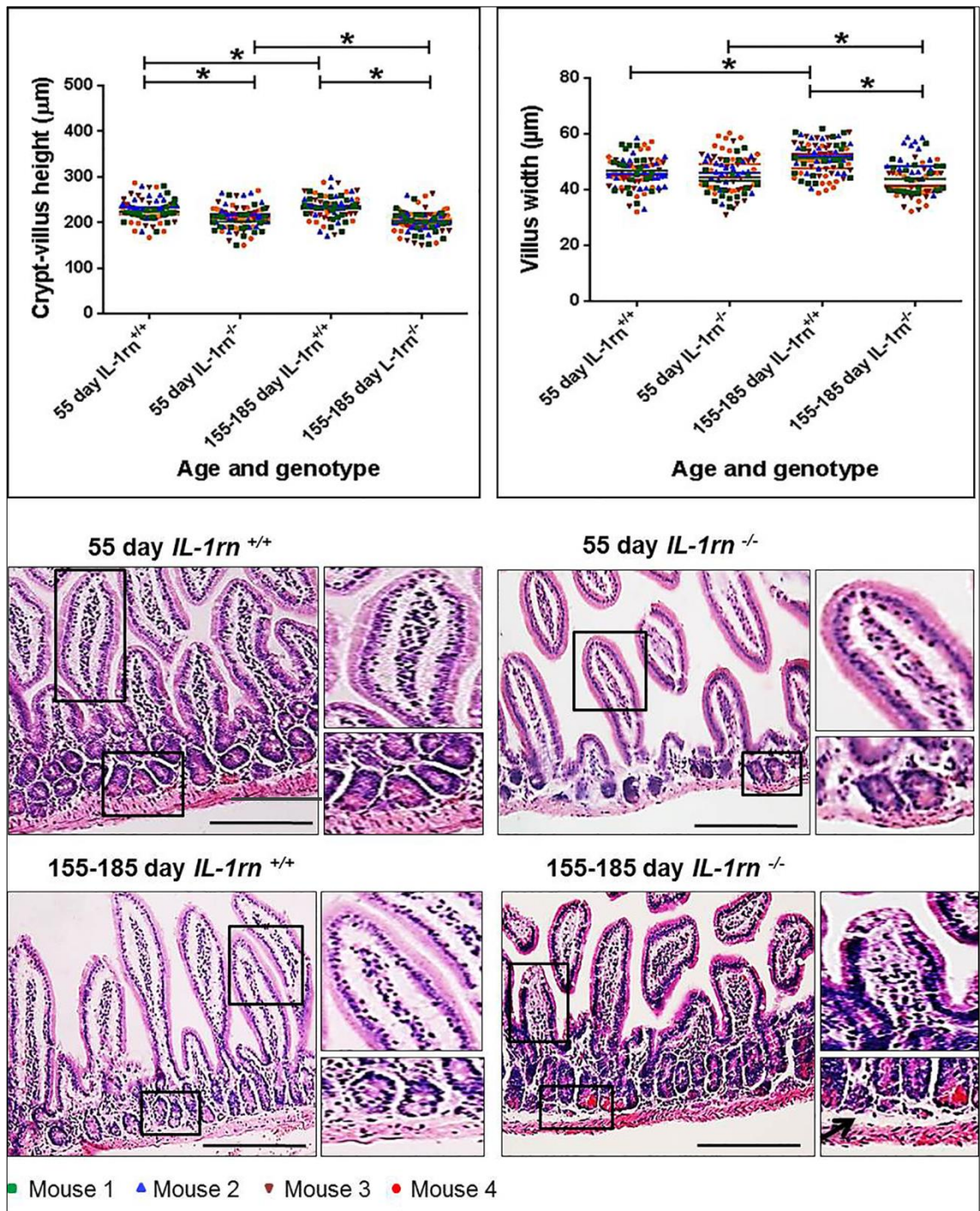


Figure 2.2: Histological analysis and morphology of the intact well-oriented crypt-villus axis heights and villus widths of ileum in the 55 day old *IL-1rn*^{-/-} mice and 155-185 day old *IL-1rn*^{-/-} mice compared to age-matched wild-type mice. Stained with H&E. Black arrows indicate enlarged space between the crypt base and the muscularis mucosa. **P* ≤ 0.05. Scale bar = 100 µm.

2.3.1.2 Number of goblet cells per crypt-villus axis

In the jejunum and ileum, there was a significant increase in the number of goblet cells per crypt-villus axis in all *IL-1rn^{-/-}* mice groups compared with WT mice ($P \leq 0.05$). Furthermore, in jejunum, there was a significant increase in the number of goblet cells per crypt-villus axis in 155-185 day old *IL-1rn^{+/+}* compared to 55 day old *IL-1rn^{+/+}* mice ($P \leq 0.05$) (Figure 2.3 A & B). Moderate and intense PAS (pink) staining was observed in 55 day old *IL-1rn^{+/+}* and *IL-1rn^{-/-}* mice and intense alcian blue staining was observed in 155-185 day old *IL-1rn^{+/+}* and *IL-1rn^{-/-}* mice (Figure 2.3 A & B). This indicated the presence of neutral mucins in younger mice, and acidic mucins in older mice in both the jejunum and the ileum.

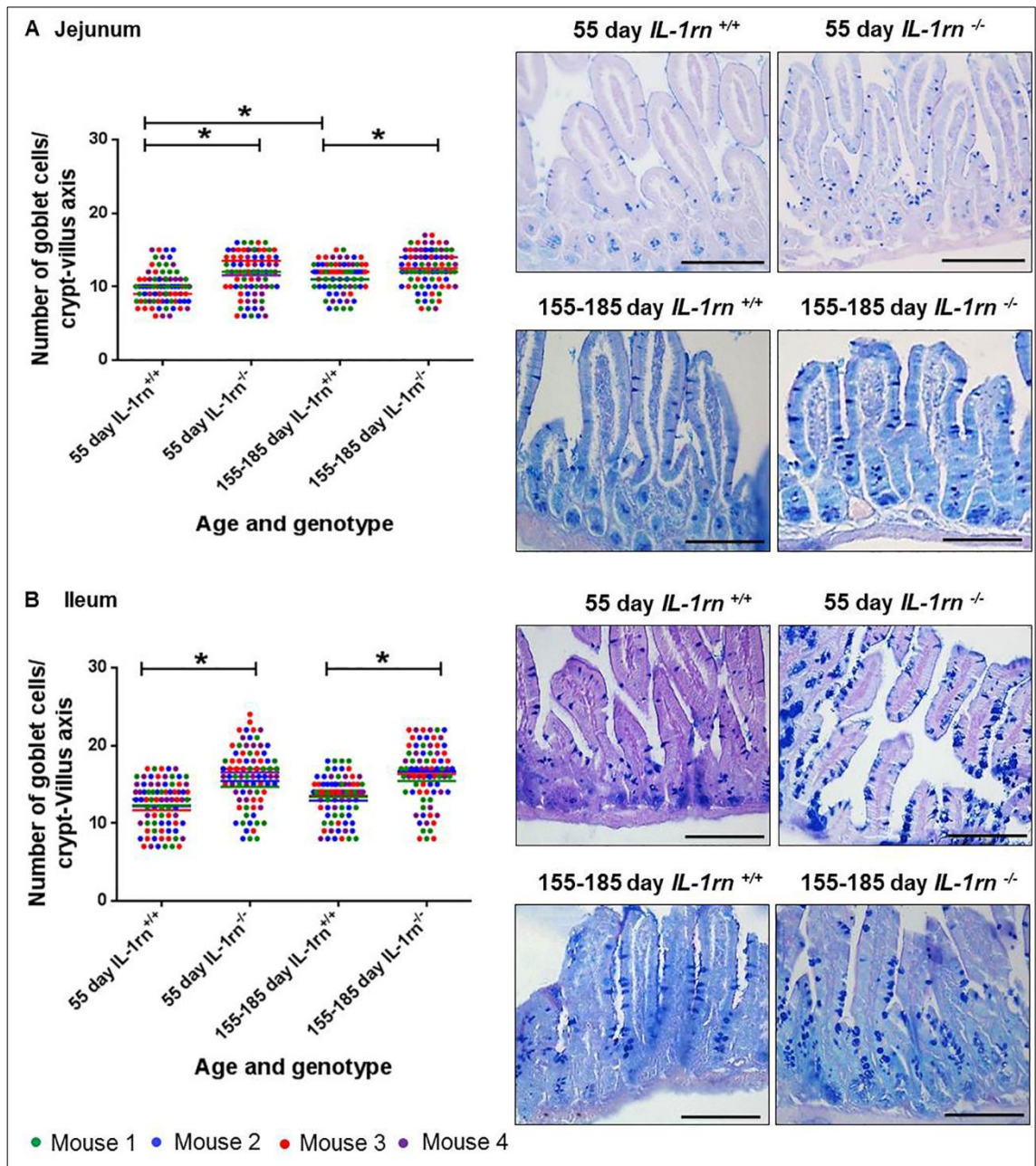


Figure 2.3: Histological analysis and morphology of goblet cells per intact well-oriented crypt-villus axis of the A: Jejunum and B: Ileum of 55 day old and 155-185 days old *IL-1rn*^{-/-} mice compared with age-matched WT mic, stained with AB-PAS. *P ≤ 0.05. Scale bar = 100 μm.

2.3.2 Immunohistochemistry staining

2.3.2.1 Assessment of pro-inflammatory cytokine expression and localization

Across the small intestine (jejunum and ileum), the expression of pro-inflammatory cytokine IL-1 α was highly expressed in both the villi and crypts. There was a significant increase in IL-1 α in 155-185 day old *IL-1rn^{-/-}* mice, compared with WT mice and 55 day *IL-1rn^{-/-}* mice ($P\leq 0.05$) (Figure 2.4 A and Figure 2.5 A & B). Whilst high levels of IL-1 α were seen in all mice, only low levels of immunopositivity was seen in WT mice with a significant increase in IL-1 β in the 55 day old and 155-185 day old *IL-1rn^{-/-}* mice, compared with WT mice ($P\leq 0.05$) (Figure 2.4 B, and Figure 2.5 C & D). The expression of IL-1R1 was primarily located in villi; however, there was a significant decrease in IL-1R1 expression in both the 55 day old and 155-185 day old *IL-1rn^{-/-}* mice compared with WT mice ($P\leq 0.05$). IL-1R1 expression in 155-185 day old *IL-1rn^{+/+}* and 155-185 day old *IL-1rn^{-/-}* mice were significantly lower than those seen in the 55 day old *IL-1rn^{+/+}* and 55 day old *IL-1rn^{-/-}* mice, respectively ($P\leq 0.05$) (Figure 2.4 C and Figure 2.5 E & F).

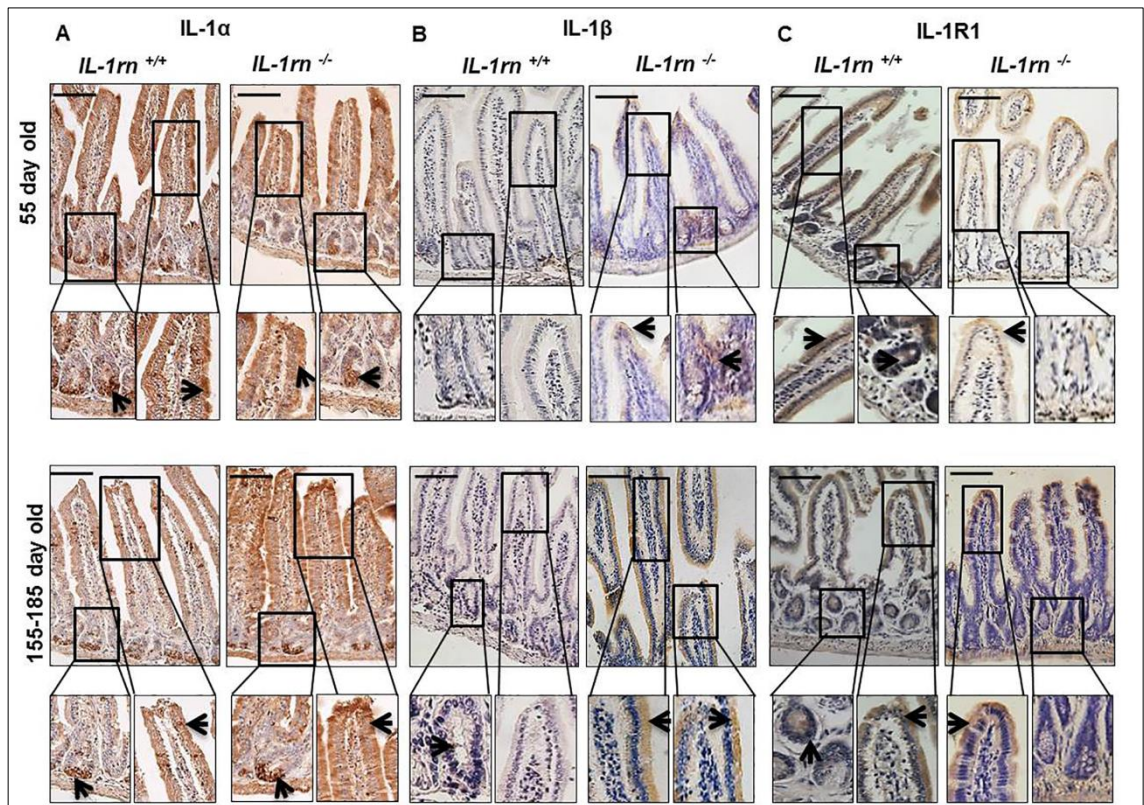


Figure 2.4: Immunohistochemistry staining of the expression and localization of pro-inflammatory cytokine A: IL-1 α ; B: IL-1 β ; C: IL-1R1 in the jejunum of the 55-day old and 155-185 days old *IL-1rn^{-/-}* mice compared with WT mice. Cell nuclei were stained with haematoxylin (blue). Black arrows indicate immunopositivity. Scale bar = 100 μ m.

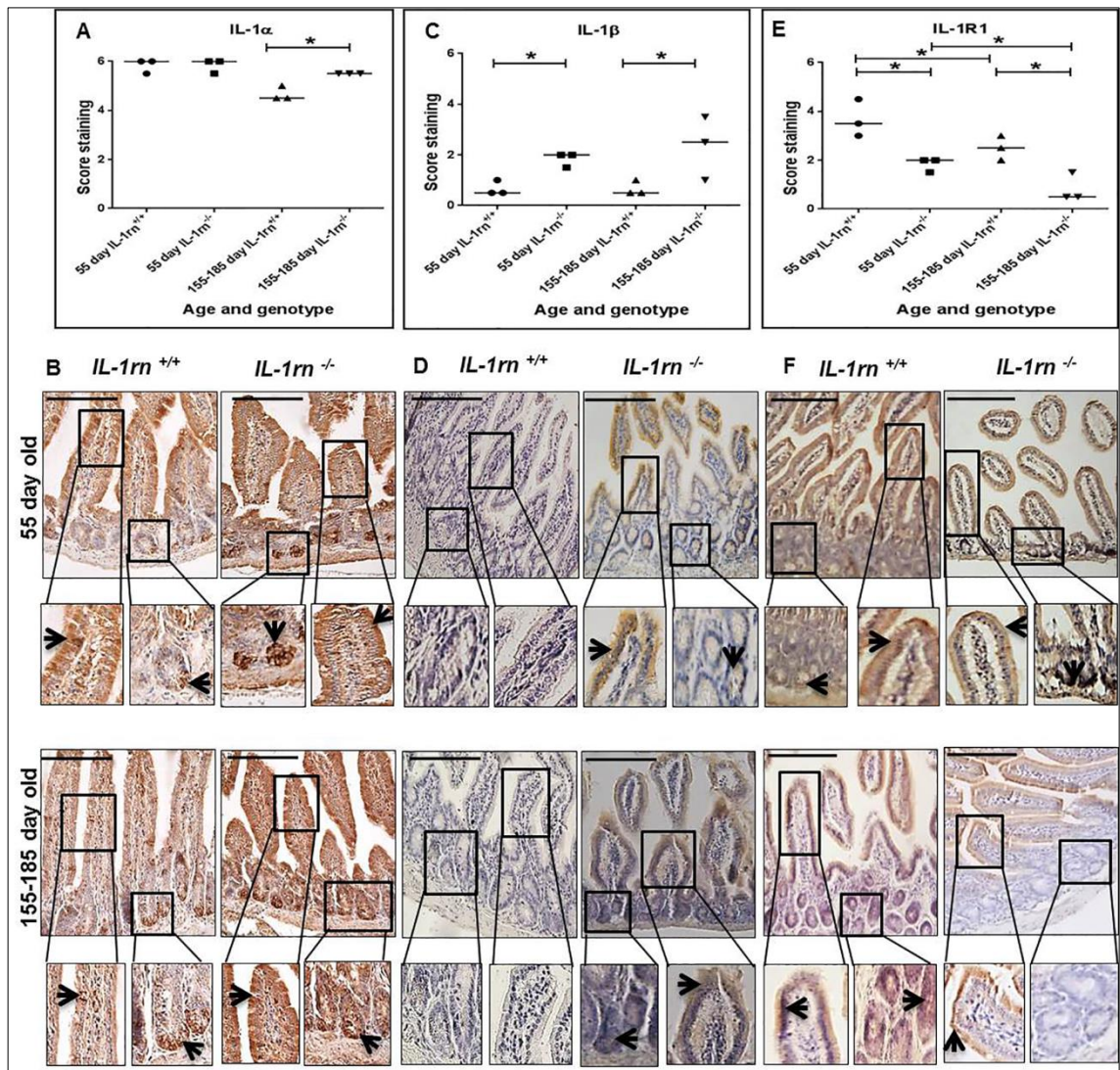


Figure 2.5: Immunohistochemistry staining of the expression and localization of pro-inflammatory cytokines: IL-1 α (A); IL-1 β (C); IL-1RI (E) showing the immunopositive intensity quantification across the small intestinal architecture. B, D, and F showing the immunopositive staining in the ileum of the 55 day old and 155-185 day old *IL-1m^{-/-}* mice compared with WT mice. Cell nuclei were stained with haematoxylin (blue). Black arrows indicate immunopositivity. * $P \leq 0.05$. Scale bar = 100 μm .

IL-15 expression was observed only at low levels in the 55 day old *IL-1m^{-/-}* mice, and localized in both the villi and crypts, but significantly increased in the 155-185 day old *IL-1m^{-/-}* mice, compared with WT mice ($P \leq 0.05$) (Figure 2.6 A and Figure 2.7 A & B). TNF α expression was also observed at low levels in the 55 day old *IL-1m^{-/-}* mice. TNF α was localized in the villi of the jejunum and in the submucosa of the ileum, and was expressed at greater levels than in the WT mice. Whereas TNF α expression was significantly increased in the 155-185

day old *IL-1rn^{-/-}* mice, where immunopositive cells were localized within the villi, crypts, and the submucosa of the jejunum and ileum, and was significantly greater than that seen in the WT mice ($P \leq 0.05$) (Figure 2.6 B and Figure 2.7 C & D).

The number of infiltrated polymorphonuclear (PMN) cells in the lamina propria were significantly increased in the 55 day old and 155-185 day old *IL-1rn^{-/-}* mice compared with WT mice ($P \leq 0.05$) (Figure 2.8 A and Figure 2.9 A & B). Crypt abscesses were observed in the ileum of 155-185 day old *IL-1rn^{-/-}* mice. Here, PMN cells were seen to clump together within the lamina propria of the villi of 55 day old *IL-1rn^{-/-}* mice and in the crypts of the 155-185 day old *IL-1rn^{-/-}* mice (Figure 2.8 A and Figure 2.9 A & B). The number of macrophages was significantly increased in 55 day old and 155-185 day old *IL-1rn^{-/-}* mice compared with WT mice ($P \leq 0.05$). Similar distributions were seen throughout the lamina propria of the villi in the young and old *IL-1rn^{-/-}* mice in the jejunum and ileum (Figure 2.8 B and Figure 2.9 C & D).

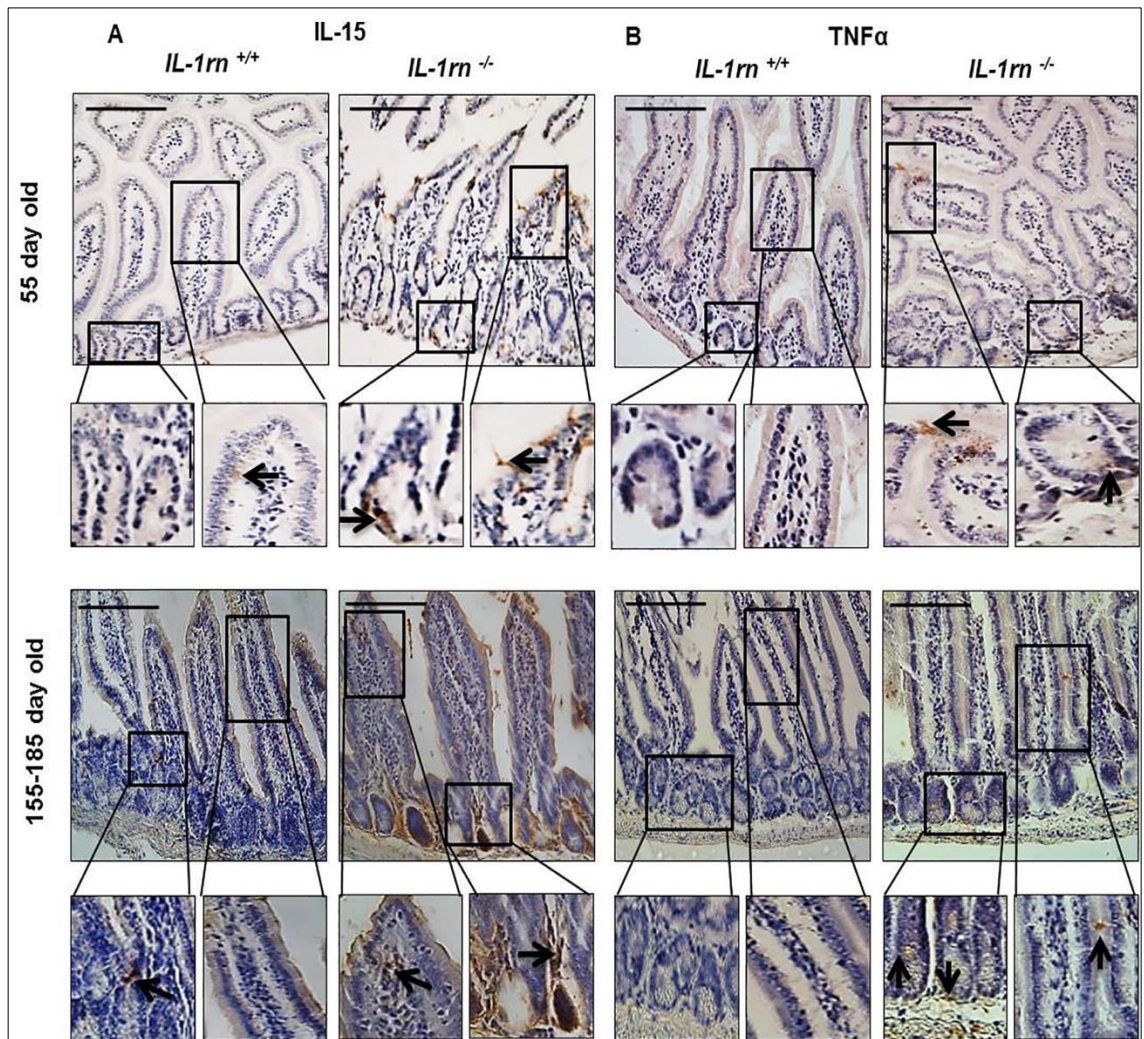


Figure 2.6: Immunohistochemistry staining of the expression and localization of pro-inflammatory cytokines IL-15 (A); TNFα (B) in the jejunum of the 55-day old and 155-185 day old $IL-1m^{-/-}$ mice compared with WT mice. Cell nuclei were stained with haematoxylin (blue). Black arrows indicate immunopositivity. Scale bar = 100 μ m.

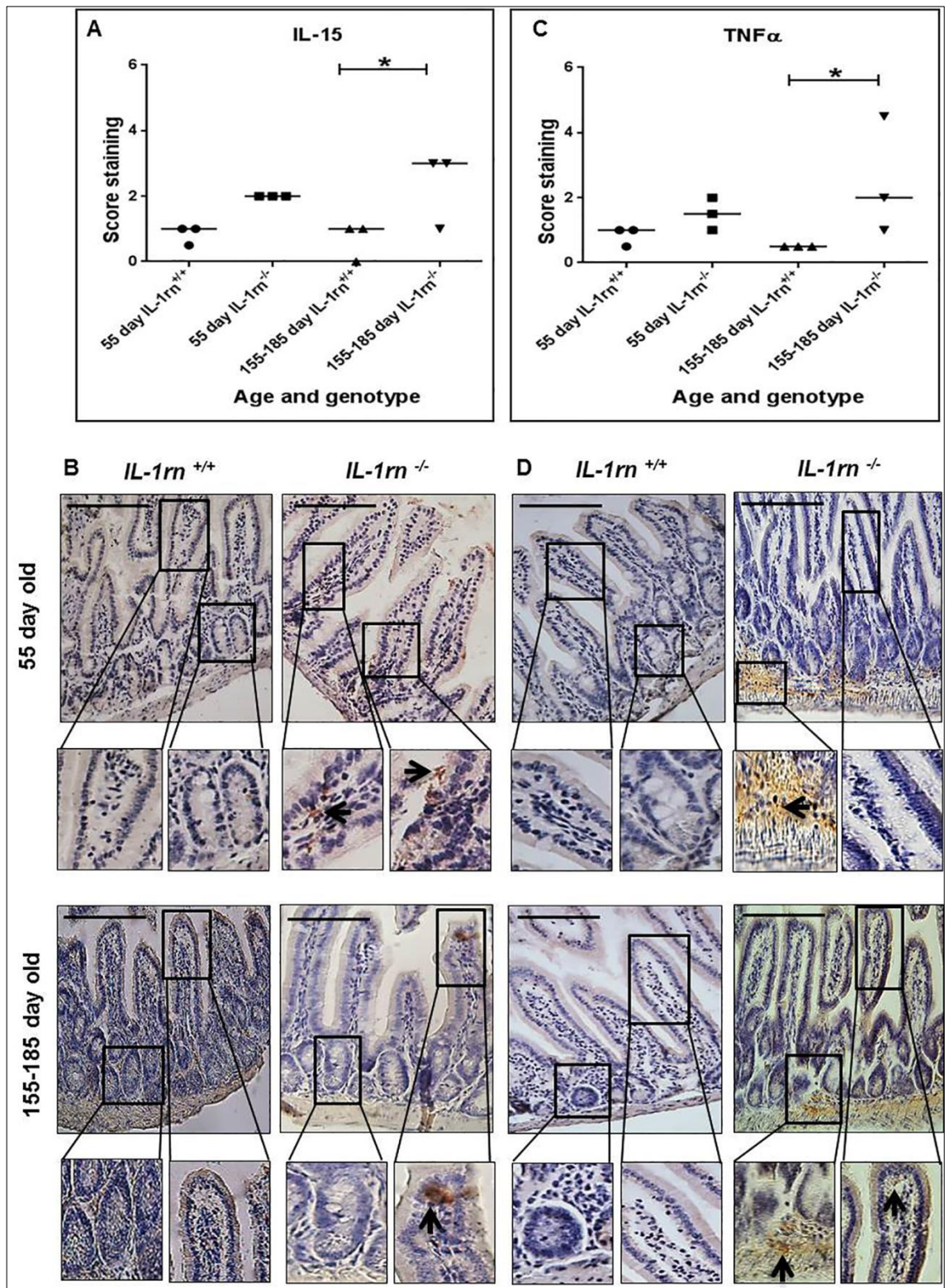


Figure 2.7: Immunohistochemistry staining of the expression and localization of pro-inflammatory cytokines: IL-15 (A); TNF α (C) showing the immunopositive intensity quantification across the small intestinal architecture. B and D showing immunopositive staining in the ileum of the 55 day old and 155-185 day old IL-1m^{-/-} mice compared with WT mice. Cell nuclei were stained with haematoxylin (blue). Black arrows indicate immunopositivity. *P \leq 0.05. Scale bar = 100 μ m.

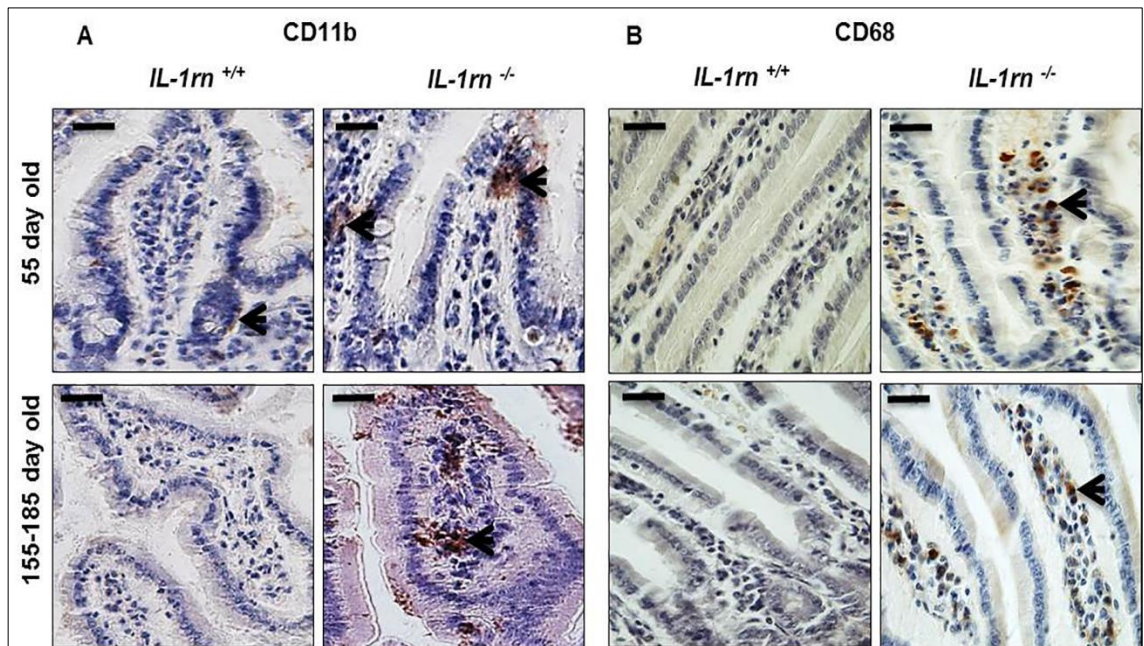


Figure 2.8: Immunohistochemistry staining of the infiltrated cells: Polymorphonuclear cells (PMNs) (A) and Macrophage cells (B) into the lamina propria of the intact well oriented crypt-villus axis in the jejunum of the 55-day old and 155-185 day old *IL-1rn*^{-/-} mice compared with WT mice. Cell nuclei were stained with haematoxylin (blue). Black arrows indicate immunopositivity. Scale bar = 25 µm.

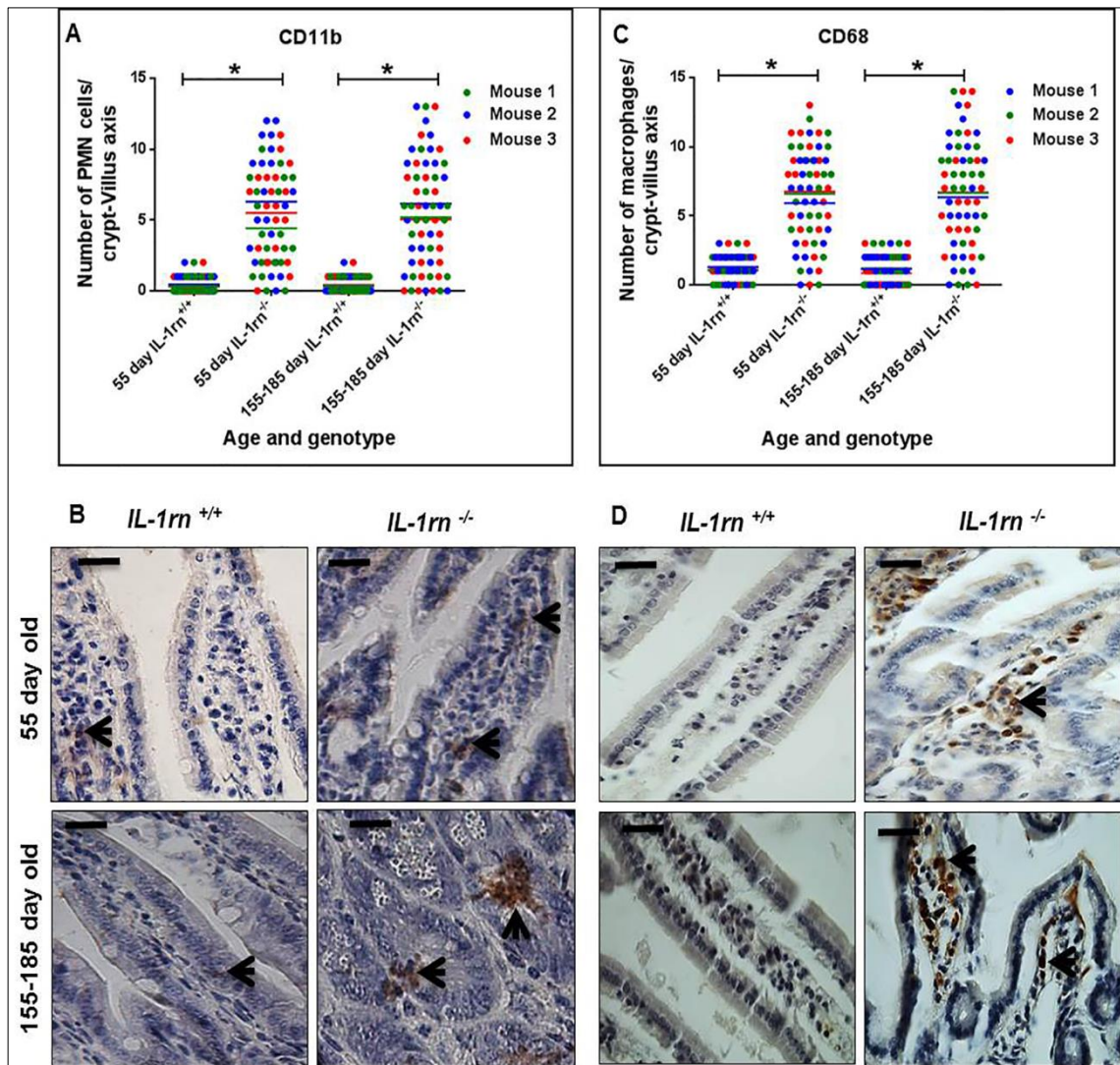


Figure 2.9: Immunohistochemistry staining of the infiltrated cells: Polymorphonuclear cells (PMNs) (A) and Macrophage cells (B) into the lamina propria of the intact well oriented crypt-villus axis in the ileum of the 55 day old and 155-185 day old *IL-1rn*^{-/-} mice compared with WT mice. Cell nuclei were stained with haematoxylin (blue). Black arrows indicate immunopositivity. *P ≤ 0.05. Scale bar = 25 μm.

2.3.2.2 Assessment of degrading enzyme expression and localization

Although MMP2 expression was higher in both the 55 day old and 155-185 day old *IL-1rn^{-/-}* mice than WT mice, this failed to reach significance. In 55 day old and 155-185 day old *IL-1rn^{-/-}* mice, MMP2 was highly expressed in the villi, crypts and muscularis mucosa (Figure 2.10 A and Figure 2.11 A and B).

MMP9 expression was limited in all groups, its expression was higher in the submucosa of the ileum than the jejunum in the 55 day old *IL-1rn^{+/+}*, *IL-1rn^{-/-}* mice and in 155-185 day old *IL-1rn^{+/+}* mice (Figure 2.10 B, Figure 2.11 C and D). Although ADAMTS1 was highly expressed in the jejunum and ileum of the *IL-1rn^{-/-}* mice, there were no significant differences between age and genotype groups (Figure 2.10 C, Figure 2.11 E and F).

2.3.2.3 Assessment of enterocyte polarity and digestive enzyme expression and localization.

ZO-1 and E-cadherin were expressed from the surface of the villi down to crypts in WT mice. The level of expression of both ZO-1 and E-cadherin was significantly decreased in both the 55 day old and 155-185 day old of *IL-1rn^{-/-}* mice compared to age-matched WT controls ($P \leq 0.05$) (Figure 2.12 A & B and Figure 2.13 A, B, C, D). In the jejunum, ZO-1 expression was localized on villi surfaces only in the 155-185 day old of *IL-1rn^{-/-}* mice, which was significantly less than that seen in younger 55 day old of *IL-1rn^{-/-}* and WT mice (Figure 2.12 A). In contrast, ZO-1 was uniformly expressed at the cell surface of the villi in the ileum and was comparable to that seen in WT mice (Figure 2.12 A and B). E-cadherin immunopositivity was lost in the jejunum and ileum of 155-185 day old of *IL-1rn^{-/-}* mice compared to WT mice (Figure 2.12 B and Figure 2.13 C & D).

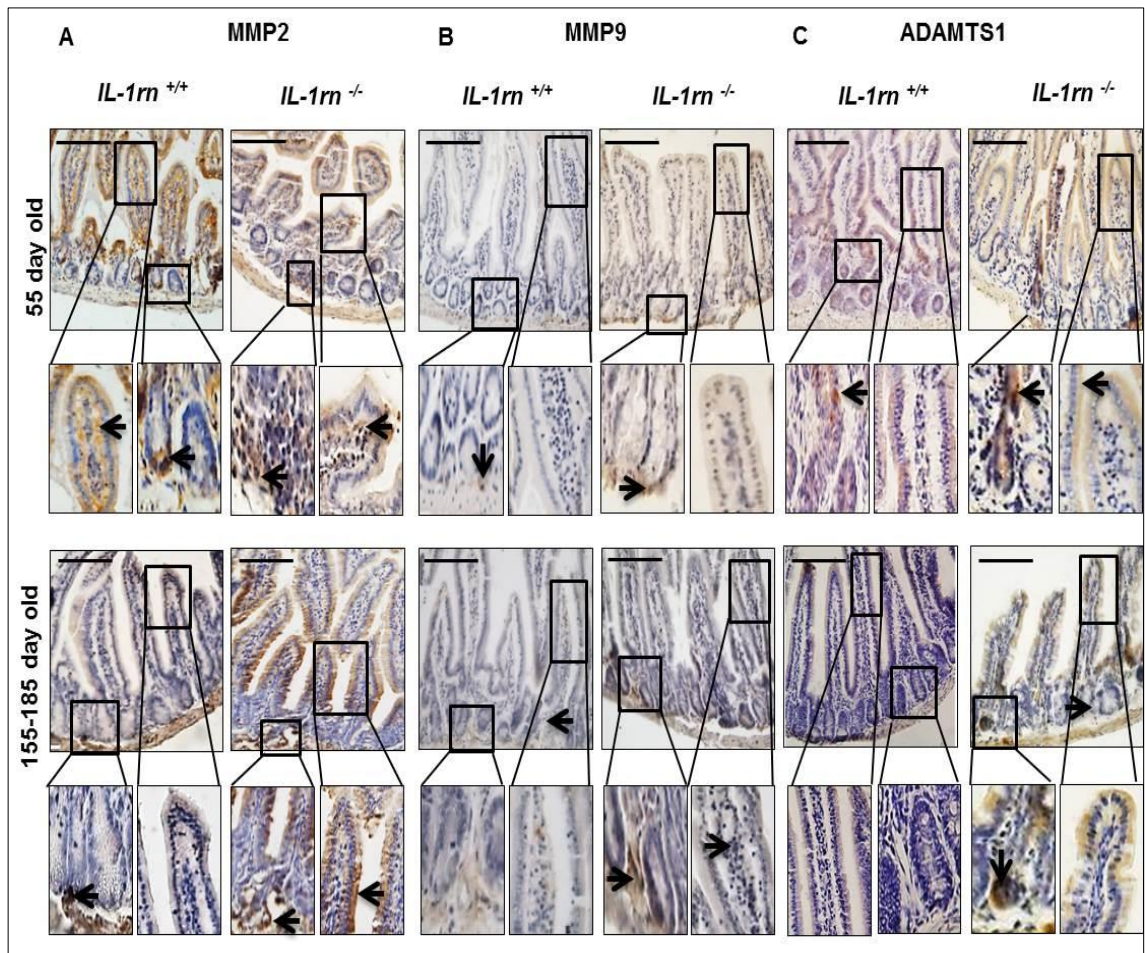


Figure 2.10: Immunohistochemistry staining of the expression and localization of degrading enzymes: MMP2 (A); MMP9 (B); ADAMTS1 (C) in the jejunum of the 55-day old and 155-185 day old *IL-1m^{-/-}* mice compared with WT mice. Cell nuclei were stained with haematoxylin (blue). Black arrows indicate immunopositivity. Scale bar = 100 μ m.

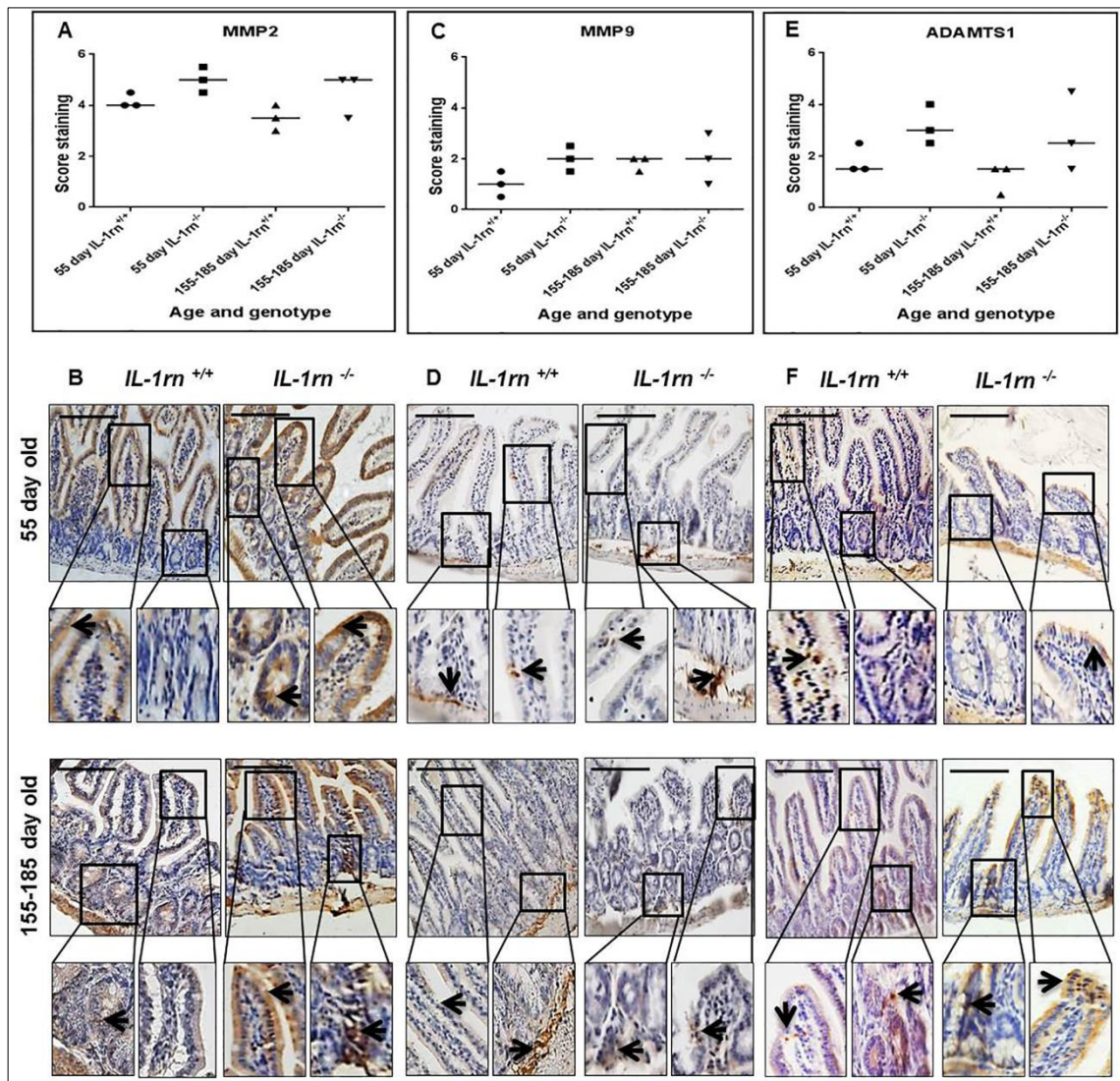


Figure 2.11: Immunohistochemistry staining of the expression and localization of degrading enzymes: MMP2 (A); MMP9 (C); ADAMTS1 (E) showing the immunopositive intensity quantification across the small intestinal architecture. B, D, and F showing the immunopositive staining in the ileum of the 55-day old and 155-185 day old *IL-1rn^{-/-}* mice compared with WT mice. Cell nuclei were stained with haematoxylin (blue). Black arrows indicate immunopositivity. Scale bar = 100 μ m.

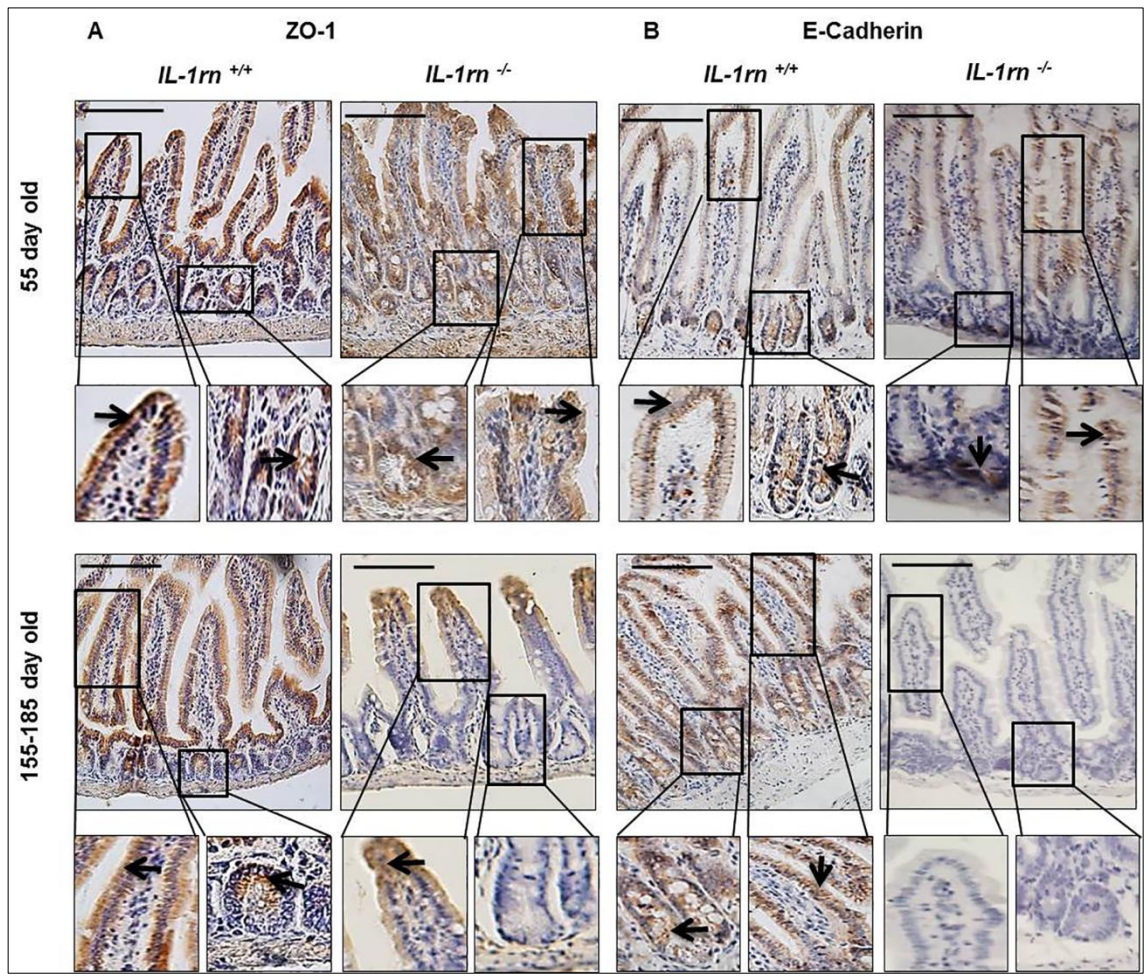


Figure 2.12: Immunohistochemistry staining of the expression and localization of junctional proteins: ZO-1 (A); E-cadherin (B) in the jejunum of the 55-day old and 155-185 day old *IL-1rn*^{-/-} mice compared with WT mice. Cell nuclei were stained with haematoxylin (blue). Black arrows indicate immunopositivity. Scale bar = 100 μ m.

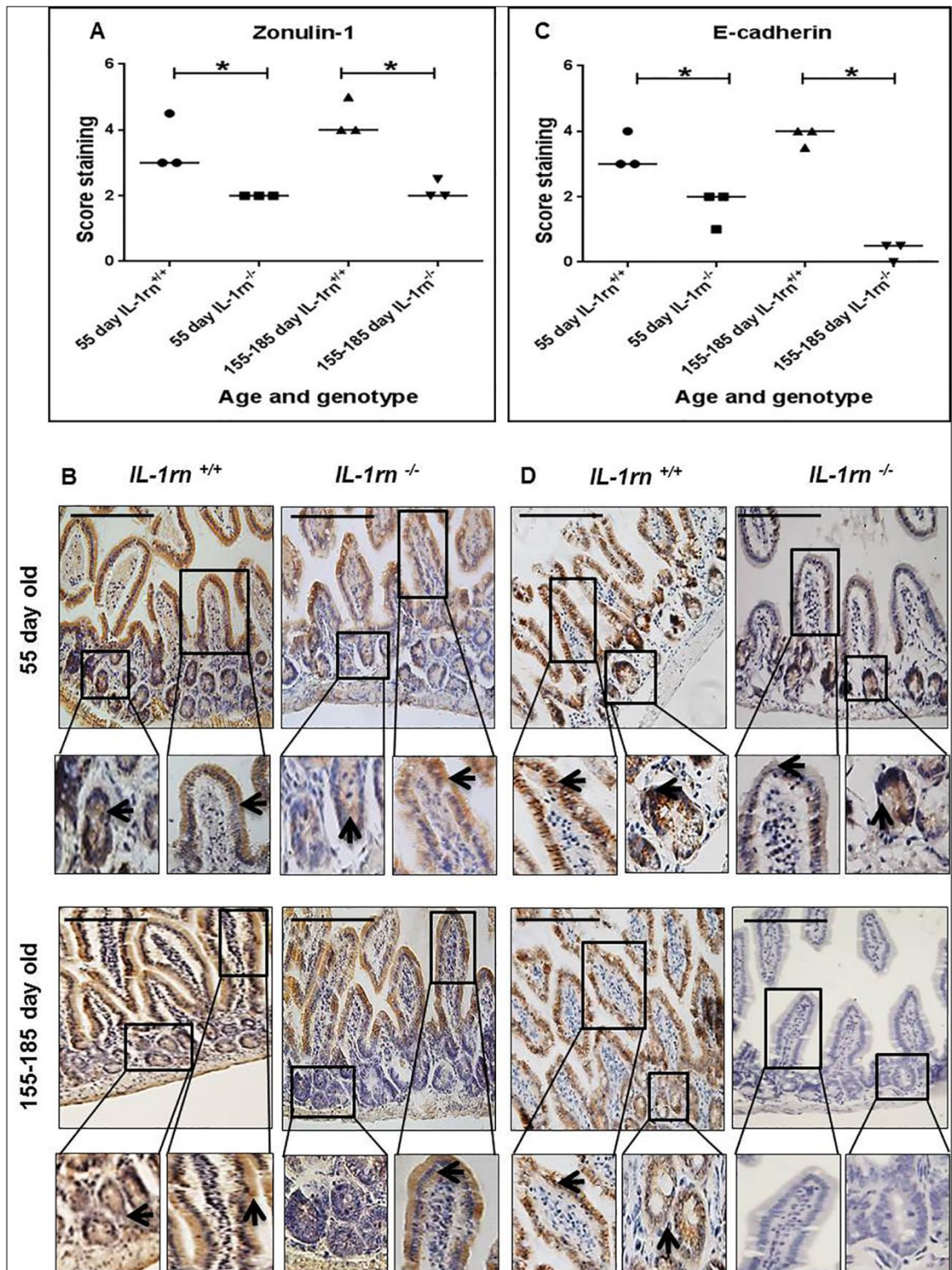


Figure 2.13: Immunohistochemistry staining of the expression and localization of junctional proteins: ZO-1 (A); E-cadherin (C) showing the immunopositive intensity quantification across the small intestinal architecture. B and D showing the immunopositive staining in the ileum of the 55 day old and 155-185 day old *IL-1rn*^{-/-} mice compared with WT mice. Cell nuclei were stained with haematoxylin (blue). Black arrow indicate immunopositivity. * $P \leq 0.05$. Scale bar = 100 μm .

ALP expression was weak in all mice; however, specific ALP immunopositivity was seen on the brush border of the enterocytes and in the lamina propria cells (Figure 2.14 A and Figure 2.15 A & B). Sucrase-isomaltase expression was localized to the apical epithelial surface and was highly expressed in all mice (Figure 2.14 B and Figure 2.15 C & D). DPP IV expression was increased in 55-day old *IL-1 α* ^{-/-} mice compared with WT mice ($P \leq 0.05$) this expression was localized on the enterocyte surface and in the lamina propria cells (Figure 2.14 C and Figure 2.15 E & F).

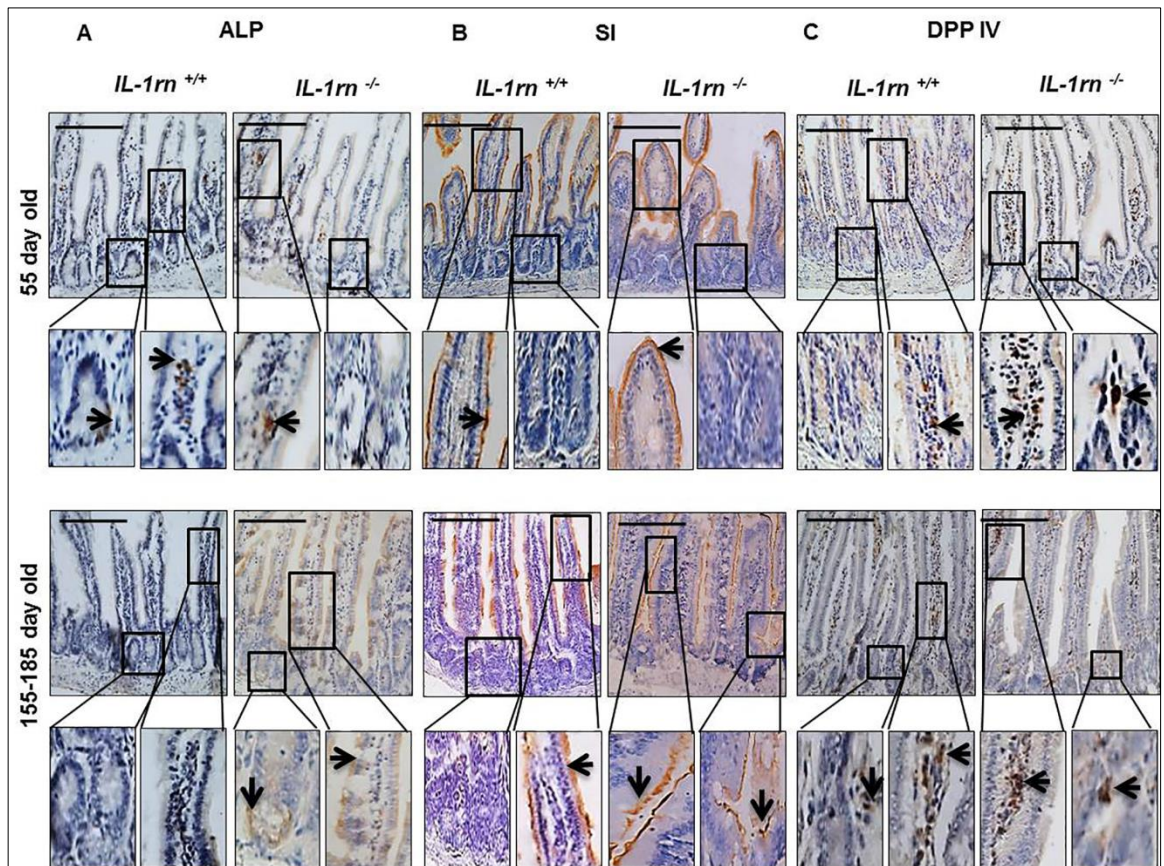


Figure 2.14: Immunohistochemistry staining of the expression and localization of digestive enzymes: ALP (A); SI (B); and DPP IV (C) in the jejunum of the 55-day old and 155-185 day old *IL-1rn^{-/-}* mice compared with WT mice. Cell nuclei were stained with haematoxylin (blue). Black arrows indicate immunopositivity. Scale bar = 100 μ m.

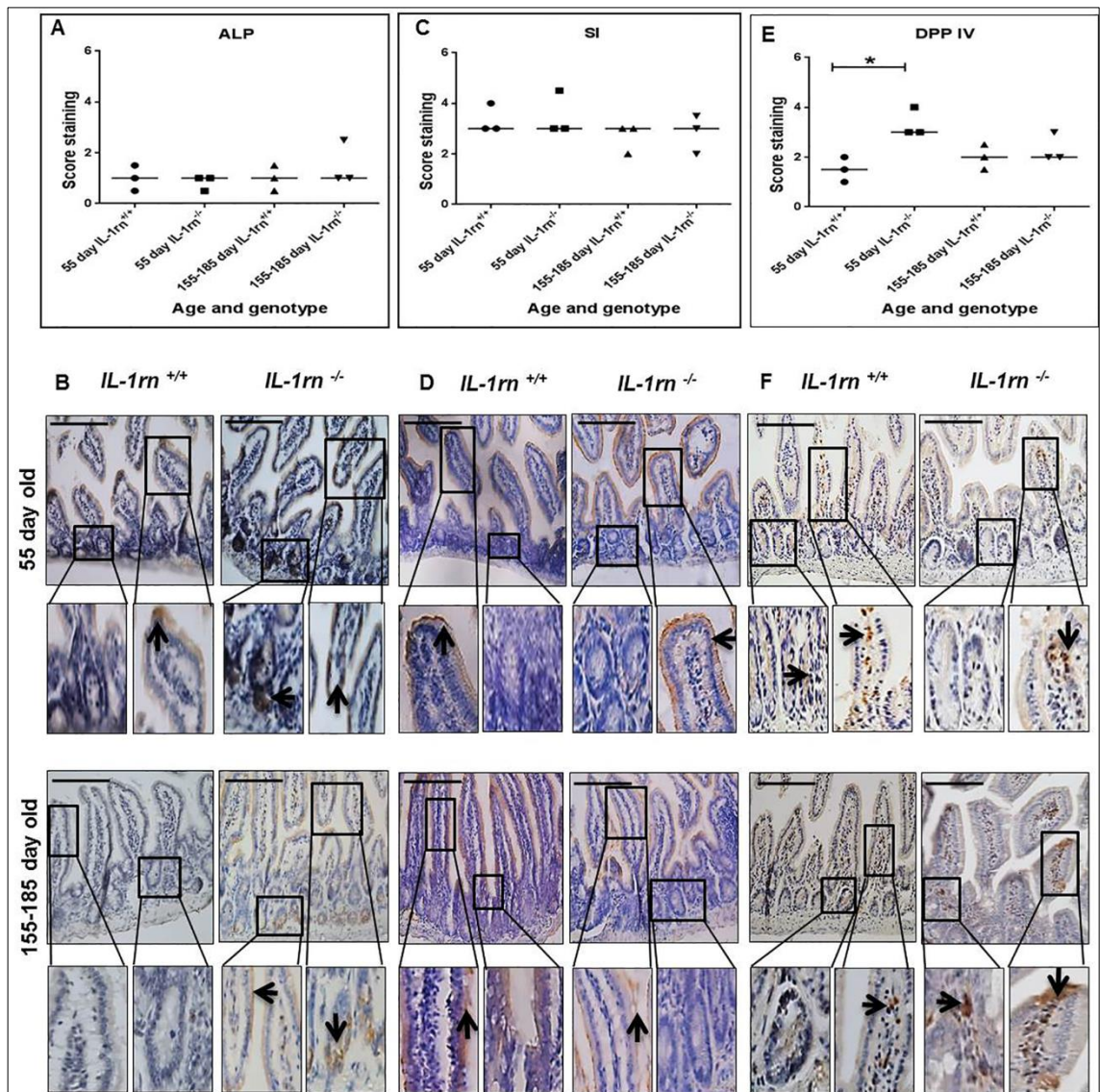


Figure 2.15: Immunohistochemistry staining of the expression and localization of the digestive enzymes: ALP (A); SI (C); and DPP IV (E) showing the immunopositive intensity quantification across the small intestinal architecture. B, D and F showing the immunopositive staining in the ileum of the 55 day old and 155-185 day old $IL-1rn^{-/-}$ mice compared with WT mice. Cell nuclei were stained with haematoxylin (blue). Black arrows indicate immunopositivity. * $P \leq 0.05$. Scale bar = 100 μ m.

2.4 Discussion

The balance between IL-1 and IL-1Ra as an endogenous inhibitor plays an essential role in stimulation and regulation of inflammation in IBD (Ludwiczek *et al.* 2004), however, whether IL-1 is an important causative factor in IBD or purely a result of inflammation is not currently understood. Thus, this study investigated whether changes seen during IBD could be induced spontaneously by the removal of IL-1Ra in mice that lack a functional *IL-1rn* gene. In *IL-1rn*^{-/-} mice, the villi were shown to be shorter in the jejunum, while shorter and thinner in the ileum. This blunting of the villi is a common microscopic feature of IBD and has been observed in patients with Crohn's disease in both the jejunum and the ileum (Rutgeerts *et al.* 1984). In contrast, in WT mice the crypt-villus axes height and villi width were shown to be comparable to the villus-crypt architecture of wild-type C57BL/6J mice of a similar age and region of the small intestine (Gulbinowicz *et al.* 2004). As seen in the WT mice, there was a decrease in height and width along a proximal-distal gradient of the small intestine. Similarly to these findings, in a wild-type C57BL/6J mice model a comparison of old and young mice, showed an increase in villi height with age, whilst the villi width was unchanged (Gulbinowicz *et al.* 2004).

Physiologically intestinal goblet cells secrete large amounts of mucus, which coat and cover the intestinal villi. This mucus plays an important role in the maintenance of the intestinal mucosal barrier and creates a milieu in which digestion and absorption take place (Atuma *et al.* 2001). Here, an increase in the number of goblet cells per crypt-villus axis in both jejunum and ileum of *IL-1rn*^{-/-} mice compared with WT mice was observed. This increase in goblet cells which accompanies the inflammatory process is believed to be caused by increased expression of the transcription factors: Hath1 (a bHLH factor) and

KLF4 (Klupper like factor 4), which are essential for goblet cell differentiation (Gersemann *et al.* 2009). This inflammatory process is believed to drive the increase in goblet cell differentiation, which is observed in Crohn's disease patients (Gersemann *et al.* 2009). However, it is important to note that this increase in goblet cells is not found in all Crohn's disease patients or throughout the whole gastrointestinal tract (Dorofeyev *et al.* 2013).

Maintenance of intestinal homeostasis is regulated by epithelial barrier integrity (Noti *et al.* 2010). Diffusion of the luminal materials into lamina propria promotes a local inflammatory response causing release of proinflammatory cytokines, release of MMPs, and epithelial degradation and inflammation (O'Sullivan *et al.* 2015). Expression of pro-inflammatory cytokines: IL-1 α , IL-1 β , TNF α , and IL-15 were increased in *IL-1rn^{-/-}* mice, and these results are in agreement with those obtained from patients with Crohn's disease (Geboes 2003). IL-1 α and IL-1 β are expressed in human intestinal epithelial cells (Garlanda *et al.* 2013). IL-1 α is released when these cells are damaged or destroyed. IL-1 α was detected in the epithelium of human IBD where released from necrotic intestinal epithelial cells and plays a crucial role in intestinal inflammation by inducing human intestinal fibroblast to produce IL-6 and IL-8 (Scarpa *et al.* 2015). The high concentrations of IL-1 β in the intestine of patients with Crohn's disease are mainly attributed to local mononuclear cell infiltration (Mahida *et al.* 1989). Increased production of IL-1 β and TNF α in inflamed Crohn's disease mucosa induces the synthesis of IL-8, which is an effective neutrophil chemoattractant (Andus *et al.* 1993). these findings agree with previous work, which showed increased numbers of TNF α positive cells in the lamina propria and submucosa of patients with Crohn's disease. Furthermore, TNF α produced by subepithelial macrophages has been shown to contribute to decreased epithelial integrity (Murch *et al.* 1993). TNF α

acts as an important mediator of inflammation through MAPK and NF- κ B activation, increasing cell proliferation and altering epithelial barrier permeability (Guan & Zhang 2017). The production of TNF α is also high in cultured mucosal mononuclear cells from Crohn's disease patients (Reinecker *et al.* 1993). However, a previous study observed no differences in TNF α mRNA expression between control and IBD mucosal biopsies (Isaacs *et al.* 1992).

IL-1RI is expressed on many cell types including T cells, fibroblasts, and intestinal epithelial cells. Despite the increased expression of IL-1 β in the *IL-1rn^{-/-}* mice, the expression of IL-1R1 was reduced; this could suggest a negative feedback loop decreasing expression of IL-1RI in the presence of uncontrolled IL-1 production. This agrees with a previous study, which showed IL-1 β and TNF α treatment downregulated the expression of mRNA IL-1RI in rat intestinal epithelial cells (IEC-6) (McGee *et al.* 1996). Similarly, IL-1 β treatment was also shown to downregulate IL-1RI protein in retinal endothelial cells (TR-iBRB2) (Aveleira *et al.* 2010). This is contrary to previous study, in which an increase in IL-1 β induced chronic intestinal inflammation in mice and an increase in IL-17A-secreting innate lymphoid cells which express high levels of IL-1R1 (Coccia *et al.* 2012). These differences may be a result of the different levels of inflammation seen in these models. Here, increased expression of IL-15 was seen in *IL-1rn^{-/-}* mice, this is in agreement with Liu *et al.* (2000), who showed increased expression of IL-15 by macrophages in the inflamed ileum of patients with Crohn's disease and that IL-15 increased local T cell activation and induced proinflammatory cytokine production by T cells and macrophages. The presence of polymorphonuclear cells and mononuclear cells play an important role in the augmentation of inflammation and tissue damage in IBD (Valatas *et al.* 2015). Increased infiltration of these CD11b and CD68 positive

cells into the lamina propria were observed in *IL-1rn^{-/-}* mice compared with WT mice. These findings are in agreement with previous findings which showed increased numbers of these cells in the inflamed mucosa of IBD patients (McKaig *et al.* 2003). Infiltration of immune cells such as macrophages and lymphocytes in the lamina propria is an important aspect of IBD, especially Crohn's disease, even in the lack of noticeable morphological, clinical, and endoscopic indication of inflammation. This is thought to be due to an increased demand of macrophages within the inflamed intestine (Fiocchi 1998).

MMPs and ADAMTS1 expression were not significantly altered in *IL-1rn^{-/-}* mice. MMPs have been demonstrated to be induced in several pathological conditions of IBD and play a key role in regulating the pathophysiology of IBD (Manicone & McGuire 2008). The main action of matrix metalloproteinases is to degrade extracellular matrix proteins. Active MMP2 and MMP9 play an important role in cell migration and cytokine stimulation. Indeed neutrophil infiltration has been shown to be induced by upregulation of MMP9 in murine inflamed intestine (Liu *et al.* 2013). Furthermore, stromal cells play an important role in intestinal inflammation and the pathogenesis of IBD. These cells secrete MMP2 and MMP9 (Drygiannakis *et al.* 2013); and MMP9 is produced by human colonic epithelium during IBD (Pedersen *et al.* 2009). In addition, infiltrating macrophages and neutrophils are the main source of MMP9 in human IBD (Koelink *et al.* 2014). Overexpression of MMP9 has been shown to cause a reduction in the differentiation of progenitor cells to goblet cells and consequently decreased MUC2 expression, which leads to decreases in the protective mucin barrier in colonic epithelium (Liu *et al.* 2013).

The maintenance of epithelial barrier function and control of paracellular permeability are regulated by tight junction proteins (Landy *et al.* 2016). Epithelial disruption and decrease in tight junctions that lead to increased intestinal permeability are the common features of Crohn's disease (Munkholm *et al.* 1994). Decreased expression of ZO-1 and loss of E-cadherin expression were observed in *IL-1rn^{-/-}* mice, suggesting a dysfunctional and leaky epithelial barrier. Inflammatory cytokines are known to affect epithelial junctional complexes, causing barrier dysfunction and increased epithelial permeability (Landy *et al.* 2016). A previous study showed that a tight junction disorder has been found in the epithelial cells of the terminal ileum from patients with Crohn's disease (Marin *et al.* 1983). In addition, it has been shown that IL-1 β and TNF α induced defects in intestinal epithelial tight junctions resulting in increased intestinal permeability (Gibson 2004).

Surprisingly, the expression of digestive enzymes were not altered in *IL-1rn^{-/-}* mice compared with WT mice. This demonstrated the resilience of the intestine to maintain function even during severe inflammation. ALP plays an essential role in maintaining small intestinal homeostasis and has been shown to prevent the activation of NF-kB, thus inhibiting release of pro-inflammatory cytokines. Decreased activity of ALP could increase intestinal inflammation, (Fawley & Gourlay 2016) and intestinal epithelial dysfunction in IBD patients has been attributed to lower intestinal expression and activity of ALP (Bilski *et al.* 2017). SI expression was also unchanged, which is contrary to decreased gene expression of SI in villus enterocytes seen in the ileum of patients with Crohn's disease (Ziambaras *et al.* 1996). DPP IV expression, however, was significantly increased in the young *IL-1rn^{-/-}* mice, but not the older *IL-1rn^{-/-}* mice compared to

WT mice. A similar loss of DPPIV activity has been seen in the serum of patients with IBD (Moran *et al.* 2012).

In conclusion, IL-1Ra deficient mice ($IL-1rn^{-/-}$) induced spontaneous intestinal inflammation which provides an effective approach to display features associated with IBD. Old $IL-1rn^{-/-}$ mice demonstrated a higher inflammatory response than young $IL-1rn^{-/-}$ mice. This model delivers an evidence for the role of the imbalance between IL-1 and IL-1Ra in the pathogenesis of IBD and could provide a useful model for testing new therapies.

Chapter 3

Use of hydrogel scaffolds to develop an *in vitro* 3D culture model of human intestinal epithelium

This chapter has been published:

Use of hydrogel scaffolds to develop an *in vitro* 3D culture model of human intestinal epithelium.

Rasha H. Dosh, Abdulsallam Essa, Nicola Jordan-Mahy, Chris Sammon, Christine L. Le Maitre.

Acta Biomaterialia, Vol. 62, 128-143, 2017.

Author Contributions:

R.H.D. performed the majority of the laboratory work, data analysis, and statistical analysis, contributed to study design and drafted the manuscript. **AE** performed the DMA and pore size analysis and associated statistical analysis. **N.J.M.**, **C.S.**, and **C.L.L.M.** conceived the study, participated in its design and analysis and critically revised the manuscript. All authors read and approved the final manuscript.

3.1 Introduction

In vitro 3D intestinal models are becoming useful tools for investigating how human intestinal cells function and are regulated (Costello *et al.* 2014b). The studies of intestinal cellular proliferation, migration, differentiation, and drug absorption using *in vivo* models have their limitations. These include difficulties in controlling cell behaviour, their responses to specific environmental prompts, and the way in which they absorb compounds (Pusch *et al.* 2011; Costello *et al.* 2014b). Hence, this has led to the development of a number of 3D *in vitro* intestinal models. It is suggested that these 3D models could be useful to investigate tissue engineering, drug discovery, and used as an alternative to *in vivo* animal models in drug toxicity studies (Pampaloni *et al.* 2007, 2009; Ravi *et al.* 2015). Previously, *in vitro* intestinal models have been limited to 2D cell culture (Pontier *et al.* 2001; Imura *et al.* 2009), however, a number of studies have attempted to develop 3D intestinal models *in vitro* to mimic the morphological characteristics and function of intestinal epithelia and represent the micro-environment seen *in vivo* (Pusch *et al.* 2011; Sung *et al.* 2011; Kim & Ingber 2013). The choice of cells within the models is a major challenge due to the restricted accessibility to obtain sufficient quantity of primary cells which are required for 3D *in vitro* intestinal models (Kauffman *et al.* 2013).

To date, a number of normal and tumour cell types have been tested for their ability to generate intestinal epithelial models. When rat intestinal epithelial cell line (IEC-6) were seeded on top of rat intestinal subepithelial myofibroblasts (ISEMF) embedded in a collagen gel, the ISEMFs were shown to induce enteroendocrine differentiation of the overlying IEC-6 cells after 3 weeks (Yoshikawa *et al.* 2011). Viney *et al.*, (2009) co-cultured IEC-6, IPI-21 (small boar ileum epithelial cell line), and CRL-2102 (human epithelial cell line derived

from colorectal adenocarcinoma) with Rat-2 (fibroblast-like cells) on collagen gel alone; or on a collagen-Matrigel scaffold. They demonstrated that the greatest epithelial growth was seen on collagen gels, supplemented with Matrigel after 20 days. They observed multi-layered intestinal epithelium containing a cluster of cells resembling native small intestinal crypts.

To reduce the cost and ethical concerns raised by using *in vivo* animal models, Caco-2 and HT29-MTX human colon adenocarcinoma cell lines have been extensively employed in *in vitro* models of the gastrointestinal tract. These two cell lines have been selected due to their capacity to differentiate into enterocyte-like cells and mucus-producing goblet cells respectively, plus they are capable of demonstrated properties which are characteristic of the small intestine *in vitro* (Ferruzza *et al.* 2012). In 2D culture, Caco-2 cells form a monolayer, and spontaneously differentiate when confluent, expressing morphological and functional characteristics of enterocytes. These cells display polarized morphology, with microvilli on the apical side, tight junctions between the adjacent cells and express high levels of hydrolase enzymes such as alkaline phosphatase, sucrase-isomaltase, and peptidase (Howell *et al.* 1992; Olejnik *et al.* 2003; Natoli *et al.* 2011). In contrast, HT29-MTX cells are characterised by the development of confluent monolayers, junction formation and express high level of mucins (Gagnon *et al.* 2013).

It has been shown, that the use of 3D scaffolds can drive cell proliferation and differentiation (Costello *et al.* 2014a, 2014b). However, the cell growth rate varies depending on the scaffold used. Hence, the selection of scaffolds and matrices depends on cell type and other culture conditions (Ravi *et al.* 2015). Previous studies have investigated a number of potential biomaterial scaffolds

for the formation of 3D models of the small intestine (Yu *et al.* 2012; Costello *et al.* 2014a). Collagen gel has been used widely as a scaffold to develop a 3D model of the small intestine, although collagen gels are limited by batch variation (Antoine *et al.* 2014). Most notably, Caco-2 cells have been investigated within 3D collagen scaffolds which were fabricated prior to seeding to match the geometry of intestinal villi. On these moulded collagen scaffolds, Caco-2 cells proliferated and migrated to form structures resembling intestinal villi (Sung *et al.* 2011; Kim *et al.* 2014; Costello *et al.* 2014a, 2014b).

Sung *et al.*, (2011) demonstrated that the fabricated micro-scale collagen structure mimicking the intestinal villi and could be used as a scaffold for Caco-2 cells investigated permeability. Alternatively, several studies have exploited biodegradable fabricated co-polymers such as poly lactic-co-glycolic acid (PLGA). These scaffold moulds have been used in co-culture studies of Caco-2 and HT29-MTX and were shown to give rise to villi-like structures (Wu & Ding 2004; Costello *et al.* 2014b). However, to date, no realistic 3D models which form intestinal villi without prefabrication of structures prior to culture have been achieved.

Hence, this study aimed to investigate alternative hydrogels which could be used to develop a 3D model of the small intestinal villi *in vitro*. A number of biomaterials have potential in the tissue engineering of small intestinal villi, interestingly all the biomaterials investigated to date have been hydrogel based. Calcium cross-linked alginate hydrogels are increasingly being used as a 3D culture system for mammalian cells in biomedical engineering studies (Gombotz & Wee 2012; Khavari *et al.* 2016). Alginate is generally softer than some of the more commonly used collagen gels and enables facile diffusion of nutrients and

cellular migration, which may be beneficial in the formation of villi structures. Here, this study investigated three hydrogels which have not been previously used in 3D culture for immortalized human intestinal epithelial cells: an alginate hydrogel; novel synthetic non-biodegradable hydrogel systems L-pNIPAM (Boyes 2012) and L-pNIPAM-co-DMAc (Thorpe *et al.* 2016). As these hydrogels are highly hydrated, it is hypothesized that they would support the growth of small intestinal cells, which could mimic the cellular phenotypes of the small intestine. The latter two have been developed by our group; these hydrogels can be closely controlled and due to their synthetic nature do not display batch variation, which is a major disadvantage of natural materials (Antoine *et al.* 2014). Furthermore, as these hydrogels display an extremely low viscosity they can be moulded into any shape required, and enable incorporation of cells either pre- or post-gelation (Boyes 2012; Thorpe *et al.* 2016). Thus, if these systems are shown to support intestinal cells here they could be utilised in more complex culture systems in the future, including its use in the lining of tube like structures to mimic more closely the closed *in vivo* structures of the intestine. Furthermore, these hydrogels have been previously shown to be cytocompatible (Thorpe *et al.* 2016). Here, the potential of these all three hydrogel systems to support the 3D culture of Caco-2 and HT29-MTX cells was investigated and determine their use as scaffolds to support formation of the villi architecture of the *in vitro* small intestine.

3.2 Materials and methods

3.2.1 Hydrogel scaffolds synthesis

3.2.1.1 Alginate hydrogel scaffolds

1.2% (w/v) medium viscosity of alginic acid sodium salt (Sigma-Aldrich, Poole, UK) was dissolved in 0.15 M NaCl (Sigma-Aldrich, Poole, UK) and filter sterilized. To prepare alginate: 300 μ L alginate was added to each well of 48 well plates for histological assessment and 100 μ L added to each well of 96 well plates for metabolic activity analysis. Alginate was carefully overlaid with 300 μ L in 48 well plates and 100 μ L in 96 well plates of 200 mM CaCl₂ and incubated at 37°C for 10 min to induce gelation.

3.2.1.2 L-pNIPAM hydrogel scaffolds

Laponite® clay nanoparticles (25–30 nm diameter, \leq 1 nm thickness) (0.1 g) were dispersed in deionised H₂O (9.0 ml) (18 m Ω) for 24 h. N-isopropyl acrylamide (BYK Additives Ltd, Cheshire, UK) was prepared by vigorous stirring of 99% NIPAM (0.9 g) (Sigma, Poole, UK) and 1% 2-2'-azobisisobutyro nitrile (AIBN) (0.009 g) (Sigma, Poole, UK) for 1 h. After passing the suspension through a 5 – 8 μ m pore filter paper, the polymerization was initiated by heating to 80°C and the reagents were allowed to react for 24 h. It was observed that after heating the monomeric suspension to 80°C, the transparent liquid transforms to a milky suspension, which is comprised of a statistical co-polymer with a composition of 1% Laponite, 9% pNIPAM, and 90% water (by weight) (Boyes 2012). This hydrogel was synthesized by Abdulsalam Essa.

Following 24 h the hydrogel suspension was cooled to 38 - 39°C prior to cell incorporation. Further cooling of the polymeric suspension to 32°C, i.e. below the lower critical solution temperature (LCST) resulted in rapid gelation to a solidified hydrogel.

3.2.1.3 L-pNIPAM-co-DMAc hydrogel scaffolds

L-pNIPAM-co-DMAc hydrogel was synthesized as previously described (Thorpe *et al.* 2016). Briefly, 0.1 g Laponite® clay nanoparticles (25-30 nm diameter, ≤1 nm thickness) were dispersed in deionised H₂O (9.0 ml) (18 mΩ) for 24 h. N-isopropyl acrylamide (BYK Additives Ltd, Cheshire, UK) was prepared by vigorous stirring 0.783 g NIPAM (Sigma, Poole, UK), 0.117 g N,N'-dimethyl acrylamide (DMAc) (Sigma, Gillingham, UK) and 0.009 g 2-2'-azobisisobutyronitrile (AIBN) (Sigma, Poole, UK) were added to the suspension and stirred for 1 h. After passing the suspension through a 5-8 μm pore filter paper, the polymerization was initiated by heating to 80°C and the reagents were allowed to react for 24 h. It was observed that after heating the monomeric suspension to 80°C, the transparent liquid transformed to a milky suspension, which is comprised of a statistical co-polymer with a composition of 1% Laponite, 7.83% pNIPAM, 1.17% DMAc and 90% water (by weight). This hydrogel was synthesized by Abdulsalam Essa.

Following 24 h the hydrogel suspension was cooled to 38-39°C prior to cell incorporation. Further cooling of the polymeric suspension to 37°C, i.e. below the LCST, resulted in rapid gelation to a solidified hydrogel.

3.2.2 Material Characterisation

3.2.2.1 Scanning electron microscopy (SEM)

The morphology of all samples was investigated using a scanning electron microscope, the samples were taken as prepared and frozen at -80°C and subsequently freeze-dried using (FD-1A-50) and fractured into two or more pieces to obtain cross-sectional edges. Samples were then mounted onto aluminum stubs and gold coated using (Q150T-ES sputter coater (Quorum, UK), (10 μA sputter current for 190 s with a 2.7 tooling factor).

The fractured samples were examined using a FEI NOVA nano-SEM 200 scanning electron microscope. Images were obtained using accelerating voltage 5 KV with a range of magnifications (1000 to 10,000). From images captured, six images were randomly selected for each sample at 2400 magnification and pore sizes measured using the Capture Pro OEM v8.0 software (Media Cybernetics, Buckinghamshire, UK). Pore sizes were determined by Abdulsalam Essa.

3.2.2.2 Dynamic mechanical analysis (DMA)

Samples were either cast directly into an in-house designed sample holder for synthetic hydrogel samples or by making 3 mm thick sheet at room temperature (2 h), and a circular biopsy punch (4.5 mm internal diameter) was used to remove cylindrical samples from the solid alginate, all sample dimensions were confirmed using digital callipers prior to measurement.

Dynamic mechanical analysis was conducted in compression mode at 25°C, using frequency testing type (0.063 - 10 Hz) at room temperature (PerkinElmer DMA 8000) and storage moduli determined. Six replicates for each sample were measured. DMA was completed by Abdulsalam Essa.

3.2.3 Cell lines

The human immortal epithelial cell lines Caco-2, (passage 18-27), and HT29-MTX cells (passage 25-30), were obtained from the American Type Culture Collection (ATCC). Cells were cultured in complete cell culture media consisting of Dulbecco's modified eagle's medium (DMEM) media (Life Technologies, Paisley, UK) supplemented with 20% (v/v) heat-inactivated foetal bovine serum (FBS) for Caco-2 cells and 10% (v/v) FBS for HT29-MTX cells (Life Technologies, Paisley, UK), 100U/M penicillin (Life Technologies, Paisley, UK), 100 µg/ml streptomycin (Life Technologies, Paisley, UK), 250ng/ml amphotericin

(Sigma, Poole, UK), 2mM glutamine (Life Technologies, Paisley, UK) and 1% (v/v) non-essential amino acids (NEAA) (Sigma, Poole, UK). Cells were maintained in an incubator at 37°C temperature and 5% CO₂ in a humid atmosphere. Culture medium was replaced every 2 days. At 70-80% confluence, cells were washed with PBS (Life Technologies, Paisley, UK) and then treated with 0.25% w/v trypsin-EDTA (Life Technologies, Paisley, UK) and sub-cultured.

3.2.3.1 Culture conditions

Caco-2 and HT29-MTX cells were seeded at a density of 1x10⁶ cells/ml and 2x10⁶ cells/ml either suspended in or layered onto the surface of the three hydrogels (alginate, L-pNIPAM, and L-pNIPAM-co-DMAc) in separated experiments.

To prepare suspended cells in alginate culture: 1x10⁶ cells/ml or 2x10⁶ cells/ml were suspended in alginate and 300 µL added to each well of 48 well plates for histological assessment and 100 µL added to each well of 96 well plates for metabolic activity analysis. Alginate was carefully overlaid with 300 µL in 48 well plates and 100 µL in 96 well plates of 200 mM CaCl₂ and incubated at 37°C for 10 min to induce gelation. CaCl₂ was removed and samples were washed twice in 0.15 M NaCl to remove free Ca²⁺, and complete media, before 500 µL of complete culture media was added to each well of 48 well plates, and 250 µL of complete media was added to each well of 96 well plates. Cells were incubated at 37°C, 5% CO₂ and maintained in culture for 2, 7, 14 and 21 days under static or dynamic 3D culture conditions using an orbital shaker at 30 rpm, with media replenished every 48 h.

To prepare L-pNIPAM and L-pNIPAM-co-DMAc suspensions: 1x10⁶ cells/ml or 2x10⁶ cells/ml were suspended within either L-pNIPAM or L-pNIPAM-co-DMAc

at 38-39°C. Three hundred microliters of hydrogel cell suspension was added to each well of 48 well plates and 100 µL of hydrogel suspension was added to each well of 96 well plates and allowed to cool below the LCST to induce gelation. Five hundred microliters of complete culture media were added to each well of 48 well plates and 250 µL of complete culture media was added to each well of 96 well plates. Cells were then incubated at 37°C, 5% CO₂ and maintained in culture for 2, 7, 14 and 21 days under static or dynamic 3D culture conditions using an orbital shaker at 30 rpm with media replenished every 48 h.

To prepare layered cultures, 300 µL of either alginate, L-pNIPAM or L-pNIPAM-co-DMAc were added to each well of 48 well plates and 100 µL added to each well of 96 well plates. Alginate culture gelation was induced by application of CaCl₂, whilst gelation of the L-pNIPAM and L-pNIPAM-co-DMAc was induced by cooling. Following gelation 300 µL or 100 µL of 1x10⁶ cells/ml or 2x10⁶ cells/ml in complete media were applied to the surface of each hydrogel construct in 48 and 96 well plates, respectively and a further 200 µL or 150 µL complete media added to each well after 30 min cell attachment period. All constructs were incubated at 37°C, 5% CO₂ and maintained in culture for 2, 7, 14 and 21 days under static and dynamic 3D culture conditions using an orbital shaker at 30 rpm, with media replenished every 48 h.

3.2.3.2 Cytospins of monolayer control cells

Monolayer cells were fixed in 4% w/v paraformaldehyde (Sigma, Poole, UK) for 20 min. To generate a cell pellet, cells were centrifuged at 300g for 5 min and resuspended in PBS to a cell density of 300 cells/µl. One hundred microliters of cell suspension was cytopun by centrifugation at 1000 rpm for 3 min (Shandon

cytochrome 3, Thermo Scientific, Loughborough, UK). Slides were then air-dried and stored at 4 °C until needed for immunohistochemical investigation.

3.2.3.3 Metabolic activity of cells

The metabolic activity of Caco-2 and HT29-MTX cells suspended within and layered on hydrogels under static and dynamic 3D culture conditions were assessed using Alamar blue assay (Life Technologies, Paisley, UK) in normal complete media after 0-21 days of culture following the manufacturer's protocol. The fluorescent intensity was recorded using a fluorescence microplate reader (CLARIOstar®, BMG LABTECH) fluorescence emission of 590 nm, excitation wavelength of 540 nm. Relative fluorescence units (RFU) were recorded for cellular hydrogel scaffolds and normalized to RFU of acellular control scaffolds as an indication of total live cells.

3.2.4 Histological assessment

Caco-2 and HT29-MTX cells were cultured suspended within or layered on each of the three hydrogel scaffolds, under static or dynamic culture conditions, together with no cell controls for 2, 7, 14 and 21 days. Triplicate samples were fixed in 4% w/v paraformaldehyde/PBS for 24 h prior to washing in PBS and processed to paraffin wax in a TP1020 tissue processor (Leica Microsystem, Milton Keynes, UK). Four-micron sections were cut and mounted onto positively charged slides (Leica Microsystem Milton Keynes, UK). Sections were deparaffinised in Sub-X and rehydrated in industrial methylated spirits (IMS) prior to rehydration in distilled water. Sections were then stained with either: Haematoxylin and Eosin; Mayer's Haematoxylin (Leica Microsystem, Milton Keynes, UK) for 2 min rinsed in water for 5 min and immersed in Eosin (Leica Microsystem, Milton Keynes, UK) for 1 min); or Alcian Blue/Periodic acid Schiff's (PAS): 1% w/v Alcian Blue (PH 2.5) (Sigma-Aldrich, Poole, UK) in 3%

(v/v) acetic acid (Sigma-Aldrich, Poole, UK) for 30 min and immersed in 0.5% (w/v) Periodic acid for 10 min and rinsed three times in deionised water. Slides were then immersed in Schiff reagent (Merck KGaA, Germany) for 10 min, and rinsed three times with deionised water. Following staining, sections were dehydrated in IMS, cleared with Sub-X and mounted in Pertex (Leica Microsystem, Milton Keynes, UK). The slides were examined with an Olympus BX 51 microscope and images captured by the camera and Capture Pro OEM V8.0 software (Media Cybernetics, Buckinghamshire, UK).

3.2.5 Immunohistochemical assessment

Immunohistochemistry was performed on Caco-2 and HT29-MTX cells harvested from monolayer cultures (cytospins) prior to hydrogel incorporation to serve as time zero controls. Together with cells cultured on the optimal hydrogel culture conditions for 21 days in culture. Briefly, 4 µm sections were de-waxed, rehydrated, and endogenous peroxidase blocked using hydrogen peroxide (Sigma-Aldrich, Poole UK). After washing in Tris-buffered saline (TBS) tissue sections were subjected to an appropriate antigen retrieval method, specific to the antibodies investigated: brush border differentiation marker using anti CD10 antibody, tight junction protein using anti ZO-1 antibody, enzyme expression using anti DPP IV antibody (enzyme antigen retrieval); enterocyte differentiation markers using anti alkaline phosphatase (ALP) antibody, anti sucrase-isomaltase antibody (SI), HT29-MTX differentiation marker using anti MUC2 antibody, and anti MUC5AC antibody (heat antigen retrieval). Following this sections were washed in TBS. Following TBS washing, nonspecific binding sites were blocked at room temperature for 90 min with 25% (w/v) serum (Abcam, Cambridge, UK) in 1% (w/v) bovine serum albumin in TBS. Sections were incubated overnight at 4°C with appropriate primary antibody: CD10

(1:100 rabbit polyclonal) (Abcam, Cambridge, UK), ZO-1 (1:50 rabbit polyclonal) (Abcam, Cambridge, UK), ALP (1:200 rabbit polyclonal) (Abcam, Cambridge, UK), DPP IV (1:50 mouse monoclonal) (Abcam, Cambridge, UK), SI (1:50, mouse monoclonal) (Santa Cruz, Heidelberg, Germany), MUC2 (1:100 rabbit polyclonal) (Abcam, Cambridge, UK), MUC5AC (1:200, mouse monoclonal) (Abcam, Cambridge, UK). For each immunohistochemistry method, a negative control was performed, replacing the primary antibody with either rabbit or mouse IgG (Abcam, Cambridge, UK) as appropriate, at a concentration equal to that of the primary antibody. Sections were washed in TBS and then incubated in 1:500 dilution of an appropriate biotinylated secondary antibody for 30 min at room temperature. Binding of the secondary antibody was visualised after exposure to horseradish peroxidase (HRP) streptavidin-biotin complex (Vector Laboratories, Peterborough, UK) for 30 min. Sections were washed in TBS, and treated with 0.08% (v/v) hydrogen peroxide in 0.65mg/ml 3, 3'-diaminobenzidine tetrahydrochloride (Sigma-Aldrich, Poole, UK) in TBS for 20 min. Sections were counterstained with Mayer's haematoxylin, dehydrated, cleared and mounted in Pertex. Immunohistochemical staining were examined with an Olympus BX51 microscope and images captured by digital camera and Capture Pro OEM V8.0 software (Media Cybernetics, Buckinghamshire, UK).

3.2.6 Scanning electron microscopy following cell culture

After 21 days in culture, samples were processed for scanning electron microscopy (SEM). Briefly, the samples were removed from the culture, frozen at -80°C then freeze-dried overnight using a FD-1A-50 freeze dryer (Genorise Scientific). The samples were then fractured to expose the interior surface morphology. The fractured samples were mounted on aluminum stubs and coated with gold using a Quorum Technology 150Q TES system set at 10µA

sputter current for 180s with a 2.7 tooling factor. The cells were examined using a FEI NOVA nano-200 scanning electron microscope.

3.2.7 Statistical analysis

All viability tests were performed at least 6 times. Normality was assessed using Stats Direct. Normality of data was tested using a Skewness, Kurtosis, Royston Chi-sq, Shapiro Wilk W and Shapiro-Francia W tests, together with a q-q plot. From this analysis, it was demonstrated that the data sets were from mixed populations with some populations displaying potential normal distribution, but others were shown to be not normally distributed, as such non-parametric tests have been performed for all data. Therefore statistical comparisons were performed by Kruskal-Wallis with a pairwise comparison (Dwass-Steel-Critchlow-Fligner) between all-time points and between culture conditions and hydrogel systems for 21 days for Alamar blue assay with statistical significance accepted at $P \leq 0.05$.

3.3 Results

3.3.1 Material properties of alginate, L-pNIPAM and L-pNIPAM-co-DMAc scaffolds.

Alginate displayed significantly larger pores (30-74 μm) and lowest storage moduli ($0.4\text{-}8.6 \times 10^5$ Pa) than both the synthetic hydrogels investigated (Figure 3.1 A & B). L-pNIPAM displayed significantly larger pores (5.6-25 μm) and lower storage moduli ($0.18\text{-}2.8 \times 10^7$ Pa) than L-pNIPAM-co-DMAc (Figure 3.1 A & B). L-pNIPAM-co-DMAc displayed the smallest pore sizes (1.5-30 μm) and highest storage moduli ($1\text{-}5 \times 10^7$ Pa) indicating this was the stiffest of the three hydrogels investigated (Figure 3.1 A & B).

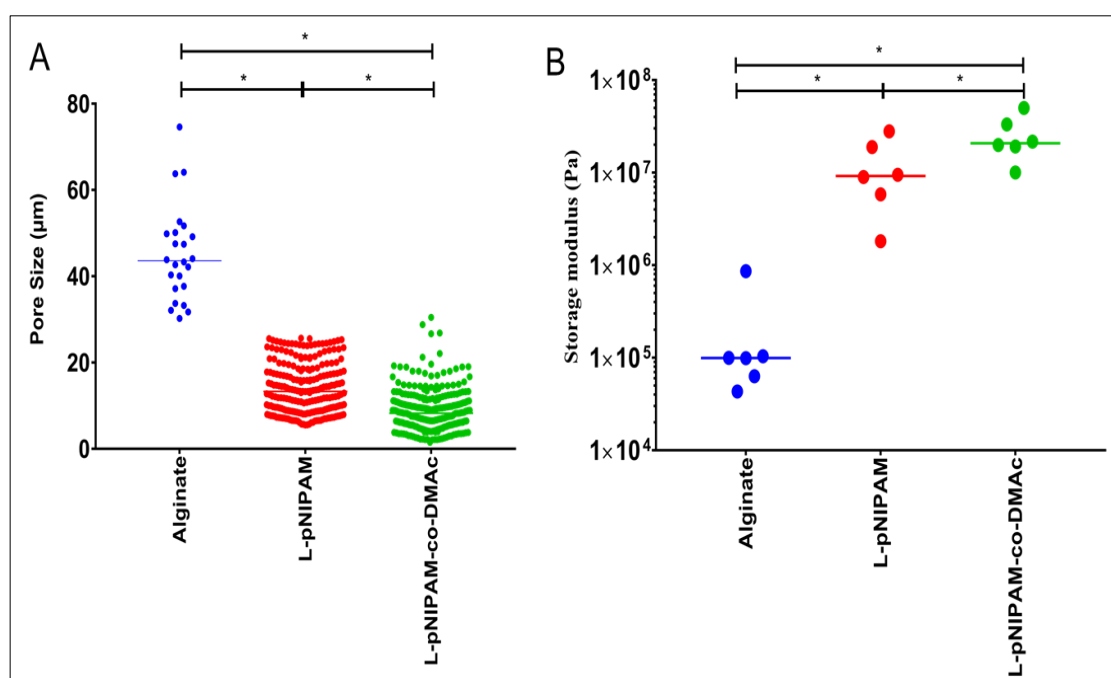


Figure 3.1: Pore size (μm) for acellular alginate, L-pNIPAM, and L-pNIPAM-co-DMAc hydrogels determined using SEM analysis. B: Storage Modulus (G') values for acellular alginate, L-pNIPAM, and L-pNIPAM-co-DMAc hydrogels determined using DMA. This figure prepared by Abdulsalam Essa.

3.3.2 Metabolic activity of Caco-2 cells in three hydrogel scaffolds

Cell densities of 1×10^6 cells/ml and 2×10^6 cells/ml were investigated in all three gel systems. The data from the 2×10^6 cells/ml cell density were selected as optimal cell density and this cell density was used for further study. At this density the viability of the cells and cellular morphology was much better in all three gel systems. This thesis will report the 2×10^6 cells/ml data only.

3.3.2.1 Alginate hydrogel scaffold

Under static layered culture conditions, there was a significant decrease in cell metabolic activity of Caco-2 cells between day 0 and 2, when grown on alginate ($P \leq 0.05$) (Figure 3.2 A). Thereafter metabolic activity was significantly increased between day 2 to 14 ($P \leq 0.05$) (Figure 3.2 A). Likewise, when Caco-2 cells were suspended in alginate and cultured under static conditions, there was a decreased metabolic activity from day 0 and 7, which was then followed by a significant increase in metabolic cell activity from day 2 and day 7 to day 14 and 21 ($P \leq 0.05$) (Figure 3.2 B). In contrast, under dynamic culture conditions, there was an increase in metabolic cell activity in Caco-2 cells between day 0 and 7 when layered on the alginate, followed by a decrease in metabolic cell activity from day 7 to 21 which failed to reach significance (Figure 3.2 C). No significant difference in metabolic cell activity was observed during the initial 7 days of culture when the Caco-2 cells were suspended within alginate was observed. This was then followed by a significant increase in metabolic cell activity from day 7 to 21 under dynamic culture ($P \leq 0.05$) (Figure 3.2 D). Across the culture conditions following 3 weeks a significant decrease in metabolic activity was observed in Caco-2 cells layered on the surface of alginate cultured under dynamic conditions compared to static conditions ($P \leq 0.05$) (Figure 3.2 A & C). Whilst cells cultured under dynamic culture in suspension showed an increase

in metabolic activity compared to layered cultures under dynamic conditions ($P \leq 0.05$) (Figure 3.2 C & D).

3.3.2.2 L-pNIPAM hydrogel scaffold

When Caco2 cells were cultured as layers on the surface of L-pNIPAM hydrogel scaffolds under either static or dynamic culture, there was no change in metabolic cell activity from day 0 to 2. This was followed by a significant increase in metabolic cell activity from day 7 to 21 ($P \leq 0.05$) (Figure 3.2 E & G). In contrast, when Caco-2 cells were suspended in L-pNIPAM and cultured under either static or dynamic conditions there was a significant decrease in metabolic cell activity ($P \leq 0.05$) (Figure 3.2 F & H). Across the culture conditions following 3 weeks a significant decrease in metabolic activity was seen in Caco-2 cells suspended in L-pNIPAM compared to layered cells under both static and dynamic culture ($P \leq 0.05$) (Figure 3.2 E - H).

3.3.2.3 L-pNIPAM-co-DMAc hydrogel scaffold

Under both static and dynamic culture conditions, there was a significant increase in metabolic cell activity from day 0 when Caco-2 cells were layered on the L-pNIPAM-co-DMAc ($P \leq 0.05$) (Figure 3.2 I & K). However, when Caco-2 cells were suspended within L-pNIPAM-co-DMAc there was a significant decrease in metabolic cell activity, under both static and dynamic culture conditions ($P \leq 0.05$) (Figure 3.2 J & L). Across the culture conditions following 3 weeks a significant decrease in metabolic activity was seen in Caco-2 cells suspended in L-pNIPAM-co-DMAc compared to layered cells under both static and dynamic culture ($P \leq 0.05$) (Figure 3.2 I - L).

3.3.2.4 Comparison of metabolic activity between three hydrogel systems.

Caco-2 cells cultured under static conditions in layers displayed no significant difference in metabolic activity following 3 weeks (Figure 3.2). Whilst Caco-2 cells cultured in suspension either under static or dynamic culture showed significantly higher metabolic activity in alginate culture compared to both L-pNIPAM and L-pNIPAM-co-DMAc following 3 weeks ($P < 0.05$) (Figure 3.2). In contrast, Caco-2 cells cultured in layers in dynamic culture showed highest metabolic activity in L-pNIPAM which was significantly higher than both L-pNIPAM-co-DMAc and alginate cultures following 3 weeks ($P < 0.05$) (Figure 3.2). Furthermore, metabolic activity of Caco-2 cells cultured in layers on L-pNIPAM-co-DMAc under dynamic culture was significantly higher than cells cultured on alginate following 3 weeks ($P < 0.05$) (Figure 3.2).

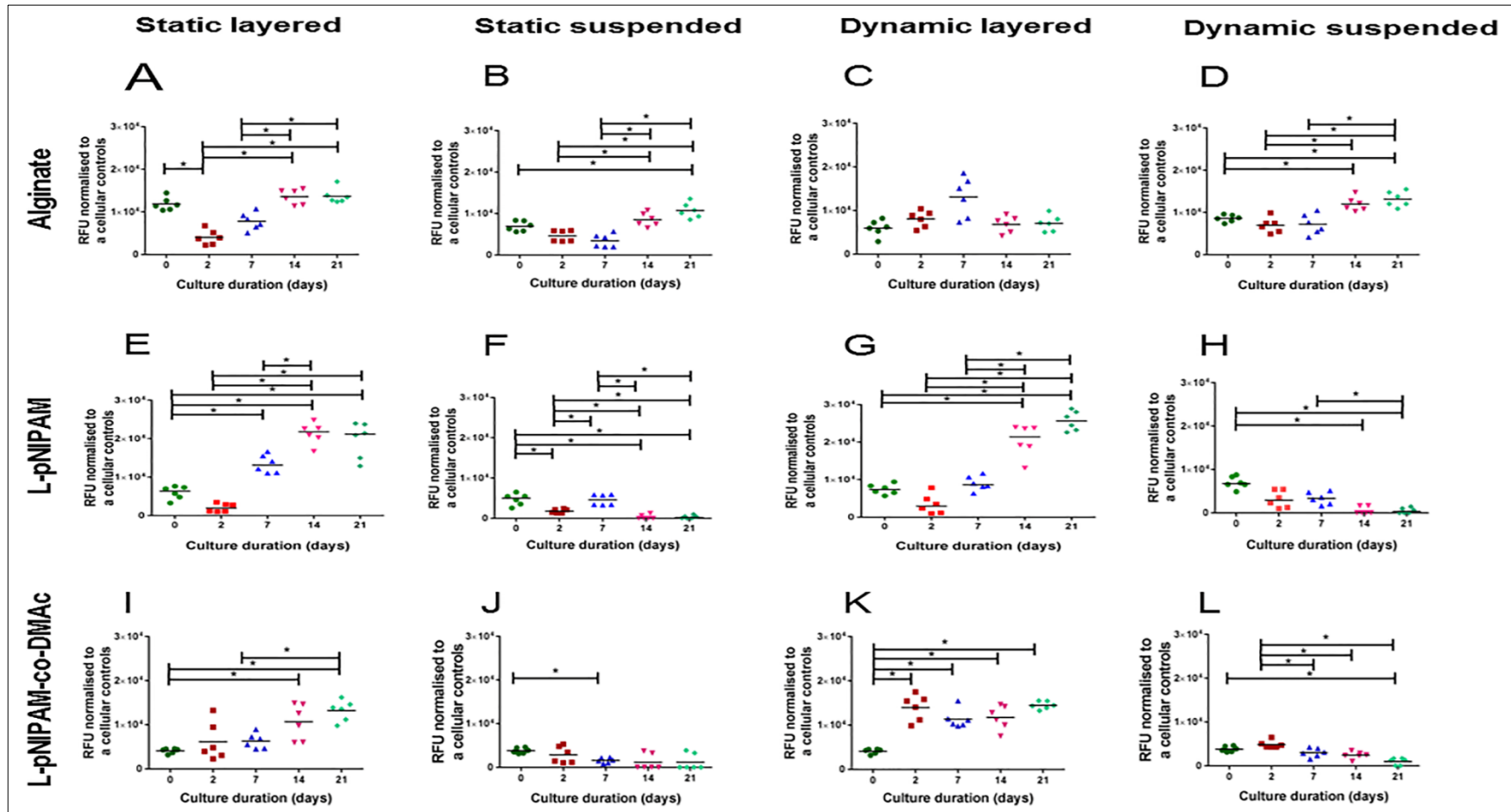


Figure 3.2: Metabolic activity of Caco-2 cells at a cell density of 2×10^6 cells/ml layered on or suspended within Alginate: (A, B, C, D); L-pNIPAM: (E, F, G, H); L-pNIPAM-co-DMAC: (I, J, K, L) following 21 days under static and dynamic culture conditions. * $P \leq 0.05$.

3.3.3 Morphological and phenotypic assessment of Caco-2 cells cultured in hydrogel systems

Caco-2 cells cultured in layers on alginate under either static or dynamic culture commonly formed multilayer spheroid structures by day 2 to 21 (Figure 3.3, Figure 3.4, Figure 3.5 A and Figure 3.6 A). When cells were suspended within alginate they formed large cell clusters which had clearly defined nuclei by day 14 to 21 (Figure 3.5 A and Figure 3.6 A). In contrast, Caco-2 cells cultured as layers on the surface of L-pNIPAM under static culture conditions formed small multicellular layers, parallel to the surface of the hydrogel between day 7 and 21 (Figure 3.5 A and Figure 3.6 A). However, when Caco-2 cells were grown as layers on the surface of L-pNIPAM under dynamic culture conditions, these cells were found to migrate into the hydrogel by day 14 (Figure 3.5 A) and then give rise to villus-like structures by day 21 (Figure 3.6 A).

However, when Caco-2 cells were suspended in L-pNIPAM and maintained under either static or dynamic culture conditions cells showed poor nuclear morphology, consistent with non-viable cells (Figure 3.4, Figure 3.5 A and Figure 3.6 A). Similarly, when Caco-2 cells were suspended within L-pNIPAM-co-DMAc and maintained under both static and dynamic culture, cells only formed a few small clusters of cells between day 7 and 21. In contrast, Caco-2 cells grown as layers on the surface of L-pNIPAM-co-DMAc under static and dynamic conditions formed multi-cellular layers (Figure 3.3, Figure 3.4, Figure 3.5 A) and villus-like structures (Figure 3.6 A).

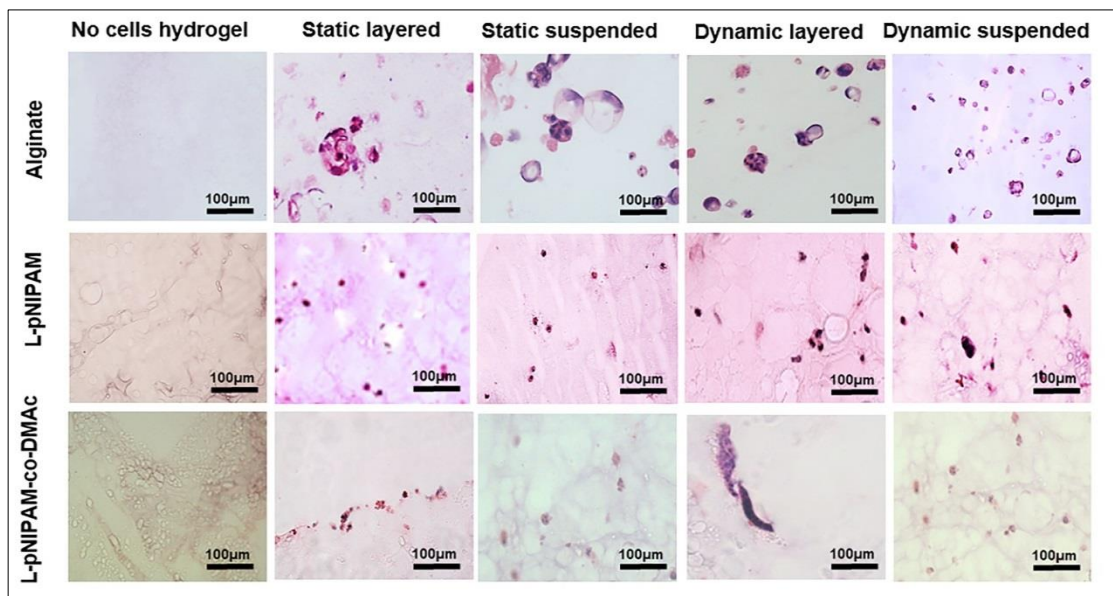


Figure 3.3: Histological analysis of Caco-2 cells layered on or suspended within alginate, L-pNIPAM, and L-pNIPAM-co-DMAC hydrogels under static or dynamic culture conditions at a cell density of 2×10^6 cells/ml following 2 days stained with H&E. Scale bar = 100µm.

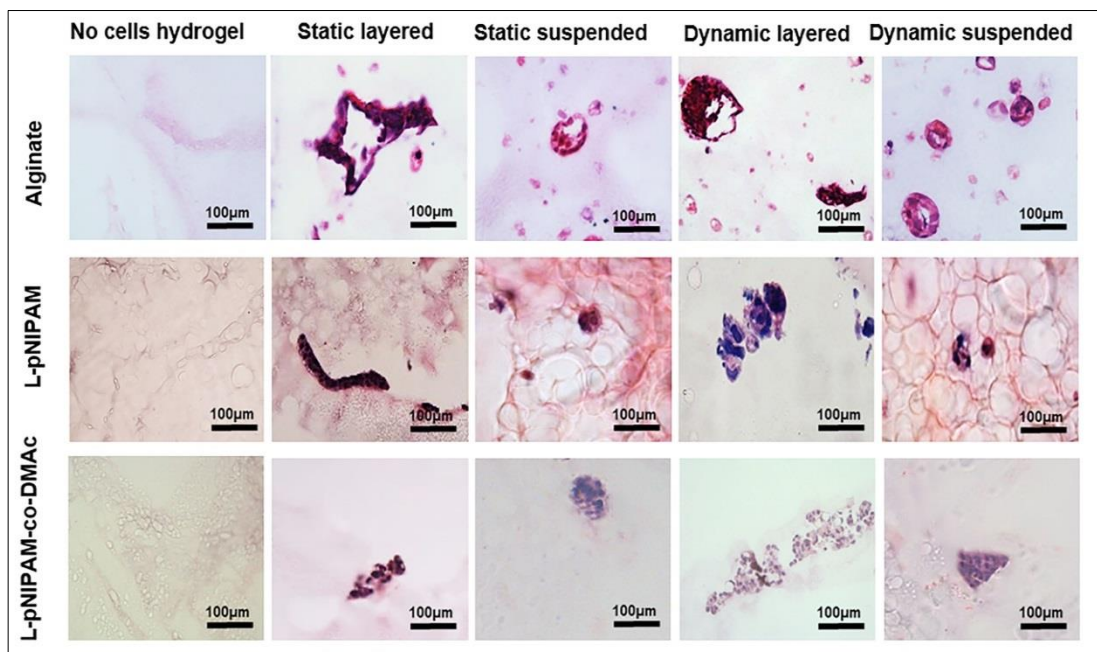


Figure 3.4 Histological analysis of Caco-2 cells layered on or suspended within alginate, L-pNIPAM, and L-pNIPAM-co-DMAC hydrogels under static or dynamic culture conditions at a cell density of 2×10^6 cells/ml following 7 days stained with H&E. Scale bar = 100 µm.

To determine potential mucin production, tissue sections of day 14 and 21 were stained using alcian blue/PAS. Whilst all three hydrogels showed background staining for alcian blue, cellular structures within them could be easily distinguished, however, due to the high levels of background staining for acidic mucins within all hydrogels, no increased staining over background was observed for acidic mucins. Within alginate scaffolds, cells were positive for neutral (pink) mucins in all culture conditions (Figure 3.5 B and Figure 3.6 B). Immunohistochemically analysis of MUC2 and MUC5AC showed Caco-2 cells did not express MUC2 and MUC5AC mucins in monolayer culture (0 h cytopsin), or in cells cultured as layers or suspended in all three hydrogels under either static or dynamic culture (Figure 3.7 A, B, and C).

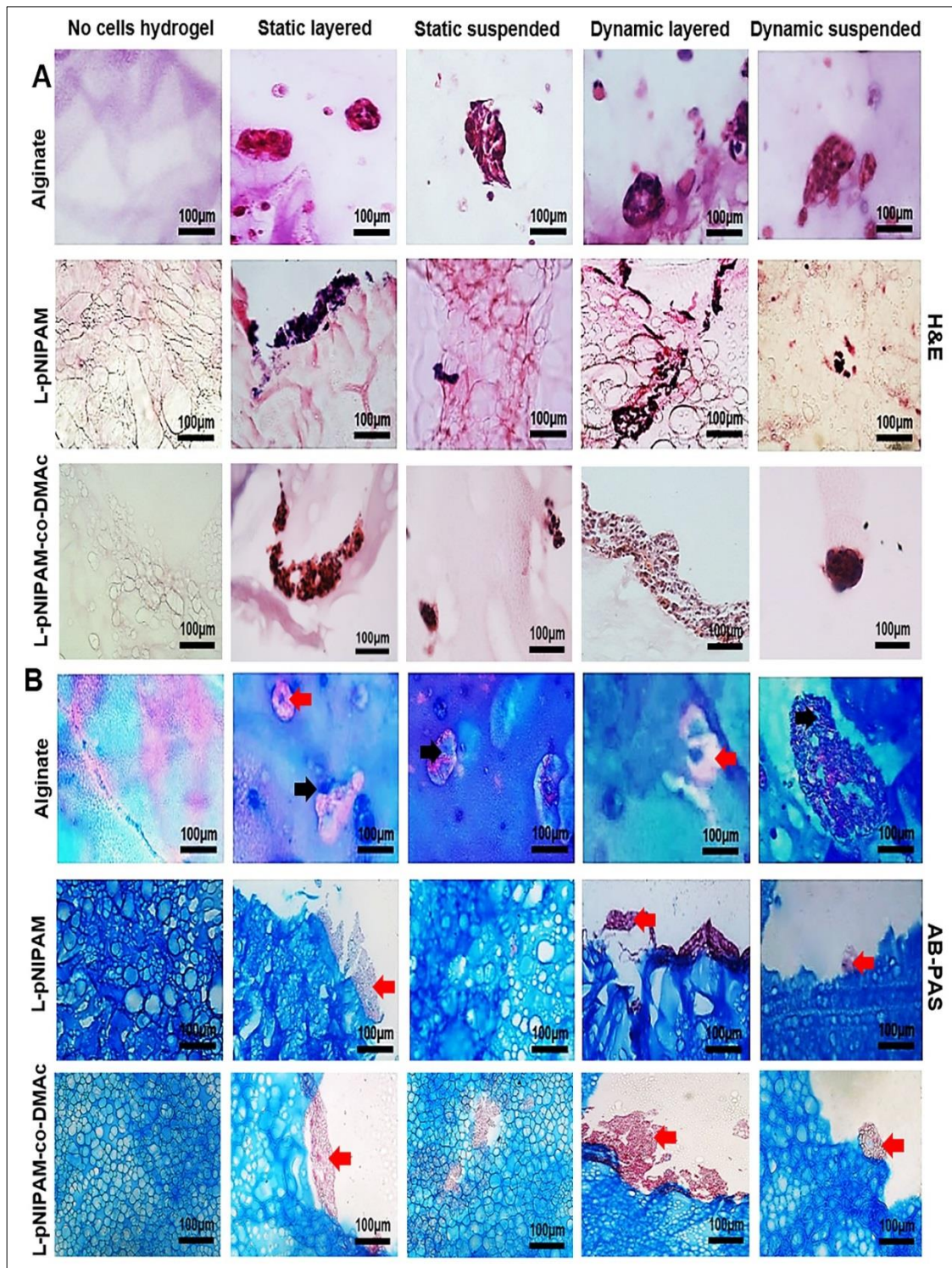


Figure 3.5: Histological analysis of Caco-2 cells layered on or suspended within alginate, L-pNIPAM, and L-pNIPAM-co-DMAC hydrogels under static or dynamic culture conditions at a cell density of 2×10^6 cells/ml following 14 days. A: Stained with H&E, and B: Stained with Alcian blue/PAS, blue: acidic mucin (black arrows); magenta: neutral mucin (red arrows). Scale bar = 100 μ m.

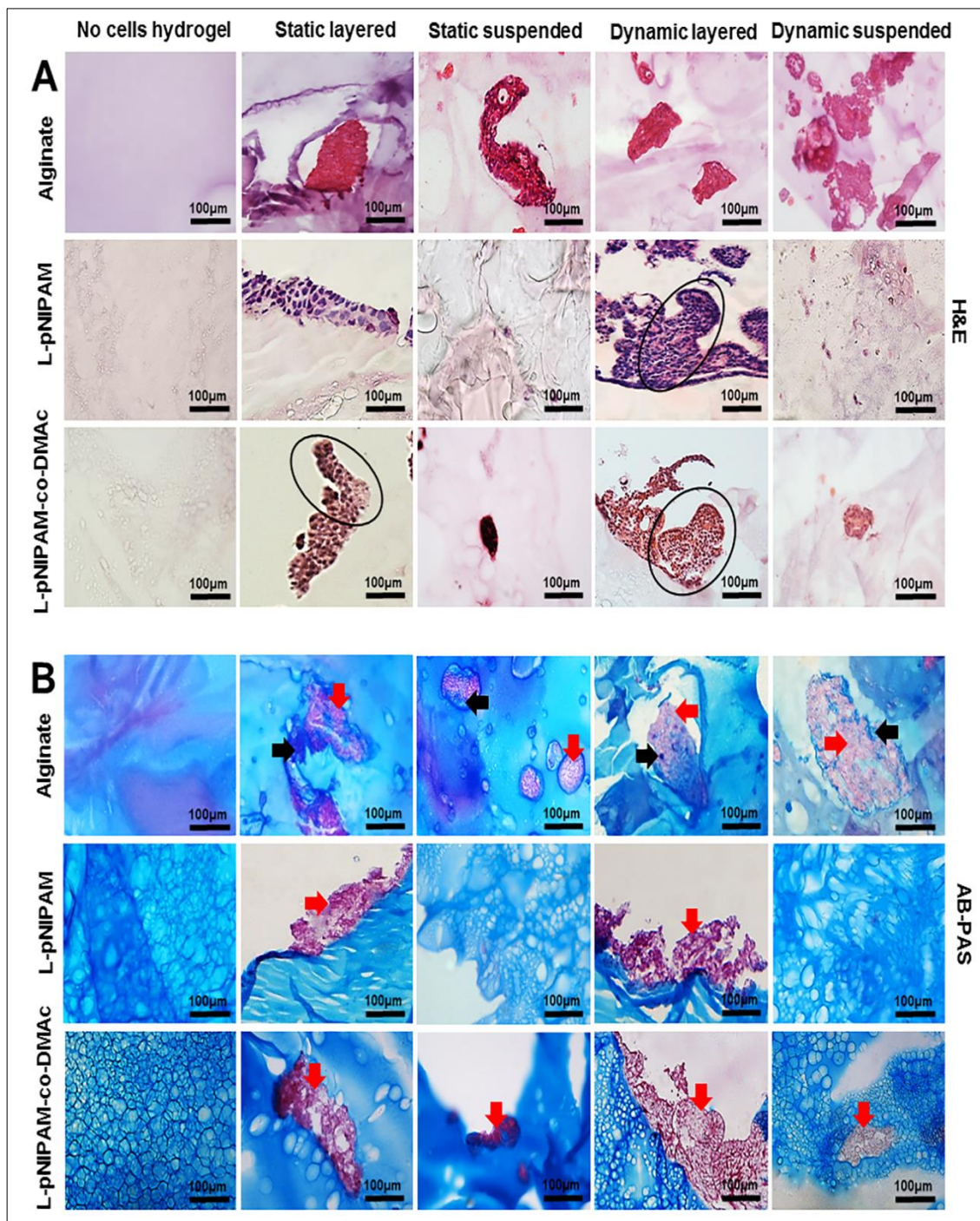


Figure 3.6: Histological analysis of Caco-2 cells layered on or suspended within alginate, L-pNIPAM, and L-pNIPAM-co-DMAC hydrogels under static or dynamic culture conditions at a cell density of 2×10^6 cells/ml following 21 day. A: Stained with H&E (circles indicate villus-like structures) and B: Stained with Alcian blue/PAS, blue: acidic mucin (black arrows); magenta: neutral mucin (red arrows). Scale bar = 100 μ m.

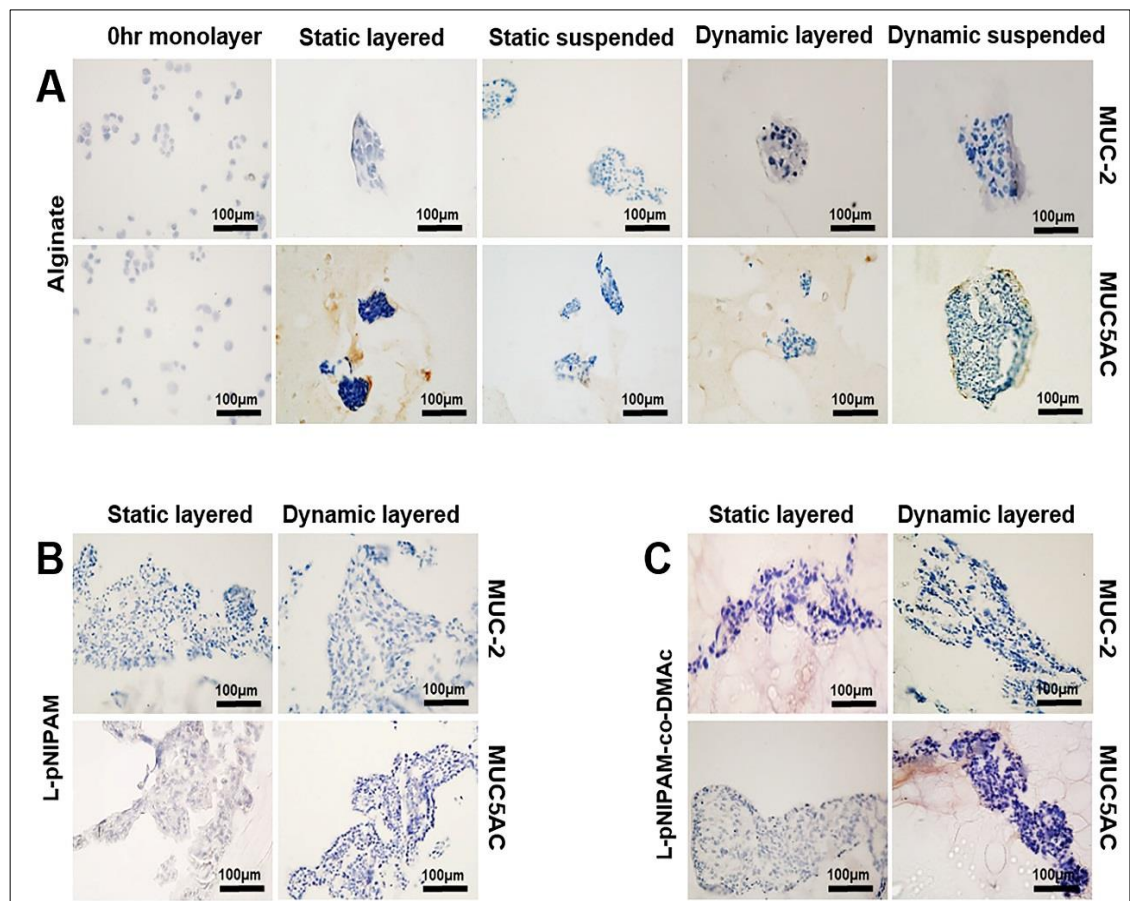


Figure 3.7: Immunohistochemistry staining of MUC2 and MUC5AC. A: Caco-2 cells monolayer and layered on or suspended within alginate; B and C: Caco-2 cells layered on L-pNIPAM, and L-pNIPAM-co-DMAc hydrogels, under static or dynamic culture conditions at a cell density of 2×10^6 cells/ml following 21 days. Cell nuclei were stained with haematoxylin (blue). Scale bar = 100 μ m.

From this analysis, L-pNIPAM was selected for further phenotypical analysis due to the superior morphological appearance and mucin production. To determine the level of Caco-2 cellular differentiation, the expression of three brush border enzymes, together with enterocyte brush border marker and a tight junction protein were investigated. Immunopositivity for CD10, ZO-1, ALP, DPP IV and SI were seen in monolayer cultures (0 h cytospin) and on the cell surface of all Caco-2 cells layered on L-pNIPAM maintained under either static or dynamic culture (Figure 3.8).

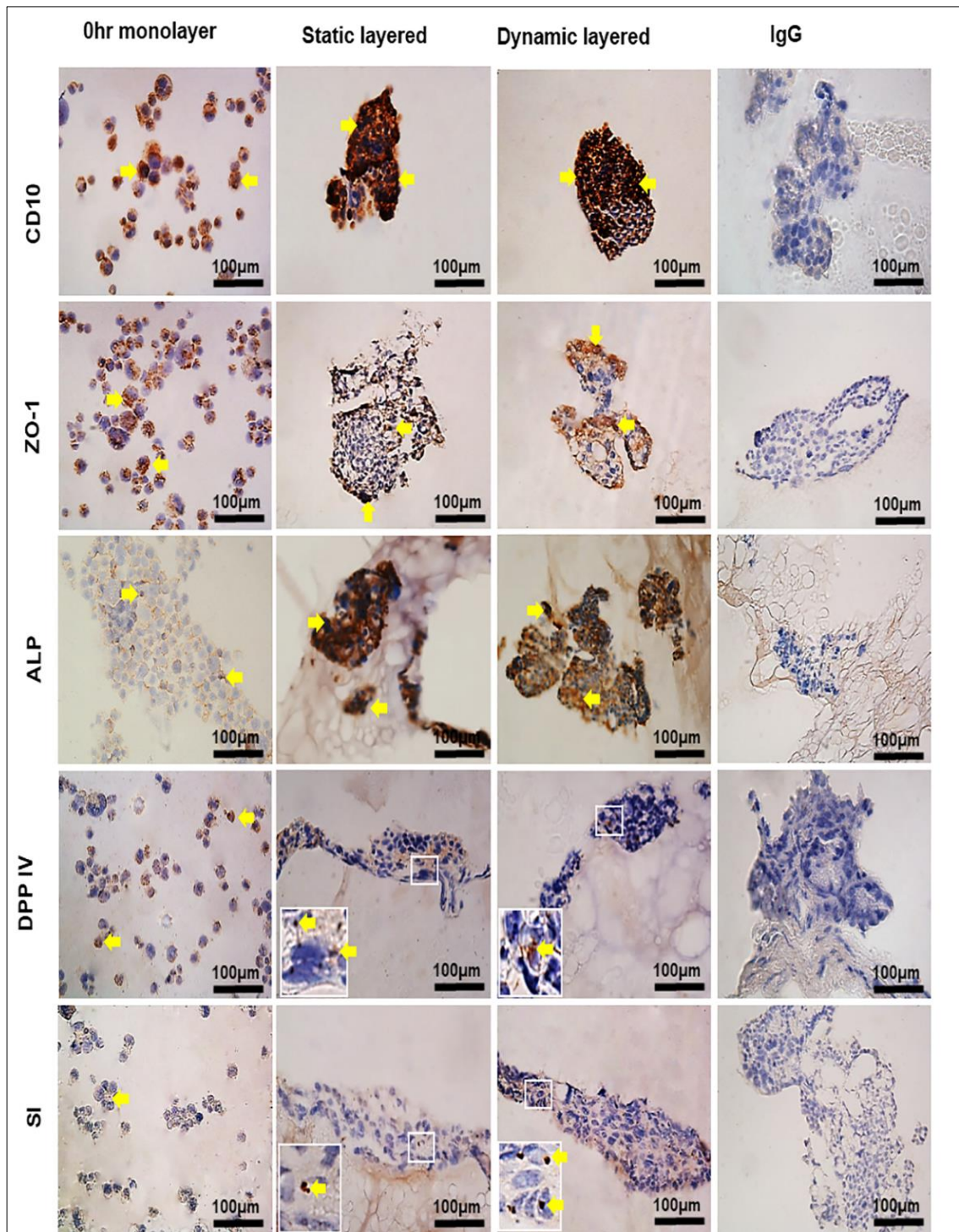


Figure 3.8: Immunohistochemistry staining (yellow arrows) for CD10, Zonulin-1 (ZO-1), Alkaline phosphatase (ALP), Dipeptidyl peptidase IV (DPP IV), and Sucrase-isomaltase (SI) of Caco-2 cells in 0 h monolayer and Caco-2 cells layered on L-pNIPAM hydrogel under static or dynamic culture conditions at a cell density of 2×10^6 cells/ml following 21 day. Cell nuclei were stained with haematoxylin (blue). IgGs is shown as a negative controls. Scale bar = 100 μ m.

3.3.4 Scanning electron microscopy of Caco-2 cells

SEM analysis of Caco-2 cell cultures in layers on the surface of L-pNIPAM and L-pNIPAM-co-DMAc hydrogel scaffolds was performed (Figure 3.9 A & B). Under static and dynamic culture conditions Caco-2 cells layered on L-pNIPAM formed comprehensive multi-layer clusters of cells which often gave rise to villi-like structures by day 21 (Figure 3.9 A and Figure 3.10). Close examination of the edges of these cell clusters showed the presence of microvilli brush borders. Surprisingly, layered Caco-2 cells when spread on the surface of L-pNIPAM-co-DMAc under static and dynamic culture conditions covered the entire surface of the scaffold (Figure 3.9 B and Figure 3.10), this contrasted with the no cell controls where hydrogels were cultured in media for 3 week, it can be seen that there were no cellular structures or disposition of matrix within the hydrogel pores (Figure 3.9).

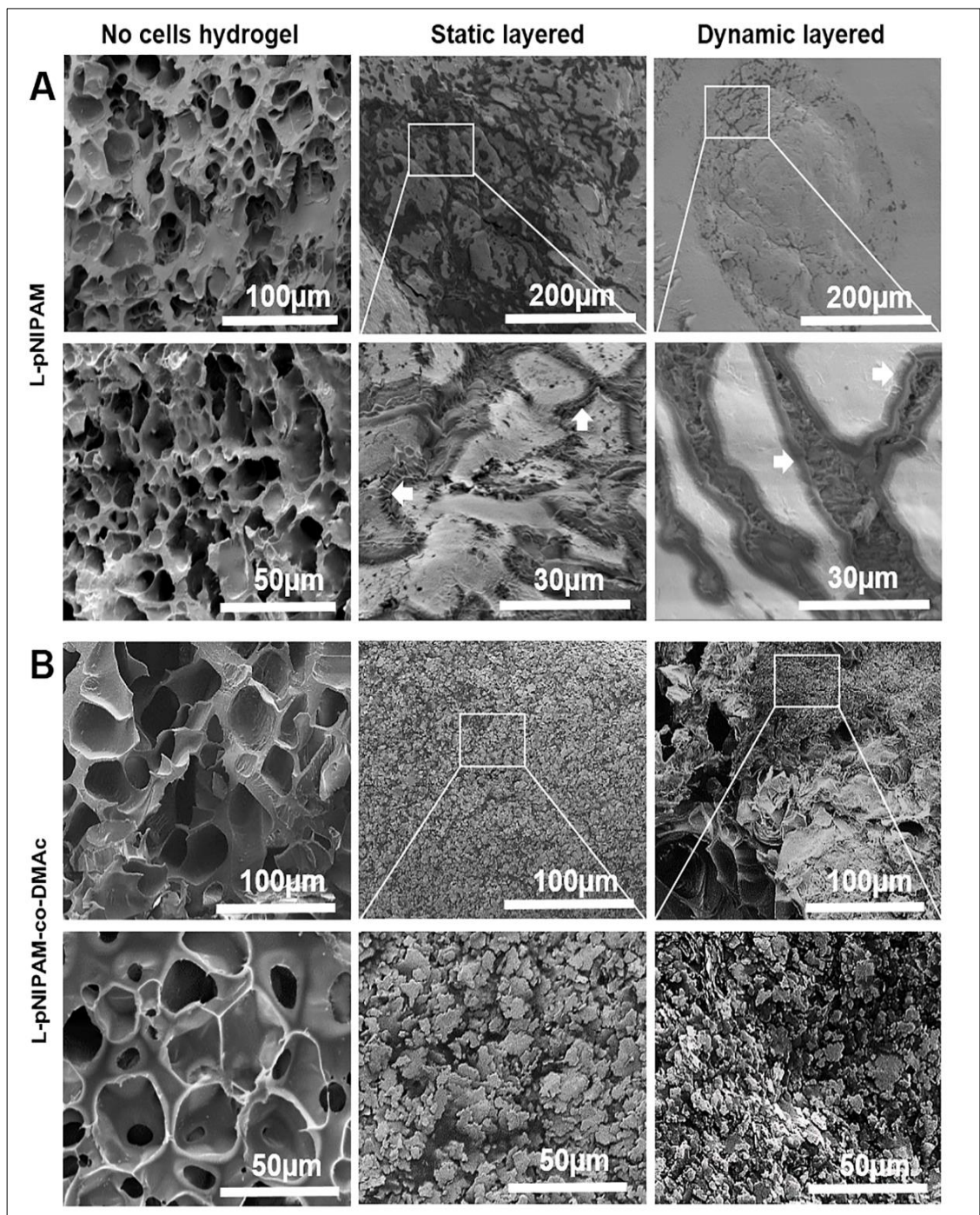


Figure 3.9: Scanning electron micrographs of Caco-2 cells layered on. A: L-pNIPAM; and B: L-pNIPAM-co-DMAc hydrogels under static or dynamic culture conditions at a cell density of 2×10^6 cells/ml following 21 day. White arrows show the microvilli-like structures. Scale bar = 30 μ m to 200 μ m.

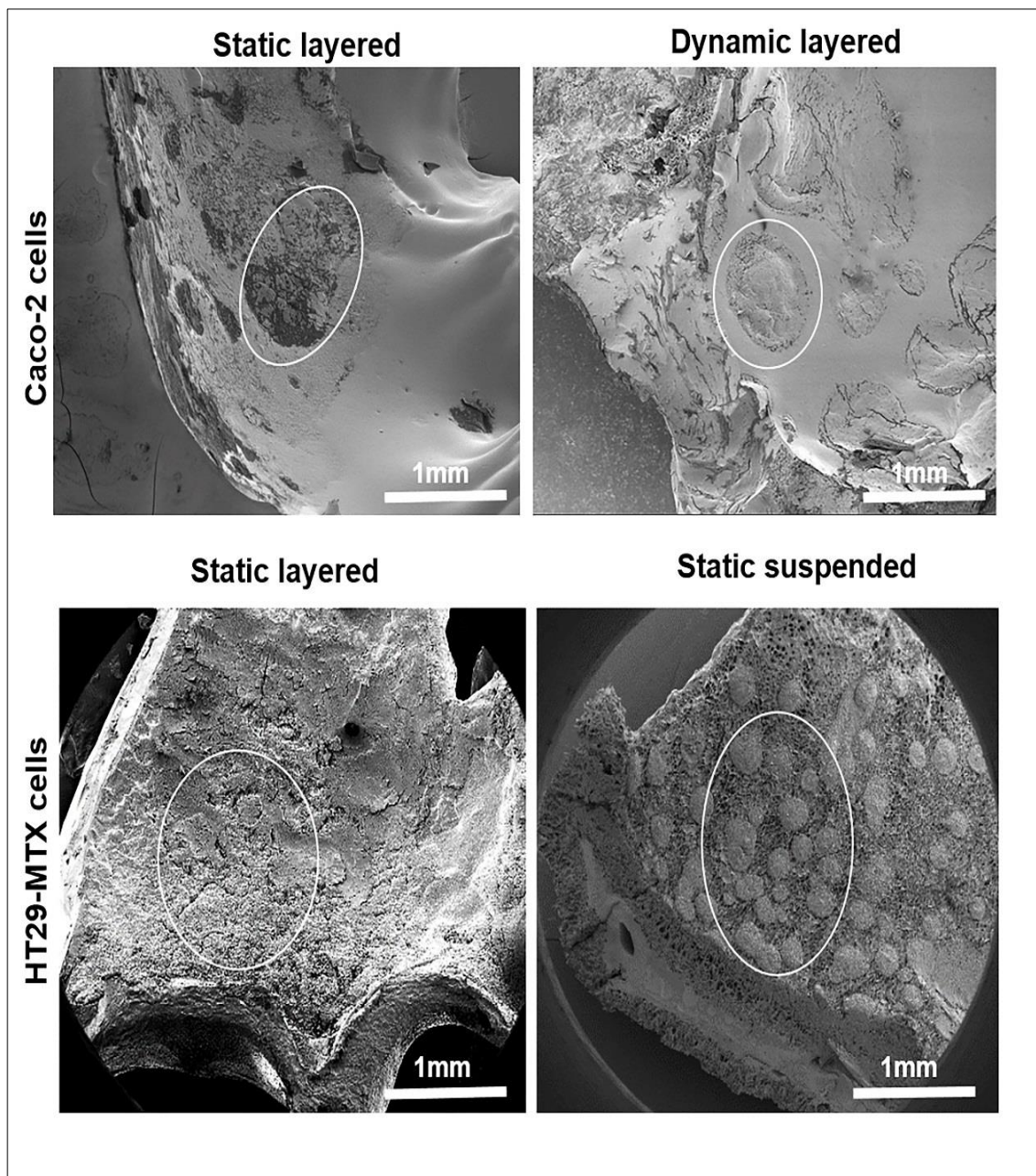


Figure 3.10: Scanning electron micrographs of Caco-2 and HT29-MTX cells layered on or suspended within L-pNIPAM hydrogel under static or dynamic culture conditions at a cell density of 2×10^6 cells/ml following 21 days. Circles indicate clusters of cells. Scale bar = 1mm.

3.3.5 Metabolic activity of HT29-MTX cells in three hydrogel scaffolds

3.3.5.1 Alginate hydrogel scaffold

Under static culture conditions, a significant increase in metabolic cell activity was observed between 0 and 21 days when HT29-MTX cells were layered on alginate ($P \leq 0.05$) (Figure 3.11 A). However, when HT29-MTX cells were suspended within alginate, a significant decrease in metabolic cell activity between day 0 and 21 ($P \leq 0.05$) (Figure 3.11 B). In contrast, under dynamic culture conditions, there was a significant increase in metabolic cell activity between day 0 and 7, 14 and 21, when HT29-MTX cells were layered on alginate ($P \leq 0.05$) (Figure 3.11 C). Whereas HT29-MTX cells, when suspended within alginate, showed a significant decrease in metabolic cell activity between day 0 and 2, which was followed by a significant increase in metabolic cell activity at day 21 ($P \leq 0.05$) (Figure 3.11 D). Across the culture conditions following 3 weeks a significant decrease in metabolic activity was observed in HT29-MTX cells suspended compared to those layered on the surface and cultured under static conditions ($P \leq 0.05$) (Figure 3.11 A & B). However, cells cultured under dynamic layered culture conditions showed an increase in metabolic activity, when compared to static layered conditions ($P \leq 0.05$) (Figure 3.11 A & C).

3.3.5.2 L-pNIPAM hydrogel scaffold

Under static culture conditions, when HT29-MTX cells were layered on or suspended in L-pNIPAM there was a significant decrease in metabolic cell activity observed between day 0 and 2, followed by a significant increase in metabolic cell activity between day 2 and 21 ($P \leq 0.05$) (Figure 3.11 E & F). Under dynamic culture conditions, initially there was a significant decrease in metabolic cell activity detected from 0 to 2 days ($P \leq 0.05$); followed by a

significant increase in metabolic cell activity from day 2 to 21 ($P \leq 0.05$) (Figure 3.11 G & H). Across the culture conditions following 3 weeks a significant difference in metabolic activity was seen in HT29-MTX cells suspended in L-pNIPAM compared to layered cells under both static and dynamic culture ($P \leq 0.05$) (Figure 3.11 E & H).

3.3.5.3 L-pNIPAM-co-DMAc hydrogel scaffold

Under static culture conditions, a significant increase in metabolic cell activity was observed at all time points where HT29-MTX cells were layered on L-pNIPAM-co-DMAc ($P \leq 0.05$) (Figure 3.11 I). In contrast, a significant increase in metabolic cell activity was observed from day 2 to 7 followed by a significant decrease in metabolic cell activity from day 7 to 21 when HT29-MTX cells were suspended in L-pNIPAM-co-DMAc ($P \leq 0.05$) (Figure 3.11 J). Under dynamic culture conditions, when HT29-MTX cells were layered on L-pNIPAM-co-DMAc there was a significant increase in metabolic cell activity from day 0 to 7 ($P \leq 0.05$) (Figure 3.11 K). Whereas, when HT29-MTX cells were suspended within L-pNIPAM-co-DMAc and maintained under dynamic culture conditions, there was a significant increase in metabolic cell activity following 14 days in culture ($P \leq 0.05$) (Figure 3.11 L). Across the culture conditions following 3 weeks HT29-MTX cells displayed significantly higher metabolic activity when cultured layered in static conditions compared to suspended in L-pNIPAM-co-DMAc under static conditions or layered under dynamic conditions ($P \leq 0.05$) (Figure 3.11 I & L).

3.3.6 Comparison of cell metabolic activity in three hydrogel systems.

HT29-MTX cells cultured under static conditions in layers displayed no significant difference in metabolic activity following 3 weeks in culture (Figure 3.11). Whilst HT29-MTX cells cultured in suspension either under static

or dynamic culture showed significantly higher metabolic activity in L-pNIPAM compared to both alginate and L-pNIPAM-co-DMAc following 3 weeks ($P < 0.05$) (Figure 3.11). In contrast, HT29-MTX cells cultured in layers in dynamic culture showed highest metabolic activity in alginate which was significantly higher than both L-pNIPAM and L-pNIPAM-co-DMAc cultures following 3 weeks ($P < 0.05$) (Figure 3.11).

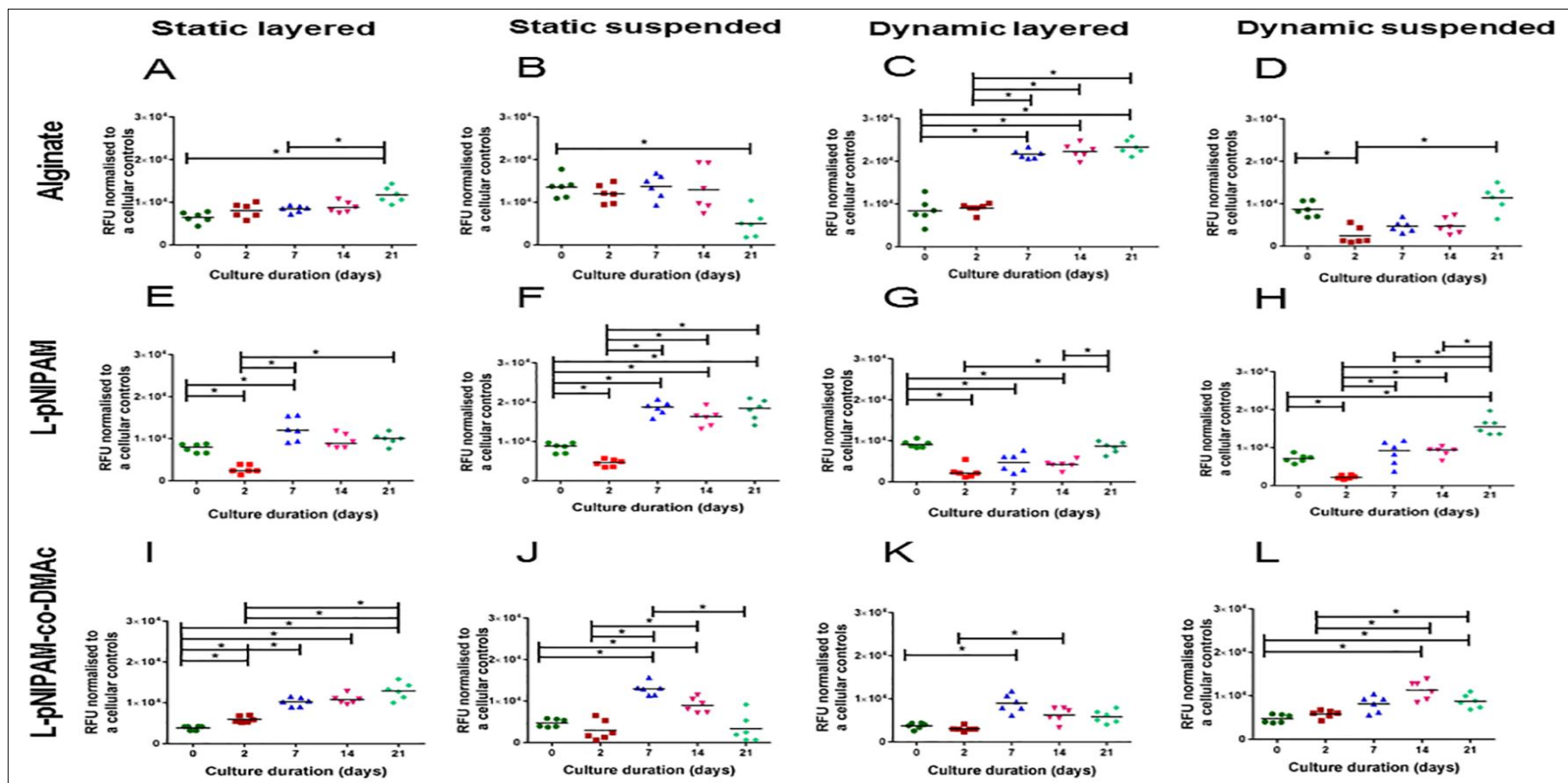


Figure 3.11: Metabolic activity of HT29-MTX cells at a cell density of 2×10^6 cells/ml layered on or suspended within Alginate: (A, B, C and D); L-pNIPAM: (E, F, G and H); L-pNIPAM-co-DMAC: (I, J, K and L) following 21 days under static or dynamic culture conditions. * $p \leq 0.05$.

3.3.7 Morphological and phenotypic assessment of HT29-MTX cells cultured in hydrogel systems

HT29-MTX cells cultured in layers on alginate under either static or dynamic culture conditions formed multilayer spheroids following 2 days (Figure 3.12), which continuously enlarged over the 21 days of culture (Figure 3.13, Figure 3.14 A, and Figure 3.15 A). However, multilayers of HT29-MTX cells were observed when cells were layered on alginate hydrogel scaffolds under static and dynamic culture at day 21 (Figure 3.14 A, and Figure 3.15 A). In contrast, HT29-MTX cells layered on L-pNIPAM under static and dynamic culture conditions at day 2, 7, 14 and 21, accumulated as multilayers of cells and formed villus-like structures at 14 and 21 days (Figure 3.12, Figure 3.13, Figure 3.14 A, and Figure 3.15 A). This differed considerably to suspended HT29-MTX cells, which migrated to the surface of L-pNIPAM and formed a multilayer of cells under static conditions propagating the formation of villus-like structures under dynamic conditions (Figure 3.14 A, and Figure 3.15 A). As a result by day 21, well-developed mucosal-like layers formed when HT29-MTX cells were layered on and suspended in L-pNIPAM-co-DMAc under both static and dynamic culture conditions (Figure 3.14 A, and Figure 3.15 A). HT29-MTX cells grown for 21 days on and in the three hydrogel systems under dynamic and static culture differentiated to form mucus-producing goblet-like cells (Figure 3.14 B, and Figure 3.15 B). Whilst background staining for acidic mucins was again high in no cell controls, clear increases in intensity for acidic mucins were observed around cells in all cultures of HT29-MTX cells (Figure 3.15). Although acidic and neutral mucins were secreted by the HT29-MTX cells in all cultures the secretion patterns varied. In alginate, acidic and neutral mucins were secreted in all culture conditions at day 14 and 21 (Figure 3.14 B, and

Figure 3.15 B). Increased secretion of acidic mucin over neutral mucin was observed in L-pNIPAM hydrogel scaffolds. Furthermore, mucus covered the HT29-MTX cells by day 21, in all culture conditions. Although the secretion of acidic mucin was observed in HT29-MTX cells layered on and suspended in L-pNIPAM-co-DMAc, neutral mucins were also detected after day 21, under both static and dynamic culture (Figure 3.14 B, and Figure 3.15 B).

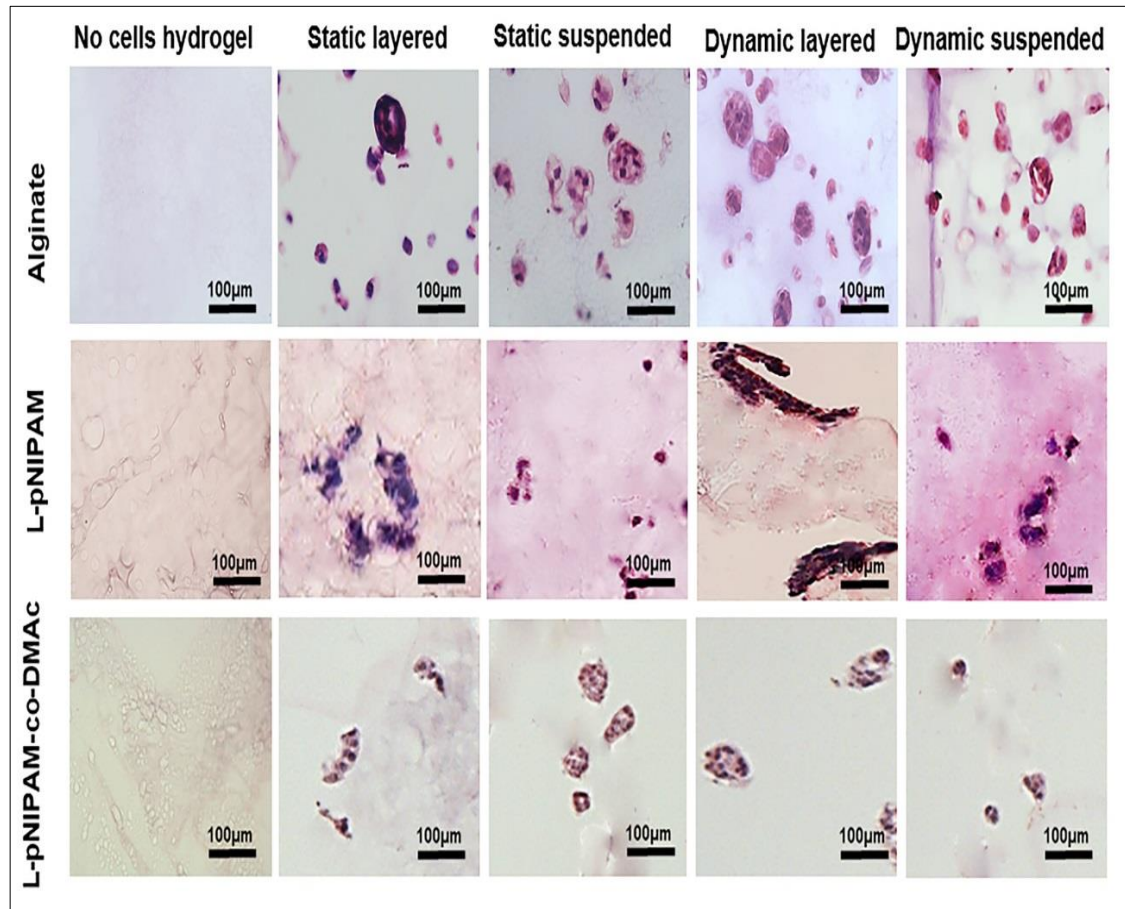


Figure 3.12: Histological analysis of HT29-MTX cells layered on or suspended within alginate, L-pNIPAM, and L-pNIPAM-co-DMAc hydrogels under static or dynamic culture conditions at a cell density of 2×10^6 cells/ml following 2 days stained with H&E. Scale bar = 100µm.

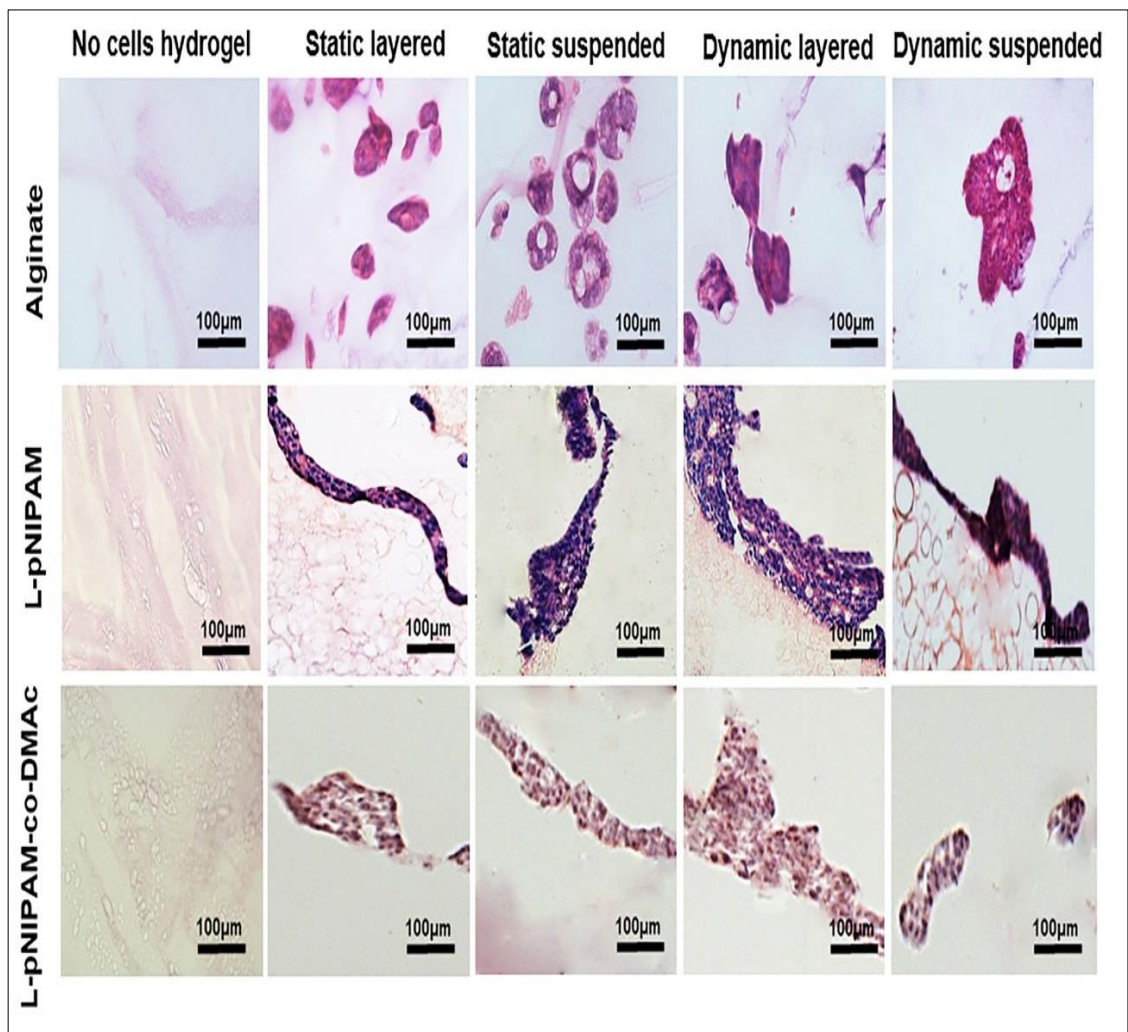


Figure 3.13: Histological analysis of HT29-MTX cells layered on or suspended within alginate, L-pNIPAM, and L-pNIPAM-co-DMAC hydrogels under static or dynamic culture conditions at a cell density of 2×10^6 cells/ml following 7 days stained with H&E. Scale bar = 100 μ m.

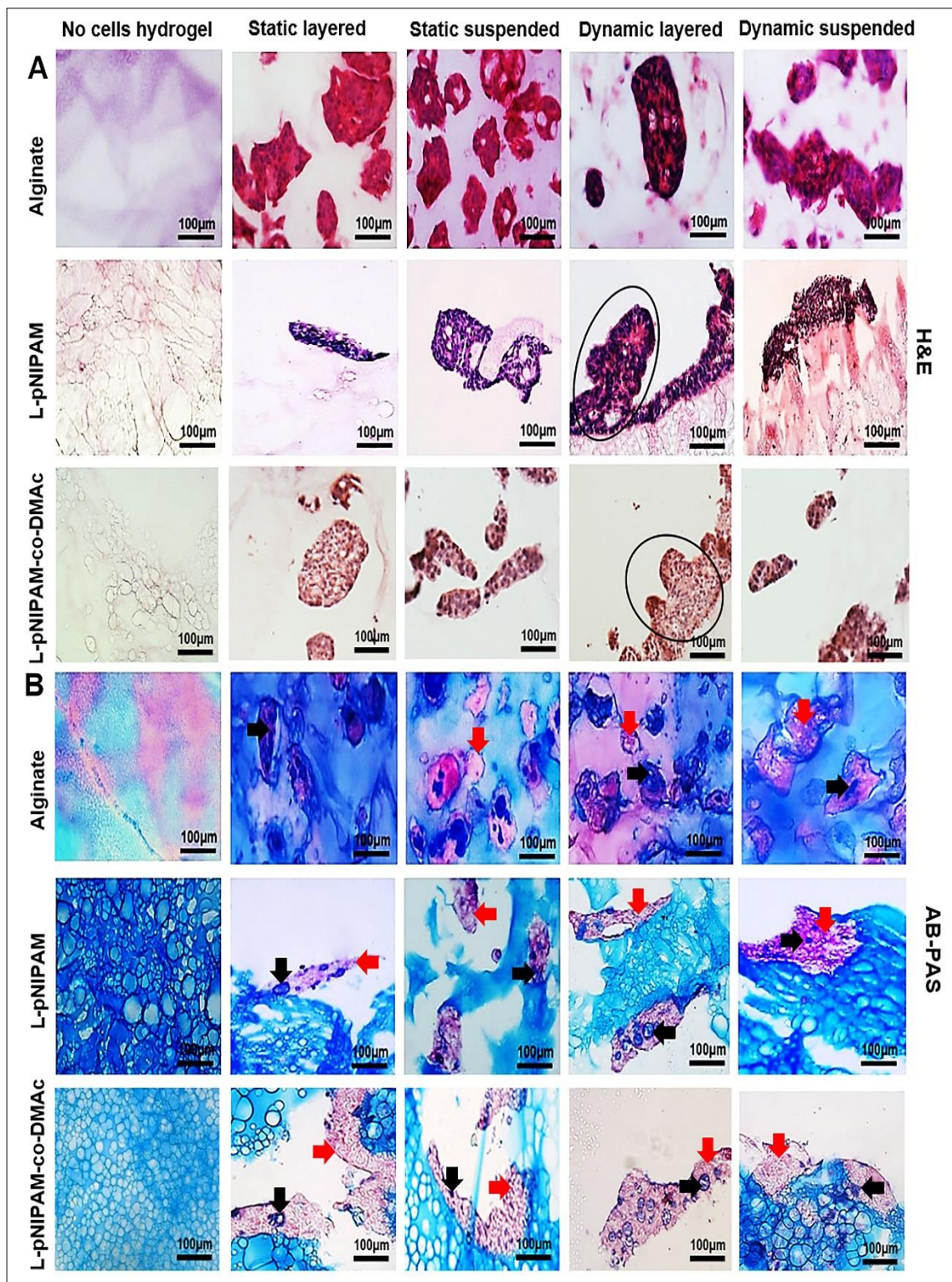


Figure 3.14: Histological analysis of HT29-MTX cells layered on or suspended within alginate, L-pNIPAM, and L-pNIPAM-co-DMAC hydrogels under static or dynamic culture conditions at a cell density of 2×10^6 cells/ml following 14 days. A: Stained with H&E (circles indicate villus like structures) and B: stained with Alcian blue/PAS, blue: acidic mucin (black arrows); magenta: neutral mucin (red arrows). Scale bar = 100 μ m.

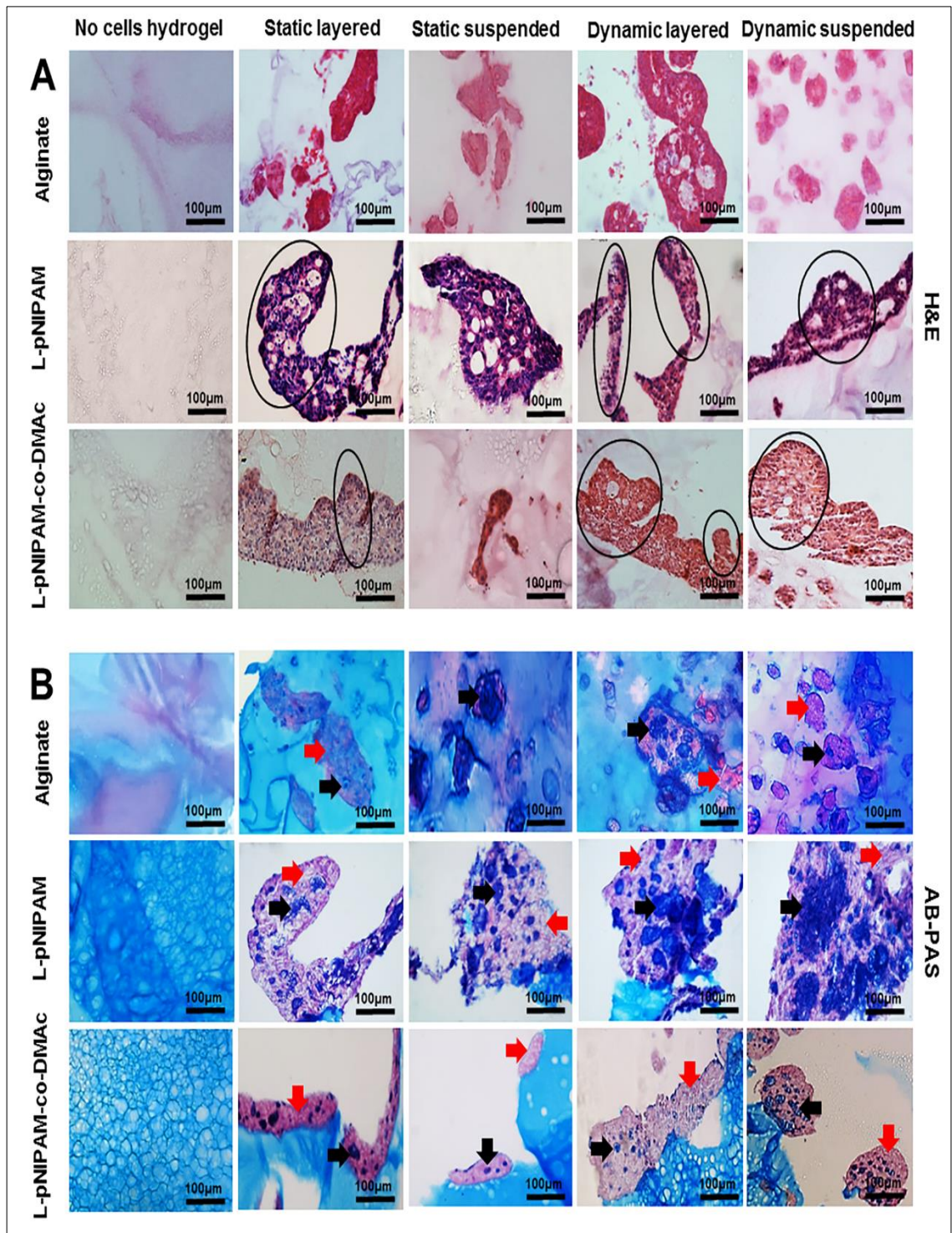


Figure 3.15: Histological analysis of HT29-MTX cells layered on or suspended within alginate, L-pNIPAM, and L-pNIPAM-co-DMAc hydrogels under static or dynamic culture conditions at a cell density of 2×10^6 cells/ml following 21 day. A: stained with H&E (circles indicate villus like structures) and B: stained with Alcian blue/PAS, blue: acidic mucin (black arrows); magenta: neutral mucin (red arrows). Scale bar = 100 μ m.

Immunopositivity for MUC2 and MUC5AC was observed in control cytospun HT29-MTX cells grown in monolayer (Figure 3.16 A). Higher levels of MUC2 immunopositivity was seen in HT29-MTX cells cultured in layers on alginate scaffolds compared to those suspended within alginate (Figure 3.16 B). Interestingly HT29-MTX cells cultured on or in L-pNIPAM hydrogel scaffolds showed some immunopositivity for MUC2 and a high level of immunopositivity for MUC5AC (Figure 3.16 C). Whereas HT29-MTX cells layered on and suspended within L-pNIPAM-co-DMAc under static and dynamic culture conditions displayed weak immunopositivity for MUC2 with high immunopositivity for MUC5AC (Figure 3.16 D).

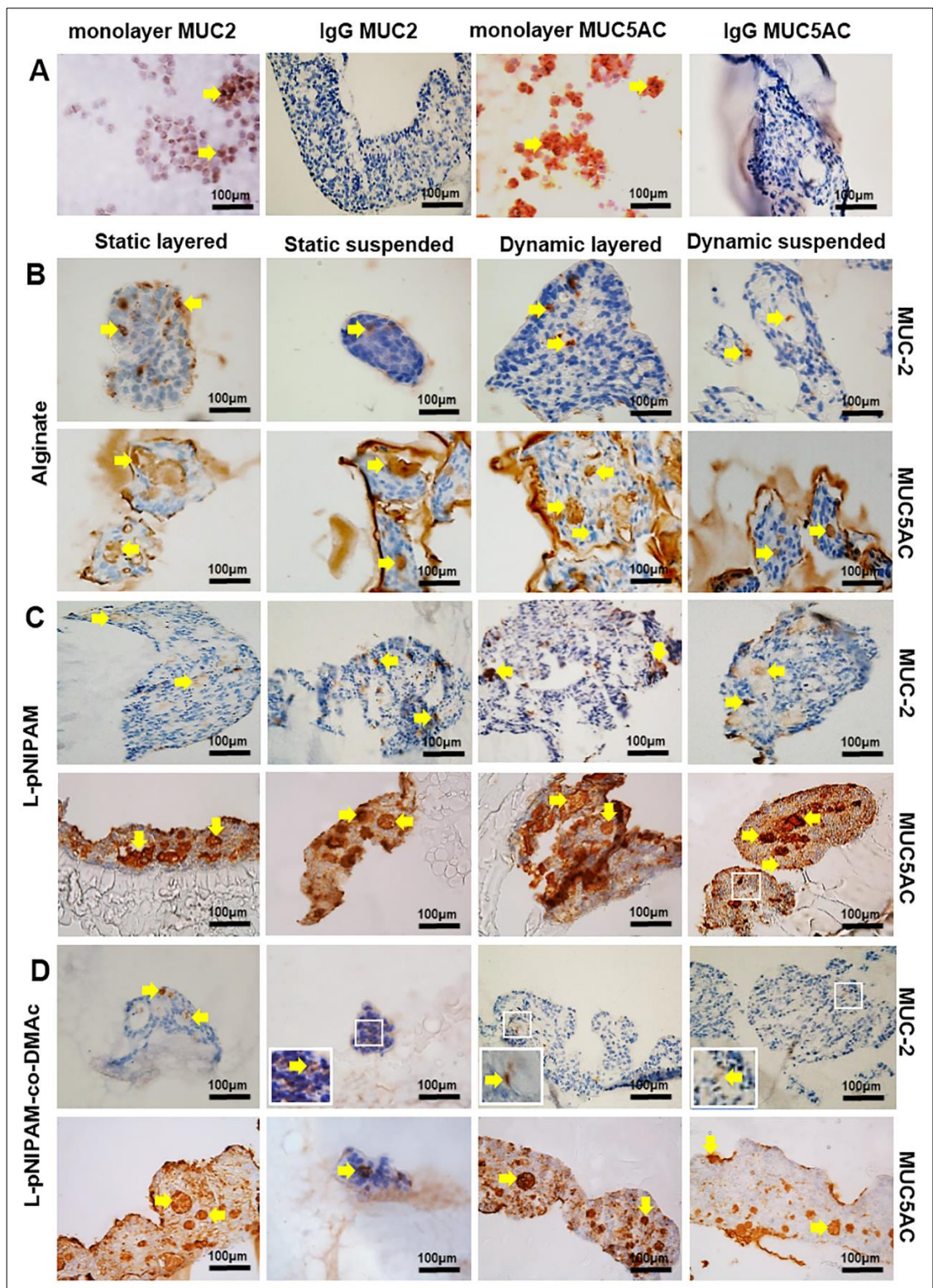


Figure 3.16: Immunohistochemistry staining (yellow arrows) of MUC2 and MUC5AC. A: monolayer and IgG negative control. HT29-MTX cells layered on or suspended within B: Alginate, C: L-pNIPAM, and D: L-pNIPAM-co-DMAc hydrogels under static or dynamic culture conditions at a cell density of 2×10^6 cells/ml following 21 day. Cell nuclei were stained with haematoxylin (blue). Scale bar = 100 μm.

3.3.8 Scanning electron microscopy of HT29-MTX cells

SEM analysis of HT29-MTX cells suspended within and layered on L-pNIPAM and L-pNIPAM-co-DMAc hydrogel scaffolds under static and dynamic culture conditions at 21 days, showed the presence of cells within or on the surface of the hydrogel (Figure 3.17 A, B). Although HT29-MTX cells were suspended within L-pNIPAM and L-pNIPAM-co-DMAc hydrogel scaffolds, cells migrated to the surface of the hydrogels, where cells formed circular clusters of cells when cultured under static and dynamic culture conditions. It was found that the HT29-MTX cells layered on the hydrogels under both static and dynamic conditions; covered the hydrogels (Figure 3.17 A, B, and Figure 3.10).

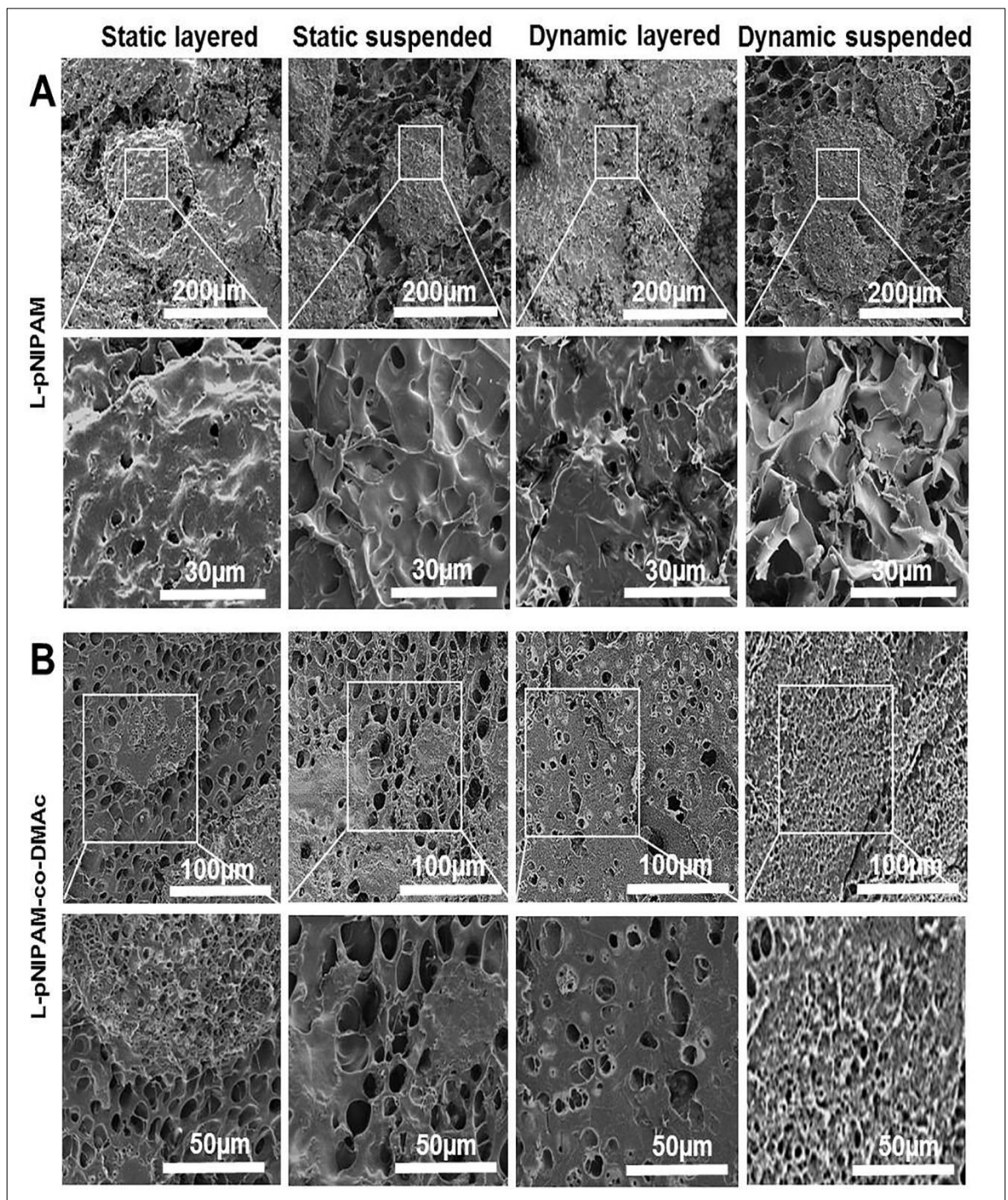


Figure 3.17: Scanning electron micrographs for HT29-MTX cells layered on or suspended within A: L-pNIPAM and B: L-pNIPAM-co-DMAc hydrogels under static or dynamic culture conditions at a cell density of 2×10^6 cells/ml following 21 day. Squares indicate areas of magnifications. Scale bar = 30 μ m to 200 μ m.

3.4 Discussion

The human intestinal Caco-2 and HT29-MTX cells have been utilized as *in vitro* models of enterocytes and goblet cells, respectively (Chen *et al.* 2010). Here, three hydrogel systems were investigated to determine which would support 3D culture of Caco-2 and HT29-MTX cells, and give rise to the villus architecture of the small intestine *in vitro*. Previous studies have reported the importance of pore size, mechanical properties, microenvironment such as pH and oxygen concentration and culture conditions in the differentiation and functionality of cells (Engler *et al.* 2006; Jaasma *et al.* 2008; Pusch *et al.* 2011; Knight *et al.* 2013; Li *et al.* 2013). Interestingly, the pH of the hydrogel used here and the microenvironment of the natural small intestine both are basic (Kozlolek *et al.* 2014). *In vitro*, pore size (pore diameter) can influence cell migration into the scaffold from its surface and this migration depends on the cell type (Knight *et al.* 2013). Thus, this study compared cell behaviour in a softer and larger pores alginate versus stiffer and smaller pores synthetic non-biodegradable scaffolds developed in our laboratory (Boyes 2012; Thorpe *et al.* 2016; Boyes *et al.* 2016); and compared cells cultured in suspension or as layers and maintained under static versus dynamic culture conditions. However, it is also worth noting that the crosslinking type will also affect cellular migration, namely the ionic crosslinking seen with alginate will form a more fixed structure preventing cellular migration. Whilst the physical entanglement seen in the L-pNIPAM hydrogels where cells can effectively push their way through the hydrogel.

Long-term static culture has been shown to contribute to decreased cell viability and extracellular matrix production (Jaasma *et al.* 2008), thus, in this study an orbital shaker was utilized as a simple way to simulate dynamic culture conditions. This study showed that not only the static or dynamic culture

conditions impacted on the metabolic activity of Caco-2 and HT29-MTX cells but also the cellular localization within or on the three hydrogels affected metabolic activity and tissue architecture.

To characterize the 3D culture models *in vitro*, the metabolic activity of Caco-2 and HT29-MTX cells were assessed within the three hydrogel scaffolds. The natural biodegradable scaffold: calcium cross-linked alginate; maintained the metabolic activity of Caco-2 and HT29-MTX cells for 21 days in some of the culture conditions and induced formation of cell spheroids. In contrast, the metabolic activity was decreased when Caco-2 cells were layered on alginate and cultured under dynamic culture and when HT29-MTX cells were suspended within alginate and cultured under static culture conditions. These differences between Caco-2 and HT29-MTX cells may be attributed to differential expression or properties of cell receptors. Simon-Assmann *et al*, (1994; 1998) and Orian-Rousseau *et al* (1998) demonstrated that Caco-2 and HT29-MTX cells produced different types of integrins and that this could affect how these cells grow in culture. Simon-Assmann *et al* (1994) showed that undifferentiated and differentiated HT29 cell populations cultured on laminin produced different laminin-binding integrins and grew differently under identical culture conditions. These differences in integrins may in part explain the difference in the growth seen in the HT29-MTX and Caco-2 cells observed in this current study. In addition, the mechanical properties of alginate may also impact on cell proliferation, migration, differentiation, and morphological organisation (Banerjee *et al*. 2009). This study demonstrated that suspended Caco-2 and HT29-MTX cells migrated into the surface of alginate following 21 days under static culture conditions due to shortage of O₂ and nutrients. The mechanical properties of alginate are time dependent, the strength of alginate decreases

gradually during the first few weeks of culture, due to the loss of calcium ions (LeRoux *et al.* 1999). Furthermore, the average pore size of alginate probably increased and shifted to larger pores due to decreased cross linking which resulted from the diffusion of calcium ions out of the alginate.

Taken together, the variable metabolic activity and spheroid morphology observed when Caco-2 and HT29-MTX cells were cultured in alginate could in part be a result of the poor stability and changing properties seen in alginate; when used as a 3D scaffold in long-term cell culture. Scaffold stability would be essential to maintain cells demanding stability and time to produce their own matrix (Wang *et al.* 2009a), alginate was shown to have low storage moduli indicating a soft hydrogel and thus could have impacted on stability with time (Shoichet *et al.* 1996). Due to the fact that the mechanical properties of the hydrogel can be controlled and strengthened by controlling the components concentrations and gelation time (Cao 2011). It would be interesting to investigate the effect of cells cultured within a range of alginate concentrations, CaCl₂ concentrations and gelation time in order to increase the storage moduli could improve the alginate stability and strength its mechanical properties.

Caco-2 and HT29-MTX cells are sensitive to calcium and express the calcium-sensing receptor (Poquet *et al.* 2008; Davies *et al.* 2008) the main effects of calcium on these cells appear to be on cellular migration (Peignon *et al.* 2006) and adhesion molecules (Bernet *et al.* 1993). Transepithelial electrical resistance (TEER) values increased in Caco-2 cells treated with 1.6 mM Ca²⁺ for 1 h (Davies *et al.* 2008). However, within alginate cultures with the exception of the 10 minute polymerisation time, where cells are exposed within the alginate to 200 mM CaCl₂, the Ca²⁺ is bound within the alginate as a cross

linker as is not freely accessible to cells. During the preparation of alginate, following polymerisation the alginate is washed with NaCl and media, and media is changed every 48 h, thus any remaining free Ca^{2+} would be rapidly removed. Chan & Mooney *et al.* (2013) demonstrated that in alginate which was unwashed following polymerisation 50% of the Ca^{2+} was released into the media over the first 10 h. Thus, following the 3 weeks of culture in this study and extensive washes following polymerisation, limited free Ca^{2+} would be available for cellular uptake. In the bound form Ca^{2+} may be involved in activation of the Ca^{2+} sensing receptor but due to its bound form is unlikely to be able to be taken up into cells and thus at the later time points of 2 and 3 weeks of culture it is unlikely to have had a major effect on the cellular behaviour.

Here, this study investigated the capacity of synthetic porous, non-biodegradable, non-fabricated, cross-linked network structures which are highly hydrated and similar to the native microenvironment of the small intestine to determine their ability to provide the mechanical support for cellular proliferation and differentiation. Interestingly, the phenotype of Caco-2 and HT29-MTX cells were similar in L-pNIPAM and L-pNIPAM-co-DMAc. The metabolic activity of Caco-2 and HT29-MTX cells were increased when layered on these hydrogels under both static and dynamic culture; with both cell lines shown to form villus-like structures under dynamic culture. The observed increases in metabolic activity and formation of the villus-like structure under dynamic culture conditions and the migration of the suspended HT29-MTX cells into the surface of the synthetic hydrogel may be due to the flow of nutrients and oxygen over cells, the fluid flow induced in these cultures will mimic the fluid flow of nutrients in the small intestine. This efficient delivery of nutrients and oxygen enabled

Caco-2 and HT29-MTX cells to reorganize into 3D villus-like structures that remained viable for the 21 days investigated. Furthermore, these synthetic hydrogels provided a hydrated space for the diffusion of nutrients and metabolites to and from the Caco-2 and HT29-MTX cells. Thus, stimulating the production of extracellular matrix (ECM) demonstrated here by the production of mucins. Moreover, increased cell adhesion seen through expression of adhesion factors, interestingly, Caco-2 cells are known to increase cell-cell adhesion through the production of E-cadherin-actin complexes (Peignon *et al.* 2006), and are shown to adhere to decellularized scaffolds and form villus-like structures when grown under dynamic culture conditions (Pusch *et al.* 2011).

In the synthetic hydrogel models, when Caco-2 cells were suspended within either L-pNIPAM or L-pNIPAM-co-DMAc the metabolic activity of cells was reduced, compared to alginate. It seems possible that these decreases in metabolic activity were due to reduced nutrient diffusion through the synthetic hydrogels. This is supported by the decreased pore size and increased stiffness seen in these synthetic hydrogels. This finding, however, is contrary to the groups' previous study with mesenchymal stem cells, which had excellent metabolic activity and cell differentiation within L-pNIPAM-co-DMAc (Thorpe *et al.* 2016). These differences in metabolic activity within the hydrogel may reflect the relatively higher metabolic rate of the Caco-2 cells compared to mesenchymal stem cells. This leads to the suggestion that Caco-2 cells are more sensitive to reduced nutrient supply and/or diffusion of waste material when suspended within either L-pNIPAM or L-pNIPAM-co-DMAc. In addition, there are many parameters which can influence cell behaviour in 3D synthetic scaffolds such as cross-linking, density, porosity, and biodegradability (Drury & Mooney 2003). Mechanical properties of biomaterials have been shown

previously to drive differentiation of cells. For example, Baker *et al* (2009) found that the stiffness of the extracellular matrix plays an important role in increasing the intracellular mechanical properties of prostate cancer cells when mixed with different concentrations of type I collagen matrix. Thus, the differential stiffness seen within these systems could explain at least in part the behaviour of cells within this study. Unfortunately comparison to the storage moduli of intestinal tissue was not possible within the current study. Recently, Stewart *et al* (2018) reported that the effective total modulus of human small bowel is 3.98 kPa.

Mucins are an intrinsic part of the small intestinal niche, and these proteins give rise to an adherent mucus layer that coat the intestinal mucosa (Kitamura *et al.* 1996). Mucins provide protection against pathogens and autodigestion and act as a medium for digestion and absorption (Kitamura *et al.* 1996; Moncada *et al.* 2003). *In vivo* MUC2 and MUC5AC mucins are secreted and gel-forming mucin types and are expressed by intestinal cells to variable amounts (Kim & Gum 1995; Bu *et al.* 2010; Kim & Ho 2010). MUC2 is highly expressed in goblet cells of the small intestine and colon (Bu *et al.* 2011); whereas MUC5AC is not normally expressed in the small and large intestinal mucosa, and are mainly expressed in the stomach (Kim & Gum 1995; Bu *et al.* 2010). Within the hydrogel models, immunohistochemical analysis showed that MUC2 and MUC5AC were not expressed by Caco-2 cells under any culture conditions. The expression of MUC5AC gene has been previously observed in Caco-2 cells; however, this was measured by qRT-PCR and was not measured as protein production (Bu *et al.* 2011).

In the HT29-MTX cells, the results showed production of MUC2 and MUC5AC when cultured in and on L-pNIPAM or L-pNIPAM-co-DMAc under static or

dynamic cultures. These findings indicated a modification of predominantly MUC2 production to mostly MUC5AC in the HT29-MTX cells. This switching in mucin phenotype is common with formation of tumours and can be attributed to changes in the cell niche (Kitamura *et al.* 1996), thus, the switching seen in the current study may be due to the fact that HT29-MTX cells are derived from human colon adenocarcinoma. During gastrointestinal cancers there is often an up-regulation of the more viscous and protective MUC5AC during disease progression especially where auto digestion can occur (Wan *et al.* 2014).

In this study, the results have shown that the cell morphology varied dramatically between the three *in vitro* systems and indeed the native small intestinal epithelium. However, it was clear that the cell morphology was greatly influenced by the 3D microenvironment; with the presence of villus like structures being more common when cells were cultured on the surface of L-pNIPAM and L-pNIPAM-co-DMAc under dynamic culture conditions.

Immunohistochemical analysis showed the presence of CD10 and ZO-1 which confirmed the brush border and tight junction expression, respectively when Caco-2 cells were layered on L-pNIPAM under static and dynamic culture conditions. Despite the colonic origins of Caco-2 cells, when grown on L-pNIPAM they expressed small intestinal digestive enzymes sucrase-isomaltase, dipeptidyl peptidase IV, and alkaline phosphatase. Previous studies have also shown differentiation of Caco-2 cells into enterocyte-like cells, which mimic the cells of the small intestine (Jumarie & Malo 1991; Basson *et al.* 1996; Olejnik *et al.* 2003). However, it is important to note that not all Caco-2 cells produced sucrase-isomaltase; this may be due to the early passage of Caco-2 cells used in this study. This patchy expression of sucrase-isomaltase has been shown to vary in Caco-2 cells depending on the passage number (Chantret *et al.* 1994).

Hence, the results show that L-pNIPAM not only stimulates Caco-2 differentiation in both culture conditions but also maintained expression of enzymes which were expressed in monolayer. These results propose a positive communication between the L-pNIPAM and the Caco-2 cells. These findings are in agreement with the previous studies which showed an increase in alkaline phosphatase activity when Caco-2 cells grown as a monolayer on polycarbonate filters (Ferruzza *et al.* 2012) and when co-cultured with HT29-MTX cells on silk scaffolds (Chen *et al.* 2015). Similarly, Caco-2 cells cultured on the extracellular matrix proteins (collagen type I and the basement membrane components collagen type IV and laminin) also showed that the activity of alkaline phosphatase, dipeptidase II, and sucrase-isomaltase were significantly higher in cells grown on laminin or collagen type IV than cells grown on collagen type I for one week after confluence as a result of the effect of extracellular matrix proteins on the differentiation phenotype (Basson *et al.* 1996).

SEM analysis further confirmed Caco-2 differentiation when cultured in layers on L-pNIPAM under static and dynamic culture conditions. The results revealed the typical finger-like projections at the apical surface of Caco-2 cells layered on L-pNIPAM suggesting differentiation and formation of microvilli. Caco-2 cells spread and covered the surface of L-pNIPAM-co-DMAc under static and dynamic culture. It seems possible that these differences in the morphological characteristics could be due to differences in mechanical stiffness of these synthetic hydrogels (Boyes 2012; Thorpe *et al.* 2016).

This study reports for the first time that synthetic non-biodegradable hydrogels could be used as scaffolds for Caco-2 and HT29-MTX cells. The most effective

scaffold which supported both cell lines and induced the formation of the optimal villus like structures was L-pNIPAM when cells were layered on the surface and cultured under dynamic conditions. Despite these promising findings, future work is required to investigate the capacity of the L-pNIPAM as a scaffold to co-culture Caco-2 and HT29-MTX cells under dynamic culture conditions to develop a 3D model of the small intestinal epithelium.

In conclusion, Caco-2 and HT29-MTX cells were successfully layered on L-pNIPAM hydrogel scaffolds under dynamic culture conditions which supported the 3D culture of these cells and stimulated them to form villus-like structures, maintained differentiation into enterocyte-like cells and mucus-producing goblet cells, respectively which expressed phenotypic markers that mimicked the native small intestinal epithelium. Thus, L-pNIPAM has the potential to deliver a 3D culture of Caco-2 and HT29-MTX cells which is promising for further investigation and characterisation of 3D *in vitro* co-culture model which could be used in drug discovery, and studies investigating inflammatory bowel disease and used as an alternative to *in vivo* animal models in drug toxicity studies.

Chapter 4

Long-term *in vitro* 3D hydrogel co-culture model of inflammatory bowel disease.

4.1 Introduction

Inflammatory bowel disease (IBD) such as Crohn's disease is characterised by increased intestinal permeability due to intestinal mucosal barrier dysfunction, which may be a critical factor in the pathogenesis of IBD (Marano *et al.* 1998; Cui *et al.* 2010). Furthermore, increased infiltration of inflammatory cells into the lamina propria and submucosa of the small and large intestines are also observed (Elson *et al.* 1995). Several inflammatory mediators are believed to be associated with the development of IBD. Interleukin-1 beta (IL-1 β) and tumor necrosis factor alpha (TNF α) are endogenous proinflammatory cytokines that are increased during inflammation of the mucosa and are involved in the pathogenesis of IBD (Stevens *et al.* 1992; Breese *et al.* 1994; Rogler & Andus 1998). IL-1 β and TNF α are secreted by activated immune cells within the lamina propria during inflammation (Guan & Zhang 2017). Many studies have shown that there is an increased expression of IL-1 β and TNF α in intestinal biopsy specimens obtained from patients with IBD (Stevens *et al.* 1992; Reinecker *et al.* 1993; Marano *et al.* 1998; Coccia *et al.* 2012).

Similarly, hypoxia has been shown to impact on the permeability of intestinal epithelial cells (Wang *et al.* 2013b), and O₂ signaling plays an important role in the response to inflammation (Shah 2016). In healthy mucosa of the small intestine, epithelial cells survive in physiologic hypoxia, this results from counter-current exchange of blood flow which diminishes oxygen tension along the crypt-villus axis. A steep O₂ gradient exists in the normal intestine where PO₂ levels at lamina propria and submucosa are 4-8%, this decreases across the epithelial and mucus layer to less than 2% in the intestinal lumen (Colgan & Taylor 2010; Zheng *et al.* 2015; Zeitouni *et al.* 2016a). Intestinal epithelial oxygen tension has an important role in intestinal inflammation, which is

dysregulated in IBD (Shah 2016; Colgan *et al.* 2016). IBD results in increased hypoxia over the inflamed mucosa due to increased oxygen demands of innate immune cells that are recruited to the site of inflammation (Zeitouni *et al.* 2016a).

The normal intestinal epithelium contains a number of different epithelial cell types with a range of metabolic, digestive, and barrier functions (Walter *et al.* 1996; Kleiveland 2015). The two main cell types lining the intestinal epithelium are absorptive enterocytes and mucus-producing goblet cells (Antunes *et al.* 2013). The *in vitro* study of the pathogenesis of IBD requires the use of a cell model demonstrating as closely as possible the characteristics of the *in vivo* intestinal epithelium. However, to date, most *in vitro* models have used a single cell type, the human intestinal epithelial cell line Caco-2; which is derived from absorptive cells of human colon adenocarcinoma (Balimane *et al.* 2000; Ranaldi *et al.* 2003). Caco-2 cells, have been widely used to study absorptive functions and permeability of the intestinal epithelium. However, compared to *in vivo* conditions, these models have many limitations (Ferruzza *et al.* 2012; Béduneau *et al.* 2014). One of these limitations, is that Caco-2 cells form closely linked tight junctions, which resemble those of the colon, rather than the small intestine. This results in a poor permeability of the cell membrane. Furthermore, Caco-2 monocultures fail to produce an adherent mucus layer which is essential when recreating an intestinal inflammatory niche (Nolleaux *et al.* 2006; Béduneau *et al.* 2014; Kim *et al.* 2014; Lozoya-Agullo *et al.* 2017). Subsequently, this has led to the creation of a co-culture model which combines Caco-2 cells with the mucus-producing HT29-MTX cells; which are derived from goblet cells of human colon adenocarcinoma (Antunes *et al.* 2013; Béduneau *et al.* 2014).

A number of 2D co-culture systems of the small intestine have been developed. An *in vitro* co-culture model combining Caco-2 cells and goblet-like HT29-H cells were first characterised by Wikman-Larhed & Artursson in 1995. Later, Walter *et al.* (1996) established an *in vitro* co-culture model using Caco-2 and HT29-MTX cells. *In vitro* monocultures and co-cultures of Caco-2 and HT29-MTX cells have been successfully developed to study intestinal permeability (Li *et al.* 2013; Chen *et al.* 2015; Lozoya-Agullo *et al.* 2017). However, when this model has been used in monolayer the cells fail to develop the crypt-villus architecture seen in the small intestine. 3D monocultures and co-culture studies using various types of 3D scaffolds such as porous silk, collagen, and Poly-lactic-co-glycolic acid (PLGA) have been investigated (Costello *et al.* 2014a; Chen *et al.* 2015; Yi *et al.* 2017). For example, Chen *et al.*, (2015) co-cultured Caco-2 and HT29-MTX cells on geometrically engineered hollow porous silk scaffolds. The Caco-2 and HT29-MTX cells formed mucus layers and the lumen of this tube became filled with mucus. However, there was a reduction in cell function following a few weeks of culture. Similarly, the culture of Caco-2 cells as a monolayer on 3D fabricated villi-shaped collagen scaffolds was used to study drug absorption. However, the collagen scaffold was a barrier to the diffusion of some drugs and Caco-2 cells were unable to live for a prolonged period as the collagen scaffold degraded (Yu *et al.* 2012; Yi *et al.* 2017). In contrast, when Caco-2 and HT29-MTX cells were co-cultured on a 3D PLGA scaffold which was designed to replicate the architecture of the intestinal villi; the co-cultured cells migrated to the tips of the villi and underwent differentiation when stimulated by epidermal growth factor (EGF) (Costello *et al.* 2014b).

A limited number of studies have investigated inflammatory mediators within these culture systems. *In vitro* monolayer culture of Caco-2 cells treated with IL-

1 β and TNF α resulted in increased permeability of tight junctions (Marano *et al.* 1998; Al-Sadi & Ma 2007; Al-Sadi *et al.* 2010) and the production of inflammatory chemokines, such as IL-8 (Van De Walle *et al.* 2010). The effects of proinflammatory cytokines have also been investigated in some co-culture models. Leonard *et al.* (2010) and Susewind (2015) developed an inflamed 3D co-culture model of Caco-2 cells cultured with either macrophage (THP-1) and dendritic cells (MUTZ-3) derived from peripheral blood monocytes or with human immune cell lines. The macrophages and dendritic cells were embedded in type I collagen layers on a transwell filter insert, and then Caco-2 cells were cultivated on top. These co-culture models were then stimulated with IL-1 β for 2 days to model the inflamed intestinal mucosa. In these models, the inflamed co-cultures released higher amounts of IL-8 and increased TNF α expression compared to non-inflamed Caco-2 monocultures. However, these studies did not include mucus-producing cells.

Some *in vitro* studies have investigated the effects of hypoxia in simple culture systems, where hypoxia increased the production of IL-1 β and TNF α by human peripheral blood mononuclear cells following treatment with endotoxin (Ghezzi *et al.* 1991). Caco-2 cells have also been used to study the intestinal epithelial response to hypoxia (Zeitouni *et al.* 2016b). Lima *et al.* (2013) studied the effect of *Shigella flexneri* on co-cultured Caco-2 cells and rat hepatocytes in normoxia and hypoxia (<1% O₂) conditions, resulted in apoptosis. Similarly, Caco-2 cells cultured on polystyrene and grown under hypoxia at 1% O₂ showed a significant decrease in brush border membrane expression of β 1 integrins, which resulted in decreased *Y. enterocolitica* entry into Caco-2 cells (Zeitouni *et al.* 2016b). However, these studies did not consider the effect of pro-inflammatory cytokines and hypoxia conditions on 3D co-culture systems. The previous study

described in Chapter 3 established 3D *in vitro* culture models of the intestinal epithelium consisting of monocultures of Caco-2 and HT29-MTX cells layered on L-pNIPAM hydrogel scaffolds under dynamic culture conditions. This model supported the 3D culture of these cells generating villus-like structures and promoted differentiation, mimicking the native intestinal epithelium (Dosh *et al.* 2017).

Hence, with the purpose of developing a model which represents the cell types seen within the intestine, and under conditions seen during pathological conditions. This study investigated a long-term *in vitro* 3D co-culture model utilising Caco-2 and HT29-MTX cells and a novel L-pNIPAM hydrogel scaffold to mimic the natural epithelial layer of the native intestine. The co-culture model developed was then investigated under conditions representative of inflammation to determine its potential to study disease processes.

4.2 Materials and Methods

4.2.1 L-pNIPAM hydrogel scaffolds synthesis

The hydrogel was synthesised as previously described in Chapter 3 Section 3.2.1.2.

4.2.2 Monocultures and co-cultures of Caco-2 and HT29-MTX layered on L-pNIPAM hydrogel scaffolds

Six different percentages of cultured cells were investigated: 100% Caco-2 monocultures, 100% HT29-MTX monocultures and co-cultures of these cells in various initial seeding percentages (90% Caco-2 / 10% HT29-MTX, 85% Caco-2 / 15% HT29-MTX, 80% Caco-2 / 20% HT29-MTX, 75% Caco-2 / 25% HT29-MTX). To prepare layered cultures, 300 μL of liquid L-pNIPAM at 38-39°C was added to each well of the 48 well plates and 100 μL was added to each well of 96 well plates. Gelation of the L-pNIPAM was induced by cooling to below 32°C. Following gelation 300 μL or 100 μL of 2×10^6 total cells/ml (for each of the 6 cell culture suspensions) in complete media were applied to the surface of hydrogel construct in 48 and 96 well plates respectively, and following a 30 minute cell attachment period a further 200 μL or 150 μL complete media (Caco-2 culture media) was added to each well. All constructs were incubated at 37°C, 5% CO_2 under dynamic conditions using an orbital shaker at 30 rpm, with media replenished every 48 h. Metabolic activity assessments utilized 96 well plates and were determined using Alamar Blue assay following 0 h, 48 h, and weekly between 1 to 7 weeks. For histological assessment 48 well plate cultures were utilised. Cultures were maintained for an initial 6 weeks in standard culture conditions, following initial model development, cultures were divided into 3 groups as: (1) control; (2) treated with 10 ng/ml recombinant human IL-1 β (Peprotech, London, UK), (concentrations were selected from prior studies (Al-

Sadi *et al.* 2010; Susewind 2015), and (3) cultured under hypoxic conditions in an oxygen controlled glove box (Coy Lab products, York, UK) at 1% O₂ (under static culture conditions) for a further week prior to harvest.

4.2.3 Long-term co-cultures

Cell percentages of 90% Caco-2 / 10% HT29-MTX, and 75% Caco-2 / 25% HT29-MTX cultures were selected for long-term co-culture. These cultures were also treated with pro-inflammatory cytokines and hypoxia conditions to mimic inflammatory conditions. Cultures were either maintained for 12 weeks in standard media and dynamic culture as a control. Alternatively following 11 weeks in standard culture, co-cultures were treated with pro-inflammatory cytokines: 10 ng/ml recombinant human IL-1 β (Peprotech, London, UK); or 10 ng/ml recombinant human TNF α (Peprotech, London, UK) (concentrations were selected from prior studies (Enss *et al.* 2000; Cui *et al.* 2010), or 1% O₂ in an oxygen controlled glove box at 1% O₂ (under static culture conditions) for a further week in culture prior to harvest.

4.2.4 Alamar blue assessment of metabolic activity

The metabolic activity of monocultures and co-cultures layered on L-pNIPAM hydrogel scaffolds under dynamic culture conditions were assessed using Alamar blue assay (Life Technologies, Paisley, UK) in complete media after 0-7 weeks of culture following the manufacturer's protocol. The fluorescent intensity was recorded using a fluorescence microplate reader (CLARIOstar®, BMG LABTECH) at a fluorescence excitation wavelength of 590 nm. Relative fluorescence units (RFU) were recorded for cellular hydrogel scaffolds and normalized to RFU of acellular control scaffolds as an indication of total live cells.

4.2.5 Histological assessment

Monocultures and different percentages of co-cultures in 48 well plates were utilised for histological assessment. Triplicate samples for each culture condition and time point (2, 3, 4, 7, and 12 weeks) were fixed in 4% w/v paraformaldehyde/PBS for 24 h prior to washing in PBS and processed to paraffin wax in a TP1020 tissue processor (Leica Microsystem, Milton Keynes, UK). Four-micron sections were stained with Haematoxylin and Eosin (H&E); and Alcian blue/periodic acid Schiff (AB-PAS) as previously described in Chapter 3 Section 3.2.4.

The slides were examined with an Olympus BX51 microscope and images captured by digital camera and Olympus Cell Sens Standard software (Media Cybernetics, Buckinghamshire, UK).

4.2.6 Immunohistochemical assessment

Due to the L-pNIPAM hydrogel scaffold being non-biodegradable (Thorpe *et al.* 2016), it is not possible to extract cells RNA / protein and thus qualifying gene / protein expression is not possible, as a result immunohistochemistry for presence / absence qualitative changes are reported. Immunohistochemistry was performed on co-cultures containing 90% Caco-2 / 10% HT29-MTX, and 75% Caco-2 / 25% HT29-MTX following 7 weeks and co-cultures containing 90% Caco-2 / 10% HT29-MTX following 12 weeks under the various culture conditions. Immunohistochemistry for anti ZO-1 antibody, anti MUC2 antibody, anti MUC5AC antibody, anti alkaline phosphatase antibody (ALP), anti MMP2 antibody, anti MMP9 antibody, anti ADAMTS1 antibody, (antibodies details reported in Chapter 2 Section 2.2.3 and Chapter 3 Section 3.2.5), and anti caspase 3 antibody (1:400 rabbit polyclonal, none antigen retrieval) (Abcam,

Cambridge, UK) were determined. The slides were examined with an Olympus BX51 microscope and images captured by digital camera and Olympus cell Sens Standard software (Media Cybernetics, Buckinghamshire, UK).

4.2.7 Scanning electron microscopy for monocultures and co-cultures

Following 7 and 12 weeks in culture, constructs cultured with 90% Caco-2 / 10% HT29-MTX, and 75% Caco-2 / 25% HT29-MTX were processed for scanning electron microscopy (SEM) as described previously in Chapter 3 Section 3.2.6.

4.2.8 Statistical analysis

All metabolic activity assessments were performed at least 6 times. Normality of data was tested using a Skewness, Kurtosis, Royston Chi-sq, Shapiro Wilk W and Shapiro-Francia W tests, together with a q-q plot. From this analysis, it was demonstrated that the data sets were from mixed populations with some populations displaying potential normal distribution, but others were shown to be not normally distributed, as such non-parametric tests have been performed for all data. Therefore statistical comparisons were performed by Kruskal-Wallis with a pairwise comparison (Conover-Inman), each time points compared to time 0 of monocultures and co-cultures for 7 weeks for Alamar blue assay with statistical significance accepted at $P \leq 0.05$. All replicates have been shown with the median value indicated to demonstrate clearly the spread of replicates.

4.3 Results

4.3.1 Metabolic activity of monocultures and co-cultures of Caco-2 and HT29-MTX cells layered on L-pNIPAM hydrogel scaffolds under dynamic culture conditions

When Caco-2 monocultures were layered on the surface of L-pNIPAM hydrogel scaffold under dynamic culture, there was a significant increase in metabolic cell activity by week 2 to week 7 ($P \leq 0.05$) (Figure 4.1 A). In layered co-cultures of 90% Caco-2 / 10% HT29-MTX, there was a significant increase in metabolic activity from week 2 to week 7 ($P \leq 0.05$) (Figure 4.1 B). In contrast, the metabolic activity of layered co-cultures of 85% Caco-2 / 15% HT29-MTX significantly decreased from week 6 to week 7 ($P \leq 0.05$) (Figure 4.1 C). In layered co-cultures of 80% Caco-2 / 20% HT29-MTX, there was only a significant increase in metabolic activity between day 0 and 2 weeks ($P \leq 0.05$) (Figure 4.1 D). In layered co-cultures of 75% Caco-2 / 25% HT29-MTX; there was a significant increase in metabolic activity by week 6 to week 7 ($P \leq 0.05$) (Figure 4.1 E). When HT29-MTX monocultures were layered alone on L-pNIPAM hydrogel under dynamic culture, there was a significant decrease in metabolic activity from day 0 to 1 week then the metabolic activity remained constant and followed by a significant decrease in metabolic cell activity by week 6 and week 7 ($P \leq 0.05$) (Figure 4.1 F).

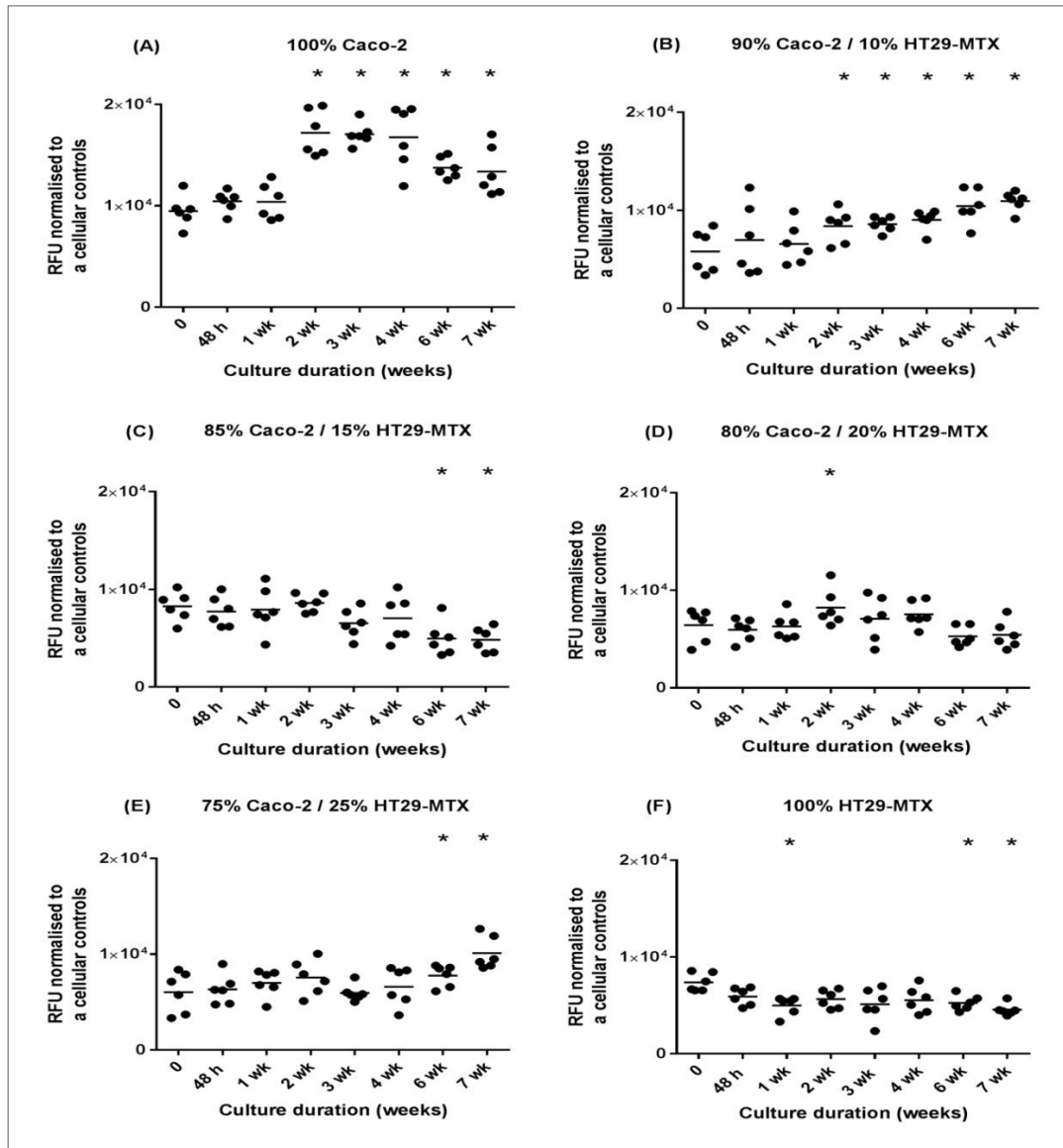


Figure 4.1: Metabolic activity of monocultures and co-cultures of Caco-2 and HT29-MTX cells at a total cell density of 2×10^6 cells/ml with different percentages A: Caco-2 cells alone; B: 90% Caco-2 / 10% HT29-MTX; C: 85% Caco-2 / 15% HT29-MTX; D: 80% Caco-2 / 20% HT29-MTX; E: 75% Caco-2 / 25% HT29-MTX; F: HT29-MTX cells alone layered on L-pNIPAM hydrogel scaffolds under dynamic culture conditions following 7 weeks. All replicates have been shown with the median ranges to clearly show the spread of replicates. * $P \leq 0.05$, and each time points was compared to time 0.

4.3.2 Morphological and phenotypic assessment of monocultures and co-cultures of Caco-2 and HT29-MTX cells layered on L-pNIPAM hydrogel scaffolds under dynamic culture conditions

When Caco-2 monocultures were layered on L-pNIPAM hydrogel scaffold and maintained under dynamic culture conditions, cells formed spheroid structures by 2 weeks which had villus-like structures between 3 to 7 weeks in culture (Figure 4.2). Layered co-cultures of 90% Caco-2 / 10% HT29-MTX formed multi-cellular layers over the surface of the hydrogel following 2 weeks. These co-cultured cells were well preserved and following 3 to 7 weeks formed villus-like structures (Figure 4.2). However, in layered co-cultures of 85% Caco-2 / 15% HT29-MTX cells and 80% Caco-2 / 20% HT29-MTX cells, multi-cellular layer were formed between 2 and 7 weeks (Figure 4.2). In layered co-cultures of 75% Caco-2 / 25% HT29-MTX, multi-cellular layers of cells were observed following 2 weeks of culture, which went on to form villus-like structures following 4 to 7 weeks (Figure 4.2). When HT29-MTX monocultures were layered on L-pNIPAM and maintained under dynamic culture conditions for 7 weeks, multi-cellular layers were observed in cultures between 2 and 3 weeks, which went on to form villus-like structures following 4 to 7 weeks in culture (Figure 4.2).

To determine potential mucin production, cell cultures following 3, 4, and 7 weeks in culture were stained using alcian blue/PAS. Alcian blue detects acidic mucins (blue) whereas PAS detects neutral mucins (pink magenta). Caco-2 monocultures were positive for neutral mucins, whereas both neutral mucins and acidic mucins were observed over all co-cultured cells and HT29-MTX monocultures following 3, 4, and 7 weeks in culture. An increase in intensity for

acidic mucins were observed in layered co-cultures of 75% Caco-2 / 25% HT29-MTX and in HT29-MTX monocultures (Figure 4.3).

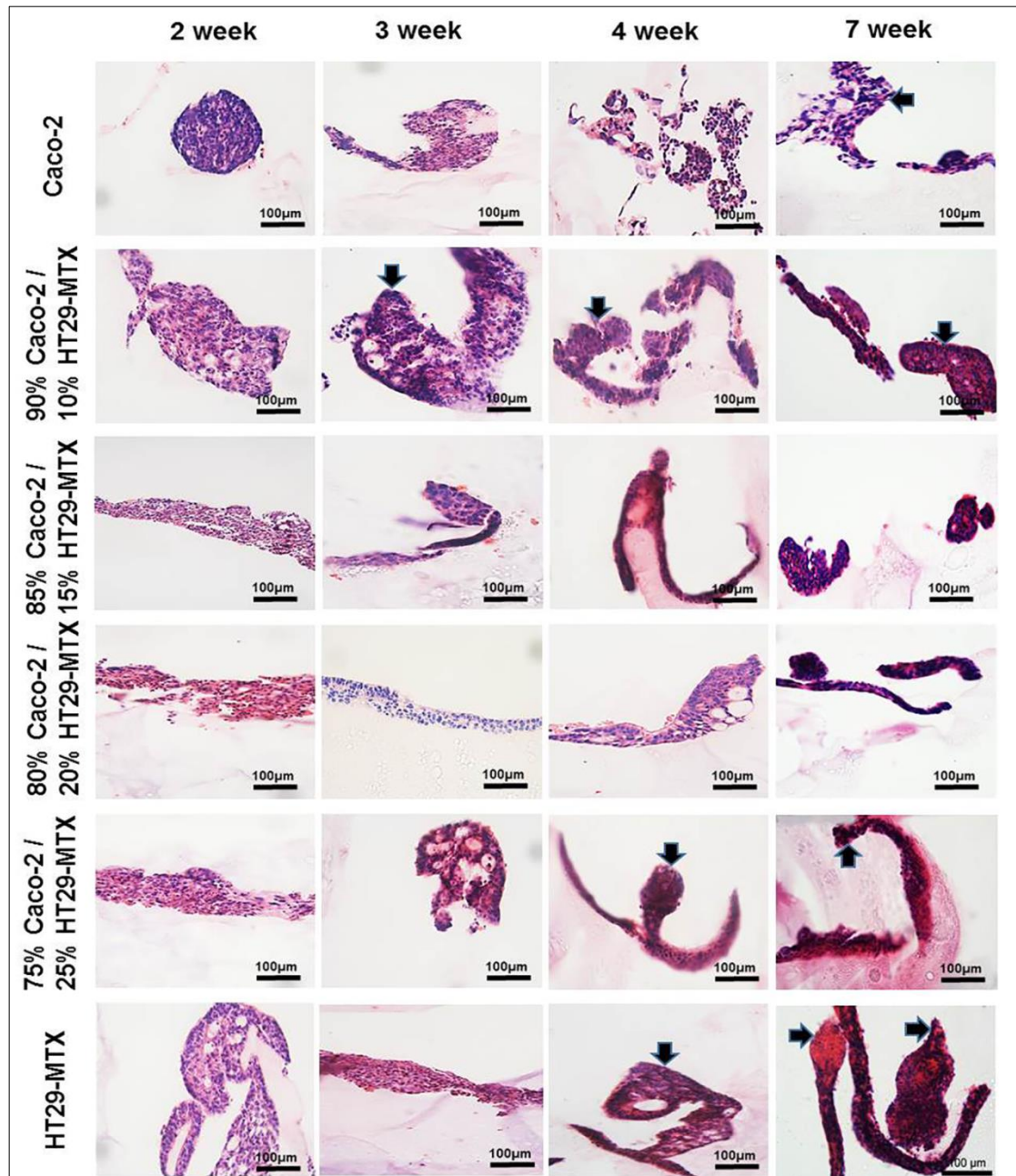


Figure 4.2: Morphology of monocultures and co-cultures of Caco-2 and HT29-MTX cells at a total cell density of 2×10^6 cells/ml with different percentages layered on L-pNIPAM hydrogel scaffolds under dynamic culture conditions following 7 weeks stained with H&E. The black arrows indicate the villus-like structures. Scale bar = 100 μ m.

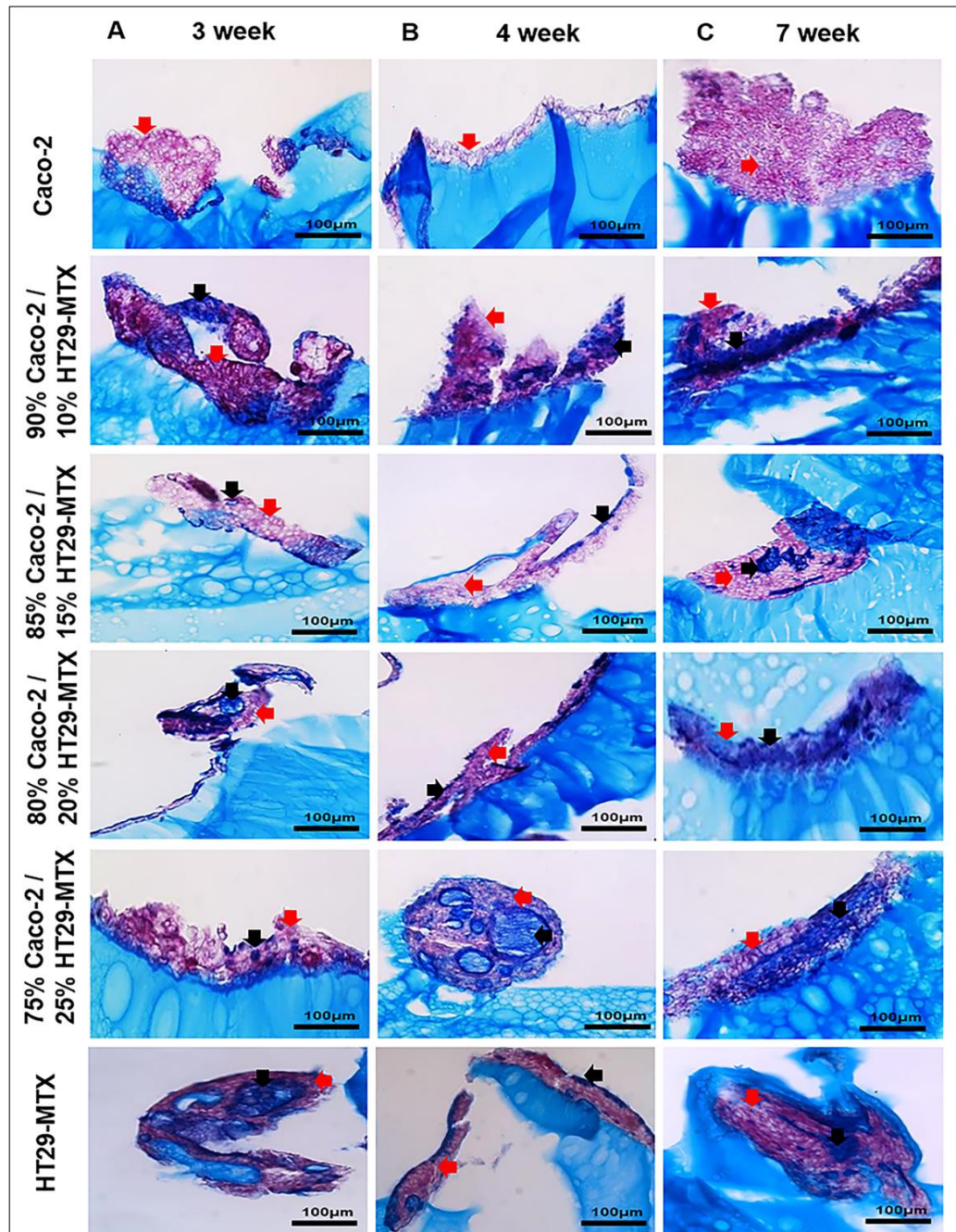


Figure 4.3: Mucin expression by monocultures and co-cultures of Caco-2 and HT29-MTX cells at different percentages layered on L-pNIPAM hydrogel scaffolds under dynamic culture conditions following A: 3 weeks; B: 4 weeks; and C: 7 weeks stained with AB-PAS, blue: acidic mucin (black arrows); magenta: neutral mucin (red arrows). Scale bar = 100 μ m.

4.3.3 Scanning electron microscopy of monocultures and co-cultures following 7 weeks

Examination of the surface of the monocultures and co-cultures by SEM showed the presence of morphological structures which resembled epithelial microvilli. These were identified in Caco-2 monocultures, and co-cultures containing: 90% Caco-2 / 10% HT29-MTX, and 75% Caco-2 / 25% HT29-MTX following 7 weeks in culture whilst HT29-MTX monocultures showed budding of the mucus producing goblet-like cells (Figure 4.4, white arrows).

4.3.4 Treatment monocultures and co-cultures with pro-inflammatory cytokines or cultured under hypoxic conditions

Following 6 weeks of dynamic culture in layers on L-pNIPAM hydrogel scaffold, monocultures and co-cultures were treated with pro-inflammatory cytokine IL-1 β (10 ng/ml) for 1 week under dynamic culture or cultured under hypoxic conditions at 1% O₂ for 1 week under static culture conditions. Among these cultures, layered co-cultures of 85% Caco-2 / 15% HT29-MTX, 80% Caco-2 / 20% HT29-MTX and HT29-MTX monocultures appeared to undergo cell death and cell debris were observed (Figure 4.5). Whilst layered Caco-2 monocultures, co-cultures of 90% Caco-2 / 10% HT29-MTX, and 75% Caco-2 / 25% HT29-MTX cells remained viable for the whole study period (Figure 4.5).

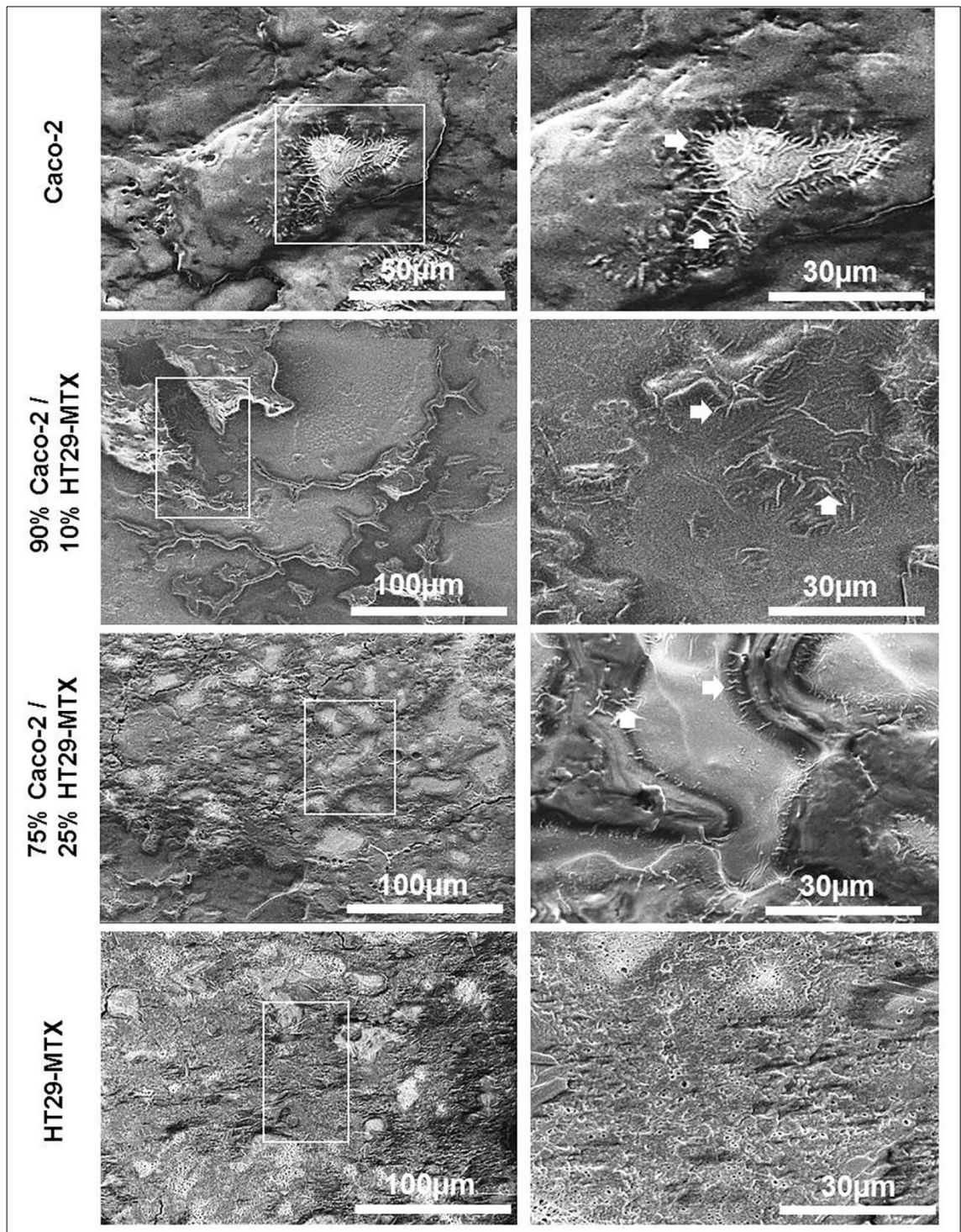


Figure 4.4: Scanning electron micrographs of monocultures and co-cultures of Caco-2 and HT29-MTX cells at different percentages layered on L-pNIPAM hydrogel scaffolds under dynamic culture conditions following 7 weeks showing microvilli-like structures (white arrows). Scale bar = 30 μm to 100 μm.

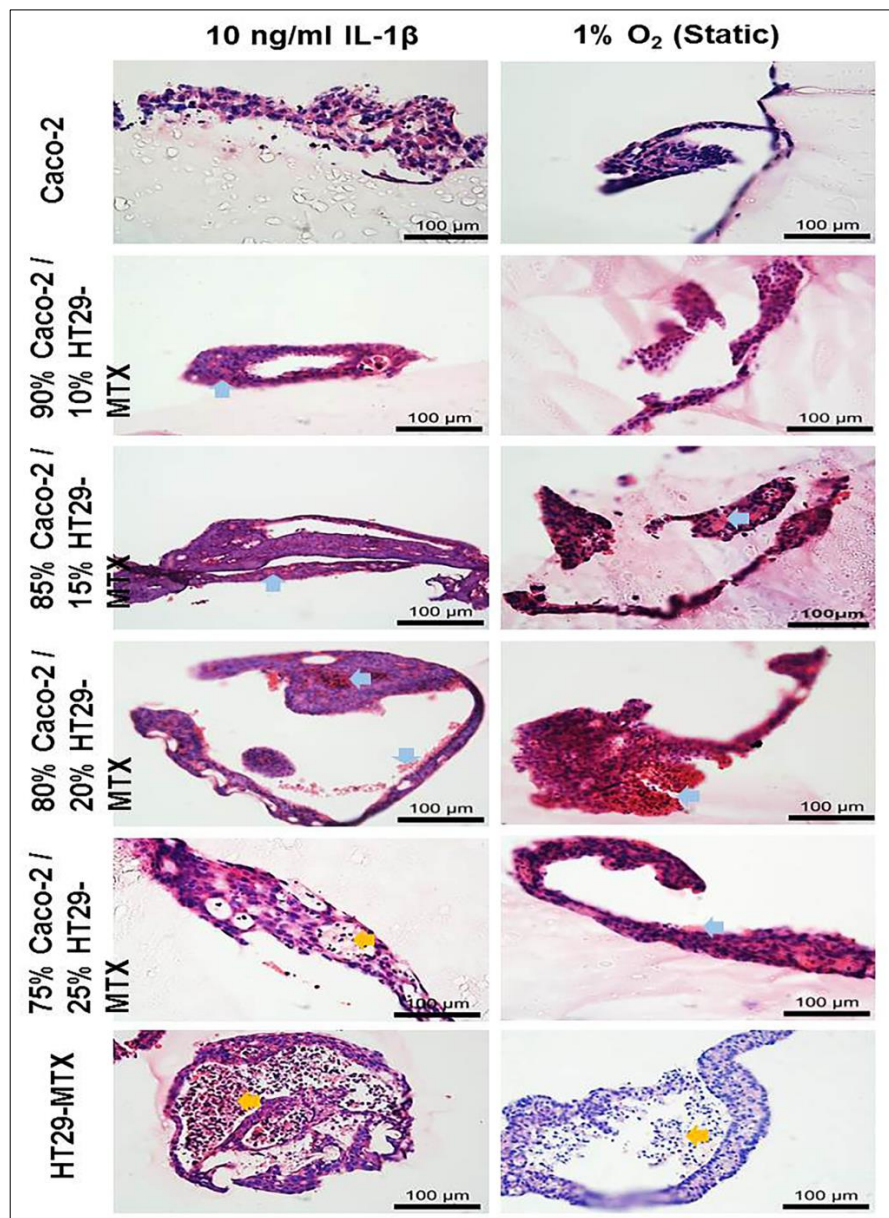


Figure 4.5: Morphology of monocultures and co-cultures of Caco-2 and HT29-MTX cells at different percentages layered on L-pNIPAM hydrogel scaffolds under dynamic culture conditions for 6 weeks and then treated with 10ng/ml IL-1 β for 1 week under dynamic culture conditions or hypoxic at 1% O₂ for 1 week under static culture conditions stained with H&E. The blue arrows indicate debris cells, the yellow arrows indicate dead cells. Scale bar = 100 μ m.

To determine features classically associated with IBD a number of markers were assessed by immunohistochemistry. In co-cultures containing 90% Caco-2 and 10% HT29-MTX cells, stimulation with IL-1 β and 1% O₂ decreased the expression of ZO-1, whilst increased expression of MUC2 compared to controls, MUC5AC was expressed in all cultures (Figure 4.6). ALP was highly expressed in the control, with less expression in cells treated with IL-1 β and 1% O₂ (Figure 4.6). MMP2 was expressed in the control and 1% O₂ cultures more than IL-1 β treated cells (Figure 4.6). Immunopositivity for MMP9 was not observed in any culture. ADAMTS1 was highly expressed in 1% O₂ culture compared to the control and IL-1 β cultures. Caspase 3 was expressed at low levels in the control but was not observed in IL-1 β and 1% O₂ treated cultures (Figure 4.6).

In co-cultures containing 75% Caco2 and 25% HT29-MTX cells, ZO-1 and MUC2 were highly expressed in the control with less expression in 1% O₂ and IL-1 β treated cultures (Figure 4.7). MUC5AC was positively expressed in all cultures. ALP was expressed in IL-1 β and 1% O₂ treated cultures compared to control (Figure 4.7). MMP2 was expressed in the control and 1% O₂ cultures more than IL-1 β treated cultures. Immunopositivity for MMP9 was not observed in any culture (Figure 4.7). ADAMTS1 was highly expressed in 1% O₂ culture compared to the control and IL-1 β treated cultures. Caspase 3 was expressed in 1% O₂ cultures but was not observed in control and IL-1 β treated cultures (Figure 4.7).

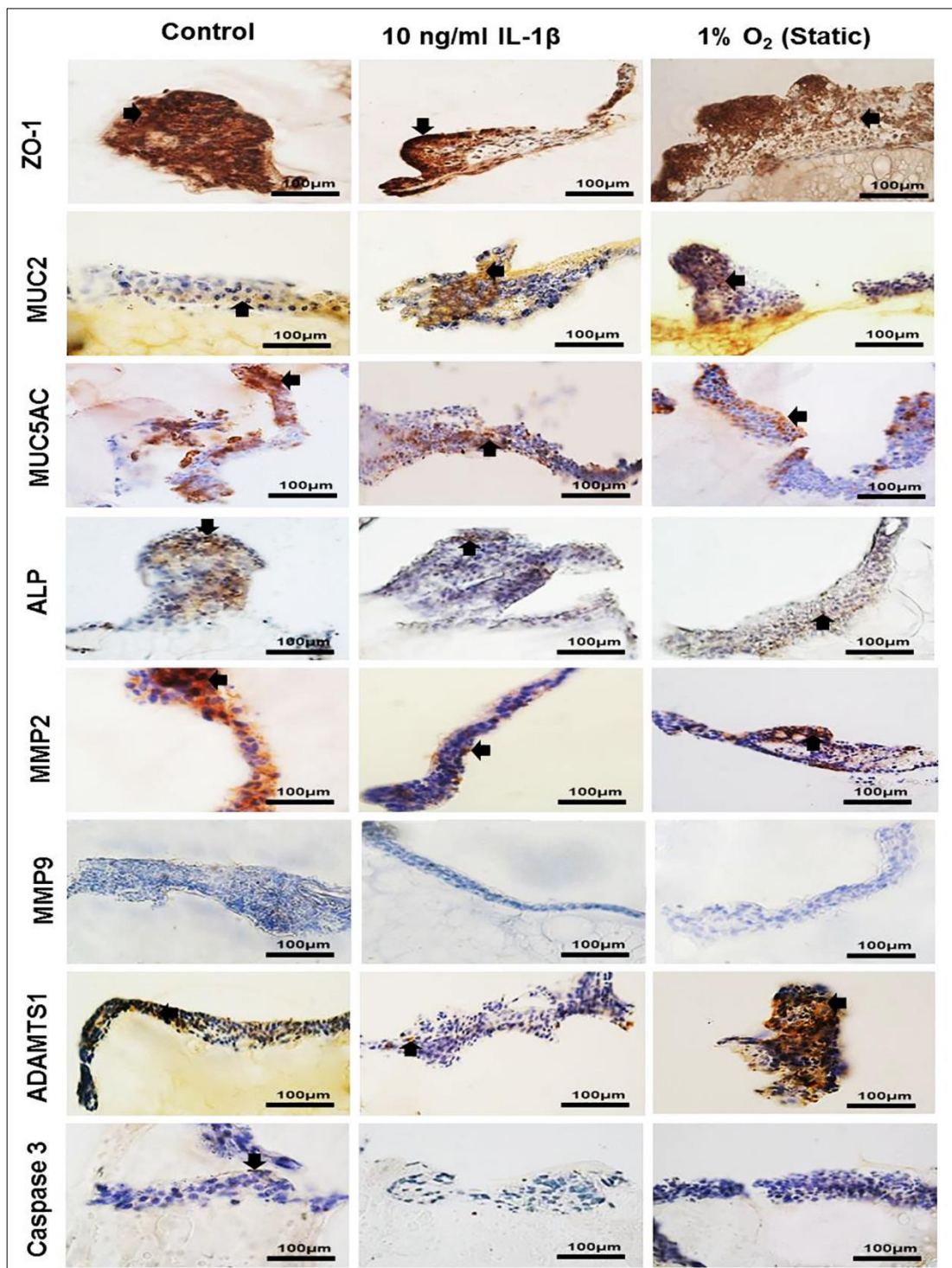


Figure 4.6: Immunopositivity (brown) of co-culture Caco-2 and HT29-MTX cells at percentages 90% Caco-2 / 10% HT29-MTX layered on L-pNIPAM hydrogel scaffolds under dynamic culture conditions following 7 weeks as a control or for 6 weeks and then treated with 10 ng/ml IL-1 β for 1 week under dynamic culture conditions or hypoxic at 1% O₂ for 1 week under static culture conditions. Cell nuclei were stained with haematoxylin (blue). The black arrows indicate positively stained cells. Scale bar = 100 μ m.

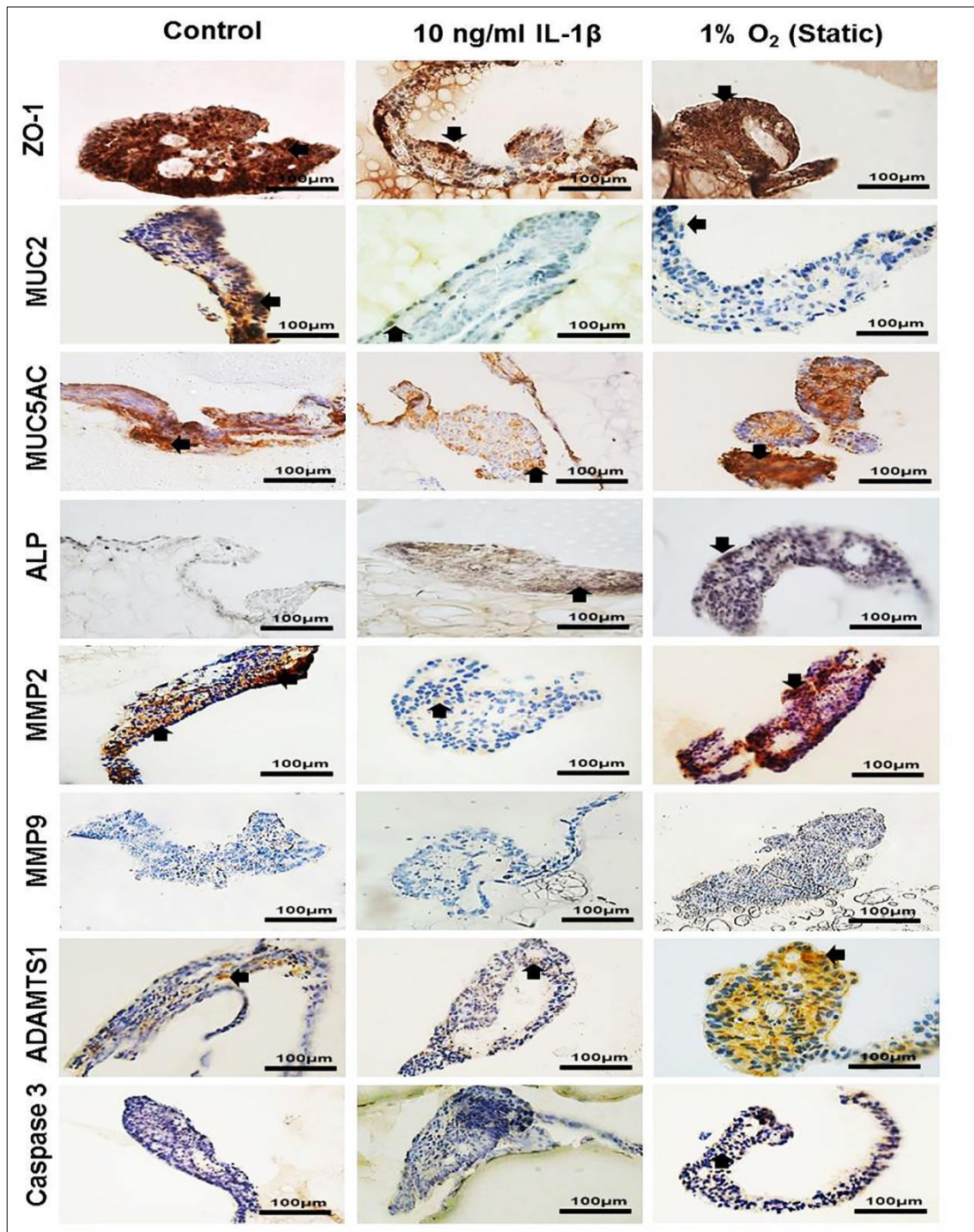


Figure 4.7: Immunopositivity (brown) of co-culture Caco-2 and HT29-MTX cells at percentages of 75% Caco-2 / 25% HT29-MTX layered on L-pNIPAM hydrogel scaffolds following 7 weeks as a control or for 6 weeks and then treated with 10ng/ml IL-1 β for 1 week under dynamic culture conditions or hypoxic at 1% O₂ for 1 week under static culture conditions. Cell nuclei were stained with haematoxylin (blue). The Black arrows indicate positively stained cells. Scale bar = 100 μ m.

To investigate the impact of long-term co-culture on cell behaviour, cell percentages of 90% Caco-2 / 10% HT29-MTX and 75% Caco-2 / 25% HT29-MTX cultures were selected for further long term culture. The non-stimulated co-culture of 90% Caco-2 / 10% HT29-MTX cultured as layers on the surface of L-pNIPAM hydrogels under dynamic culture conditions were well preserved and formed multicellular layers. In contrast, when co-cultured cells were treated with IL-1 β , only small cell clusters were seen. Whilst those cultures treated with TNF α cells showed poor nuclear morphology which is consistent with non-viable cells (Figure 4.8 A). This was confirmed by an increase in caspase 3 expression within these cells (Figure 4.9). However, when co-cultured cells were maintained at 1% O₂ for the final week of culture, cells formed multicellular spheroid like structures (Figure 4.8 A). Neutral and acidic mucins were observed in the control cultures and cultures maintained under 1% O₂ for the final week of culture, whilst lower levels of mucin were seen in cultures treated with IL-1 β and TNF α (Figure 4.8 A). In cultures containing 75% Caco-2 / 25% HT29-MTX, cells showed evidence of cell death following stimulation with IL-1 β and TNF α (Figure 4.8 B & Figure 4.9). Neutral and acidic mucins were observed in the control and at 1% O₂ (Figure 4.8 B). From this morphological assessment, co-cultures containing 90% Caco-2 and 10% HT29-MTX were selected for further investigation of the inflammatory response using immunohistochemistry staining.

As an indication of inflammation in the 90% Caco-2 / 10% HT29-MTX co-culture model, ZO-1, MUC2, ALP, MMP2, MMP9, and caspase 3 were investigated in the co-cultures stimulated with IL-1 β , TNF α , and 1% O₂ together with unstimulated controls using immunohistochemistry. ZO-1 was decreased in IL-1 β , TNF α and 1% O₂ compared to control suggesting an increase in membrane

permeability. IL-1 β , TNF α and 1% O₂ increased the expression of MUC2 compared to the control (Figure 4.9). ALP was highly expressed in the control and 1% O₂ compared to those treated with IL-1 β and TNF α . MMP2 was expressed in the control and 1% O₂ cultures but was not observed in IL-1 β and TNF α treated cultures (Figure 4.9). MMP9 was highly expressed in TNF α treated cultures with less expression in IL-1 β but was not observed in control and 1% O₂ cultures. Caspase 3 was highly expressed in TNF α treated cultures compared with IL-1 β and 1% O₂ cultures but was not observed in control (Figure 4.9).

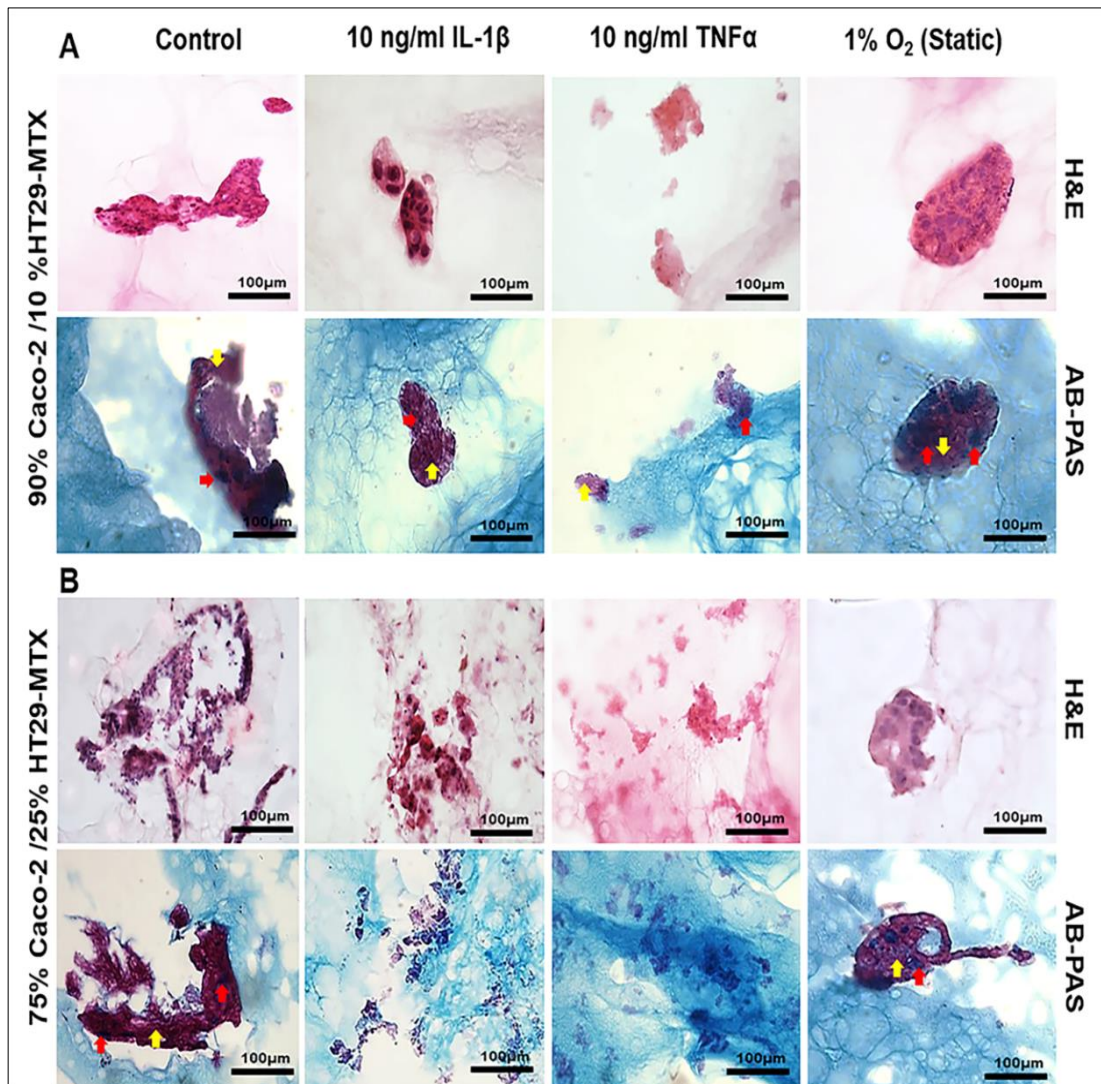


Figure 4.8: Morphology of long term co-culture of Caco-2 and HT29-MTX cells at percentages A: 90% Caco-2 / 10% HT29-MTX; B: 75% Caco-2 / 25% HT29-MTX layered on L-pNIPAM hydrogel scaffolds under dynamic culture conditions following 12 weeks as a control or for 11 weeks and then treated with 10 ng/ml IL-1 β or 10 ng/ml TNF α for 1 week under dynamic culture conditions or hypoxic at 1% O₂ for 1 week under static culture conditions. Cells were stained with H&E and AB-PAS (blue shows acidic mucin (red arrows) and magenta shows neutral mucin (yellow arrows)). Scale bar = 100 μ m.

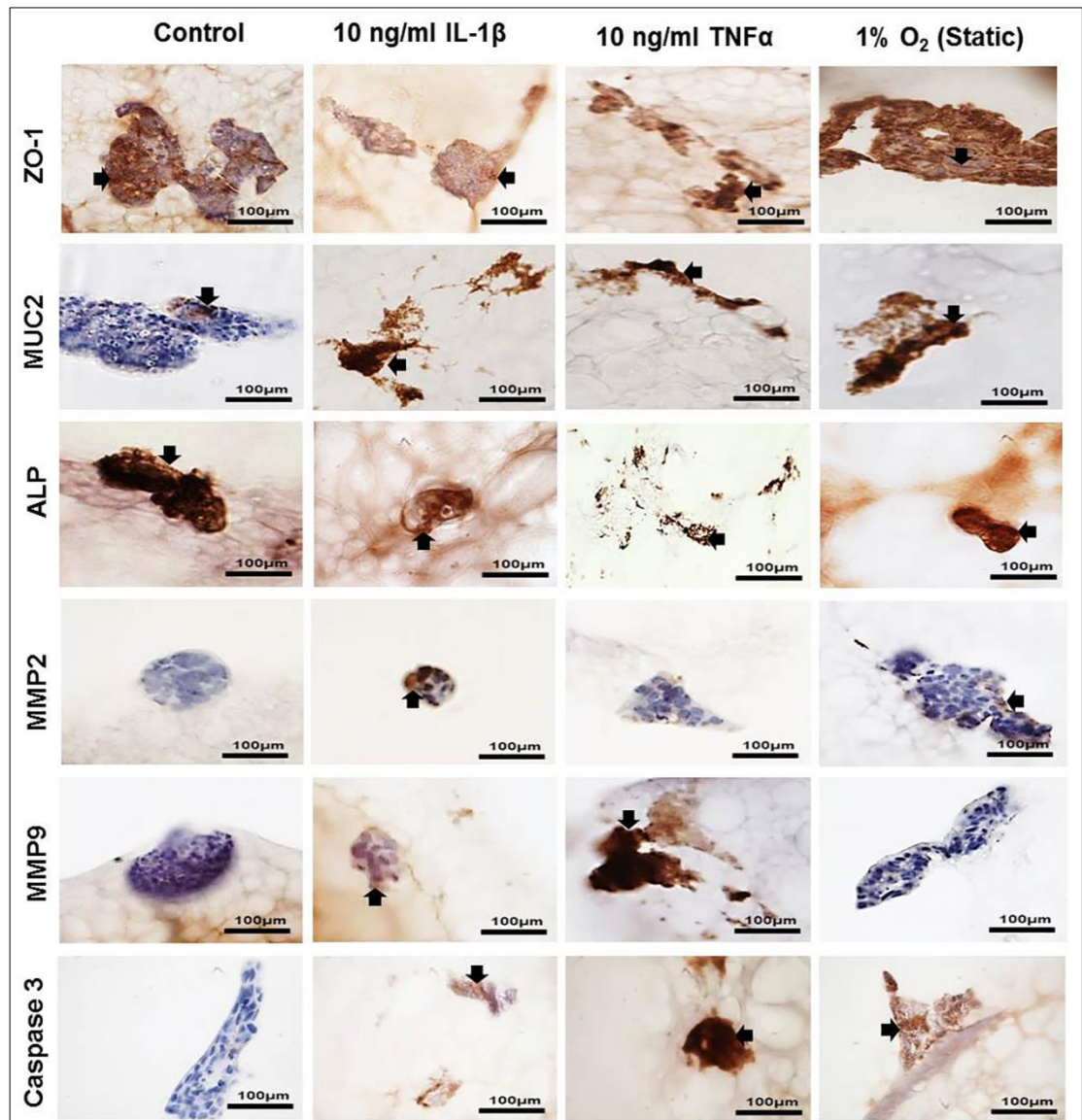


Figure 4.9: Immunopositivity (brown) of co-culture Caco-2 and HT29-MTX cells at percentages 90 %Caco-2 / 10% HT29-MTX layered on L-pNIPAM hydrogel scaffolds under dynamic culture conditions following 12 weeks as a control or for 11 weeks and then treated with 10 ng/ml IL-1 β or 10 ng/ml TNF α for 1 week under dynamic culture conditions or hypoxic at 1% O₂ for 1 week under static culture conditions. Cell nuclei were stained with haematoxylin (blue). The black arrows indicate positively stained cells. Scale bar = 100 μ m.

4.3.5 Scanning electron microscopy of long-term co-cultures following 12 weeks

The SEM observations suggested that the cell morphology and spreading were affected by pro-inflammatory cytokines. When co-cultures containing 90% Caco-2 / 10% HT29-MTX, and 75% Caco-2 / 25% HT29-MTX cells layered on L-pNIPAM hydrogel scaffold for 12 weeks, cells were completely spread out with extending projections was observed in control, whereas co-cultures treated with IL-1 β and TNF α were still rounded (Figure 4.10 & Figure 4.11). Hypoxic co-cultures at 1% O₂ were spread out with distinct microvilli on their apical surfaces of 90% Caco-2 / 10% HT29-MTX (white arrows) (Figure 4.10). Whilst small rounded cells were observed in 75% Caco-2 / 25% HT29-MTX co-cultures at 1% O₂ (Figure 4.11).

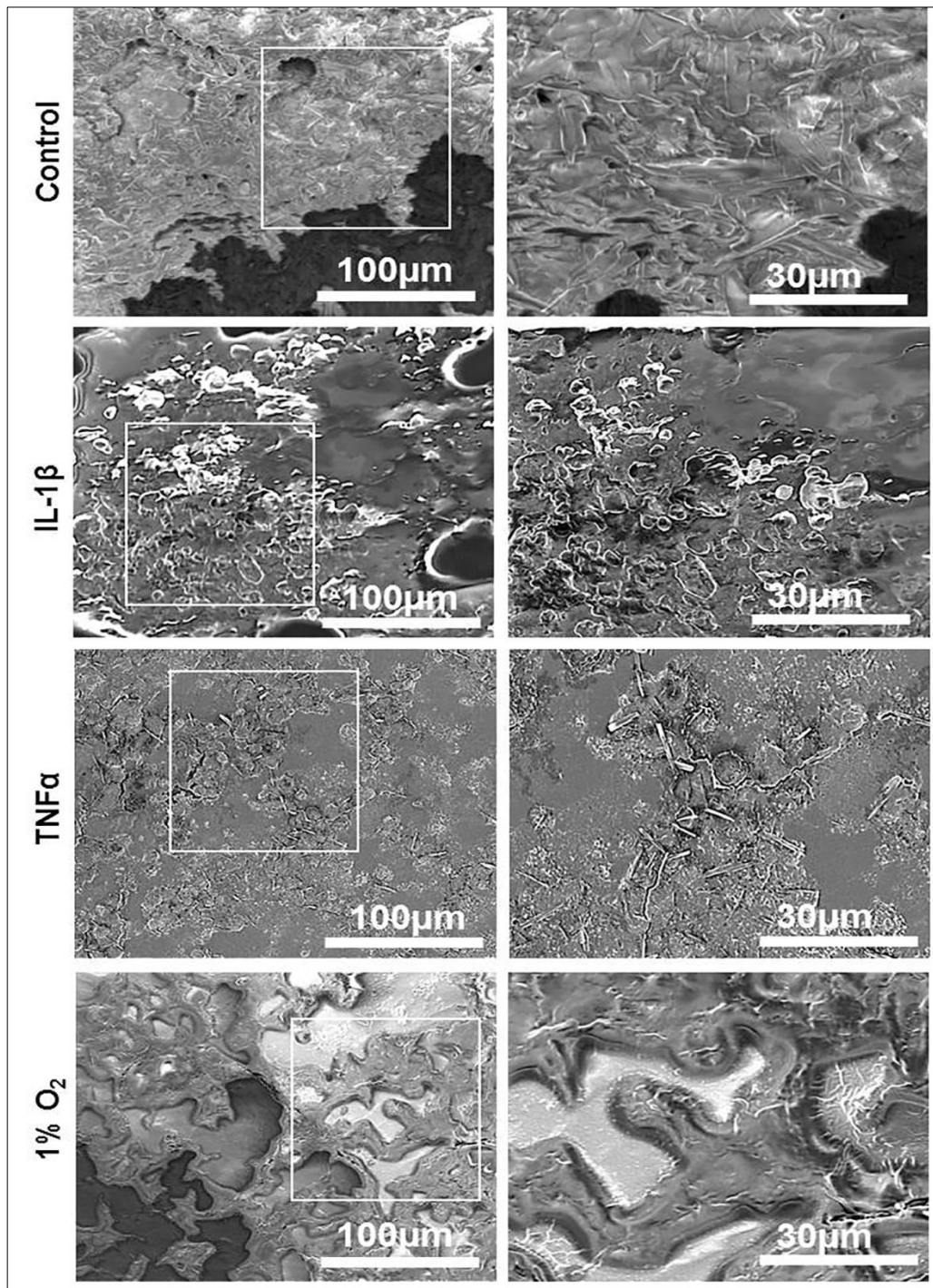


Figure 4.10: Scanning electron micrographs of long-term co-culture Caco-2 and HT29-MTX cells at percentages 90% Caco-2 / 10%HT29-MTX cells layered on L-pNIPAM hydrogel scaffolds under dynamic culture conditions following 12 weeks as a control or for 11 weeks and then treated with 10 ng/ml IL-1 β or 10 ng/ml TNF α for 1 week under dynamic culture conditions or hypoxic at 1% O $_2$ for 1 week under static culture conditions. The white arrows indicate the microvilli-like structures. Scale bar = 30 μ m, 100 μ m.

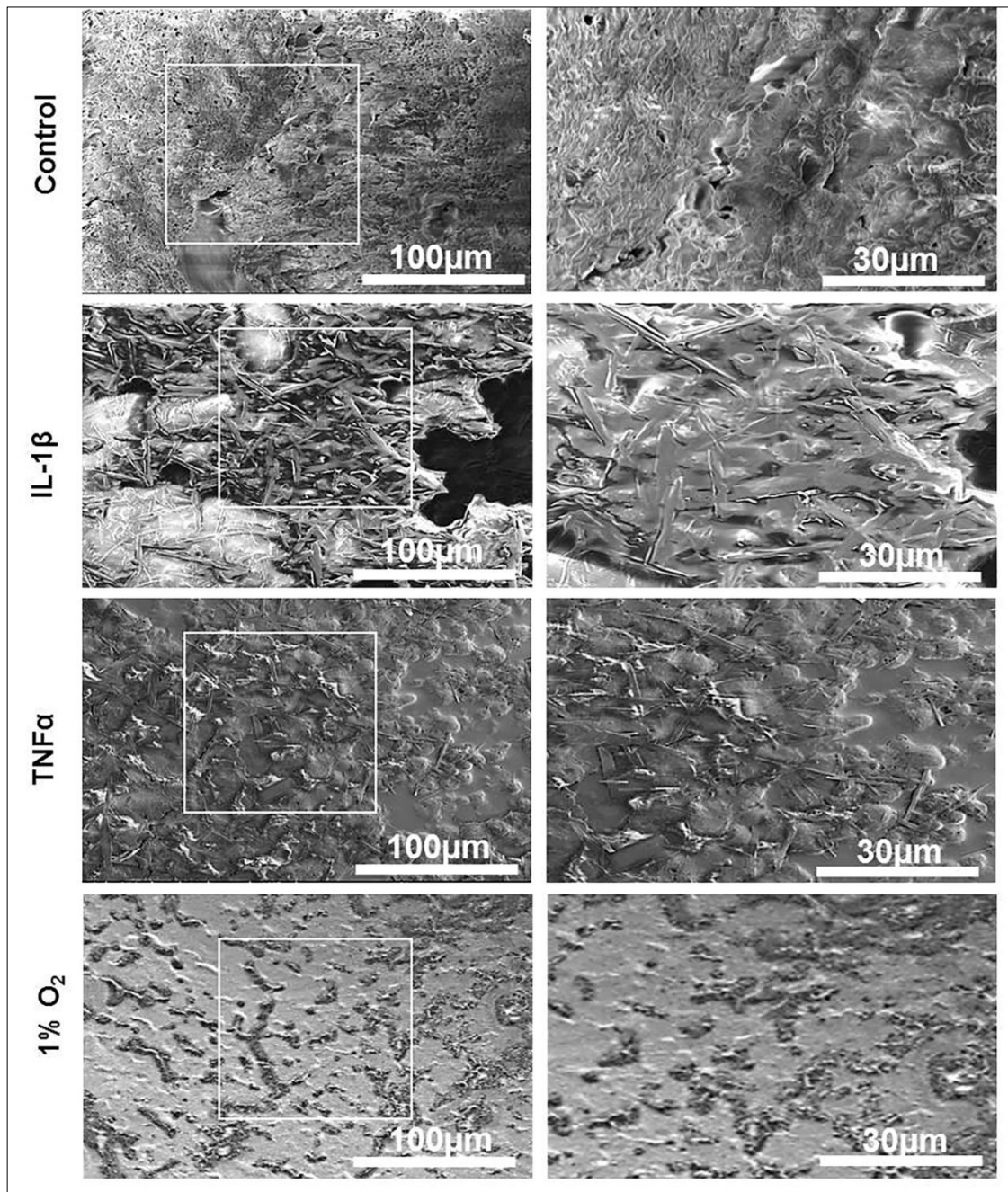


Figure 4.11: Scanning electron micrographs of long term co-culture Caco-2 and HT29-MTX cells at percentages 75% Caco-2 / 25% HT29-MTX cells layered on L-pNIPAM hydrogel scaffolds under dynamic culture conditions following 12 weeks as a control or for 11 weeks and then treated with 10ng/ml IL-1 β or 10ng/ml TNF α for 1 week under dynamic culture conditions or hypoxic at 1% O $_2$ for 1 week under static culture conditions. Scale bar = 30 μ m, 100 μ m.

4.4 Discussion

Co-culture of intestinal epithelial cells: Caco-2 and HT29-MTX have been extensively used as 2D *in vitro* models to study intestinal epithelial barrier functions (Hilgendorf *et al.* 2000; Chen *et al.* 2010; Antunes *et al.* 2013). Here, L-pNIPAM hydrogel scaffold was investigated to determine its ability to provide the mechanical support for long-term layered monocultures and co-cultures of Caco-2 and HT29-MTX cells under dynamic conditions to develop an *in vitro* intestinal epithelium model. This model was then treated with proinflammatory cytokines IL-1 β , TNF α , or hypoxic conditions at 1% O₂ to mimic the environment observed during inflammatory bowel disease (Muzes *et al.* 2012; Colgan *et al.* 2016).

To characterise the 3D mono- and co-culture models *in vitro*, the metabolic activity, and phenotype of these cultures were assessed. The metabolic activity of Caco-2 monoculture or 90% Caco-2 / 10% HT29-MTX co-cultures were increased when layered on L-pNIPAM hydrogel scaffold under dynamic culture. Cells formed a multi-cellular layer which became undulated and gave rise to villus-like structures. Importantly, this was not observed when co-cultures contained more than 10% HT29-MTX cells. This contradicts previous work in which HT29-MTX were found to have a faster proliferation rate than Caco-2 cells grown in monolayers (Berger *et al.* 2017). The mono- and co-culture of Caco-2 and HT29-MTX cells were differentiated after 3 weeks. This was evident by the expression of alkaline phosphatase and the presence of microvilli-like structures of Caco-2 cells, plus the expression of MUC2 by HT29-MTX cells. However, dynamic culture conditions using an orbital shaker as a simplified way with non-directional flow probably resulted in formation of non-aligned microvilli.

Thus, utilising a perfusion bioreactor system may be useful to enable development of one-directional microvilli.

The differentiation of Caco-2 and HT29-MTX cells was accompanied by a decrease in metabolic activity at 3 weeks. This was seen both in Caco-2 monoculture after 3 weeks and in co-cultures where differentiation had taken place. Furthermore, in monoculture and co-culture models no loss of metabolic activity was observed, which may be due to increased flow of nutrients and oxygen by the use of dynamic culture conditions, this effect has been previously seen in Chapter 3 when cells are grown under dynamic culture conditions (Dosh *et al.* 2017). For long-term co-culture experiments, the optimal seeding percentages were 90% Caco-2 / 10% HT29-MTX cells and 75% Caco-2 / 25% HT29-MTX cells. These percentages more closely mimic the cell percentages found in the small (90% / 10%) and large (75% / 25%) intestine (Mahler *et al.* 2009; Umar 2010). Both HT29-MTX cells and Caco-2 cells were shown to produce mucus. Caco-2 cells produced neutral mucins, whilst HT29-MTX cells produced acidic mucins when cultured as mono- and co-cultures. This agreed with previous observation seen when 90% Caco-2 / 10% HT29-MTX and 75% Caco-2 / 25% HT29-MTX cell were cultured in monolayer (Mahler *et al.* 2009).

Inflammatory bowel diseases such as Crohn's disease and ulcerative colitis are chronic inflammatory diseases that can affect the intestine by increasing intestinal paracellular permeability resulted in alterations of function and expression of tight junction proteins such as ZO-1 (Neuman 2007). Several inflammatory cytokines such as IL-1 β and TNF α play a crucial role in the development of IBD. These cytokines have been linked to the dysfunctional intestinal epithelium which leads to permeability defects which are key symptom

of IBD (Pearson *et al.* 1982; Ukabam *et al.* 1983). Thus, *in vitro* cell monolayers have often been utilised to investigate their effects on epithelial permeability using trans epithelial electrical resistance (TEER), where Caco-2 or HT29 cells on semi-permeable filters form luminal and basolateral compartments and the electrical resistance is measured between compartments (Press & Di Grandi 2008). IL-1 β and TNF α expression in patients with Crohn's disease has been shown to lead to increased intestinal permeability (Gibson 2004; Landy *et al.* 2016). However, few studies have investigated the role of IL-1 β and TNF α in intestinal permeability within 3D culture systems. In this study as a proxy measure of intestinal permeability, expression of ZO-1 (tight junction protein) was utilised due to its role in maintaining barrier function, as TEER is difficult to measure within this system (Lee 2015). This study showed IL-1 β and TNF α reduced ZO-1, which would lead to an increase in paracellular permeability of co-culture following 7 and 12 weeks. This observation is consistent with a previous studies by Wang *et al.*, (2006) and Al-sadi *et al.*, (2007) where IL-1 β and TNF α increased Caco-2 tight junction permeability by inducing increase in Myosin L Chain Kinase (MLCK) expression and activity.

The Mucus layer provides protective function for intestinal mucosa against physical and chemical injury, assist the clearance of pathogens, and play important role in maintaining mucosal integrity (McGuckin *et al.* 2008; Johansson *et al.* 2011; Kim & Khan 2013). Alteration in mucin production was detected in patients with IBD (Dorofeyev *et al.* 2013). Moderate expression of MUC2 was observed in patients with Crohn's disease, whereas low expression of MUC2 was detected in patients with ulcerative colitis. In co-culture model, MUC2 mucin was produced at 7 and 12 weeks in 90% Caco-2 / 10% HT29-MTX co-cultures. This expression of MUC2 was increased when these cultures

were treated with IL-1 β and TNF α . This agrees with previous studies that displayed IL-1 and TNF α stimulates secretion of mucin via IL-1R1 on the basolateral surface of cultured HT29-C1.6E cells and via NF-KappaB pathway in HM3 colon cancer cells (Jarry *et al.* 1996; Ahn *et al.* 2005).

Although Caco-2 cells originated from colon adenocarcinoma, they resemble the epithelial cells of the foetal ileum and are believed to differentiate and express proteins phenotypically similar to normal small intestine (Sambuy *et al.* 2005). Culture duration and seeding cell densities can impact on the cellular differentiation and senescence. Differentiation of Caco-2 cells is time-dependent (Sambuy *et al.* 2005), and a marker of the enterocyte phenotype is the expression of ALP. Intestinal ALP is a brush border membrane protein which is expressed by enterocytes and is used as a marker for crypt-villus differentiation (Goldberg *et al.* 2008). Thus, the expression of ALP was used here to select the optimal co-culture percentage in these models. The results showed the expression of ALP was increased with the increase in the percentage of Caco-2 cells in the co-cultures. The 90% Caco-2 / 10% HT29MTX co-cultured cells produced the highest level of ALP activity and hence differentiation of the Caco-2 cells to enterocyte-like cells. As a consequence, these co-culture percentages were used in a further study of pro-inflammatory conditions. However, Nollevaux *et al* (2006) developed co-culture model comprising 75% Caco-2 / 25% HT29-MTX which were grown in serum-free medium. This model produced monolayers which expressed alkaline phosphatase. This suggests that differences in culture conditions, as well as the percentage of each cell line, may affect cell differentiation and the expression of alkaline phosphatase. Subsequently, here all investigations of inflammation in co-culture model were

performed in 90% Caco-2 / 10% HT29MTX and 75% Caco-2 / 25% HT29MTX co-cultures.

An increased expression of matrix metalloproteinases (MMPs) is associated with intestinal inflammation and Crohn's disease. Here, the expression of MMP2 and MMP9 as these are biomarkers for inflammation was investigated (O'Sullivan *et al.* 2015). Following 7 weeks, MMP2 was seen in control cells, IL-1 β treated and hypoxic conditions in both 90% Caco-2 / 10% HT29MTX and 75% Caco-2 / 25% HT29MTX co-cultures. In contrast, following 12 weeks MMP2 was only slightly expressed in IL-1 β treated co-cultures; whereas increased expression of MMP9 was seen in cultures treated with TNF α . These results are consistent with other results which showed increases in MMP9 activity indicating an activation in tissue degrading process resulting from TNF α overproduction by intestinal epithelial cells in TNF $\Delta^{\text{ARE}/+}$ mice model, whereas MMP2 activity was not altered in this model (Roulis *et al.* 2011). MMP2 has been shown to be upregulated in pediatric Crohn's disease (Sim *et al.* 2012) whilst other studies have shown high levels of MMP9 compared to low levels of MMP2 in inflamed mucosa (Baugh *et al.* 1999). IL-1 β and TNF α have been shown to induce synthesis of MMP2 and MMP9 in inflammatory cells and epithelial cells (Saren *et al.* 1996). Gan *et al.* (2001) demonstrated that MMP9 is highly expressed in Caco-2 cells stimulated with IL-1 β and TNF α . In this study, the observed increased expression of MMP2 in control could be due to the Caco-2 and HT29-MTX cells are tumour cells in origin and indeed the expression and activity of MMPs are upregulated in many cancerous cells (Egeblad & Werb 2002).

Here, this study also investigated the expression of ADAMTS 1, which plays a critical role in the inflammation (Tang 2001). In normal tissues, ADAMTS1 is not highly expressed, but increases during inflammation (Hirohata *et al.* 2017). In this model, ADAMTS1 was highly expressed in control cells compared to IL-1 β treated cells in both co-culture percentages. This could be due to the fact that Caco-2 and HT29-MTX cells are cancer cell lines and the proteolytic activity of ADAMTS1 has been related to local tissue invasion in cancer (Filou *et al.* 2015). These results are in agreement with Demircan *et al.* (2005) and Kalinski *et al.* (2007), who reported a decrease in ADAMTS1 expression in a chondrosarcoma cell line (OUMS-27) and chondrosarcoma cell line (C3842) stimulated with IL-1 β . However, Filou *et al.* (2015) stated that RNA levels of ADAMTS1 were upregulated in the muscular tissue of healthy colons, while downregulated in colon cancer. Additionally, in this study, western blot analysis showed that ADAMTS1 have been detected in both Caco-2 and HT-29 cells.

The normal intestinal epithelium has been shown to be in a physiologic state of hypoxia (Zheng *et al.* 2015). The intestinal epithelial cells response to hypoxia through the transcription factor called hypoxia-inducible factor (HIF-1 α and HIF-2 α) and are believed to be essential in maintaining intestinal homeostasis. Intestinal epithelial cells are expressed high amounts of HIF-1 α and HIF-2 α in Crohn's disease (Colgan & Taylor 2010; Shah 2016; Colgan *et al.* 2016). Similarly, a decreased partial pressure of O₂ has been observed in mouse models of ulcerative colitis (Karhausen *et al.* 2004). It is thought to be brought about increased O₂ consumption of intestinal epithelial cells during inflammation. Inflammation raises local vasculitis thus reduced O₂ availability to the inflamed region, furthermore, transmigration of neutrophils can consume regional O₂ (Karhausen *et al.* 2004). In addition, hypoxia can alter gene expression, intra-

and extra-cellular pH and membrane receptors (Lima *et al.* 2013). In the current study, the influence of hypoxia on the cellular behaviour in monocultures and co-cultures was examined. Following 7 weeks, histological assessment of Caco-2 monocultures and in co-culture 90% Caco-2 / 10% HT29-MTX showed that 1% O₂ hypoxia for 1 week had no effects. Only in the 100% HT29-MTX monoculture and in co-cultures where the number of HT29-MTX cells were increased an increase in cell debris and cell death was observed.

Under hypoxic conditions, decreased expression of ZO-1 in 90% Caco-2 / 10% HT29-MTX and 75% Caco-2 / 25% HT29-MTX co-cultures following 7 weeks and 12 weeks was observed. This findings is in agreement with previous study which has demonstrated that hypoxia can induce decrease expression and reorganization of tight junction proteins including ZO-1 due to hypoxia increased the expression of MLCK (Wang *et al.* 2009b). In contrast, increased expression of MUC2 in 90% Caco-2 / 10% HT29-MTX co-culture following 7 weeks and 12 weeks. This is in agreement with a recent study which showed increased MUC2 expression in response to hypoxia in LS174T colorectal cancer cells (Dilly *et al.* 2016). Importantly, hypoxia is an important factor that induces cancer metastasis (Munoz-Najar *et al.* 2006; Jing *et al.* 2012), following 7 weeks, hypoxia increased expression of MMP2 and ADAMTS1 in both percentages. This agrees with a previous study which showed that in breast carcinoma cells hypoxia-induced invasion by increased expression of MMP2 (Munoz-Najar *et al.* 2006) while hypoxia had no significant influence on ADAMTS1 transcription in chondrosarcomas cell line (C3842) (Kalinski *et al.* 2007). In addition, induced hypoxia-mimicking conditions using CoCl₂ (100 µmol/L) for 24 h increased expression of MMP2 in human esophageal cancer cells (Eca109) (Jing *et al.* 2012). Apoptotic cells were less frequent in 90% Caco-2 / 10% HT29-MTX than

seen in 75% Caco-2 / 25% HT29-MTX co-culture. Caco-2 cells consume less oxygen under hypoxia and thus may be better adapted to hypoxic conditions (Lima *et al.* 2013).

In conclusion, the successful application of an *in vitro* model depends on how closely this model mimics the characteristics of the *in vivo* intestinal epithelium; In this study, an intestinal epithelial model that could mimic healthy and diseased conditions was developed. The L-pNIPAM hydrogel scaffold and dynamic culture condition makes long-term co-culture possible and allows investigation of pro-inflammatory cytokines effect on intestinal cell behaviour. However, the ability of L-pNIPAM hydrogel as a scaffold for more physiologically relevant intestinal cells such as intestinal organoids rather than the cancerous cells in this study would be important to investigate.

Chapter 5

**Isolation and *in vitro* expansion of small intestinal stem cells
from mice using L-pNIPAM hydrogel**

5.1 Introduction

The intestinal mucosa is composed of columnar epithelia which form intestinal villi and crypts. These crypts are the site of intestinal stem cell (ISC) production (Clevers 2009). The intestinal epithelium rapidly self-renews every 3-5 days (Barker *et al.* 2007). The self-renewal process is driven by ISCs or crypt base columnar cells (CBCs), which reside at the bottom of the intestinal crypts, and are scattered amongst Paneth cells which support them and contribute to stem cell niche (Yeung *et al.* 2011; Foulke-Abel *et al.* 2014). These stem cells symmetrically divide every 24 h and generate new cells, which are known as transit amplifying cells. The transit amplifying cells proliferate rapidly, and either migrate towards the villi tips and terminally differentiate into the mature intestinal epithelial cell types (enterocytes, goblet cells or enteroendocrine cells) or alternatively move toward the crypt base and differentiate into Paneth cells (Leedham *et al.* 2005; Sato *et al.* 2009, 2011a; Sato & Clevers 2015). These stem cells within the crypts are capable of responding to local environment changes ensuring that the correct cellular populations are produced within the villi. Hence, this stem cell niche regulates cellular proliferation in the villi whilst maintaining a stem cell population (Scoville *et al.* 2008; Barker *et al.* 2008, 2010; Munoz *et al.* 2012). This stem cell population within the stem cell niche expresses a leucine-rich repeat-containing G-protein coupled receptor 5 (Lgr5), which is a target gene for WNT signalling. A single Lgr5 positive stem cell (Lgr5⁺) is capable of regenerating all cell types within the intestinal epithelium (Barker *et al.* 2007, 2012, 2013; Clevers 2013).

It has previously been shown that when small intestinal crypt cells, isolated from mice, are embedded within Matrigel, and cultured in the presence of R-spondin 1, Noggin, and epidermal growth factors to mimic the physiological conditions of

the intestinal stem cell niche; these cells expanded in culture without significant genetic or physiologic alterations (Sato *et al.* 2009, 2011b; Fuller *et al.* 2012; Wang *et al.* 2013a; Xinaris *et al.* 2015; Sasaki *et al.* 2017). Under these conditions, cells organised themselves into 3D tissue constructs: described as organoids, consisting of a central sphere-shaped domain, composed mostly of differentiated cells, and numerous bud-like structures similar to that of an intestinal crypt. Found within these crypt like structures are Lgr5⁺ intestinal stem cells. Similarly Paneth cells are found at the base of the crypt (Sato *et al.* 2009, 2011a; Wong *et al.* 2012; Sato & Clevers 2012, 2013; Date & Sato 2015; Zachos *et al.* 2016; Scott *et al.* 2016). A noticeable feature of the epithelial organoid system is its ability to grow cells almost infinitely from a small number of cells, or tiny pieces of tissue (Sato *et al.* 2011a; Mahe *et al.* 2013; Liu *et al.* 2016).

Similarly, isolation of Lgr5⁺ stem cells grown in culture also resulted in the formation of organoids. These organoids contain crypt and villus domains which recapitulate essential processes of the native intestinal epithelium (Sato *et al.* 2009, 2011a; Sato & Clevers 2013; Yin *et al.* 2014; Date & Sato 2015; Sato & Clevers 2015). Wang *et al.* (2017) reported that when pre-isolated stem cells or crypts from the human small intestine were cultured within Matrigel they formed cystic organoids. These organoids formed an enclosed lumen surrounded by a single layer of non-polarized epithelial cells made up of both proliferated cells randomly mixed with differentiated cells. These organoids did not reflect tissue of the *in vivo* intestine and were unsuitable for studying of intestinal functions. This led to the development of alternative scaffolds to support the growth of intestinal stem cells. Those that have been investigated, including type 1 collagen gels, which have been shown to support long-term (28 days)

maintenance and expansion of organoids formed from the co-culture of human small intestinal crypts with intestinal sub-epithelial myofibroblast (ISEMFs) (Jabaji *et al.* 2014). Sachs *et al.* (2017) showed that mice intestinal organoids could be formed from a single Lgr5⁺ stem cell, when embedded in Matrigel for 3 days. These organoids were released from Matrigel and grown in contracting floating type 1 collagen, where, they continued to align, fuse and self-organize into a hollow tube-like structure which became lined with the stem cells and differentiated into the various intestinal epithelial cell types.

Although these organoid systems have a huge impact on the intestinal research, the size, structure, and function of the epithelial components in these organoids are not exactly the same as that in the *in vivo* intestine. For example, differentiated epithelial cells in small intestinal organoids fail to form finger-like structures that accurately mimic native intestinal villi (Nakamura & Sato 2018). Thus, recent studies have utilised a variety of bio-fabrication to produce functional intestine that attempts to mimic the villus-crypt architecture of the *in vivo* intestine. A recent study, demonstrated that micro-engineered collagen scaffolds with appropriate extracellular matrix and stiffness (modulus young's = approximately 10 KPa) generated an *in vitro* human small intestinal epithelium with a polarized monolayer which mimicked *in vivo* crypt-villus structure with a suitable cell lineage and an open luminal surface (Wang *et al.* 2017). Although current organoid culture systems are dependent on animal-derived hydrogels such as Matrigel and collagen gels, these scaffolds are complex and vary in their composition (Sachs *et al.*, 2017) which makes them inappropriate for organoid expansion with clinical applications. Hence, this has led to the use of synthetic matrices in tissue engineering of the small intestine (Gjorevski *et al.* 2016). Cromeens *et al.* (2016) produced tissue-engineered intestine from

organoids. These organoids were expanded in Matrigel then released and suspended in poly-glycolic acid (PGA) scaffold coated with type 1 collagen this was then implanted in the peritoneal cavity of immunosuppressed NOD/SCID mice for 4 wks. Tissue-engineered intestine showed the presence of crypts and short villi, which contained all intestinal epithelial cell lineages. This study demonstrated that a synthetic extracellular matrix could provide a suitable scaffold for maintenance and expansion of crypts and intestinal stem cells. Thus, the current study investigated the potential of the novel synthetic L-pNIPAM hydrogel, (which have previously demonstrated the ability to support villus like structures formation in Caco-2 cells and HT29-MTX cells (Dosh *et al.* 2017) as a 3D scaffold for crypt cells and to support long-term culture of Lgr5⁺ intestinal stem cells under dynamic culture conditions. In addition, the capacity of these cells to differentiate into intestinal epithelial cells *in vitro* when suspended within or layered on L-pNIPAM hydrogel were also investigated.

5.2 Materials and methods

5.2.1 Mice

BALB/c mice (n=22) (Charles River Laboratories) aged 6 to 12 weeks old were used for the extraction of intestinal crypts and isolation of single Lgr5⁺ stem cells.

5.2.2 Culture media

The basal culture media (Advanced Dulbecco's Modified Eagle Medium (DMEM/F12) (Life Technologies, Paisley, UK) supplemented with 100 µg/ml penicillin/ streptomycin (Life Technologies, Paisley, UK), 250 ng/ml amphotericin (Sigma, Poole, UK), 2 mM glutamine (Life Technologies, Paisley, UK), and 1 M HEPES buffer to maintain physiological PH (Sigma, Poole, UK). The crypt basal media was made by supplementing with B-27 (50 x) (to promote growth and proliferation of stem cells without differentiation in this serum free media) (Life Technologies, Paisley, UK), N-2 (100 x) (Life Technologies, Paisley, UK), and 0.5 M N-Acetyl-L-cysteine (as an antioxidant that directly scavenging ROS and also acts as a mucolytic) (Sigma, Poole, UK).

5.2.3 Small intestinal crypt extraction

Isolation of small intestinal crypts was performed, as described previously (Sato & Clevers 2012; Mahe *et al.* 2013; Pastuła & Quante 2014). Briefly, the abdomen of Balb/c mice, were cleaned with 70% (v/v) ethanol in dH₂O. A mid-sagittal incision was made into the abdominal cavity. The intestine was excised from the stomach at the pyloric sphincter, the mesentery dissected away and the distal segment was cut at the ileocecal junction. The intestines were then separated from adipose and connective tissues. Intestines were then flushed with ice-cold washing solution (10% (v/v) heat-inactivated foetal bovine serum

(FBS) (Life Technologies, Paisley, UK) in PBS without Ca^{2+} and Mg^{2+} (Life Technologies, Paisley, UK) using a 10 ml syringe fixed with a 18 gauge needle. All luminal content was removed. In order to extract the crypts, dissected intestines were opened lengthwise and villi of intestines were scraped off using a coverslip, and discarded. The rest of the intestine (including the crypts) were washed with washing buffer and cut with scissors into 2-4 mm pieces. These pieces were then transferred into a 50 ml Falcon tube and further washed with ice-cold washing solution (approximately 10 times), and pipetting up and down, until the supernatant was clear. The tissue fragments were transferred into 50 ml falcon tubes and incubated in 25 ml of chelating buffer (2 mM EDTA (Sigma, Poole, UK) in PBS) on ice and shaken gently on an orbital shaker for 15 mins. The tubes were inverted gently, and cell fragments were allowed to settle at bottom of tubes. The chelating buffer was carefully removed and the crypts were re-suspended in 20 ml of washing solution for 5 min. Tissues were then passed through a 70 μm cell strainer to remove any remaining tissue debris and the crypt fraction was collected. The fraction (Fraction I) was stored on ice. The remaining tissue fragments were re-suspended in ice-cold washing solution, pipetted 5-10 times and the supernatant was passed through 70 μm cell strainers (Fraction II). The previous step was repeated a second time and a third fraction was collected (Fraction III). The three fractions were combined and centrifuged at 200 g for 5 min at 4°C. The pellet was re-suspended in 10 ml ice-cold basal culture medium and centrifuged at 300 g for 5 min at 4°C to remove single cells and tissue debris. The number of crypts was counted under the inverted microscope. The crypts were subsequently either directly embedded in either Matrigel or L-pNIPAM hydrogel, or further dissociated into a single stem cell population (Section 5.2.8).

5.2.4 Suspension of small intestinal crypts within Matrigel

Matrigel (basement membrane matrix, growth factor reduced and phenol red-free) (Corning, UK) was mixed with growth factors (recombinant human R-Spondin 1 (1 µg/ml) (PeproTech, London, UK), recombinant murine Noggin (100 ng/ml) (PeproTech, London, UK) and recombinant murine EGF (50 ng/ml) (PeproTech, London, UK)) on ice. One to five hundred crypts were re-suspended in 50 µl of Matrigel. The suspension was pipetted in the middle of the well of pre-warmed 24 well-plates which had been allowed to cool to room temperature for 2-3 min. The plates were then transferred to 37°C for 15 min to allow complete polymerization of the Matrigel. Five hundred microliters of crypt basal media supplemented with epidermal growth factor (EGF) (50 ng/ml), Noggin (100 ng/ml), and R-Spondin 1 (1 µg/ml) (ENR) was added to each well. Cultures were maintained at 37°C, 5% CO₂ for up to 14 days, crypt basal media supplemented with ENR was replaced every 48 h.

5.2.5 Suspension of small intestinal crypts within L-pNIPAM hydrogel

One to five hundred crypts were re-suspended in 300 µl of liquid L-pNIPAM hydrogel at 38-39°C. The suspension was added in each well of 48 well plates and allowed to cool below the lower critical solution temperature of the L-pNIPAM hydrogel to induce gelation. Five hundred microliters of crypt basal medium supplemented with ENR was added per well. Cultures were maintained at 37°C, 5% CO₂ and for up to 14 days under dynamic conditions, which were created using an orbital shaker set at 30 rpm. Media was replaced with fresh crypt basal media supplemented with ENR every 48 h.

5.2.6 Layering of small intestinal crypts on L-pNIPAM hydrogel

Three hundred microliters of L-pNIPAM was added to each well of 48 well plates. Following gelation 300 μ l of crypt culture media (Section 5.2.2) containing 100-500 crypts was applied to the surface of hydrogel construct. After 30 min cell attachment period, 200 μ l of crypt basal media (Section 5.2.2) was added to each well. All plates were incubated at 37°C, 5% CO₂ and maintained in culture for up to 14 days under dynamic culture conditions, which were created using an orbital shaker set at 30 rpm. Fresh crypt basal media supplemented with ENR was replenished every 48 h.

5.2.7 Suspension of small intestinal crypts within Matrigel followed by suspension within or layered on L-pNIPAM hydrogel

The extracted crypt pellet was suspended and cultured in Matrigel for 7 days (Section 5.2.4). The resultant organoid were released from the Matrigel on 7 days and were either suspended within or layered on L-pNIPAM hydrogel. Briefly, to release organoid from Matrigel the media was removed from the organoids and 500 μ l of cold PBS was added to each well. Matrigel containing organoids was broken up by pipetting up and down. The suspension was transferred into 15 ml conical tubes then the organoids were pipetted up and down 50-100 times to mechanically disassociate the organoids into smaller fragments. Seven milliliters of cold PBS was added to the tube and pipetted up and down a further 20 times. The suspension was centrifuged at 200 g for 5 min at 4°C. The pellet containing the crypt cells was either suspended within or layered on L-pNIPAM hydrogel (Section 5.2.5 and 5.2.6) and maintained for up to 14 days at 37°C, 5% CO₂ under dynamic culture condition created using an orbital shaker set at 30 rpm. Media was replaced with fresh crypt basal media supplemented with ENR every 48 h.

5.2.8 Isolation of small intestinal stem cells

Crypts were extracted from BALB/c mice as described in (Section 5.2.3). The crypt pellet was re-suspended with 2 ml of pre-warmed single cell dissociation medium (basal medium supplemented with Rock inhibitor, Y-27632, (10 μ M/ml) (Sigma, Poole, UK)) for 30-45 min at 37°C until cells dissociated. During incubation, the crypt suspension was mechanically pipetted with fire-polished pasteur pipette every 5-10 min until the crypts were dissociated into single cells or 2-3 cell clusters. The cell suspension was filtered through 40 μ m cell strainers to remove any remaining cell clumps then resuspended with basal medium and centrifuged at 300 g at 4°C. The pellet was re-suspended with 1 ml single-cell dissociation medium (basal medium supplemented with Y-27632 (10 μ M/ml)), and centrifuged at 500 g for 10 min and the supernatant was completely removed in preparation of Magnetic Activated Cell Sorting (MACS).

5.2.9 Magnetic Activated Cell Sorting (MACS) separation

Following the manufacturer's protocol the cell pellet was resuspended up to 10^6 nucleated cells in 45 μ l of degassed MACS buffer solution (PBS plus 0.5% (w/v) bovine serum albumin (BSA), and 2 mM EDTA). This MACS buffer solution was prepared by diluting 1 ml MACS BSA stock solution (Miltenyi Biotec, UK) with 20 ml autoMACS rinsing solution (Miltenyi Biotec, UK). Five μ l of FcR blocking reagent (Miltenyi Biotec, UK) was added to the suspension to block unwanted binding of Lgr 5 antibody to mouse cells expressing Fc receptors (e.g. B cells, monocytes or macrophages); and mixed well, then refrigerated for 10 min at 2-8°C. Cells were labeled by adding 5 μ l of the biotinylated Lgr5 antibody (Miltenyi Biotec, UK), mixed well and refrigerated for 10 min. Cells were then washed by adding 1-2 ml of degassed MACS buffer and centrifuged at 500 g for 10 min. The supernatant was completely removed and the cell pellet was re-suspended

in 70 μ l of degassed MACS buffer. Cells were magnetically labeled by adding 20 μ l of anti-biotin microbeads (Miltenyi Biotec, UK), mixed well and refrigerated for 15 min. The cells were washed in 1-2 ml of degassed MACS buffer and centrifuged at 500 g for 10 min. The supernatant was removed and the cell pellet re-suspended in 500 μ l of degassed MACS buffer and magnetic separated.

The MACS MS column (Miltenyi Biotec, UK) was inserted into the column holder on the MACS separator. The column was rinsed with 500 μ l of degassed buffer and the effluent was discarded. The magnetically labeled cell suspension was loaded onto a MACS MS column; unlabelled cells were flushed through the column with 3 x 500 μ l degassed MACS buffer. Unlabelled cell fraction was collected and a new collection tube was placed under the column. The column was removed from the magnetic holder, 1 ml of degassed MACS buffer was pipetted onto the column and plunger applied causing the magnetically labeled Lgr5 positive cell to be released and collected from the column. To increase the purity of the magnetically labeled fraction, the Lgr5 positive fraction was applied onto a new freshly prepared MS column as described above, and the MACS sorting of these cells was repeated. The number of Lgr5⁺ cells/ml were counted following sorting and cell suspensions were centrifuged at 500 g for 5 min and the supernatant discarded. The cell pellet was used for subsequent culture experiments.

5.2.10 Cytospin of Lgr5⁺ sorted cells

A sample of the Lgr5⁺ sorted cells was fixed in 4% w/v paraformaldehyde (Sigma, Poole, UK) for 20 min. The cells were centrifuged at 300 g for 5min and suspended in PBS at a cell density of 300 cells/ μ l. One hundred microliters of cell suspension was cytopun by centrifugation at 1000 rpm for 3 min (Shandon

cytochrome 3, Thermo Scientific, Loughborough, UK). Slides were then air-dried and stored at 4°C until needed for immunohistochemical investigation.

5.2.11 Suspension of Lgr5⁺ stem cells within Matrigel

Matrigel was mixed with growth factors: Notch ligand Jagged-1 peptide (1 µM/ml) (Eurogentec, Southampton, UK), and ENR on ice. One to two hundred Lgr5⁺ stem cells were re-suspended in 10 µl of Matrigel and pipetted into the middle of the well of a pre-warmed 96 well-plate. Following 2-3 min at room temperature, they were transferred to 37°C for 15 min to allow complete polymerization of the Matrigel. One hundred microliters of fresh crypt basal media supplemented with 2.5 µM/ml GSK3β inhibitor (CHIR99021) (Sigma, Poole, UK) (to activate β-catenin and other survival pathways), Rock activity inhibitor (Thiazovivin) (2.5 µM/ml (Sigma, Poole, UK) to decrease anoikis by increasing the stability of E-cadherin), and ENR was added to each well. Cultures were incubated at 37°C, 5% CO₂ for up to 14 days, media was replaced with fresh crypt basal media supplemented with ENR every 48 h. To reduce apoptosis and promote the survival of single stem cells during the first 2 days of culture a Notch agonist Jagged-1 peptide (1 µM/ml) was also added to the cell culture media.

5.2.12 Suspension of Lgr5⁺ stem cells within L-pNIPAM hydrogel

One to two hundred Lgr5⁺ stem cells were re-suspended in 100 µl of liquid L-pNIPAM hydrogel at 38-39°C and added to each well of 96 well-plate, and allowed to cool below the lower critical solution temperature to induce gelation of the hydrogel. Two hundred and fifty microliters of crypt basal media supplemented with CHIR99021 (2.5 µM/ml), Thiazovivin (2.5 µM/ml), Jagged-1 peptide (1 µM/ml) and ENR was added to each well. Cultures were incubated at 37°C, 5% CO₂ and maintained for up to 14 days under dynamic conditions

created using an orbital shaker set at 30 rpm. Media was replaced with fresh crypt basal media supplemented with ENR every 48 h. Jagged-1 peptide (1 $\mu\text{M}/\text{ml}$) was added to the cell culture media during the first 2 days of culture.

5.2.13 Layering of Lgr5⁺ stem cells on L-pNIPAM hydrogel

One hundred microliters of L-pNIPAM was added to each well of 96 well plates. Following gelation, 100 μl of crypt culture media containing 100-200 Lgr5⁺ stem cells were applied to the surface of hydrogel construct in each well of the 96 well plates. After an attachment period of 30 minutes, a further 150 μl basal crypt media supplemented with CHIR99021 (2.5 $\mu\text{M}/\text{ml}$), Thiazovivin (2.5 $\mu\text{M}/\text{ml}$), Jagged-1 peptide (1 $\mu\text{M}/\text{ml}$), and ENR was added to each well. All plates were incubated at 37°C, 5% CO₂ and maintained in culture for up to 14 days under dynamic culture conditions created using an orbital shaker set at 30 rpm. The basal crypt media supplemented with ENR was replenished every 48 h. Jagged-1 peptide (1 $\mu\text{M}/\text{ml}$) was added to the cell culture media during the first 2 days of culture.

5.2.14 Suspension of Lgr5⁺ stem cells within Matrigel followed by suspension within or layered on L-pNIPAM hydrogel

Isolated Lgr5⁺ stem cells pellet were suspended in Matrigel (Section 5.2.11), the organoids which formed from Lgr5⁺ stem cells were released from Matrigel at day 7. Briefly, media was removed and 100 μl of cold PBS was added to each well. Matrigel was broken up by pipetting up and down to mechanically disassociate the organoid into single cells. The suspension was transferred into 1.5 ml Eppendorf and centrifuged at 300 g for 5 min. The pellet was either suspended within or layered on L-pNIPAM hydrogel (Section 5.2.12 and 5.2.13) and maintained for 1 to 4 weeks at 37°C, 5% CO₂ under dynamic culture conditions using an orbital shaker set at 30 rpm. Media was replaced with fresh

crypt basal media supplemented with ENR every 48 h. Jagged-1 peptide (1 $\mu\text{M}/\text{ml}$) was added to the cell culture media during the first 2 days of culture.

5.2.15 Characterisation of crypts and Lgr5⁺ stem cells

5.2.15.1 A bright field images of the crypts and Lgr5⁺ stem cells

Crypts and Lgr5⁺ stem cells were suspended within Matrigel for up to 14 days. Bright field images were examined using an inverted microscope (Olympus IX8, UK) and images captured using Cell-F software.

5.2.15.2 Histological assessment

Crypts and Lgr5⁺ stem cells either suspended within or layered on L-pNIPAM hydrogel together with those suspended in Matrigel for 7 days then released from Matrigel and suspended within or layered on L-pNIPAM hydrogel were assessed. Triplicate samples were fixed in 4% w/v paraformaldehyde/PBS for 24 h prior to washing in PBS and processed to paraffin wax in a TP1020 tissue processor (Leica Microsystem, Milton Keynes, UK). Four-micron sections were cut and mounted onto positively charged slides (Leica Microsystem Milton Keynes, UK). Sections were stained with Haematoxylin and Eosin or Alcian Blue/Periodic acid Schiff's (PAS) as described in (Chapter 2 Section 2.2.2).

5.2.15.3 Immunohistochemical Assessment

Immunohistochemistry was performed to investigate: Adhesion junction protein (using anti-E-cadherin antibody (1:200 mouse monoclonal, heat antigen retrieval) (Abcam, Cambridge, UK); MUC2 production using anti-MUC2 antibody (1:100 rabbit polyclonal, heat antigen retrieval) (Santa Cruz, Heidelberg, Germany); Chromogranin A production as an indication of enteroendocrine cell presence using anti-Chromogranin A antibody (1:100 rabbit polyclonal, heat antigen retrieval) (Abcam, Cambridge, UK); and

lysozyme production as an indication of Paneth cell presence (using anti-Lysozyme antibody (1:2000 rabbit monoclonal, heat antigen retrieval) (Abcam, Cambridge, UK). Immunohistochemistry was performed as previously described in (Chapter 2 Section 2.2.3).

5.3 Results

5.3.1 Morphological assessment of crypts isolated from the small intestine suspended within Matrigel, L-pNIPAM hydrogel or layered on L-pNIPAM hydrogel

When isolated crypts were suspended in Matrigel, they formed spheroid-like structures within 1 day (Figure 5.1). After 2 days, these structures began to develop crypt-like buds. Larger mature buds made up of several well-defined cells were seen by day 6 to 7, suggesting the presence of stem cells within the crypt buds (Figure 5.1). Between day 7 and 14, the organoids enlarged with increasing number of crypt-like buds. These organoids were passaged after 7 days and continued to grow (Figure 5.1).

When isolated crypts were directly suspended within or layered on L-pNIPAM hydrogel under dynamic culture conditions, H&E staining showed that they formed spheroid-like structures consisting of a central core surrounded by multiple cells by day 10 to 14 (Figure 5.2 A). Alcian blue/PAS staining of these organoids showed the presence of mucin-producing cells which resembled goblet cells scattered throughout the organoid structures, associated with an adherent mucus layer covering the organoids by day 14 (Figure 5.2 B).

5.3.2 Morphological assessment of the organoids when released from Matrigel, dissociated and suspended within or layered on L-pNIPAM hydrogel.

When organoids were formed in Matrigel for 7 days, and dissociated into small fragments and then transferred to L-pNIPAM hydrogel they formed new organoids with numerous crypt-like buds within 10 days when cultured under dynamic culture conditions when suspended within or layered on the L-pNIPAM

hydrogel (Figure 5.3 A & B). Mucin-producing cells were distributed throughout the organoid structures when dissociated organoids were suspended within or layered on L-pNIPAM hydrogel following 10 days (Figure 5.3 A & B).

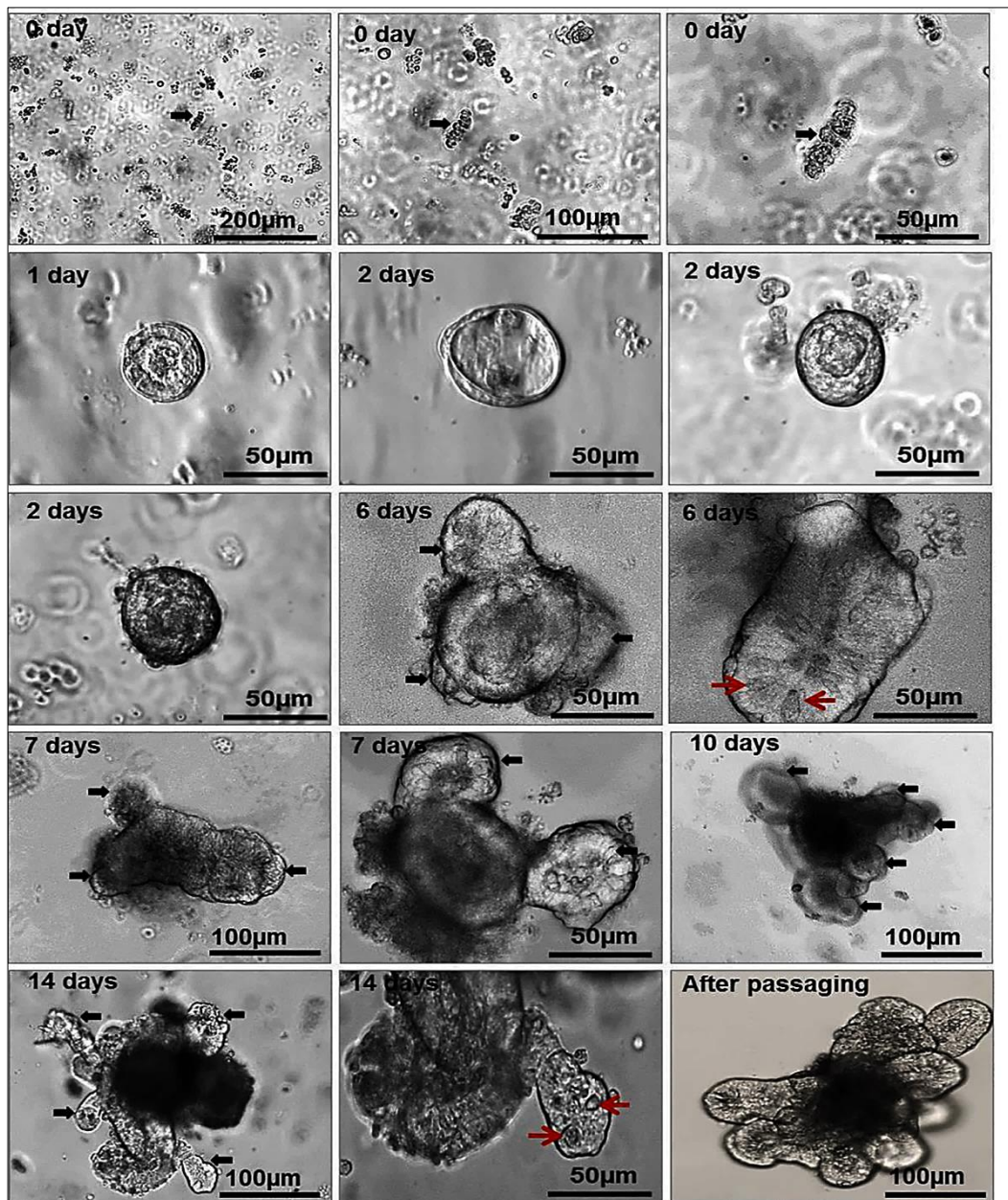


Figure 5.1: Bright-field morphology of the isolated small intestinal crypts suspended within Matrigel for 0-14 days. Representative organoids with black arrows indicating crypt buds; red arrows suggesting the presence of stem cells within crypt-like buds. Organoid growth was shown to continue after passage at day 7 with the continual growth of crypt-like buds. Scale bar = 50 µm - 200 µm.

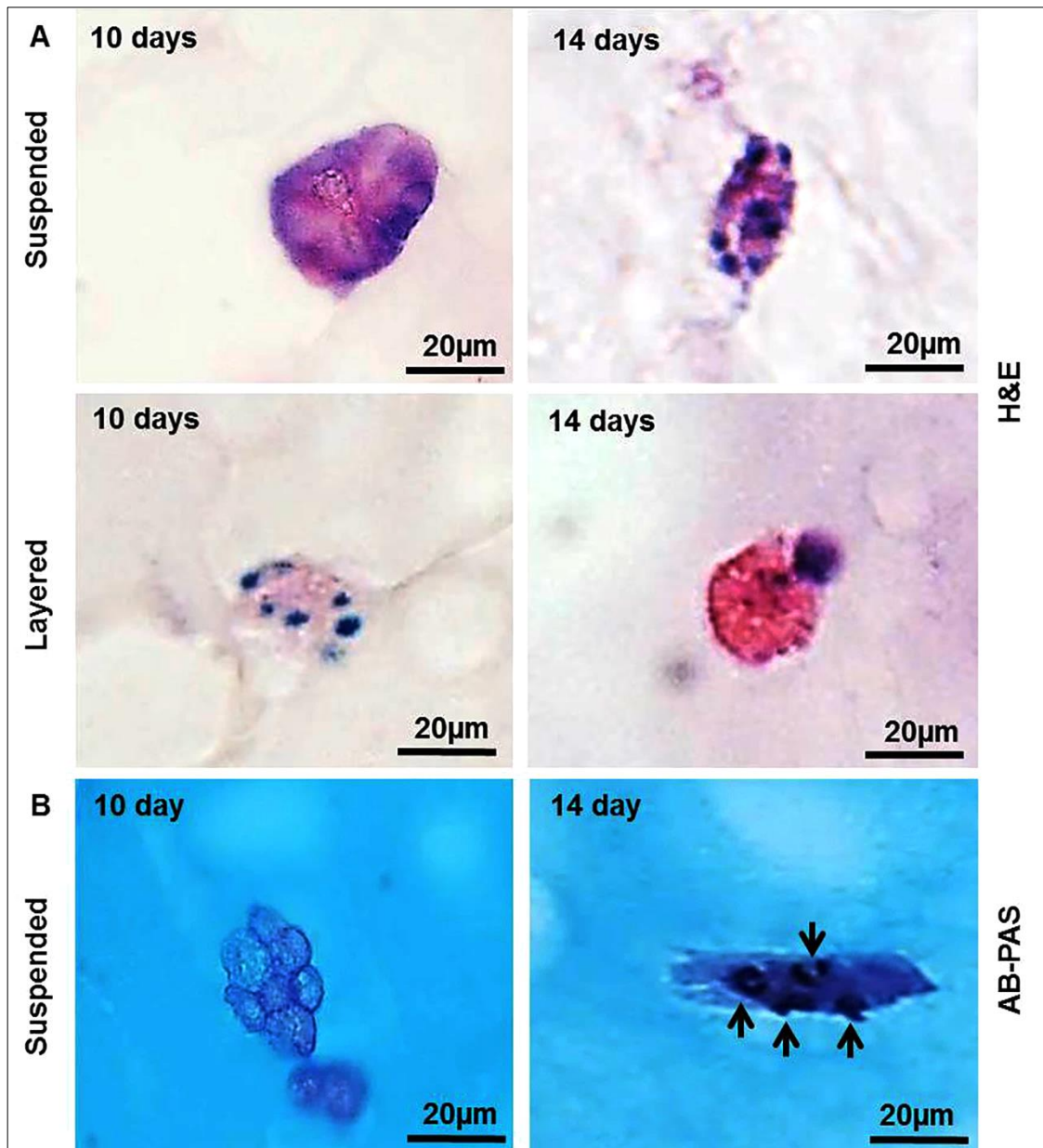


Figure 5.2: Morphology of the isolated small intestinal crypts when suspended directly within or layered on L-pNIPAM hydrogel under dynamic culture conditions for 14 days. The cells stained with: (A) H&E and (B) AB-PAS. Black arrows indicate mucin-producing goblet cells. Scale bar = 20 μ m.

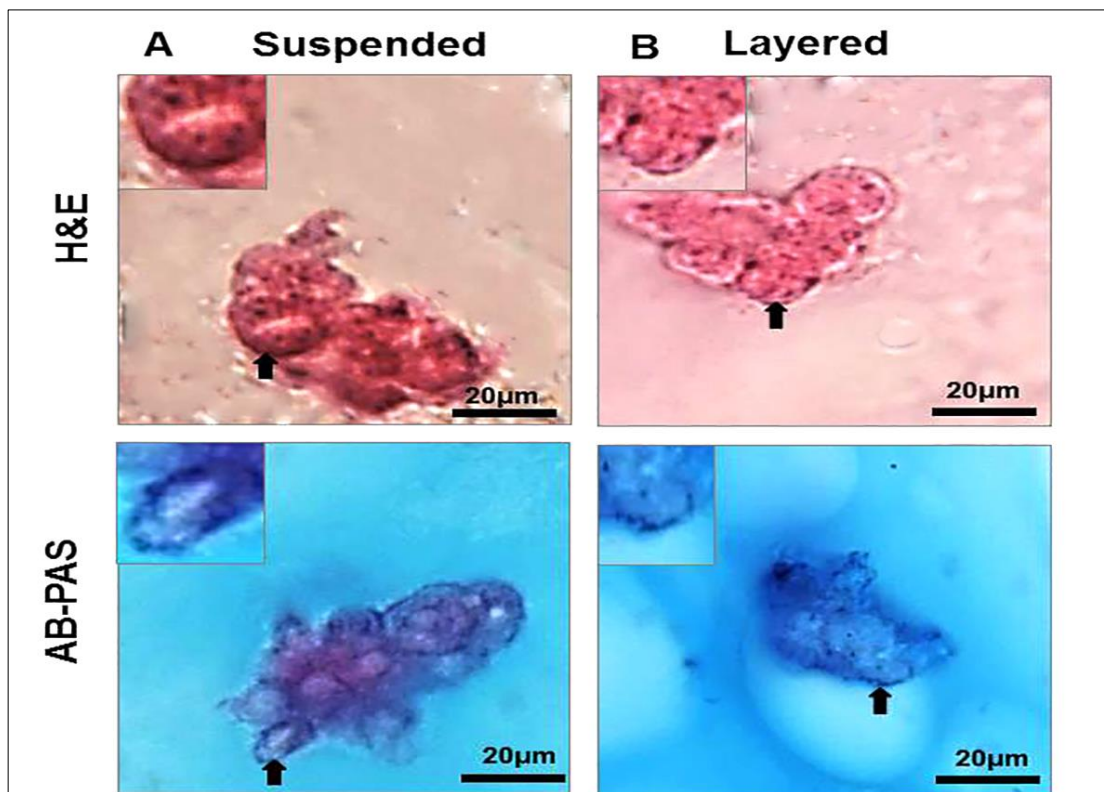


Figure 5.3: Morphology of the isolated small intestinal crypts when suspended within Matrigel for 7 days then the derived organoids were released from Matrigel and dissociated into small fragments and then (A) re-suspended within or (B) layered on L-pNIPAM hydrogel under dynamic culture conditions for 10 days. Stained with H&E: the black arrows indicate the crypt-like buds and AB-PAS: the black arrows indicate the adherent mucus layer coating the organoids and mucin-producing goblet cells. Scale bar = 20 μm .

5.3.3 Phenotypical assessment of the organoids derived from crypts suspended directly in L-pNIPAM hydrogel or in Matrigel for 7 days then dissociated and re-suspended in L-pNIPAM for 10 days

Immunohistochemistry staining was used to determine the cellular composition of the organoids derived from crypts when suspended within L-pNIPAM hydrogel following 10 days culture (Figure 5.4 A-E) or derived from dissociated organoids re-suspended and cultured within L-pNIPAM hydrogel (Figure 5.4 F-J). Lgr5 expression of intestinal stem cells was shown within the crypt-like structure; this was expressed alongside markers for all terminally differentiated epithelial cell lineages which identified the presence of enterocytes, goblet cells, enteroendocrine cells and paneth cells by day 10. Stem cell marker Lgr5 was expressed at the base of the crypt-like buds of the organoids (Figure 5.4 A and F). Cell-cell adhesion marker: E-cadherin was expressed under all culture conditions, but was most highly expressed in the Matrigel to L-pNIPAM organoids (Figure 5.4 B and G). Goblet cell marker MUC2 showed the presence of goblet cells and the adherent mucus layer covering the organoids (Figure 5.4 C and H). The enteroendocrine cell marker: chromogranin A, showed immunopositive cells scattered throughout the organoid structure (Figure 5.4 D and I). Paneth cell marker lysozyme, was seen at the base of the organoids in those crypts which were suspended directly into L-pNIPAM hydrogel; whilst organoids which were grown in Matrigel and then moved to L-pNIPAM hydrogel showed a scattered distribution of lysosome positive cells throughout the organoid (Figure 5.4 E and J).

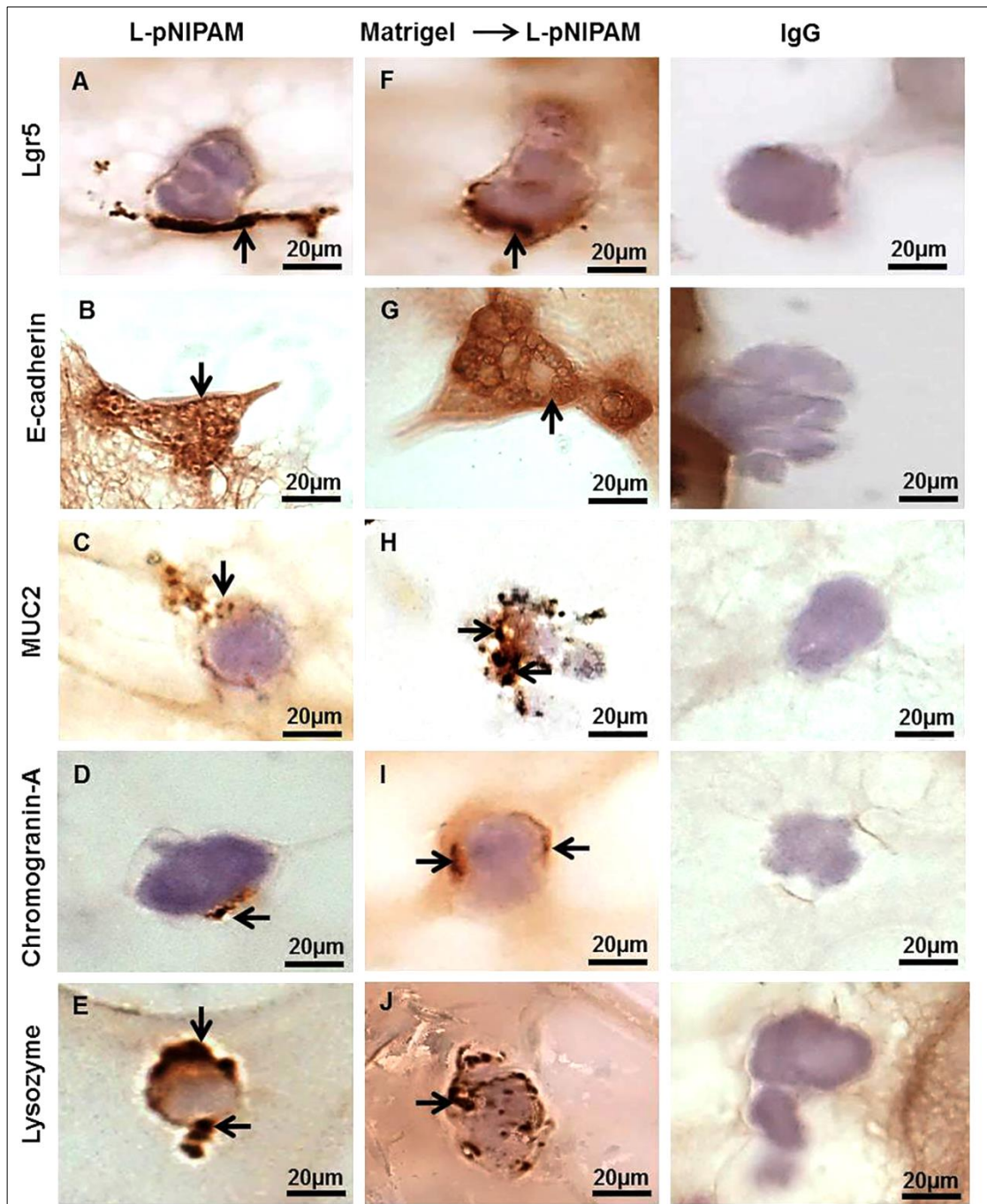


Figure 5.4: Immunohistochemistry staining (black arrows) for Lgr5, E-cadherin, MUC2, Chromogranin-A, and Lysozyme of the isolated small intestinal crypts: A-E suspended directly within L-pNIPAM hydrogel under dynamic culture conditions for 10 days; F-J suspended within Matrigel for 7 days then the organoids were released from Matrigel and dissociated into small fragments then suspended within L-pNIPAM hydrogel under dynamic culture conditions for 10 days. Cell nuclei were stained with haematoxylin (blue). IgG as negative controls. Scale bar = 20 µm.

5.3.4 Morphological assessment of the isolated Lgr5⁺ small intestinal stem cells suspended within Matrigel, L-pNIPAM hydrogel, or layered on L-pNIPAM hydrogel

Single Lgr5⁺ intestinal cells suspended within Matrigel formed intestinal spheroids following 5 days in culture. Between day 10 and 14, the intestinal organoids formed numerous buds (Figure 5.5).

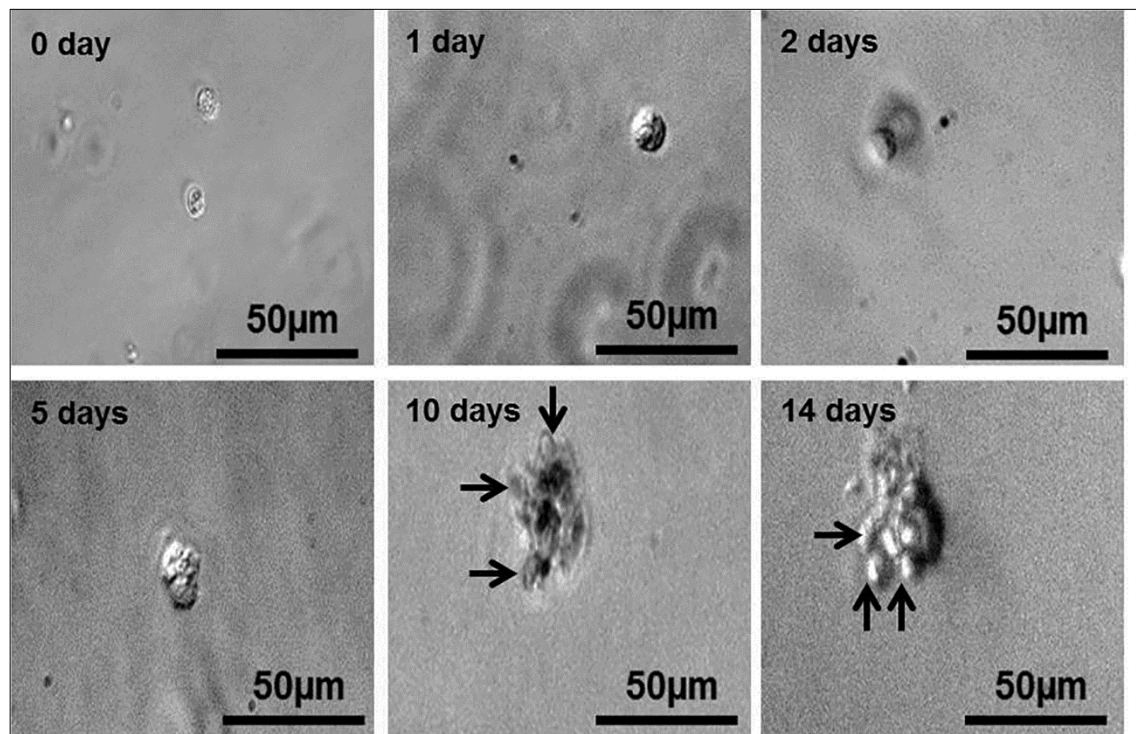


Figure 5.5: Bright-field morphology of the isolated Lgr5⁺ intestinal stem cells suspended within Matrigel from day 0 to 14. Black arrows indicate organoid buds. Scale bar= 50 µm.

When single Lgr5⁺ intestinal cells were suspended within L-pNIPAM hydrogel they proliferated and formed spheroid-like structures composed of multiple cells and started to form buds from day 10 to 14 (Figure 5.6 A). In contrast, when single Lgr5⁺ intestinal cells layered on L-pNIPAM hydrogel the spheroid structure was not observed (Figure 5.6 B).

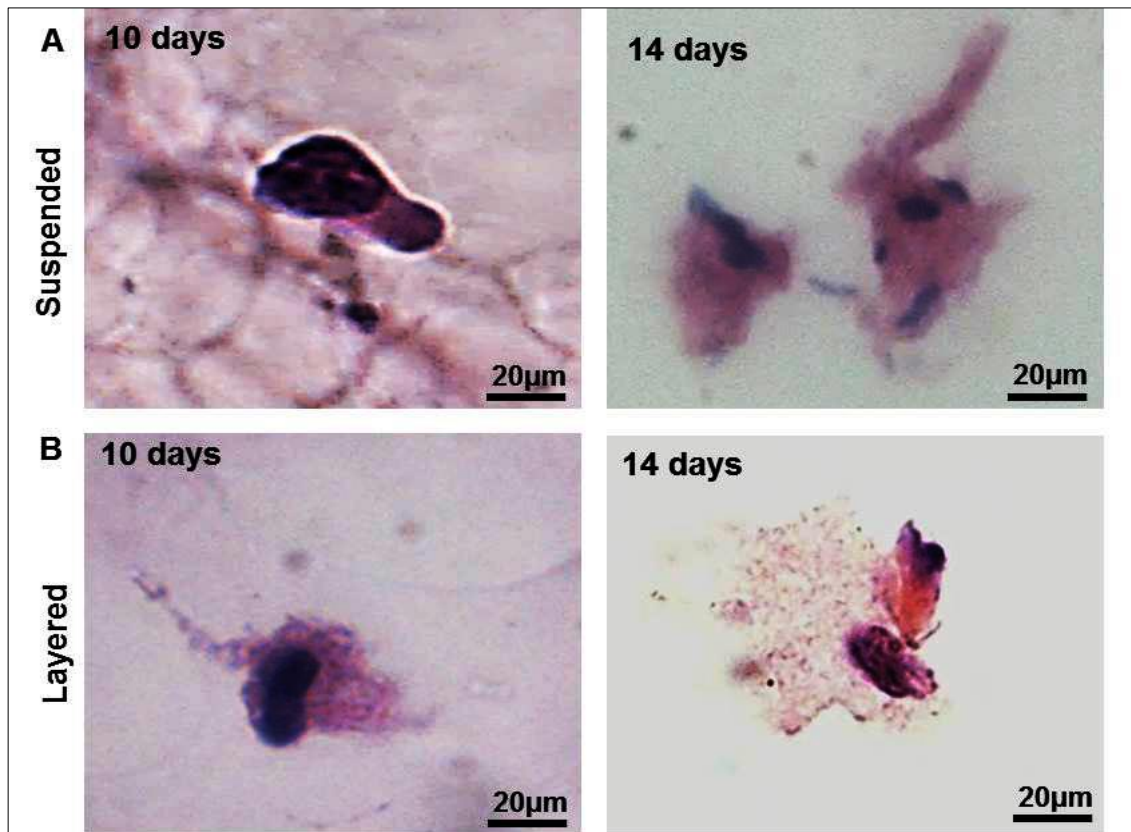


Figure 5.6: Morphology of the isolated $Lgr5^+$ intestinal stem cells: (A) suspended within L-pNIPAM hydrogel and (B) Layered on L-pNIPAM hydrogel under dynamic culture conditions for 10 to 14 days. Stained with H&E. Scale bar = 20 μm .

To determine the ability of $Lgr5^+$ intestinal stem cells to maintain their stemness and differentiation *in vitro* using L-pNIPAM hydrogel; single sorted $Lgr5^+$ stem cells were suspended within Matrigel for 7 days. The derived organoids were released from Matrigel and dissociated into single cells then re-suspended within or layered on L-pNIPAM hydrogel under dynamic culture conditions for up to 28 days. When suspended within or layered on L-pNIPAM hydrogel $Lgr5^+$ cells proliferated and started to form buds and differentiated. The presence of goblet cells was seen after 7 days, and by day 21 to 28 the organoids had numerous buds containing mucin-secreting goblet cells and the organoid was surrounded by an adherent mucus layer (Figure 5.7 A & B).

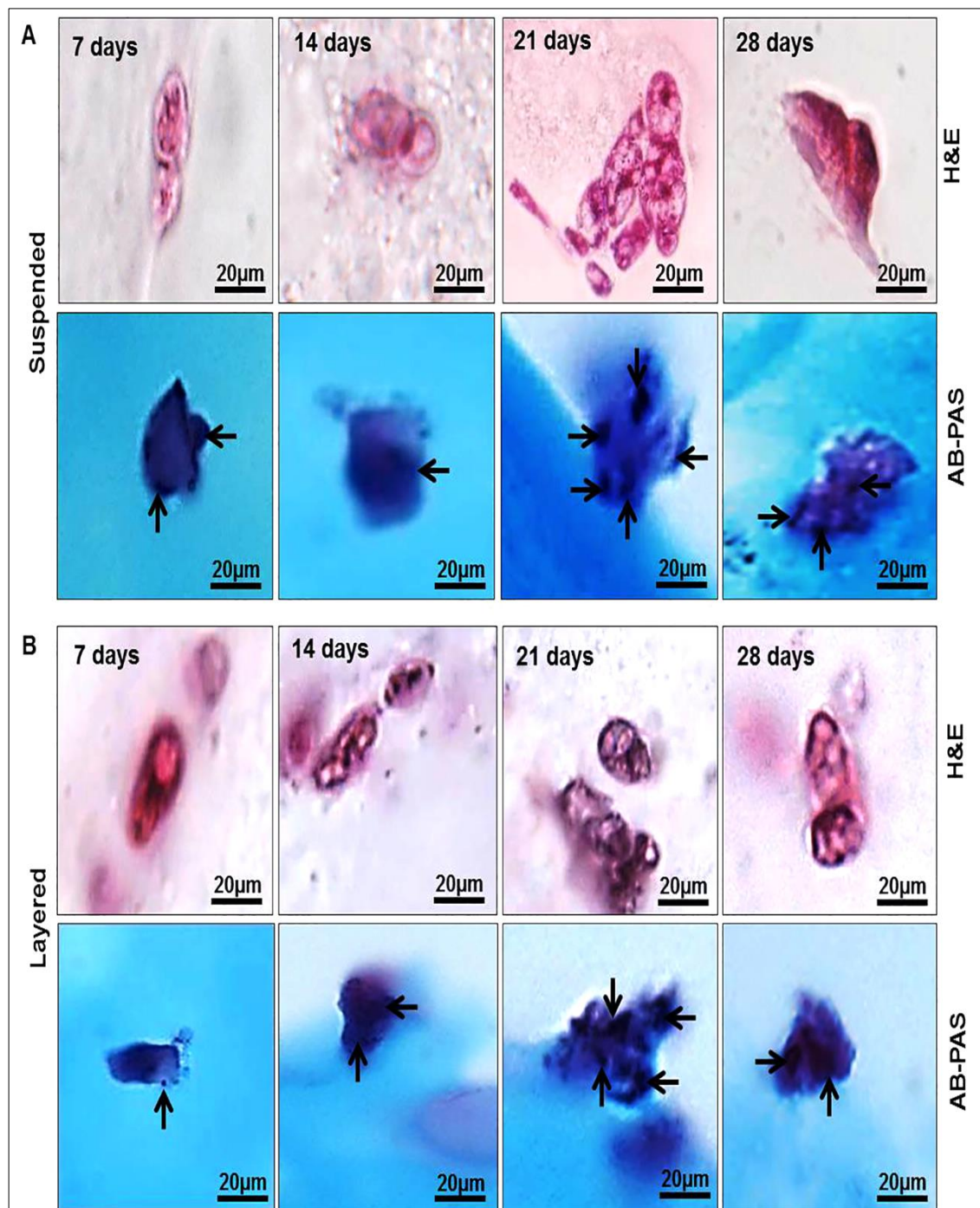


Figure 5.7: Morphology of the isolated $Lgr5^+$ intestinal stem cells suspended within Matrigel for 7 days then the organoids were released from Matrigel and dissociated into single cells and (A) were suspended in L-pNIPAM hydrogel or (B) were layered on L-pNIPAM hydrogel under dynamic culture conditions for 7 to 28 days. Cells were stained with H&E and AB-PAS. The black arrows indicate goblet cells. Scale bar = 20 μm .

Immunohistochemical staining for Lgr5 showed that Lgr5 was expressed by the stem cells located at the base of the small intestinal crypts isolated from mice (Figure 5.8 A). When Lgr5⁺ stem cells were isolated, Lgr5 immunopositivity staining was observed in single sorted Lgr5⁺ intestinal stem cells in day 0 cytopins (Figure 5.8 B). To investigate the specific binding of Lgr5 antibody to the stem cells, two cell lines (Caco-2 and HT29-MTX) were also investigated for Lgr5 positivity. Both cytopins of Caco-2 and HT29-MTX cells showed no expression of Lgr5 (Figure 5.8 C and D).

Immunohistochemistry staining for differentiation markers of isolated Lgr5⁺ stem cells showed immunopositivity for E cadherin only (Figure 5.9 A). There was no immunopositivity for MUC2, Chromogranin A, and Lysozyme (Figure 5.9 B, C, and D).

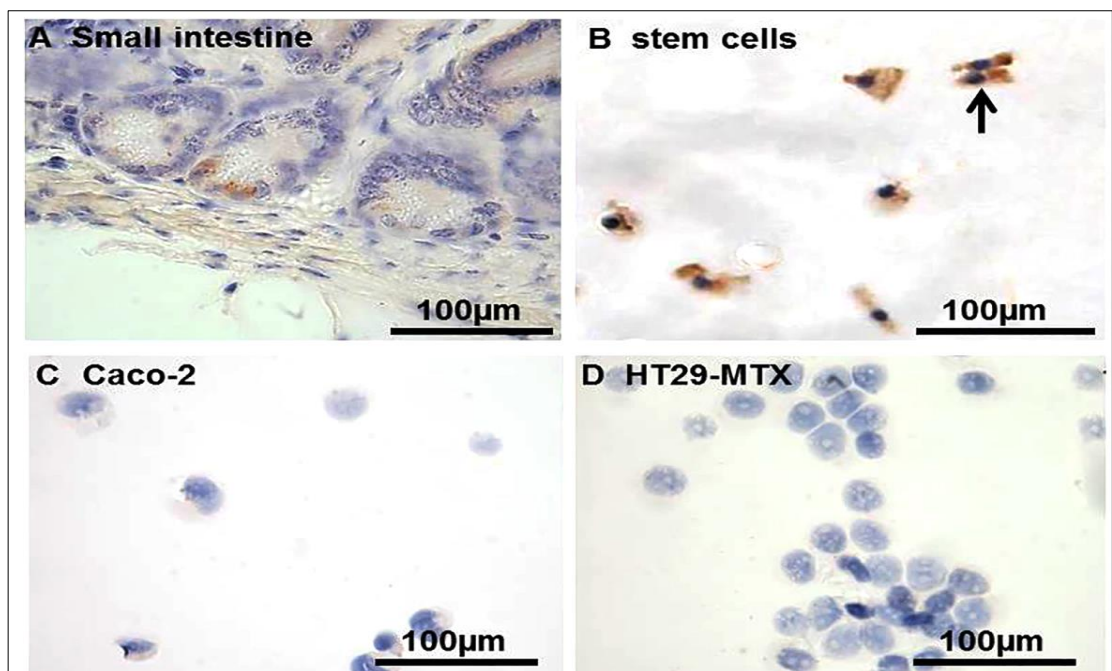


Figure 5.8: Immunohistochemistry staining (black arrows) for Lgr5 in: (A) the intact mouse small intestine, (B) cytopin of Lgr5⁺ intestinal stem cells, (C) Caco-2 cells and (D) HT29-MTX cell lines. Cell nuclei were stained with haematoxylin (blue). Scale bar = 100

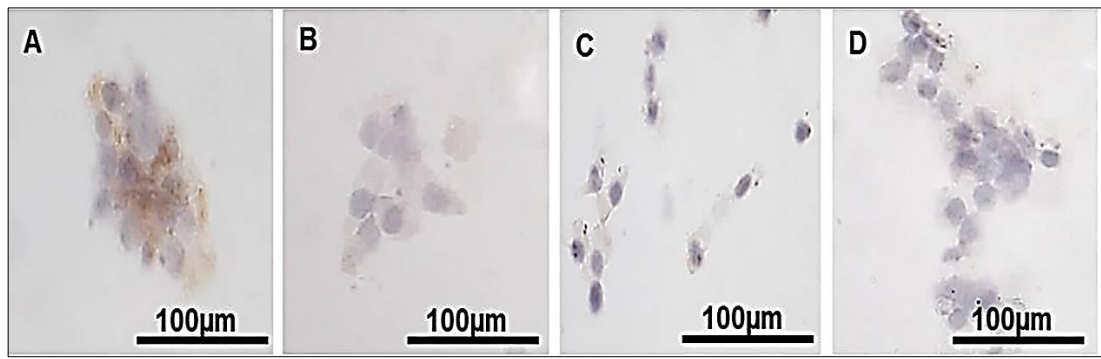


Figure 5.9: Immunohistochemistry staining for (A) E-cadherin; (B) MUC2; (C) Chromogranin-A and (D) Lysozymes in cytospin of the isolated Lgr5⁺ intestinal stem cells. Cell nuclei were stained with haematoxylin (blue). Scale bar = 100 μm.

Immunohistochemistry staining for the intestinal epithelial differentiation markers were used to investigate the differentiation capability of single Lgr5⁺ intestinal stem cells derived from dissociated organoids which were suspended within or layered on L-pNIPAM hydrogel. Lgr5 was expressed in the organoids throughout the entire 28 days study period (Figure 5.10 A and B). There were many Lgr5⁺ cells with the highest levels at the base of crypt-like structures at day 21 to 28 under dynamic culture conditions (Figure 5.10 A). Cell-cell adhesion was investigated in the differentiated cells by E-cadherin expression. At the later time points of 21 and 28 days, E-cadherin was highly expressed in the differentiated cells of the organoids derived from Lgr5⁺ intestinal stem cells when suspended in or layered on L-pNIPAM hydrogel under dynamic culture conditions (Figure 5.11 A and B). Lgr5⁺ intestinal stem cells were differentiated into mucin-producing goblet cells. However, MUC2 expression was time-dependent, with the highest levels of MUC2 immunopositivity observed in the organoids at the later time points of 21 and 28 days (Figure 5.12 A and B). Chromogranin-A immunopositivity which is indicative of the presence of enteroendocrine cells, was not consistently observed during the early stages of

organoid development, but was expressed following prolonged culture at 21 to 28 days, when $Lgr5^+$ intestinal stem cells were suspended within L-pNIPAM hydrogel (Figure 5.13 A).

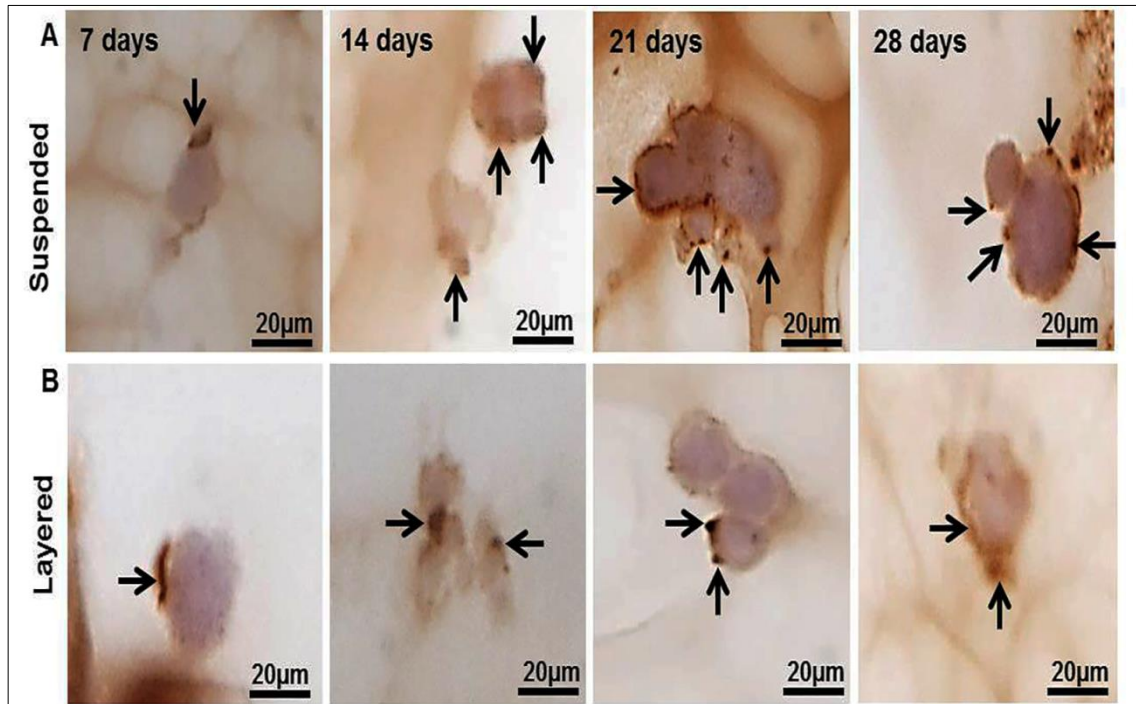


Figure 5.10: Immunohistochemistry staining (black arrows) for $Lgr5$ in isolated $Lgr5^+$ intestinal stem cells when suspended within Matrigel for 7 days then the organoids were released from Matrigel and dissociated into single cells then (A) suspended within L-pNIPAM hydrogel or (B) layered on L-pNIPAM hydrogel under dynamic culture conditions for 7 to 28 days. Cell nuclei were stained with haematoxylin (blue). Scale bar = 20 μ m.

In contrast, Chromogranin-A was expressed in the organoids following 14 days when $Lgr5^+$ intestinal stem cells were layered on L-pNIPAM hydrogel (Figure 5.13 B). Lysozyme expression was seen at day 7-28 indicating the differentiation of Paneth cells when suspended within or layered on L-pNIPAM hydrogel (Figure 5.14 A and B). The highest expression was observed in the organoids when layered on L-pNIPAM hydrogel (Figure 5.14 B).

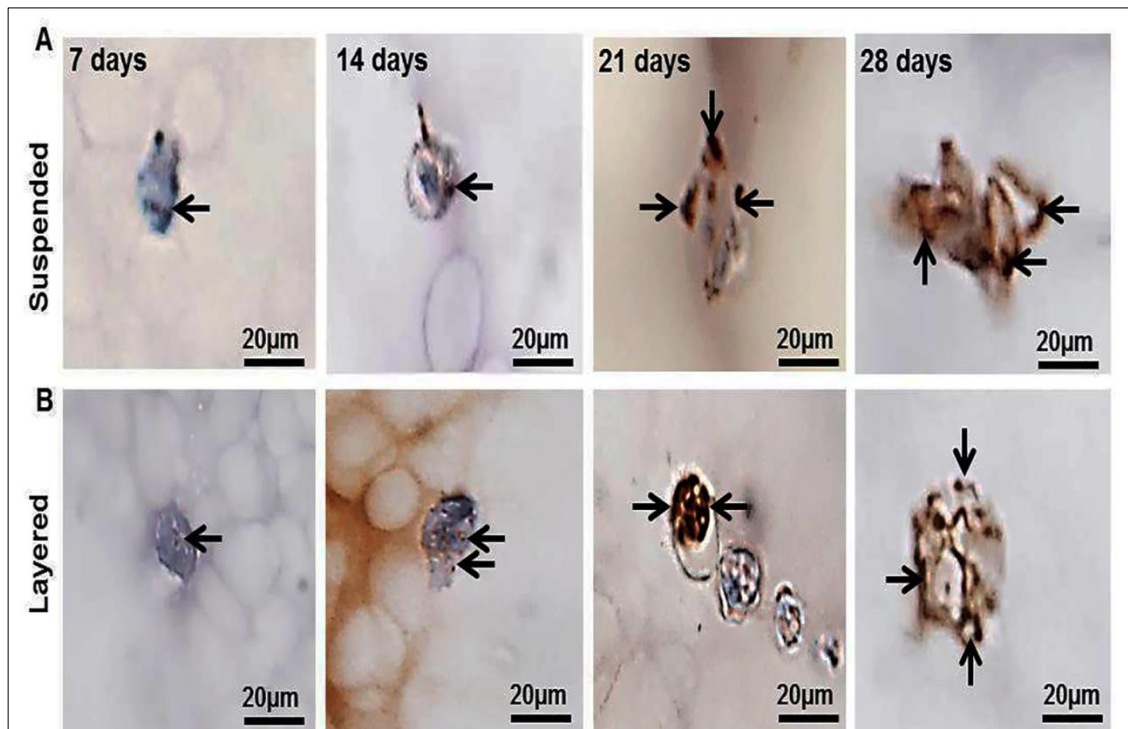


Figure 5.11: Immunohistochemistry staining (black arrows) for E-cadherin of the isolated $Lgr5^+$ intestinal stem cells suspended within Matrigel for 7 days then the organoids were released from Matrigel and dissociated into single cells and (A) suspended within L-pNIPAM hydrogel; (B) layered on L-pNIPAM hydrogel under dynamic culture conditions for 7 to 28 days. Cell nuclei were stained with haematoxyline (blue). Scale bar = 20 μm .

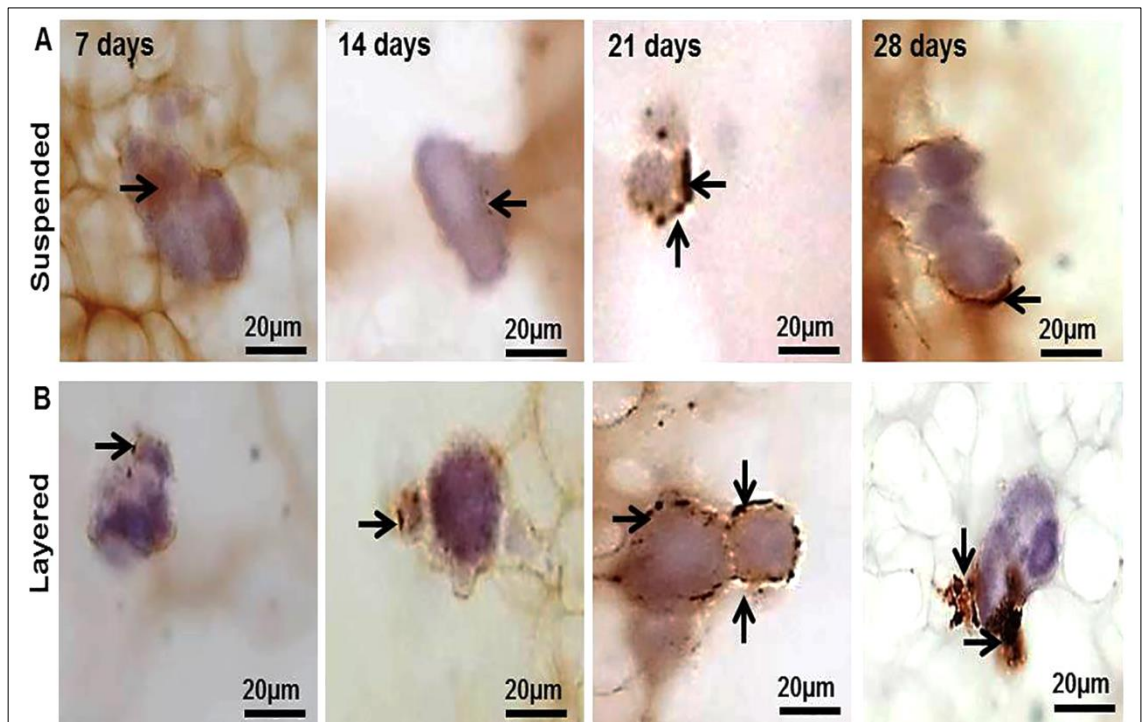


Figure 5.12: Immunohistochemistry staining (black arrows) for MUC2 of the isolated $Lgr5^+$ intestinal stem cells suspended within Matrigel for 7 days then the organoids were released from Matrigel and dissociated into single cells and (A) suspended within L-pNIPAM hydrogel; (B) layered on L-pNIPAM hydrogel under dynamic culture conditions for 7 to 28 days. Cell nuclei were stained with haematoxylin (blue). Scale bar = 20 μm .

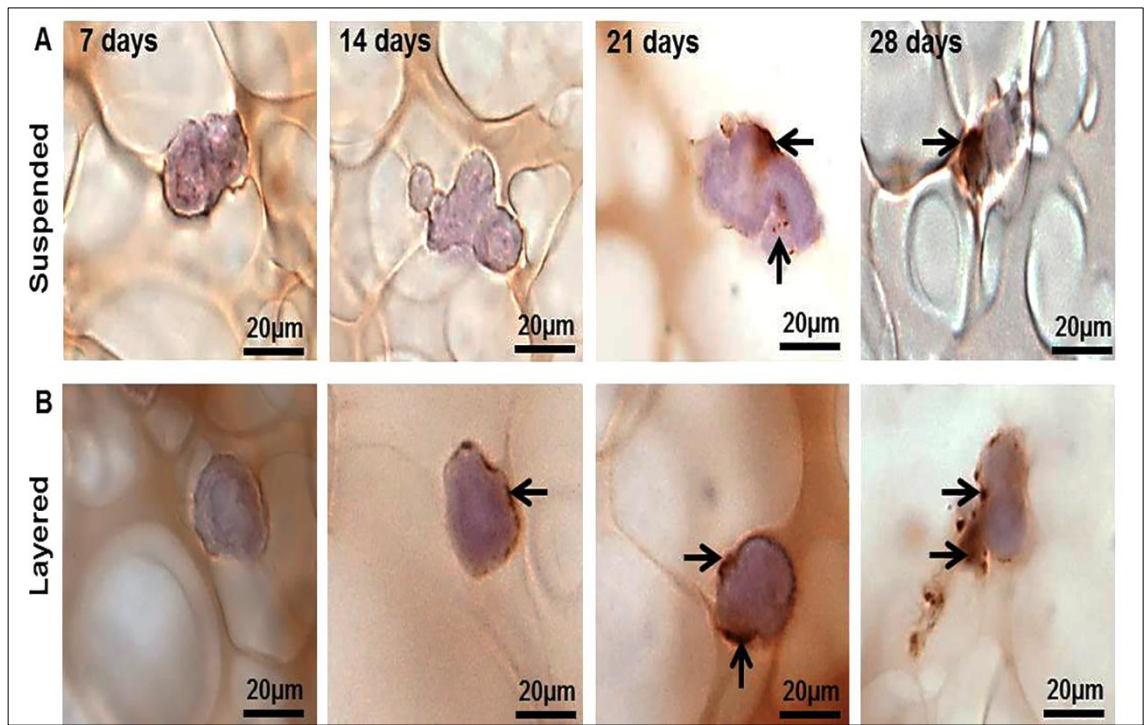


Figure 5.13: Immunohistochemistry staining (black arrows) Chromogranin-A of the isolated $Lgr5^+$ intestinal stem cells suspended within Matrigel for 7 days then the organoids were released from Matrigel and dissociated into single cells and (A) suspended within L-pNIPAM hydrogel; (B) layered on L-pNIPAM hydrogel under dynamic culture conditions for 7 to 28 days. Cell nuclei were stained with haematoxylin (blue). Scale bar = 20 μm .

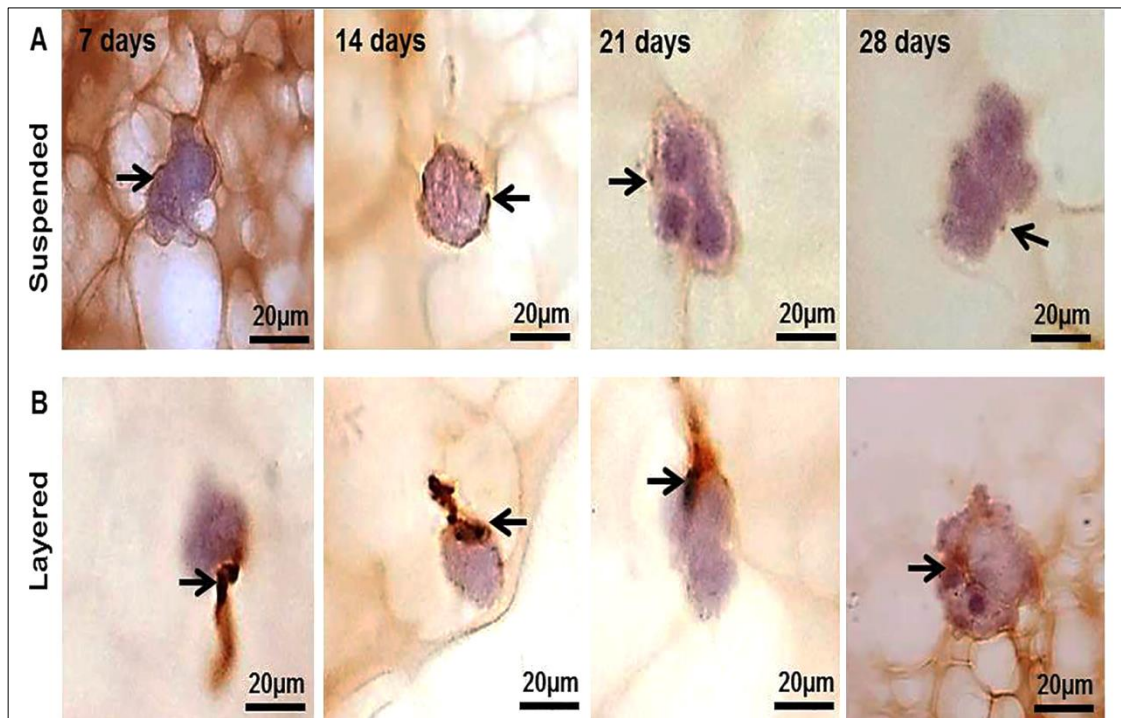


Figure 5.14: Immunohistochemistry staining (black arrows) for lysozyme production of the isolated Lgr5+ intestinal stem cells suspended within Matrigel for 7 days then the organoids were released from Matrigel and dissociated into single cells and (A) suspended within L-pNIPAM hydrogel; (B) layered on L-pNIPAM hydrogel under dynamic culture conditions for 7 to 28 days. Cell nuclei were stained with haematoxylin (blue). Scale bar = 20 µm.

5.4 Discussion

In vivo, intestinal stem cells are positioned at the base of the intestinal crypts and have the ability to renew the epithelium by differentiation into multiple epithelial progenies and initiate mucosal regeneration (Bjerknes & Cheng 2006). Thus, these intestinal stem cells hold great potential in tissue regeneration of the intestine and research groups worldwide are investigating different biomaterial or biological approaches to their use such as Matrigel, collagen type 1, PGA, PLA, PLGA, (Agopian *et al.* 2009; Sato *et al.* 2009; Fuller *et al.* 2013; Liu *et al.* 2014; Mochel *et al.* 2018). Matrigel was the first system utilised to culture these intestinal stem cells and form organoid cultures (Sato *et al.* 2009), however, Matrigel has a number of disadvantages and is not appropriate for use clinically. Therefore, researchers have explored the use of synthetic biomaterials for organoid formation with mixed success (Lahar *et al.* 2011; Boomer *et al.* 2014; Cromeens *et al.* 2016). This study investigated the potential of synthetic porous L-pNIPAM hydrogel as a 3D scaffold for organoid development from crypts and Lgr5⁺ intestinal stem cells under dynamic culture conditions. The capacity of these cells to differentiate into intestinal epithelial cells *in vitro* when suspended within or layered on L-pNIPAM hydrogel was investigated.

Laminin and collagen rich Matrigel 3D scaffold was originally used to develop intestinal epithelial culture (Sato *et al.* 2009); as this was rich in both laminin α 1 and α 2 which are highly expressed in the base of native mice intestinal crypts and are required to support normal villus-crypt morphology (Sasaki *et al.* 2002) Sato *et al.* 2009 developed an *in vitro* culture system capable of developing intestinal organoids from crypt cells and single Lgr5⁺ stem cells. In these systems, the growth media was supplemented with epidermal growth factor

(EGF), the BMP antagonist Noggin, and the Wnt agonist R-spondin 1. Here, this culture system was replicated and successfully demonstrated the development of organoids in Matrigel. These organoids showed the presence of a central core lined with villus-like domains surrounding by crypt-like structures by day 14. These crypt-like domains maintained the basic crypt-villus morphology of the intestinal epithelium and later the central core became filled with dead cells. The structure of these organoids was maintained over several passages. These observations agree with those previously seen utilising Matrigel (Sato *et al.* 2009, 2011a; Fuller *et al.* 2012) which revealed organoids derived from crypt cells consisted of crypts (with occupant Lgr5 cells, Paneth cells and transit amplifying cells (TA)) surrounded a central lumen lined by all terminally differentiated epithelial lineages. In Matrigel, cells proliferated, differentiated, and shed into the central lumen following 5 days which mimics *in vivo* behaviour (Clevers 2013). Despite the potential advantages of Matrigel, particularly the similarity to native ECM (Reed *et al.* 2008), there are also a number of disadvantages, which make Matrigel inappropriate for clinical applications including: high batch variability; sourced from cancerous tissues (Engelbreth-Holm-Swarm mouse sarcoma) and low mechanical stiffness (Reed *et al.* 2008; Soofi *et al.* 2009).

Hence, this has led to the used of synthetic scaffolds with well-defined biochemical and biophysical properties as a scaffold for intestinal tissue engineering (Choi & Vacanti 1997; Gjorevski *et al.* 2014; Shaffiey *et al.* 2016). This current study demonstrated that the synthetic highly porous L-pNIPAM hydrogel facilitated crypt cell seeding and adhesion, however, bud structures were not observed when crypt cells were directly layered on the L-pNIPAM hydrogel. Nevertheless, immunohistochemical staining demonstrated Lgr5

positive stem cells together with all cells expressing positive markers for all differentiated cells (enterocytes, goblet cells, enteroendocrine cells and Paneth cells) were seen in these organoids despite the lack of bud formation. In contrast, when crypts were suspended within Matrigel for 7 days then released from Matrigel, dissociated into small fragments and re-suspended within or layered on L-pNIPAM hydrogel for 10 days under dynamic culture conditions the organoids had multiple buds containing mucin-secreting goblet cells. This suggests that isolated crypts require ECM signals to form organoids with crypt-like buds which was provided by the Matrigel.

Synthetic scaffolds have been used previously to culture intestinal crypts, these crypts have been seeded directly into porous PLGA scaffold (young's modulus = 1-2 GPa) (Costello *et al.* 2014b), or into PLGA coated in either Matrigel (Shaffiey *et al.* 2016) or collagen (Cromeens *et al.* 2016). It has been shown that microfabricated PLGA scaffolds which mimic the villus structure, coated with Matrigel could be utilised to co-culture mice intestinal crypts alongside myofibroblasts and macrophages. Here, intestinal organoids proliferated and filled the entire synthetic villus. Furthermore the cells were shown to differentiate into all the intestinal cell lineages. However, these fabricated scaffolds did not form true-villi, but the scaffolds moulded to form villi like structures for cells to grow on. In contrast co-cultured human colon carcinoma cell lines Caco-2 and HT29-MTX cells grown on L-pNIPAM have been shown to spontaneously give rise to villus-like structures (Dosh *et al.* 2017). In the current study, cultures demonstrated the early stages of organoid formation and cellular differentiation. It remains to be determined if longer cultures of these organoids were performed whether spontaneous villi formation would be seen. Alternatively, transplantation of the L-pNIPAM organoids in *in vivo* models may

induce villi formation as has been seen previously with transplantation of organoids using PLGA scaffolds (Agopian *et al.* 2009; Yui *et al.* 2012; van Rijn *et al.* 2016).

Similarly to the crypt culture, Matrigel has been used as a basement membrane matrix for stem cells due to its capacity to maintain self-renewal (undifferentiated state) of the stem cells (Hughes *et al.* 2010). Here, Lgr5⁺ ISCs were cultured in Matrigel and / or L-pNIPAM hydrogel in the presence of growth factors and the Rho kinase inhibitor Y-27632 (which inhibits stem cell anoikis). The current study found that the isolated Lgr5⁺ stem cells formed organoids with multiple crypt-like buds when grown in Matrigel. These agree with previous studies which showed that organoids were generated in Matrigel from single Lgr5⁺ stem cells after 5 days (Sato *et al.* 2009, 2011a; Sato & Clevers 2012, 2013, 2015).

Lgr5⁺ stem cells also survived, proliferated and started to form buds following 10 days when suspended directly within L-pNIPAM hydrogel. Similarly, when organoids were initially formed in Matrigel, then dissociated into single cells and suspended within or layered on L-pNIPAM hydrogel the stem cells generated crypt-like buds within 21 days. Furthermore, expression of markers of enterocytes, mucus producing goblet cells, enteroendocrine, and Paneth cells together with a residing population of Lgr5 stem cells were observed, suggesting that expanded Lgr5⁺ stem cells can be differentiated into the four main types of the intestinal epithelial cells when suspended within or layered on L-pNIPAM hydrogel. However, it is unknown whether the cells released from the organoid cultures developed in the Matrigel were stem cells or differentiated cells. It has been shown previously that enterocyte progenitors can become

proliferative stem cells and Paneth-like cells during crypt regeneration to replenish stem cell loss. Not only enterocyte progenitors dedifferentiated to stem cells but also secretory progenitors, which derived from Lgr5⁺ stem cells and generate goblet cells, enteroendocrine cells and Paneth cells de-differentiated to stem cells *in vivo* to replace lost stem cells (Van Es *et al.* 2012). Thus, the cells derived from the dissociated Matrigel organoids could have been stem cells or differentiated cells which then de-differentiated to an earlier progenitor cell which then went on to form later organoids in L-pNIPAM hydrogels.

Gjorevski *et al* (2016) reported the first synthetic matrix for the expansion of mouse and human ISCs. They tested the effect of matrix mechanical properties on the ISC survival, proliferation, expansion and differentiation. It has been shown that varying stiffness of polyethylene glycol (PEG) hydrogel and ECM components were required for ISC expansion and organoid formation. Fibronectin based adhesion was required for intestinal stem cells survival and proliferation, whilst ISC expansion required high matrix stiffness. Soft matrix and laminin-based adhesion was required for intestinal stem cells differentiation and organoid formation. To study the relation between the matrix stiffness and the intestinal crypt and stem cell behaviours, the low stiffness Matrigel (young's modulus < 500 Pa) was compared to the high stiffness of L-pNIPAM hydrogel (storage modulus= 0.18-2.8 MPa) (Chapter 3). The results have shown that the stiff L-pNIPAM hydrogel and the soft Matrigel, supported intestinal crypts and stem cells survival, differentiation and organoid formation under dynamic culture conditions. These findings are in agreement with (Chapter 3) study which demonstrated the potential of L-pNIPAM hydrogel to maintain, differentiate, and stimulate of both Caco-2 and HT29-MTX cells to form villus-like structures

compared to low stiffness alginate where the cells formed spheroid-like structures under dynamic culture conditions (Dosh *et al.* 2017). Despite these promising findings, future work is required to investigate the ability of L-pNIPAM hydrogel as scaffold to crypts and Lgr5⁺ stem cells isolated from human small intestine and colon.

In conclusion, L-pNIPAM hydrogel was a suitable scaffold to support the formation of organoids *in vitro* from small intestinal crypts and Lgr5⁺ stem cells isolated from mice and supported appropriate cell differentiation. Thus, further studies are required to investigate host-pathogen interactions, or to test drug delivery and toxicity.

Chapter 6: General discussion

The small intestine is a complicated hollow organ with numerous histological and functional layers that enable digestive functions. This active tube is comprised of an inner layer of absorptive mucosa, a middle layer of connective tissue, and smooth muscle, and an outer layer of serosa (McCance & Huether 1998; Tortora & Derrickson 2016). Inflammatory bowel diseases (IBD) such as Crohn's disease and ulcerative colitis are characterised by inflammation at the mucosal surface, which has defects in its barrier and secretory functions, resulting from a disruption of the gut immune homeostasis (Munkholm *et al.* 1994; Landy *et al.* 2016). The exact pathophysiology of IBD is not fully understood and curative therapies are lacking. Several effective models for the intestinal epithelium exist, each model has a number of advantages and limitations, and thus choosing the appropriate model for a specific research problem is essential. The best of these models are combining all cells types that are implicated in the IBD disease process.

The overall aim of the studies presented in this thesis was to develop several models of the small intestine that can be used to investigation of IBD. Studies were performed by: (1) Using genetically engineered model of IL-1Ra knockout mice to develop a model of inflammatory bowel disease; (2) using human adenocarcinoma-derived intestinal cell lines (Caco-2 and HT29-MTX cell) cultured on natural and synthetic hydrogel systems to investigated potential hydrogel which could be used to develop an *in vitro* 3D model of the small intestinal villi, and then these cells were co-cultured on L-pNIPAM hydrogel scaffolds under conditions which mimic those of inflammatory bowel disease to develop an *in vitro* inflamed human intestinal epithelium; (3) mice intestinal crypts or stem cells were used to investigate the differentiation capacity of these

stem cells when suspended within or layered on L-pNIPAM hydrogel scaffolds to develop an *in vitro* 3D model of intestinal organoids.

Development of genetically engineered murine models of intestinal inflammation is a useful tool to understand the intestinal inflammation seen during inflammatory bowel disease (Cominelli *et al.* 1990; McCall *et al.* 1994; Al-Sadi *et al.* 2008). In this thesis, a number of essential features associated with IBD were investigated in the small intestine of IL-1Ra knockout mice model. Histological staining was performed on jejunum and ileum of BALB/c *IL-1rn^{+/+}* and *IL-1rn^{-/-}* mice from two age groups to characterize the crypt-villus height, villus width, and number of goblet cells per crypt-villus axis. Pro-inflammatory cytokines; immune cell infiltration; matrix-degrading enzymes; the production of intestinal enzymes and the integrity of tight and adherent junction proteins was determined using immunohistochemistry. Genetically engineered model of IL-1Ra knockout mice studies within Chapter 2, demonstrated that the height of crypt-villus axes were significantly reduced in BALB/c *IL-1rn^{-/-}* mice, whilst villi width was decreased in the ileum compared to wild-type mice. Goblet cells per crypt-villus were increased, as was the expression of mucin. Proinflammatory cytokines expression were increased, whilst IL-1R1 expression was decreased in *IL-1rn^{-/-}* mice, with IL-15 and TNF α expression being increased in older *IL-1rn^{-/-}* mice. Increased polymorphonuclear and macrophage cell infiltration was also seen in *IL-1rn^{-/-}* mice, whilst expression of matrix-degrading enzymes and digestive enzymes were unchanged, except for dipeptidyl peptidase IV which was increased in younger *IL-1rn^{-/-}* mice. The expression of tight and adhesion junctions were dramatically decreased in *IL-1rn^{-/-}* mice. These data highlighted the importance of IL-1 in the pathogenesis of inflammatory bowel disease.

While genetically-modified IL-1Ra knockout mice are able to readily induce symptoms of IBD, this *in vivo* animal model shows some limitations. *In vivo* animal testing is expensive and ethically debatable in comparison to *in vitro* studies. Furthermore, species differences between rodents and humans make the interpretation of data from animal testing more complicated. Thus, to reduce the cost and ethical issues raised by using *in vivo* animal models, cell culture-based *in vitro* models have been suggested as an alternative to animal testing.

Caco-2 and HT29-MTX human colon adenocarcinoma cell lines were used in this thesis to develop an *in vitro* 3D cell culture model of intestinal epithelium using highly hydrated natural and synthetic hydrogels. Several hydrogel systems have been developed for 3D cell culture applications to develop villus-like structures (Kim *et al.* 2014; Costello *et al.* 2014b; Yi *et al.* 2017), however to date, none of these systems have demonstrated the formation of villus-like structures without fabrication of these systems using a 3D villi scaffolds. In order to assess the metabolic activity and differentiation of Caco-2 and HT29-MTX cells into enterocytes and goblet-like cells respectively; alginate, L-pNIPAM, and L-pNIPAM-co-DMAc hydrogels scaffolds were used, alongside different cell culture conditions to investigate if it is possible to develop a 3D model of the small intestinal villi *in vitro*. Caco-2 and HT29-MTX cells were suspended within or layered on these hydrogel scaffolds. Both static and dynamic culture conditions were used to mimic the fluid flow of luminal content over the intestinal surface. *In vitro* cell culture studies performed in Chapter 3 demonstrated that the L-pNIPAM hydrogel scaffolds supported layered Caco-2 growth in 3D culture under dynamic culture conditions and gave rise to villus-like structures. Caco-2 cells showed cell polarization of enterocytes like cells which had microvilli on their apical side. There was the expressed neutral mucin,

small intestinal enzymes, and the presence of functional tight junction protein. Similarly, L-pNIPAM hydrogel scaffolds supported growth of layered HT29-MTX cells in 3D culture and formed villus-like structures, where they expressed MUC2 mucin, a characteristic of the small intestine.

However, one cell type alone cannot mimic the whole tissue behavior in case of IBD. The *in vitro* study of the pathogenesis of IBD requires a cell model which closely reflects the characteristics of the *in vivo* intestinal epithelium. Thus, an investigation was made of the potential of L-pNIPAM hydrogel scaffolds to develop long-term 3D co-cultures of layered Caco-2 and HT29-MTX cells under conditions representative of inflammation by treatment with IL-1 β , TNF α , and hypoxia (1% O₂) for 1 week. In this thesis, a number of critical features associated with IBD were investigated in the co-culture model, including: metabolic activity, morphology and the expression of tight junction protein (ZO-1), mucins, digestive enzyme, matrix degrading enzymes, and the induction of apoptosis. *In vitro* studies performed in Chapter 4 demonstrated that L-pNIPAM hydrogel scaffold successfully supported long-term co-cultures under dynamic culture conditions. Furthermore, these co-cultured cells had the ability to mimic the state of inflammation with the increased expression of intestinal inflammation markers.

However, these findings might not always be physiologically relevant to epithelial tissue *in vivo* due to the fact that the cells utilised are derived from tumours. Thus, this thesis went on to determine whether the hydrogel system could be utilised to support growth and differentiation of intestinal stem cells. Lgr5 has been identified as a robust intestinal stem cell marker (Barker *et al.* 2007), and subsequently the formation of the 3D organoid model when isolated

single Lgr5⁺ stem cells or crypt fractions are embedded in Matrigel (Sato *et al.* 2009), has enhanced studies of the intestinal epithelium. Therefore, the potential of L-pNIPAM hydrogel scaffolds to develop 3D intestinal stem cell organoid model was investigated. In this thesis, small intestinal crypt cells, and Lgr5⁺ stem cells were isolated from mice and cultured within matrigel or within or on L-pNIPAM hydrogel in variable conditions, in the presence of R-spondin, Noggin, and epidermal growth factors to mimic the physiological conditions of the intestinal stem cell niche. In order to investigate the ability of single Lgr5⁺ intestinal stem cells or crypt fractions to form crypt-like buds and the differentiation capacity of intestinal stem cells into four different intestinal epithelial cells, morphology and expression of differentiation markers were investigated. The *in vitro* study in Chapter 5 demonstrated that stem cells generated crypt-like buds within 21 days. Moreover, expression of markers of enterocytes, mucus producing goblet cells, enteroendocrine, and Paneth cells indicating that expanded Lgr5⁺ stem cells can be differentiated into the four main types of the intestinal epithelial cells when suspended within or layered on L-pNIPAM hydrogel.

Overall the work from this thesis presents a number of models of small intestine. This thesis has shown that *IL-1rn*^{-/-} mice developed spontaneous abnormalities which displayed features associated with IBD suggesting a causative role in IBD rather than simply an increase due to inflammation. In addition, this thesis has demonstrated that L-pNIPAM hydrogel supported long-term 3D co-culture model and stimulation with factors seen during inflammation recapitulated features of IBD. Together this thesis has shown the ability of L-pNIPAM hydrogel as scaffold to support organoid formation and cell differentiation *in vitro* from small intestinal crypts and Lgr5⁺ stem cells isolated from mice.

6.1 Future directions

6.1.1 Genetically engineered animal model

The genetically engineered IL-1Ra knockout mice model discussed in this thesis has demonstrated its potential as a valuable model in understanding the role of IL-1 in the pathogenesis of IBD. This model could be used for preclinical efficacy testing of new therapeutic candidates. Although within this model the innate immune response to intestinal inflammation was investigated, the responses of adaptive immune system such as T, B lymphocytes, and T helper cells to intestinal inflammation need to be investigated. Furthermore, it would be useful to investigate the effects of IL-1Ra knockout within different mice backgrounds to ensure these effects are not strain dependent.

6.1.2 Epithelial cell culture model

Work accomplished in this thesis demonstrated the potential of L-pNIPAM hydrogel to develop an *in vitro* 3D co-culture model to mimic the state of inflammation under dynamic culture conditions. However, in the further studies of the inflammatory process it is necessary to investigate the crosstalk between epithelial cells and immune cells such as macrophages, lymphocytes, or dendritic cells, which are responsible for the production of pro-inflammatory cytokines. This will enable a model which can combine different cell types and accurately reflect the *in vivo* model to study the interaction between cell types and evaluation of their role in barrier integrity. In the intestine, fluid flow and peristalsis-like motion stimulate the proliferation and differentiation of epithelial cells (Kang & Kim 2016). Hence, in human intestinal disease model, it is very important to engage peristalsis-like mechanical deformation. Thus, the ability to develop a perfusion bioreactor lined by L-pNIPAM hydrogel to cultivate co-culture cells need to be developed. The ease of manipulation of the L-pNIPAM

hydrogel should allow this to be formed inside a tube system where cells can be seeded on the surface and through which media could be passed.

6.1.3 Intestinal stem cell organoid model

The survival and differentiation of intestinal crypts and Lgr5⁺ stem cells isolated from mice cultured on L-pNIPAM hydrogel for up to 28 days is extremely promising for future studies to investigate host - pathogen interactions or to test drug delivery and toxicity. Successful trials in the transplantation of organoids, derived from a single Lgr5 colon stem cell, in murine models of experimental colitis Yui *et al.* (2012) and Fukuda *et al.* (2014) suggests that intestinal stem cell transplantation may establish a new treatment strategy for repairing mucosal barrier function in patients with IBD or indeed Crohn's disease. In this thesis, a mice intestinal organoid model was developed, however, mice models may have limitations in their ability to accurately model human intestinal physiology, future work is required to investigate the potential of L-pNIPAM hydrogel to generate organoids from human intestinal crypts isolated from healthy and diseased biopsies or surgically resected tissues alongside cultivation of isolated human intestinal stem cells to provide an opportunity to advance gastrointestinal research and therapy. In addition, the L-pNIPAM system would be interesting to investigate the ability of the organoid model to include other cellular components such as nerve, muscle, and immune cells. Advanced studies in this field could result in the development of alternative therapies for human intestinal disease.

Together the data presented in this thesis has developed a number of models which can be utilised in the study of the pathogenesis of IBD and determine efficacy of new therapeutic treatments for IBD. Their further development will

enable a more complex *in vitro* model which closely reflects the *in vivo* small intestine.

References

Abadie V. & Jabri B. 2014. IL-15: A central regulator of celiac disease immunopathology. *Immunological Reviews*, 260, 221-234.

Adamczak M. I., Hagesaether E., Smistad G. & Hiorth M. 2016. An *in vitro* study of mucoadhesion and biocompatibility of polymer coated liposomes on HT29-MTX mucus-producing cells. *International Journal of Pharmaceutics*, 498, 225-233.

Ader M. & Tanaka E. M. 2014. Modeling human development in 3D culture. *Current Opinion in Cell Biology*, 31, 23-28.

Agopian V. G., Chen D. C., Avansino J. R. & Stelzner M. 2009. Intestinal stem cell organoid transplantation generates neomucosa in dogs. *Journal of Gastrointestinal Surgery*, 13, 971-982.

Ahn D. H., Crawley S. C., Hokari R., Kato S., Yang S. C., Li J. D. & Kim Y. S. 2005. TNF- α activates MUC2 transcription via NF- κ B but inhibits via JNK activation. *Cellular Physiology and Biochemistry*, 15, 29-40.

Akitsu A., Kakuta S., Saijo S. & Iwakura Y. 2014. Rag2-deficient IL-1 receptor antagonist-deficient mice are a novel colitis model in which innate lymphoid cell-derived IL-17 is involved in the pathogenesis. *Experimental Animals*, 63, 235-246.

Al-Sadi R., Ye D., Said H. M. & Ma T. Y. 2010. IL-1 β -induced increase in intestinal epithelial tight junction permeability is mediated by MEKK-1 activation of canonical NF- κ B pathway. *The American Journal of Pathology*, 177, 2310-2322.

Al-Sadi R., Ye D., Dokladny K. & Ma T. Y. 2008. Mechanism of IL-1 β -induced increase in intestinal epithelial tight junction permeability. *Journal of Immunology*, 180, 5653-5661.

Al-Sadi R. M. & Ma T. Y. 2007. IL-1 β causes an increase in intestinal epithelial tight junction permeability. *Journal of Immunology*, 178, 4641-4649.

Andus T., Targan S. R., Deem R. & Toyoda H. 1993. Measurement of tumor necrosis factor alpha mRNA in small numbers of cells by quantitative polymerase chain reaction. *Regional Immunology*, 5, 11-17.

Antoine E. E., Vlachos P. P. & Rylander M. N. 2014. Review of collagen I hydrogels for bioengineered tissue microenvironments: characterization of mechanics, structure, and transport. *Tissue Engineering Part B: Reviews*, 20, 683-696.

Antunes F., Andrade F., Araújo F., Ferreira D. & Sarmiento B. 2013. Establishment of a triple co-culture *in vitro* cell models to study intestinal absorption of peptide drugs. *European Journal of Pharmaceutics and Biopharmaceutics*, 83, 427-435.

Araujo F. & Sarmiento B. 2013. Towards the characterization of an *in vitro* triple co-culture intestine cell model for permeability studies. *International Journal of Pharmaceutics*, 458, 128-134.

Arend W. P. 2002. The balance between IL-1 and IL-1Ra in disease. *Cytokine & Growth Factor Reviews*, 13, 323-340.

Atuma C., Strugala V., Allen A. & Holm L. 2001. The adherent gastrointestinal mucus gel layer: thickness and physical state *in vivo*. *American Journal of Physiology-Gastrointestinal and Liver Physiology*, 280, G922-G929.

Aveleira C., Castilho Á, Baptista F., Simões N., Fernandes C., Leal E. & Ambrósio A. F. 2010. High glucose and interleukin-1 β downregulate interleukin-1 type I receptor (IL-1RI) in retinal endothelial cells by enhancing its degradation by a lysosome-dependent mechanism. *Cytokine*, 49, 279-286.

Baker E. L., Bonnecaze R. T. & Zaman M. H. 2009. Extracellular matrix stiffness and architecture govern intracellular rheology in cancer. *Biophysical Journal*, 97, 1013-1021.

Balimane P. V. & Chong S. 2005. Cell culture-based models for intestinal permeability: a critique. *Drug Discovery Today*, 10, 335-343.

Balimane P. V., Chong S. & Morrison R. A. 2000. Current methodologies used for evaluation of intestinal permeability and absorption. *Journal of pharmacological and toxicological methods*, 44, 301-312.

Banerjee A., Arha M., Choudhary S., Ashton R. S., Bhatia S. R., Schaffer D. V. & Kane R. S. 2009. The influence of hydrogel modulus on the proliferation and differentiation of encapsulated neural stem cells. *Biomaterials*, 30, 4695-4699.

Barker N. 2014. Adult intestinal stem cells: critical drivers of epithelial homeostasis and regeneration. *Nature Reviews Molecular Cell Biology*, 15, 19-33.

Barker N., Van Oudenaarden A. & Clevers H. 2012. Identifying the stem cell of the intestinal crypt: strategies and pitfalls. *Cell Stem Cell*, 11, 452-460.

Barker N., Bartfeld S. & Clevers H. 2010. Tissue-resident adult stem cell populations of rapidly self-renewing organs. *Cell Stem Cell*, 7, 656-670.

Barker N., Van de Wetering M. & Clevers H. 2008. The intestinal stem cell. *Genes & Development*, 22, 1856-1864.

Barker N., Van Es J. H., Kuipers J., Kujala P., Van den Born M., Cozijnsen M., Haegebarth A., Korving J., Begthel H. & Peters P. J. 2007. Identification of stem cells in small intestine and colon by marker gene *Lgr5*. *Nature*, 449, 1003-1007.

Barker N., Tan S. & Clevers H. 2013. *Lgr* proteins in epithelial stem cell biology. *Development*, 140, 2484-2494.

Basson M. D., Turowski G. & Emenaker N. J. 1996. Regulation of human (Caco-2) intestinal epithelial cell differentiation by extracellular matrix proteins. *Experimental Cell Research*, 225, 301-305.

Basu J. & Bertram T. A. 2014. Regenerative medicine of the gastrointestinal tract. *Toxicologic Pathology*, 42, 82-90.

Baugh M. D., Perry M. J., Hollander A. P., Davies D. R., Cross S. S., Lobo A. J., Taylor C. J. & Evans G. S. 1999. Matrix metalloproteinase levels are elevated in inflammatory bowel disease. *Gastroenterology*, 117, 814-822.

Baumgart D. C. & Carding S. R. 2007. Inflammatory bowel disease: cause and immunobiology. *The Lancet*, 369, 1627-1640.

Beck P. L. & Wallace J. L. 1997. Cytokines in inflammatory bowel disease. *Mediators of Inflammation*, 6, 95-103.

Becker L., Huang Q. & Mashimo H. 2008. Immunostaining of Lgr5, an intestinal stem cell marker, in normal and premalignant human gastrointestinal tissue. *The Scientific World Journal*, 8, 1168-1176.

Béduneau A., Tempesta C., Fimbel S., Pellequer Y., Jannin V., Demarne F. & Lamprecht A. 2014. A tunable Caco-2/HT29-MTX co-culture model mimicking variable permeabilities of the human intestine obtained by an original seeding procedure. *European Journal of Pharmaceutics and Biopharmaceutics*, 87, 290-298.

Behrens I., Stenberg P., Artursson P. & Kissel T. 2001. Transport of lipophilic drug molecules in a new mucus-secreting cell culture model based on HT29-MTX cells. *Pharmaceutical Research*, 18, 1138-1145.

Bein A., Shin W., Jalili-Firoozinezhad S., Park M., Sontheimer-Phelps A., Tovaglieri A., Chalkiadaki A., Kim H. & Ingber D. 2018. Microfluidic organ-on-a-chip models of human intestine. *Cellular and Molecular Gastroenterology and Hepatology*, 5, 659-668.

Belchior, G. G., Sogayar M. C. & Grikscheit T. C. (2014). Stem cells and biopharmaceuticals: vital roles in the growth of tissue-engineered small intestine. *Seminars in Pediatric Surgery*, 23, 141-149.

Berger E., Nassra M., Atgié C., Plaisancié P. & Géoën A. 2017. Oleic acid uptake reveals the rescued enterocyte phenotype of colon cancer Caco-2 by HT29-MTX cells in co-culture model. *International Journal of Molecular Sciences*, 18, 1-21

Bernet M. F., Brassart D., Neeser J. R. & Servin A. L. 1993. Adhesion of human bifidobacterial strains to cultured human intestinal epithelial cells and inhibition

of enteropathogen-cell interactions. *Applied and Environmental Microbiology*, 59, 4121-4128.

Biasi F., Leonarduzzi G., Oteiza P. I. & Poli G. 2013. Inflammatory bowel disease: mechanisms, redox considerations, and therapeutic targets. *Antioxidants & Redox Signaling*, 19, 1711-1747.

Bilski J., Mazur-Bialy A., Wojcik D., Zahradnik-Bilska J., Brzozowski B., Magierowski M., Mach T., Magierowska K. & Brzozowski T. 2017. The role of intestinal alkaline phosphatase in inflammatory disorders of gastrointestinal tract. *Mediators of Inflammation*, 2017, 1-9.

Bitar K. N. & Zakhem E. 2013. Tissue engineering and regenerative medicine as applied to the gastrointestinal tract. *Current Opinion in Biotechnology*, 24, 909-915.

Bjerknes M. & Cheng H. 2006. Intestinal epithelial stem cells and progenitors. *Methods in Enzymology*, 419, 337-383.

Blumberg R. S., Saubermann L. J. & Strober W. 1999. Animal models of mucosal inflammation and their relation to human inflammatory bowel disease. *Current Opinion in Immunology*, 11, 648-656.

Boomer L., Liu Y., Mahler N., Johnson J., Zak K., Nelson T., Lannutti J. & Besner G. E. 2014. Scaffolding for challenging environments: materials selection for tissue engineered intestine. *Journal of Biomedical Materials Research Part A*, 102, 3795-3802.

Bosca-Watts M. M., Tosca J., Anton R., Mora M., Minguez M. & Mora F. 2015. Pathogenesis of Crohn's disease: Bug or no bug. *World Journal of Gastrointestinal Pathophysiology*, 6, 1-12.

Boyes V. 2012. The synthesis and development of novel, easily processable poly (n-isopropylacrylamide)-based hydrogels. Sheffield Hallam University, Faculty of Arts, Computing, Engineering and Sciences. doi: Thesis no. 27578.

Boyes V. L., Sammon C., Lemaitre C. & Breen C. 2013. Composite hydrogel-clay particles, Patent, i.d: WO2013027051A1.

Breese E. J., Michie C. A., Nicholls S. W., Murch S. H., Williams C. B., Domizio P., Walker-Smith J. A. & Macdonald T. T. 1994. Tumor necrosis factor α -producing cells in the intestinal mucosa of children with inflammatory bowel disease. *Gastroenterology*, 106, 1455-1466.

Bu X., Li N., Tian X. & Huang P. 2011. Caco-2 and LS174T cell lines provide different models for studying mucin expression in colon cancer. *Tissue and Cell*, 43, 201-206.

Bu X. D., Li N., Tian X. Q., Li L., Wang J. S., Yu X. J. & Huang P. L. 2010. Altered expression of MUC2 and MUC5AC in progression of colorectal carcinoma. *World Journal of Gastroenterology*, 16, 4089-4094.

Cao N. 2011. Fabrication of alginate hydrogel scaffolds and cell viability in calcium-crosslinked alginate hydrogel. Thesis

Carr D. A. & Peppas N. A. 2010. Assessment of poly (methacrylic acid-co-N-vinyl pyrrolidone) as a carrier for the oral delivery of therapeutic proteins using Caco-2 and HT29-MTX cell lines. *Journal of Biomedical Materials Research Part A*, 92, 504-512.

Casini-Raggi V., Kam L., Chong Y. J., Fiocchi C., Pizarro T. T. & Cominelli F. 1995. Mucosal imbalance of IL-1 and IL-1 receptor antagonist in inflammatory bowel disease. A novel mechanism of chronic intestinal inflammation. *Journal of Immunology*, 154, 2434-2440.

Chan G. & Mooney D. J. 2013. Ca^{2+} released from calcium alginate gels can promote inflammatory responses *in vitro* and *in vivo*. *Acta Biomaterialia*, 9, 9281-9291.

Chantret I., Rodolosse A., Barbat A., Dussaulx E., Brot-Laroche E., Zweibaum A. & Rousset M. 1994. Differential expression of sucrase-isomaltase in clones isolated from early and late passages of the cell line Caco-2: evidence for glucose-dependent negative regulation. *Journal of Cell Science*, 107, 213-225.

Chen C., Kono H., Golenbock D., Reed G., Akira S. & Rock K. L. 2007. Identification of a key pathway required for the sterile inflammatory response triggered by dying cells. *Nature Medicine*, 13, 851-856.

Chen X., Elisia I. & Kitts D. D. 2010. Defining conditions for the co-culture of Caco-2 and HT29-MTX cells using Taguchi design. *Journal of Pharmacological and Toxicological Methods*, 61, 334-342.

Chen Y., Lin Y., Davis K. M., Wang Q., Rnjak-Kovacina J., Li C., Isberg R. R., Kumamoto C. A., Mecsas J. & Kaplan D. L. 2015. Robust bioengineered 3D functional human intestinal epithelium. *Scientific Reports*, 5, 13708.

Cheng H. & Leblond C. 1974. Origin, differentiation and renewal of the four main epithelial cell types in the mouse small intestine. *American Journal of Anatomy*, 141, 461-479.

Choi R. S., Riegler M., Pothoulakis C., Kim B. S., Mooney D., Vacanti M. & Vacanti J. P. 1998. Studies of brush border enzymes, basement membrane components, and electrophysiology of tissue-engineered neointestine. *Journal of Pediatric Surgery*, 33, 991-997.

Choi R. & Vacanti J. (1997). Preliminary studies of tissue-engineered intestine using isolated epithelial organoid units on tubular synthetic biodegradable scaffolds. *Transplant Proc*, 29, 848-851.

Clatworthy J. P. & Subramanian V. 2001. Stem cells and the regulation of proliferation, differentiation and patterning in the intestinal epithelium: emerging insights from gene expression patterns, transgenic and gene ablation studies. *Mechanisms of Development*, 101, 3-9.

Clevers H. 2016. Modeling development and disease with organoids. *Cell*, 165, 1586-1597.

Clevers H. 2013. The intestinal crypt, a prototype stem cell compartment. *Cell*, 154, 274-284.

Clevers H. 2009. Searching for adult stem cells in the intestine. *EMBO Molecular Medicine*, 1, 255-259.

Coccia M., Harrison O. J., Schiering C., Asquith M. J., Becher B., Powrie F. & Maloy K. J. 2012. IL-1beta mediates chronic intestinal inflammation by promoting the accumulation of IL-17A secreting innate lymphoid cells and CD4(+) Th17 cells. *The Journal of Experimental Medicine*, 209, 1595-1609.

Colgan S. P. & Taylor C. T. 2010. Hypoxia: an alarm signal during intestinal inflammation. *Nature Reviews Gastroenterology and Hepatology*, 7, 281.

Colgan S. P., Campbell E. L. & Kominsky D. J. 2016. Hypoxia and mucosal inflammation. *Annual Review of Pathology*, 11, 77-100.

Cominelli F., Nast C. C., Duchini A. & Lee M. 1992. Recombinant interleukin-1 receptor antagonist blocks the proinflammatory activity of endogenous interleukin-1 in rabbit immune colitis. *Gastroenterology*, 103, 65-71.

Cominelli F., Nast C. C., Clark B. D., Schindler R., Lierena R., Eysselein V. E., Thompson R. C. & Dinarello C. A. 1990. Interleukin 1 (IL-1) gene expression, synthesis, and effect of specific IL-1 receptor blockade in rabbit immune complex colitis. *The Journal of Clinical Investigation*, 86, 972-980.

Costello C. M., Sorna R. M., Goh Y., Cengic I., Jain N. K. & March J. C. 2014a. 3-D intestinal scaffolds for evaluating the therapeutic potential of probiotics. *Molecular Pharmaceutics*, 11, 2030-2039.

Costello C. M., Hongpeng J., Shaffiey S., Yu J., Jain N. K., Hackam D. & March J. C. 2014b. Synthetic small intestinal scaffolds for improved studies of intestinal differentiation. *Biotechnology and Bioengineering*, 111, 1222-1232.

Cromeens B. P., Liu Y., Stathopoulos J., Wang Y., Johnson J. & Besner G. E. 2016. Production of tissue-engineered intestine from expanded enteroids. *Journal of Surgical Research*, 204, 164-175.

Cui W., Li L., Sun C., Wen Y., Zhou Y., Dong Y. & Liu P. 2010. Tumor necrosis factor alpha increases epithelial barrier permeability by disrupting tight junctions in Caco-2 cells. *Brazilian Journal of Medical and Biological Research*, 43, 330-337.

Cukierman E., Pankov R. & Yamada K. M. 2002. Cell interactions with three-dimensional matrices. *Current Opinion in Cell Biology*, 14, 633-640.

Cukierman E., Pankov R., Stevens D. R. & Yamada K. M. 2001. Taking cell-matrix adhesions to the third dimension. *Science*, 294, 1708-1712.

Daig R., Rogler G., Aschenbrenner E., Vogl D., Falk W., Gross V., Scholmerich J. & Andus T. 2000. Human intestinal epithelial cells secrete interleukin-1 receptor antagonist and interleukin-8 but not interleukin-1 or interleukin-6. *Gut*, 46, 350-358.

Date S. & Sato T. 2015. Mini-gut organoids: reconstitution of the stem cell niche. *Annual Review of Cell and Developmental Biology*, 31, 269-289.

Davie, S. L., Gibbons C. E., Steward M. C. & Ward D. T. 2008. Extracellular calcium-and magnesium-mediated regulation of passive calcium transport across Caco-2 monolayers. *Biochimica et Biophysica Acta*, 1778, 2318-2324.

Day R. M. 2006. Epithelial stem cells and tissue engineered intestine. *Current stem cell research & therapy*, 1, 113-120.

Dedhia P. H., Bertaux-Skeirik N., Zavros Y. & Spence J. R. 2016. Organoid models of human gastrointestinal development and disease. *Gastroenterology*, 150, 1098-1112.

Demircan K., Hirohata S., Nishida K., Hatipoglu O. F., Oohashi T., Yonezawa T., Apte S. S. & Ninomiya Y. 2005. ADAMTS-9 is synergistically induced by interleukin-1 β and tumor necrosis factor α in OUMS-27 chondrosarcoma cells and in human chondrocytes. *Arthritis & Rheumatology*, 52, 1451-1460.

Dilly A. K., Lee Y. J., Zeh H. J., Guo Z. S., Bartlett D. L. & Choudry H. A. 2016. Targeting hypoxia-mediated mucin 2 production as a therapeutic strategy for mucinous tumors. *Translational Research*, 169, 19-30.

Dinarello C. A. 2009. Immunological and inflammatory functions of the interleukin-1 family. *Annual Review of Immunology*, 27, 519-550.

Dinarelo C. A. 2011. Interleukin-1 in the pathogenesis and treatment of inflammatory diseases. *Blood*, 117, 3720-3732.

Dorofeyev A. E., Vasilenko I. V., Rassokhina O. A. & Kondratiuk R. B. 2013. Mucosal barrier in ulcerative colitis and Crohn's disease. *Gastroenterology Research and Practice*, 2013, 431231.

Dosh R., Essa A., Jordan-Mahy N., Sammon C. & Le Maitre C. 2017. Use of hydrogel scaffolds to develop an *in vitro* 3D culture model of human intestinal epithelium. *Acta Biomaterialia*, 62, 128-143.

Drury J. L. & Mooney D. J. 2003. Hydrogels for tissue engineering: scaffold design variables and applications. *Biomaterials*, 24, 4337-4351.

Drygiannakis I., Valatas V., Sfakianaki O., Bourikas L., Manousou P., Kambas K., Ritis K., Kolios G. & Kouroumalis E. 2013. Proinflammatory cytokines induce crosstalk between colonic epithelial cells and subepithelial myofibroblasts: implication in intestinal fibrosis. *Journal of Crohn's & Colitis*, 7, 286-300.

Egeblad M. & Werb Z. 2002. New functions for the matrix metalloproteinases in cancer progression. *Nature Reviews Cancer*, 2, 161-174.

Ehrbar M., Sala A., Lienemann P., Ranga A., Mosiewicz K., Bittermann A., Rizzi S., Weber F. & Lutolf M. 2011. Elucidating the role of matrix stiffness in 3D cell migration and remodeling. *Biophysical Journal*, 100, 284-293.

Elson C. O., Sartor R. B., Tennyson G. S. & Riddell R. H. 1995. Experimental models of inflammatory bowel disease. *Gastroenterology*, 109, 1344-1367.

Eltzschig H. K., Bratton D. L. & Colgan S. P. 2014. Targeting hypoxia signalling for the treatment of ischaemic and inflammatory diseases. *Nature Reviews Drug Discovery*, 13, 852-869.

Engler A. J., Sen S., Sweeney H. L., Discher D. E. 2006. Matrix elasticity directs stem cell lineage specification. *Cell*, 125, 677-689.

Enss M., Cornberg M., Wagner S., Gebert A., Henrichs M., Eisenblätter R., Beil W., Kownatzki R. & Hedrich H. 2000. Proinflammatory cytokines trigger MUC

gene expression and mucin release in the intestinal cancer cell line LS180. *Inflammation Research*, 49, 162-169.

Fawley J. & Gourlay D. M. 2016. Intestinal alkaline phosphatase: a summary of its role in clinical disease. *Journal of Surgical Research*, 202, 225-234.

Ferraretto A., Gravaghi C., Donetti E., Cosentino S., Donida B. M., Bedoni M., Lombardi G., Fiorilli A. & Tettamanti G. 2007. New methodological approach to induce a differentiation phenotype in Caco-2 cells prior to post-confluence stage. *Anticancer Research*, 27, 3919-3925.

Ferretti M., Casini-Raggi V., Pizarro T. T., Eisenberg S. P., Nast C. C. & Cominelli F. 1994. Neutralization of endogenous IL-1 receptor antagonist exacerbates and prolongs inflammation in rabbit immune colitis. *The Journal of Clinical Investigation*, 94, 449-453.

Ferruzza S., Rossi C., Scarino M. L. & Sambuy Y. 2012. A protocol for in situ enzyme assays to assess the differentiation of human intestinal Caco-2 cells. *Toxicology in Vitro*, 26, 1247-1251.

Filou S., Korpetinou A., Kyriakopoulou D., Bounias D., Stavropoulos M., Ravazoula P., Papachristou D. J., Theocharis A. D. & Vynios D. H. 2015. ADAMTS expression in colorectal cancer. *PloS One*, 10, e0121209.

Finkbeiner S. R., Freeman J. J., Wieck M. M., El-Nachef W., Altheim C. H., Tsai Y. H., Huang S., Dyal R., White E. S., Grikscheit T. C., Teitelbaum D. H. & Spence J. R. 2015. Generation of tissue-engineered small intestine using embryonic stem cell-derived human intestinal organoids. *Biology Open*, 4, 1462-1472.

Fiocchi C. 1998. Inflammatory bowel disease: etiology and pathogenesis. *Gastroenterology*, 115, 182-205.

Foss A. C. & Peppas N. A. 2004. Investigation of the cytotoxicity and insulin transport of acrylic-based copolymer protein delivery systems in contact with Caco-2 cultures. *European Journal of Pharmaceutics and Biopharmaceutics*, 57, 447-455.

Foulke-Abel J., In J., Kovbasnjuk O., Zachos N. C., Ettayebi K., Blutt S. E., Hyser J. M., Zeng X., Crawford S. E. & Broughman J. R. 2014. Human enteroids as an *ex-vivo* model of host–pathogen interactions in the gastrointestinal tract. *Experimental Biology and Medicine*, 239, 1124-1134.

Fukuda M., Mizutani T., Mochizuki W., Matsumoto T., Nozaki K., Sakamaki Y., Ichinose S., Okada Y., Tanaka T., Watanabe M. & Nakamura T. 2014. Small intestinal stem cell identity is maintained with functional Paneth cells in heterotopically grafted epithelium onto the colon. *Genes & Development*, 28, 1752-1757.

Fuller M. K., Faulk D. M., Sundaram N., Shroyer N. F., Henning S. J. & Helmrath M. A. 2012. Intestinal crypts reproducibly expand in culture. *Journal of Surgical Research*, 178, 48-54.

Fuller M. K., Faulk D. M., Sundaram N., Mahe M. M., Stout K. M., Von Furstenberg R. J., Smith B. J., McNaughton K. K., Shroyer N. F. & Helmrath M. A. 2013. Intestinal stem cells remain viable after prolonged tissue storage. *Cell and Tissue Research*, 354, 441-450.

Gagnon M., Berner A. Z., Chervet N., Chassard C. & Lacroix C. 2013. Comparison of the Caco-2, HT-29 and the mucus-secreting HT29-MTX intestinal cell models to investigate Salmonella adhesion and invasion. *Journal of Microbiological Methods*, 94, 274-279.

Gamsiz E. D., Thombre A. G., Ahmed I. & Carrier R. L. 2011. Drug salts and solubilization: modeling the influence of cyclodextrins on oral absorption. *Annals of Biomedical Engineering*, 39, 455-468.

Gan X., Wong B., Wright S. D. & Cai T. 2001. Production of matrix metalloproteinase-9 in Caco-2 cells in response to inflammatory stimuli. *Journal of Interferon & Cytokine Research*, 21, 93-98.

Garg P., Vijay-Kumar M., Wang L., Gewirtz A. T., Merlin D. & Sitaraman S. V. 2009. Matrix metalloproteinase-9-mediated tissue injury overrides the protective effect of matrix metalloproteinase-2 during colitis. *American journal of physiology. Gastrointestinal and Liver Physiology*, 296, G175-84.

- Garlanda C., Dinarello C. A. & Mantovani A. 2013. The interleukin-1 family: back to the future. *Immunity*, 39, 1003-1018.
- Garrett W. S., Gordon J. I. & Glimcher L. H. 2010. Homeostasis and inflammation in the intestine. *Cell*, 140, 859-870.
- Geboes K. 2003. Histopathology of Crohn's disease and ulcerative colitis. *Inflammatory Bowel Diseases*, 4, 255-276.
- Gersemann M., Becker S., Kübler I., Koslowski M., Wang G., Herrlinger K. R., Griger J., Fritz P., Fellermann K. & Schwab M. 2009. Differences in goblet cell differentiation between Crohn's disease and ulcerative colitis. *Differentiation*, 77, 84-94.
- Ghezzi P., Dinarello C. A., Bianchi M., Rosandich M. E., Repine J. E. & White C. W. 1991. Hypoxia increases production of interleukin-1 and tumor necrosis factor by human mononuclear cells. *Cytokine*, 3, 189-194.
- Gibson P. R. 2004. Increased gut permeability in Crohn's disease: is TNF the link? *Gut*, 53, 1724-1725.
- Gjorevski N., Sachs N., Manfrin A., Giger S., Bragina M. E., Ordóñez-Morán P., Clevers H. & Lutolf M. P. 2016. Designer matrices for intestinal stem cell and organoid culture. *Nature*, 539, 560-564.
- Gjorevski N., Ranga A. & Lutolf M. P. 2014. Bioengineering approaches to guide stem cell-based organogenesis. *Development*, 141, 1794-1804.
- Goldberg R. F., Austen W. G., Zhang X., Munene G., Mostafa G., Biswas S., McCormack M., Eberlin K. R., Nguyen J. T., Tatlidede H. S., Warren H. S., Narisawa S., Millan J. L. & Hodin R. A. 2008. Intestinal alkaline phosphatase is a gut mucosal defense factor maintained by enteral nutrition. *Proceedings of the National Academy of Sciences*, 105, 3551-3556.
- Gombotz W. R. & Wee S. F. 2012. Protein release from alginate matrices. *Advanced Drug Delivery Reviews*, 64, 194-205.

Gracz A. D., Ramalingam S. & Magness S. T. 2010. Sox9 expression marks a subset of CD24-expressing small intestine epithelial stem cells that form organoids *in vitro*. American Journal of Physiology-Gastrointestinal and Liver Physiology, 298, G590-G600.

Grant C. N., Mojica S. G., Sala F. G., Hill J. R., Levin D. E., Speer A. L., Barthel E. R., Shimada H., Zachos N. C. & Grikscheit T. C. 2015. Human and mouse tissue-engineered small intestine both demonstrate digestive and absorptive function. American Journal of Physiology-Gastrointestinal and Liver Physiology, 308, G664-677.

Grikscheit T. C., Siddique A., Ochoa E. R., Srinivasan A., Alsberg E., Hodin R. A. & Vacanti J. P. 2004. Tissue-engineered small intestine improves recovery after massive small bowel resection. Annals of Surgery, 240, 748-754.

Guan Q. & Zhang J. 2017. Recent Advances: The imbalance of cytokines in the pathogenesis of inflammatory bowel disease. Mediators of Inflammation, 2017, 1-8.

Gulbinowicz M., Berdel B., Wójcik S., Dziewiątkowski J., Oikarinen S., Mutanen M., Kosma V., Mykkänen H. & Moryś J. 2004. Morphometric analysis of the small intestine in wild type mice C57BL/6L-a developmental study. Folia Morphologica, 63, 423-430.

Haycock J. W. 2011. 3D cell culture: A review of current approaches and techniques. Methods Molecular Biology, 695, 1-15.

He X. C., Zhang J., Tong W., Tawfik, O., Ross J., Scoville D. H., Tian Q., Zeng X., He X. & Wiedemann L. M. 2004. BMP signaling inhibits intestinal stem cell self-renewal through suppression of Wnt- β -catenin signaling. Nature Genetics, 36, 1117-1121.

Henning S. J. & Furstenberg R. J. 2016. GI stem cells—new insights into roles in physiology and pathophysiology. The Journal of Physiology, 594, 4769-4779.

Hilgendorf C., Spahn-Langguth H., Regårdh C. G., Lipka E., Amidon G. L. & Langguth P. 2000. Caco-2 versus Caco-2/HT29-MTX co-cultured cell lines:

permeabilities via diffusion, inside-and outside-directed carrier-mediated transport. *Journal of Pharmaceutical Sciences*, 89, 63-75.

Hirohata S., Inagaki J. & Ohtsuki T. 2017. Diverse functions of a disintegrin and metalloproteinase with thrombospondin motif-1. *Journal of the Pharmaceutical Society of Japan*, 137, 811-814.

Hirsch E., Irikura V. M., Paul S. M. & Hirsh D. 1996. Functions of interleukin 1 receptor antagonist in gene knockout and overproducing mice. *Proceedings of the National Academy of Sciences*, 93, 11008-11013.

Holmberg F., Seidelin J., Yin X., Mead B., Tong Z., Li Y., Karp J., & Nielsen O. 2017. Culturing human intestinal stem cells for regenerative applications in the treatment of inflammatory bowel disease. *EMBO Molecular Medicine*, 9, 558-570.

Hori Y., Nakamura T., Kimura D., Kaino K., Kurokawa Y., Satomi S. & Shimizu Y. 2002. Experimental study on tissue engineering of the small intestine by mesenchymal stem cell seeding. *Journal of Surgical Research*, 102, 156-160.

Howell S., Kenny A. J. & Turner A. J. 1992. A survey of membrane peptidases in two human colonic cell lines: Caco-2 and HT-29. *The Biochemical Journal*, 284, 595-601.

Hughes C. S., Postovit L. M. & Lajoie G. A. 2010. Matrigel: a complex protein mixture required for optimal growth of cell culture. *Proteomics*, 10, 1886-1890.

Huh D., Hamilton G. A. & Ingber D. E. 2011. From 3D cell culture to organs-on-chips. *Trends in Cell Biology*, 21, 745-754.

Imura Y., Asano Y., Sato K. & Yoshimura E. 2009. A microfluidic system to evaluate intestinal absorption. *Analytical Sciences*, 25, 1403-1407.

Isaacs K. L., Sartor R. B. & Haskill S. 1992. Cytokine messenger RNA profiles in inflammatory bowel disease mucosa detected by polymerase chain reaction amplification. *Gastroenterology*, 103, 1587-1595.

Jaasma M. J., Plunkett N. A. & O'Brien F. J. 2008. Design and validation of a dynamic flow perfusion bioreactor for use with compliant tissue engineering scaffolds. *Journal of Biotechnology*, 133, 490-496.

Jabaji Z., Brinkley G. J., Khalil H. A., Sears C. M., Lei N. Y., Lewis M., Stelzner M., Martín M. G. & Dunn J. C. 2014. Type I collagen as an extracellular matrix for the *in vitro* growth of human small intestinal epithelium. *PLoS One*, 9, e107814.

Jabaji Z., Sears C. M., Brinkley G. J., Lei N. Y., Joshi V. S., Wang J., Lewis M., Stelzner M., Martín M. G. & Dunn J. C. 2013. Use of collagen gel as an alternative extracellular matrix for the *in vitro* and *in vivo* growth of murine small intestinal epithelium. *Tissue Engineering Part C: Methods*, 19, 961-969.

Jarry A., Vallette G., Branka J. E. & Laboisse C. 1996. Direct secretory effect of interleukin-1 via type I receptors in human colonic mucous epithelial cells (HT29-C1.16E). *Gut*, 38, 240-242.

Jing S. W., Wang Y. D., Kuroda M., Su J. W., Sun G. G., Liu Q., Cheng Y. J. & Yang C. R. 2012. HIF-1 α contributes to hypoxia-induced invasion and metastasis of esophageal carcinoma via inhibiting E-cadherin and promoting MMP-2 expression. *Acta Medica Okayama*, 66, 399-407.

Johansson M. E., Ambort D., Pelaseyed T., Schütte A., Gustafsson J. K., Ermund A., Subramani D. B., Holmén-Larsson J. M., Thomsson K. A. & Bergström J. H. 2011. Composition and functional role of the mucus layers in the intestine. *Cellular and Molecular Life Sciences*, 68, 3635-3641.

Jumarie C. & Malo C. 1991. Caco-2 cells cultured in serum-free medium as a model for the study of enterocytic differentiation *in vitro*. *Journal of Cellular Physiology*, 149, 24-33.

Kalinski T., Krueger S., Sel S., Werner K., Ropke M. & Roessner A. 2007. ADAMTS1 is regulated by interleukin-1 β , not by hypoxia, in chondrosarcoma. *Human Pathology*, 38, 86-94.

Kang T. H. & Kim H. J. 2016. Farewell to animal testing: innovations on human intestinal Microphysiological systems. *Micromachines*, 7, 107.

Karhausen J., Furuta G. T., Tomaszewski J. E., Johnson R. S., Colgan S. P. & Haase V. H. 2004. Epithelial hypoxia-inducible factor-1 is protective in murine experimental colitis. *The Journal of Clinical Investigation*, 114, 1098-1106.

Kauffman A. L., Gyurdieva A. V., Mabus J. R., Ferguson C., Yan Z. & Hornby P. J. 2013. Alternative functional *in vitro* models of human intestinal epithelia. *Frontiers in Pharmacology*, 4, 1-18.

Khalil H. A., Lei N. Y., Brinkley G., Scott A., Wang J., Kar U. K., Jabaji Z. B., Lewis M., Martín M. G. & Dunn J. C. 2016. A novel culture system for adult porcine intestinal crypts. *Cell and Tissue Research*, 365, 123-134.

Khavari A., Nydén M., Weitz D. A. & Ehrlicher A. J. 2016. Composite alginate gels for tunable cellular microenvironment mechanics. *Scientific Reports*, 6, 30854.

Kiesler P., Fuss I. J. & Strober W. 2015. Experimental models of inflammatory bowel diseases. *Cellular and Molecular Gastroenterology and Hepatology*, 1, 154-170.

Kim H. J. & Ingber D. E. 2013. Gut-on-a-Chip microenvironment induces human intestinal cells to undergo villus differentiation. *Integrative Biology*, 5, 1130-1140.

Kim H. J., Huh D., Hamilton G. & Ingber D. E. 2012. Human gut-on-a-chip inhabited by microbial flora that experiences intestinal peristalsis-like motions and flow. *Lab on a Chip*, 12, 2165-2174.

Kim J. & Khan W. 2013. Goblet cells and mucins: Role in innate defence in enteric infections. *Pathogens*, 2, 55-70.

Kim S. H., Chi M., Yi B., Kim S. H., Oh S., Kim Y., Park S. & Sung J. H. 2014. Three-dimensional intestinal villi epithelium enhances protection of human intestinal cells from bacterial infection by inducing mucin expression. *Integrative Biology*, 6, 1122-1131.

Kim S. S., Penkala R. & Abrahimi P. 2007. A perfusion bioreactor for intestinal tissue engineering. *Journal of Surgical Research*, 142, 327-331.

Kim Y. S. & Ho S. B. 2010. Intestinal goblet cells and mucins in health and disease: recent insights and progress. *Current Gastroenterology Reports*, 12, 319-330.

Kim Y. S. & Gum J. R. 1995. Diversity of mucin genes, structure, function, and expression. *Gastroenterology*, 109, 999-1013 .

Kitamura H., Cho M., Lee B., Gum J., Siddiki B., Ho S., Toribara N., Lesuffleur T., Zweibaum A. & Kitamura Y. 1996. Alteration in mucin gene expression and biological properties of HT29 colon cancer cell subpopulations. *European Journal of Cancer*, 32, 1788-1796.

Kleiveland C. R. 2015. Co-cultivation of Caco-2 and HT29-MTX. In: Verhoeckx K., Cotter P., Lopez-Exposito L., Kleiveland C., Lea T., Mackie A., Requena T., Swiatecka D., Wichers H., eds. *The impact of food bioactive on health*. New York: Springer International Publishing 135-140.

Knight T., Basu J., Rivera E., Spencer T., Jain D., and Payne R. 2013. Fabrication of a multi-layer three-dimensional scaffold with controlled porous micro-architecture for application in small intestine tissue engineering. *Cell Adhesion & Migration*, 7, 267–274.

Koelink P. J., Overbeek S. A., Braber S., Morgan M. E., Henricks P. A., Abdul Roda M., Verspaget H. W., Wolfkamp S. C., Te velde A. A., Jones C. W., Jackson P. L., Blalock J. E., Sparidans R. W., Kruijtzter J. A., Garssen J., Folkerts G. & Kraneveld A. D. 2014. Collagen degradation and neutrophilic infiltration: a vicious circle in inflammatory bowel disease. *Gut*, 63, 578-587.

Kosiewicz M. M., Nast C. C., Krishnan A., Rivera-Nieves J., Moskaluk C. A., Matsumoto S., Kozaiwa K. & Cominelli F. 2001. Th1-type responses mediate spontaneous ileitis in a novel murine model of Crohn's disease. *The Journal of Clinical Investigation*, 107, 695-702.

Kozlilek M., Grimm M., Becker D., Iordanov V., Zou H., Shmizu J., Wanki C., Garbakz G., Weitschies W. 2014. Investigation of pH and Temperature Profiles in the GI Tract of Fasted Human Subjects Using the Intellicap System. *Pharmaceutics, Journal of Pharmaceutical Sciences*, 104, 2855-2863.

Kropp B. P. & Cheng E. Y. 2000. Bioengineering organs using small intestinal submucosa scaffolds: *in vivo* tissue-engineering technology. *Journal of Endourology*, 14, 59-62.

Kühn R., Löhler J., Rennick D., Rajewsky K. & Müller W. 1993. Interleukin-10-deficient mice develop chronic enterocolitis. *Cell*, 75, 263-274.

Kulkarni A. B., Huh C. G., Becker D., Geiser A., Lyght M., Flanders K. C., Roberts A. B., Sporn M. B., Ward J. M. & Karlsson S. 1993. Transforming growth factor beta 1 null mutation in mice causes excessive inflammatory response and early death. *Proceedings of the National Academy of Sciences*, 90, 770-774.

Lahar N., Lei N. Y., Wang J., Jabaji Z., Tung S. C., Joshi V., Lewis M., Stelzner M., Martín M. G. & Dunn J. C. 2011. Intestinal subepithelial myofibroblasts support *in vitro* and *in vivo* growth of human small intestinal epithelium. *PloS One*, 6, e26898.

Landy J., Ronde E., English N., Clark S. K., Hart A. L., Knight S. C., Ciclitira P. J. & Al-Hassi H. O. 2016. Tight junctions in inflammatory bowel diseases and inflammatory bowel disease associated colorectal cancer. *World Journal of Gastroenterology*, 22, 3117-3126.

Le Maitre C. L., Freemont A. J. & Hoyland J. A. 2005. The role of interleukin-1 in the pathogenesis of human intervertebral disc degeneration. *Arthritis Research & Therapy*, 7, R732-R745.

Lea T. 2015. Caco-2 cell line. In: Verhoeckx K., Cotter P., Lopez-Exposito L., Kleiveland C., Lea T., Mackie A., Requena T., Swiatecka D., Wichers H., eds. *The impact of food bioactive on health*. New York: Springer International Publishing, 103-111.

Lee K. Y. & Mooney D. J. 2012. Alginate: properties and biomedical applications. *Progress in Polymer Science*, 37, 106-126.

Lee S. H. 2015. Intestinal permeability regulation by tight junction: implication on inflammatory bowel diseases. *Intestinal Research*, 13, 11-18.

Leedham S., Brittan M., McDonald S. & Wright N. 2005. Intestinal stem cells. *Journal of Cellular and Molecular Medicine*, 9, 11-24.

Lelièvre S. A., Kwok T. & Chittiboyina S. 2017. Architecture in 3D cell culture: An essential feature for *in vitro* toxicology. *Toxicology in Vitro*, 45, 287-295.

Leonard F., Collnot E. & Lehr C. 2010. A three-dimensional coculture of enterocytes, monocytes and dendritic cells to model inflamed intestinal mucosa *in vitro*. *Molecular Pharmaceutics*, 7, 2103-2119.

LeRoux M. A., Guilak F. & Setton L. A. 1999. Compressive and shear properties of alginate gel: effects of sodium ions and alginate concentration. *Journal of Biomedical Materials Research*, 47, 46-53.

Leushacke M. & Barker N. 2014. *Ex vivo* culture of the intestinal epithelium: strategies and applications. *Gut*, 63, 1345-1354.

Levin D. E., Barthel E. R., Speer A. L., Sala F. G., Hou X., Torashima Y. & Grikscheit T. C. 2013. Human tissue-engineered small intestine forms from postnatal progenitor cells. *Journal of Pediatric Surgery*, 48, 129-137.

Li N., Wang D., Sui Z., Qi X., Ji L., Wang X. & Yang L. 2013. Development of an improved three-dimensional *in vitro* intestinal mucosa model for drug absorption evaluation. *Tissue Engineering Part C: Methods*, 19, 708-719.

Lievin-Le Moal V. & Servin A. L. 2013. Pathogenesis of human enterovirulent bacteria: lessons from cultured, fully differentiated human colon cancer cell lines. *Microbiology and Molecular Biology Reviews*, 77, 380-439.

Lima C. B. C., Santos S. A. d. & Andrade J. D. R. 2013. Hypoxic stress, hepatocytes and CACO-2 viability and susceptibility to *Shigella flexneri* invasion. *Revista do Instituto de Medicina Tropical de São Paulo*, 55, 341-346.

Liu F., Huang J., Ning B., Liu Z., Chen S. & Zhao W. 2016. Drug discovery via human-derived stem cell organoids. *Frontiers in Pharmacology*, 7, 334.

Liu Y., Rager T., Johnson J., Enmark J. & Besner G. E. (2014). Enriched intestinal stem cell seeding improves the architecture of tissue engineered intestine. *Tissue Engineering: Part C*, 21, 816-825.

Liu H., Patel N. R., Walter L., Ingersoll S., Sitaraman S. V. & Garg P. 2013. Constitutive expression of MMP9 in intestinal epithelium worsens murine acute colitis and is associated with increased levels of proinflammatory cytokine Kc. *American journal of Physiology. Gastrointestinal and Liver Physiology*, 304, G793-803.

Liu Y., Oi Z., Li X., Du Y., & Chen Y. 2018. Monolayer culture of intestinal epithelium sustains Lgr5⁺ intestinal stem cells. *Cell Discovery*, 4, 1-3.

Liu Z., Geboes K., Colpaert S., D'Haens G. R., Rutgeerts P. & Ceuppens J. L. 2000. IL-15 is highly expressed in inflammatory bowel disease and regulates local T cell-dependent cytokine production. *Journal of Immunology*, 164, 3608-3615.

Longenecker G. & Kulkarni A. B. 2009. Generation of gene knockout mice by ES cell microinjection. *Current Protocols in Cell Biology*, 44, 1-36.

Lozoya-Agullo I., Araújo F., González-Álvarez I., Merino-Sanjuán M., González-Álvarez M., Bermejo M. & Sarmiento B. 2017. Usefulness of Caco-2/HT29-MTX and Caco-2/HT29-MTX/Raji B coculture models to predict intestinal and colonic permeability compared to Caco-2 monoculture. *Molecular Pharmaceutics*, 14, 1264-1270.

Ludwiczek O., Vannier E., Borggraefe I., Kaser A., Siegmund B., Dinarello C. & Tilg H. 2004. Imbalance between interleukin-1 agonists and antagonists: relationship to severity of inflammatory bowel disease. *Clinical & Experimental Immunology*, 138, 323-329.

Lutolf M. P., Gilbert P. M. & Blau H. M. 2009. Designing materials to direct stem-cell fate. *Nature*, 462, 433-441.

Mahe M. M., Brown N. E., Poling H. M. & Helmrath M. A. 2017. *In vivo* model of small intestine. *Methods Molecular Biology*, 1597, 229-245.

Mahe M. M., Aihara E., Schumacher M. A., Zavros Y., Montrose M. H., Helmrath M. A., Sato T. & Shroyer N. F. 2013. Establishment of gastrointestinal epithelial organoids. *Current Protocols in Mouse Biology*, 3, 217-240.

Mahida Y. R., Wu K. & Jewell D. P. 1989. Enhanced production of interleukin 1-beta by mononuclear cells isolated from mucosa with active ulcerative colitis of Crohn's disease. *Gut*, 30, 835-838.

Mahler G. J., Shuler M. L. & Glahn R. P. 2009. Characterization of Caco-2 and HT29-MTX co-cultures in an *in vitro* digestion/cell culture model used to predict iron bioavailability. *The Journal of Nutritional Biochemistry*, 20, 494-502.

Malyak M., Smith M. F., Abel A. A., Hance K. R. & Arend W. P. 1998. The differential production of three forms of IL-1 receptor antagonist by human neutrophils and monocytes. *Journal of Immunology*, 161, 2004-2010.

Manicone A. M. & McGuire J. K. (2008). Matrix metalloproteinases as modulators of inflammation. *Seminars in Cell & Developmental Biology*, 19, 34-41.

Manresa M. C. & Taylor C. T. 2017. Hypoxia inducible factor (HIF) hydroxylases as regulators of intestinal epithelial barrier function. *Cellular and Molecular Gastroenterology and Hepatology*, 3, 303-315.

Marano C., Lewis S., Garulacan L., Soler A. P. & Mullin J. 1998. Tumor necrosis factor- α increases sodium and chloride conductance across the tight junction of CACO-2 BBE, a human intestinal epithelial cell line. *The Journal of Membrane Biology*, 161, 263-274.

Marin M. L., Greenstein A. J., Geller S. A., Gordon R. E. & Aufses Jr, A. H. 1983. A freeze fracture study of Crohn's disease of the terminal ileum: changes in epithelial tight junction organization. *American Journal of Gastroenterology*, 9, 537-547.

Martin P., Palmer G., Vigne S., Lamacchia C., Rodriguez E., Talabot-Ayer D., Rose-John S., Chalaris A. & Gabay C. 2013. Mouse neutrophils express the

decoy type 2 interleukin-1 receptor (IL-1R2) constitutively and in acute inflammatory conditions. *Journal of Leukocyte Biology*, 94, 791-802.

Martínez-Maqueda D., Miralles B. & Recio I. 2015. HT29 cell line. In: Verhoeckx K., Cotter P., Lopez-Exposito L., Kleiveland C., Lea T., Mackie A., Requena T., Swiatecka D., Wichers H., eds. *The impact of food bioactives on health*. New York: Springer International Publishing, 113-124.

Masungi C., Mensch J., Willems B., Dijck A. V., Borremans C., Noppe M., Brewster M. & Augustijns P. 2009. Usefulness of a novel Caco-2 cell perfusion system II. Characterization of monolayer properties and peptidase activity. *International Journal of Pharmaceutical Sciences*, 64, 36-42.

Masungi C., Borremans C., Willems B., Mensch J., Dijck A. V., Augustijns P., Brewster M. E. & Noppe M. 2004. Usefulness of a novel Caco-2 cell perfusion system. I. *In vitro* prediction of the absorption potential of passively diffused compounds. *Journal of Pharmaceutical Sciences*, 93, 2507-2521.

Mazzucchelli L., Hauser C., Zraggen K., Wagner H., Hess M., Laissue J. A. & Mueller C. 1994. Expression of interleukin-8 gene in inflammatory bowel disease is related to the histological grade of active inflammation. *The American Journal of Pathology*, 144, 997-1007.

McCall R. D., Haskill S., Zimmermann E. M., Lund P. K., Thompson R. C. & Sartor R. B. 1994. Tissue interleukin 1 and interleukin-1 receptor antagonist expression in enterocolitis in resistant and susceptible rats. *Gastroenterology*, 106, 960-972.

McCance K. L. & Huether S. E. 1998. *Pathophysiology: The Biologic Basis for Disease in Adults and Children*. Third edition . Mosby-Year Book, Inc.

McGee D. W., Vitkus S. J. & Lee P. 1996. The effect of cytokine stimulation on IL-1 receptor mRNA expression by intestinal epithelial cells. *Cellular Immunology*, 168, 276-280.

McGuckin M. A., Eri R., Simms L. A., Florin T. H. & Radford-Smith G. 2008. Intestinal barrier dysfunction in inflammatory bowel diseases. *Inflammatory Bowel Diseases*, 15, 100-113.

McKaig B. C., McWilliams D., Watson S. A. & Mahida Y. R. 2003. Expression and regulation of tissue inhibitor of metalloproteinase-1 and matrix metalloproteinases by intestinal myofibroblasts in inflammatory bowel disease. *The American Journal of Pathology*, 162, 1355-1360.

Meunier V., Bourrie M., Berger Y. & Fabre G. 1995. The human intestinal epithelial cell line Caco-2; pharmacological and pharmacokinetic applications. *Cell Biology and Toxicology*, 11, 187-194.

Mizoguchi A., Takeuchi T., Himuro H., Okada T. & Mizoguchi E. 2016. Genetically engineered mouse models for studying inflammatory bowel disease. *The Journal of Pathology*, 238, 205-219.

Mochel J. P., Jergens A. E., Kingsbury D., Kim H. J., Martín M. G. & Allenspach K. 2018. Intestinal stem cells to advance drug development, precision, and regenerative medicine: A paradigm shift in translational research. *American Association of Pharmaceutical Scientists journal*, 20, 17.

Moncada D. M., Kammanadiminti S. J. & Chadee K. 2003. Mucin and Toll-like receptors in host defense against intestinal parasites. *Trends in Parasitology*, 19, 305-311.

Montgomery R. K. & Breault D. T. 2008. Small intestinal stem cell markers. *Journal of Anatomy*, 213, 52-58.

Moran G., O'Neill C., Padfield P. & McLaughlin J. 2012. Dipeptidyl peptidase-4 expression is reduced in Crohn's disease. *Regulatory Peptides*, 177, 40-45.

Morton D. A., Foreman K. B. & Albertine K. H. 2011. *The Big Picture: Gross anatomy*. New York, N.Y.: McGraw Hill Medical.

Munkholm P., Langholz E., Hollander D., Thornberg K., Orholm M., Katz K. D. & Binder V. 1994. Intestinal permeability in patients with Crohn's disease and ulcerative colitis and their first degree relatives. *Gut*, 35, 68-72.

Munoz J., Stange D. E., Schepers A. G., Van de Wetering M., Koo B. K., Itzkovitz S., Volckmann R., Kung K. S., Koster J., Radulescu S., Myant K., Versteeg R., Sansom O. J., Van Es J. H., Barker N., Van Oudenaarden A., Mohammed S., Heck A. J. & Clevers H. 2012. The Lgr5 intestinal stem cell signature: robust expression of proposed quiescent '+4' cell markers. *The European Molecular Biology Organization*, 31, 3079-3091.

Munoz-Najar U., Neurath K., Vumbaca F. & Claffey K. 2006. Hypoxia stimulates breast carcinoma cell invasion through MT1-MMP and MMP-2 activation. *Oncogene*, 25, 2379-2392.

Murch S. H., Braegger C. P., Walker-Smith J. A. & MacDonald T. T. 1993. Location of tumour necrosis factor alpha by immunohistochemistry in chronic inflammatory bowel disease. *Gut*, 34, 1705-1709.

Muzes G., Molnar B., Tulassay Z. & Sipos F. 2012. Changes of the cytokine profile in inflammatory bowel diseases. *World Journal of Gastroenterology*, 18, 5848-5861.

Nakamura T. & Sato T. 2018. Advancing intestinal organoid technology toward regenerative medicine. *Cellular and Molecular Gastroenterology and Hepatology*, 5, 51-60.

Natoli M., Leoni B. D., D'Agnano I., Zucco F. & Felsani A. 2012. Good Caco-2 cell culture practices. *Toxicology in vitro*, 26, 1243-1246.

Natoli M., Leoni B. D., D'Agnano I., D'Onofrio M., Brandi R., Arisi I., Zucco F. & Felsani A. 2011. Cell growing density affects the structural and functional properties of Caco-2 differentiated monolayer. *Journal of Cellular Physiology*, 226, 1531-1543.

Navabi N., McGuckin M. A. & Lindén S. K. 2013. Gastrointestinal cell lines form polarized epithelia with an adherent mucus layer when cultured in semi-wet interfaces with mechanical stimulation. *PloS One*, 8, e68761.

Neuman M. G. 2007. Immune dysfunction in inflammatory bowel disease. Translational research. *The Journal of Laboratory and Clinical Medicine*, 149, 173-186.

Nicklin M. J., Hughes D. E., Barton J. L., Ure J. M. & Duff G. W. 2000. Arterial inflammation in mice lacking the interleukin 1 receptor antagonist gene. *The Journal of Experimental Medicine*, 191, 303-312.

Nolleaux G., Deville C., El Moulaj B., Zorzi W., Deloyer P., Schneider Y. J., Peulen O. & Dandrifosse G. 2006. Development of a serum-free co-culture of human intestinal epithelium cell-lines (Caco-2/HT29-5M21). *BMC Cell Biology*, 7, 20.

Noti M., Corazza N., Mueller C., Berger B. & Brunner T. 2010. TNF suppresses acute intestinal inflammation by inducing local glucocorticoid synthesis. *The Journal of Experimental Medicine*, 207, 1057-1066.

Olejnik A., Lewandowska M., Grajek W. & Czaczyk K. 2003. New rapid method of Caco-2 cell differentiation. *Polish Journal of Food and Nutrition Sciences*, 12, 60-64.

Olson T. S., Reuter B. K., Scott K. G., Morris M. A., Wang X. M., Hancock L. N., Burcin T. L., Cohn S. M., Ernst P. B., Cominelli F., Meddings J. B., Ley K. & Pizarro T. T. 2006. The primary defect in experimental ileitis originates from a nonhematopoietic source. *The Journal of Experimental Medicine*, 203, 541-552.

Orian-Rousseau V., Aberdam D., Rousselle P., Messent A., Gavrilovic J., Meneguzzi G., Keding M. & Simon-Assmann P. 1998. Human colonic cancer cells synthesize and adhere to laminin-5. Their adhesion to laminin-5 involves multiple receptors among which is integrin alpha2beta1. *Journal of Cell Science*, 111, 1993-2004.

O'Sullivan S., Gilmer J. F. & Medina C. 2015. Matrix metalloproteinases in inflammatory bowel disease: an update. *Mediators of Inflammation*, 2015, 964131.

Pampaloni F., Stelzer E. H. & Masotti A. 2009. Three-dimensional tissue models for drug discovery and toxicology. *Recent Patents on Biotechnology*, 3, 103-117.

Pampaloni F., Reynaud E. G. & Stelzer E. H. 2007. The third dimension bridges the gap between cell culture and live tissue. *Nature Reviews Molecular Cell Biology*, 8, 839-845.

Pastuła A. & Quante M. 2014. Isolation and 3-dimensional culture of primary murine intestinal epithelial cells. *Bio-Protocol*, 4, 1-8.

Pastuła A., Middelhoff M., Brandtner A., Tobiasch M., Höhl B., Nuber A. H., Demir I. E., Neupert S., Kollmann P. & Mazzuoli-Weber G. 2016. Three-dimensional gastrointestinal organoid culture in combination with nerves or fibroblasts: a method to characterize the gastrointestinal stem cell niche. *Stem Cells International*, 2016, 1-16.

Pearson A. D., Eastham E. J., Laker M. F., Craft A. W. & Nelson R. 1982. Intestinal permeability in children with Crohn's disease and coeliac disease. *British Medical Journal*, 285, 20-21.

Pedersen G., Saermark T., Kirkegaard T. & Brynskov J. 2009. Spontaneous and cytokine induced expression and activity of matrix metalloproteinases in human colonic epithelium. *Clinical & Experimental Immunology*, 155, 257-265.

Peignon G., Thenet S., Schreider C., Fouquet S., Ribeiro A., Dussaulx E., Chambaz J., Cardot P., Pincon-Raymond M. & Le Beyec J. 2006. E-cadherin-dependent transcriptional control of apolipoprotein A-IV gene expression in intestinal epithelial cells: a role for the hepatic nuclear factor 4. *The Journal of Biological Chemistry*, 281, 3560-3568.

Pinto M. 1983. Enterocyte-like differentiation and polarization of the human colon carcinoma cell line Caco-2 in culture. *Biol.cell*, 47, 323-330.

Pontier C., Pachot J., Botham R., Lenfant B. & Arnaud P. 2001. HT29-MTX and Caco-2/TC7 monolayers as predictive models for human intestinal absorption: Role of the mucus layer. *Journal of Pharmaceutical Sciences*, 90, 1608-1619.

- Poquet L., Clifford M. N. & Williamson G. 2008. Transport and metabolism of ferulic acid through the colonic epithelium. *Drug Metabolism and Disposition*, 36, 190-197.
- Potten C. S., Kovacs L. & Hamilton E. 1974. Continuous labelling studies on mouse skin and intestine. *Cell Proliferation*, 7, 271-283.
- Potten C. S., Hume W. J., Reid P. & Cairns J. 1978. The segregation of DNA in epithelial stem cells. *Cell*, 15, 899-906.
- Potten C. S. 1998. Stem cells in gastrointestinal epithelium: numbers, characteristics and death. *Philosophical Transactions of the Royal Society of London. Series B*, 353, 821-830.
- Press B. & Di Grandi D. 2008. Permeability for intestinal absorption: Caco-2 assay and related issues. *Current Drug Metabolism*, 9, 893-900.
- Pusch J., Votteler M., Göhler S., Engl J., Hampel M., Walles H. & Schenke-Layland K. 2011. The physiological performance of a three-dimensional model that mimics the microenvironment of the small intestine. *Biomaterials*, 32, 7469-7478.
- Quante M. & Wang T. C. 2009. Stem cells in gastroenterology and hepatology. *Nature Reviews Gastroenterology and Hepatology*, 6, 724-737.
- Ranaldi G., Consalvo R., Sambuy Y. & Scarino M. L. 2003. Permeability characteristics of parental and clonal human intestinal Caco-2 cell lines differentiated in serum-supplemented and serum-free media. *Toxicology in vitro*, 17, 761-767.
- Rao L. & Sankar G. 2009. Caco-2 cells: an overview. *Asian Journal of Pharmaceutical Research and Health Care*, 1, 260-275.
- Ravi M., Paramesh V., Kaviya S., Anuradha E. & Solomon F. 2015. 3D Cell Culture Systems: Advantages and Applications. *Journal of Cellular Physiology*, 230, 16-26.

Re F., Sironi M., Muzio M., Matteucci C., Introna M., Orlando S., Penton-Rol G., Dower S. K., Sims J. E., Colotta F. & Mantovani A. 1996. Inhibition of interleukin-1 responsiveness by type II receptor gene transfer: a surface "receptor" with anti-interleukin-1 function. *The Journal of Experimental Medicine*, 183, 1841-1850.

Reed J., Walczak W. J., Petzold O. N. & Gimzewski J. K. 2008. In situ mechanical interferometry of matrigel films. *Langmuir*, 25, 36-39.

Reinecker H., Steffen M., Witthoeft T., Pflueger I., Schreiber S., MacDermott R. & Raedler A. 1993. Enhand secretion of tumour necrosis factor-alpha, IL-6, and IL-1 β by isolated lamina propria mononuclear cells from patients with ulcerative colitis and Crohn's disease. *Clinical & Experimental Immunology*, 94, 174-181.

Rider P., Carmi Y., Guttman O., Braiman A., Cohen I., Voronov E., White M. R., Dinarello C. A. & Apte R. N. 2011. IL-1alpha and IL-1beta recruit different myeloid cells and promote different stages of sterile inflammation. *Journal of Immunology*, 187, 4835-4843.

Rimann M. & Graf-Hausner U. 2012. Synthetic 3D multicellular systems for drug development. *Current Opinion in Biotechnology*, 23, 803-809.

Rocha R., Vélez D. & Devesa V. 2012. *In vitro* evaluation of intestinal fluoride absorption using different cell models. *Toxicology Letters*, 210, 311-317.

Rogler G. & Andus T. 1998. Cytokines in inflammatory bowel disease. *World Journal of Surgery*, 22, 382-389.

Roulis M., Armaka M., Manoloukos M., Apostolaki M. & Kollias G. 2011. Intestinal epithelial cells as producers but not targets of chronic TNF suffice to cause murine Crohn-like pathology. *Proceedings of the National Academy of Sciences*, 108, 5396-5401.

Rousset M. 1986. The human colon carcinoma cell lines HT-29 and Caco-2: two *in vitro* models for the study of intestinal differentiation. *Biochimie*, 68, 1035-1040.

Rubin W. 1971. The epithelial "membrane" of the small intestine. *The American Journal of Clinical Nutrition*, 24, 45-64.

Rutgeerts P., Geboes K., Vantrappen G., Kerremans R., Coenegrachts J. L. & Coremans G. 1984. Natural history of recurrent Crohn's disease at the ileocolonic anastomosis after curative surgery. *Gut*, 25, 665-672.

Sachs N., Tsukamoto Y., Kujala P., Peters P. J. & Clevers H. 2017. Intestinal epithelial organoids fuse to form self-organizing tubes in floating collagen gels. *Development*, 144, 1107-1112.

Sadlack B., Merz H., Schorle H., Schimpl A., Feller A. C. & Horak I. 1993. Ulcerative colitis-like disease in mice with a disrupted interleukin-2 gene. *Cell*, 75, 253-261.

Sailaja B. S., He X. C. & Li L. 2016. The regulatory niche of intestinal stem cells. *The Journal of Physiology*, 594, 4827-4836.

Sala F. G., Kunisaki S. M., Ochoa E. R., Vacanti J. & Grikscheit T. C. 2009. Tissue-engineered small intestine and stomach form from autologous tissue in a preclinical large animal model. *Journal of Surgical Research*, 156, 205-212.

Sambuy Y., De Angelis I., Ranaldi G., Scarino M., Stammati A. & Zucco F. 2005. The Caco-2 cell line as a model of the intestinal barrier: influence of cell and culture-related factors on Caco-2 cell functional characteristics. *Cell Biology and Toxicology*, 21, 1-26.

Saren P., Welgus H. G. & Kovanen P. T. 1996. TNF-alpha and IL-1beta selectively induce expression of 92-kDa gelatinase by human macrophages. *Journal of Immunology*, 157, 4159-4165.

Sartor R. B. 2006. Mechanisms of disease: pathogenesis of Crohn's disease and ulcerative colitis. *Nature Reviews Gastroenterology and Hepatology*, 3, 390-407.

Sasaki N., Sato T. & Clevers H. 2017. Intestinal epithelial Lgr5 stem cell niche and organoids. *Biology and Engineering of Stem Cell Niches*, 111-125.

Sasaki T., Giltay R., Talts U., Timpl R. & Talts J. F. 2002. Expression and distribution of laminin α 1 and α 2 chains in embryonic and adult mouse tissues: an immunochemical approach. *Experimental Cell Research*, 275, 185-199.

Sato T. & Clevers H. 2015. SnapShot: growing organoids from stem cells. *Cell*, 161, 1700-1700.

Sato T. & Clevers H. 2012. Primary mouse small intestinal epithelial cell cultures. *Epithelial Cell Culture Protocols*, 319-328.

Sato T., Van Es J. H., Snippert H. J., Stange D. E., Vries R. G., Van den Born M., Barker N., Shroyer N. F., Van de Wetering M. & Clevers H. 2011a. Paneth cells constitute the niche for Lgr5 stem cells in intestinal crypts. *Nature*, 469, 415-418.

Sato T., Vries R. G., Snippert H. J., Van De Wetering M., Barker N., Stange D. E., Van Es J. H., Abo A., Kujala P. & Peters P. J. 2009. Single Lgr5 stem cells build crypt villus structures *in vitro* without a mesenchymal niche. *Nature*, 459, 262-265.

Sato T. & Clevers H. 2013. Growing self-organizing mini-guts from a single intestinal stem cell: mechanism and applications. *Science*, 340, 1190-1194.

Sato T., Stange D. E., Ferrante M., Vries R. G., Van Es J. H., Van den Brink S., Van Houdt W. J., Pronk A., Van Gorp J., Siersema P. D. & Clevers H. 2011b. Long-term expansion of epithelial organoids from human colon, adenoma, adenocarcinoma, and Barrett's epithelium. *Gastroenterology*, 141, 1762-1772.

Scarpa M., Kessler S., Sadler T., West G., Homer C., McDonald C., De La Motte C., Fiocchi C. & Stylianou E. 2015. The epithelial danger signal IL-1 α is a potent activator of fibroblasts and reactivator of intestinal inflammation. *The American Journal of Pathology*, 185, 1624-1637.

Scott A., Rouch J. D., Jabaji Z., Khalil H. A., Solorzano S., Lewis M., Martín M. G., Stelzner M. G. & Dunn J. C. 2016. Long-term renewable human intestinal epithelial stem cells as monolayers: a potential for clinical use. *Journal of Pediatric Surgery*, 51, 995-1000.

Scoville D. H., Sato T., He X. C. & Li L. 2008. Current view: intestinal stem cells and signaling. *Gastroenterology*, 134, 849-864.

Seldenrijk C. A., Morson B. C., Meuwissen S. G., Schipper N. W., Lindeman J. & Meijer C. J. 1991. Histopathological evaluation of colonic mucosal biopsy specimens in chronic inflammatory bowel disease: diagnostic implications. *Gut*, 32, 1514-1520.

Shaffiey S. A., Jia H., Keane T., Costello C., Wasserman D., Quidgley M., Dziki J., Badylak S., Sodhi C. P. & March J. C. 2016. Intestinal stem cell growth and differentiation on a tubular scaffold with evaluation in small and large animals. *Regenerative Medicine*, 11, 45-61.

Shah P., Jogani V., Bagchi T. & Misra A. 2006. Role of Caco-2 cell monolayers in prediction of intestinal drug absorption. *Biotechnology Progress*, 22, 186-198.

Shah Y. M. 2016. The role of hypoxia in intestinal inflammation. *Molecular and Cellular Pediatrics*, 3, 1.

Shih D. Q. & Targan S. R. 2008. Immunopathogenesis of inflammatory bowel disease. *World Journal of Gastroenterology*, 14, 390-400.

Shoichet M. S., Li R. H., White M. L. & Winn S. R. 1996. Stability of hydrogels used in cell encapsulation: An *in vitro* comparison of alginate and agarose. *Biotechnology and Bioengineering*, 50, 374-381.

Sim W. H., Wagner J., Cameron D. J., Catto-Smith A. G., Bishop R. F. & Kirkwood, C. D. 2012. Expression profile of genes involved in pathogenesis of pediatric Crohn's disease. *Journal of Gastroenterology and Hepatology*, 27, 1083-1093.

Simon-Assmann P., Leberquier C., Molto N., Uezato T., Bouziges F. & Kedinger M. 1994. Adhesive properties and integrin expression profiles of two colonic cancer populations differing by their spreading on laminin. *Journal of Cell Science*, 107, 577-587.

Simons B. D. & Clevers H. 2011. Stem cell self-renewal in intestinal crypt. *Experimental Cell Research*, 317, 2719-2724.

Snippert H. J., Van Der Flier Laurens G, Sato T., Van Es J. H., Van Den Born M., Kroon-Veenboer C., Barker N., Klein A. M., Van Rheenen J. & Simons B. D. 2010. Intestinal crypt homeostasis results from neutral competition between symmetrically dividing Lgr5 stem cells. *Cell*, 143, 134-144.

Soofi S. S., Last J. A., Liliensiek S. J., Nealey P. F. & Murphy C. J. 2009. The elastic modulus of Matrigel™ as determined by atomic force microscopy. *Journal of Structural Biology*, 167, 216-219.

Spence J. R., Mayhew C. N., Rankin S. A., Kuhar M. F., Vallance J. E., Tolle K., Hoskins E. E., Kalinichenko V. V., Wells S. I. & Zorn A. M. 2011. Directed differentiation of human pluripotent stem cells into intestinal tissue *in vitro*. *Nature*, 470, 105-109.

Stevens C., Walz G., Singaram C., Lipman M. L., Zanker B., Muggia A., Antonioli D., Peppercorn M. A. & Strom T. B. 1992. Tumor necrosis factor- α , interleukin-1 β , and interleukin-6 expression in inflammatory bowel disease. *Digestive Diseases and Sciences*, 37, 818-826.

Stewart D.C., Berrie D., Li J., Liu X., Rickerson C., Mkoji D., Iqbal A., Tan S., Doty A., Glover S., Simmonse C. 2018. Quantitative assessment of intestinal stiffness and associations with fibrosis in human inflammatory bowel disease. *PLoS ONE*, 13, e0200377.

Sung H., Meredith C., Johnson C. & Galis Z. S. 2004. The effect of scaffold degradation rate on three-dimensional cell growth and angiogenesis. *Biomaterials*, 25, 5735-5742.

Sung J. H., Yu J., Luo D., Shuler M. L. & March J. C. 2011. Microscale 3-D hydrogel scaffold for biomimetic gastrointestinal (GI) tract model. *Lab on a Chip*, 11, 389-392.

Susewind J. 2015. A 3D co-culture of three human cell lines to model the inflamed intestinal mucosa for safety testing of nanomaterials. *Nanotoxicology*, 10, 53-62.

Tabriz A. G., Hermida M. A., Leslie N. R. & Shu W. 2015. Three-dimensional bioprinting of complex cell laden alginate hydrogel structures. *Biofabrication*, 7, 045012.

Tan S. & Barker N. (2015). Epithelial stem cells and intestinal cancer. *Seminars in Cancer Biology*, 32, 40-53.

Tang B. L. 2001. ADAMTS: a novel family of extracellular matrix proteases. *The International Journal of Biochemistry & Cell biology*, 33, 33-44.

Terada S., Sato M., Sevy A. & Vacanti J. P. 2000. Tissue engineering in the twenty-first century. *Yonsei Medical Journal*, 41, 685-691.

Thomas T., Will P., Srivastava A., Wilson C., Harbison M., Little J., Chesonis R., Pignatello M., Schmolze D. & Symington J. 1991. Evaluation of an interleukin-1 receptor antagonist in the rat acetic acid-induced colitis model. *Agents and Actions*, 34, 187-190.

Thorpe A., Boyes V., Sammon C. & Le Maitre C. 2016. Thermally triggered injectable hydrogel, which induces mesenchymal stem cell differentiation to nucleus pulposus cells: potential for regeneration of the intervertebral disc. *Acta Biomaterialia*, 36, 99-111.

Tian H., Biehs B., Warming S., Leong K. G., Rangell L., Klein O. D. & de Sauvage F. J. 2011. A reserve stem cell population in small intestine renders Lgr5-positive cells dispensable. *Nature*, 478, 255-259.

Tibbitt M. W. & Anseth K. S. 2009. Hydrogels as extracellular matrix mimics for 3D cell culture. *Biotechnology and Bioengineering*, 103, 655-663.

Tortora J. & Derrickson, B. 2016. *Principles of Anatomy and Physiology*. 15th ed. Hoboken: John Wiley Inc. 898-952

Totonelli G., Maghsoudlou P., Garriboli M., Riegler J., Orlando G., Burns A. J., Sebire N. J., Smith V. V., Fishman J. M. & Ghionzoli M. 2012. A rat decellularized small bowel scaffold that preserves villus-crypt architecture for intestinal regeneration. *Biomaterials*, 33, 3401-3410.

Ukabam S., Clamp J. & Cooper B. 1983. Abnormal small intestinal permeability to sugars in patients with Crohn's disease of the terminal ileum and colon. *Digestion*, 27, 70-74.

Umar S. 2010. Intestinal stem cells. *Current Gastroenterology Reports*, 12, 340-348.

Vacanti J. P., Morse M. A., Saltzman W. M., Domb A. J., Perez-Atayde A. & Langer R. 1988. Selective cell transplantation using bioabsorbable artificial polymers as matrices. *Journal of Pediatric Surgery*, 23, 3-9.

Valatas V., Bamias G. & Kolios G. 2015. Experimental colitis models: Insights into the pathogenesis of inflammatory bowel disease and translational issues. *European Journal of Pharmacology*, 759, 253-264.

Van Beers E. H., Al R. H., Rings E., Einerhand A., Dekker J. & Buller H. A. 1995. Lactase and sucrase-isomaltase gene expression during Caco-2 cell differentiation. *Biochemical journal*, 308, 769-775.

Van De Walle J., Hendrickx A., Romier B., Larondelle Y. & Schneider Y. 2010. Inflammatory parameters in Caco-2 cells: effect of stimuli nature, concentration, combination and cell differentiation. *Toxicology in Vitro*, 24, 1441-1449.

Van Der Flier Laurens G & Clevers H. 2009. Stem cells, self-renewal, and differentiation in the intestinal epithelium. *Annual Review of Physiology*, 71, 241-260.

Van der Sluis M., De Koning B. A., De Bruijn A. C., Velcich A., Meijerink J. P., Van Goudoever J. B., Büller H. A., Dekker J., Van Seuningen I. & Renes I. B. 2006. Muc2-deficient mice spontaneously develop colitis, indicating that MUC2 is critical for colonic protection. *Gastroenterology*, 131, 117-129.

Van Es J. H., Sato T., Van de Wetering M., Lyubimova A., Yee Nee A. N., Gregorieff A., Sasaki N., Zeinstra L., Van den Born M., Korving J., Martens A. C. M., Barker N., Van Oudenaarden A. & Clevers H. 2012. Dll1+ secretory progenitor cells revert to stem cells upon crypt damage. *Nature Cell Biology*, 14, 1099-1104.

Van Heel D. A. 2006. Interleukin 15: its role in intestinal inflammation. *Gut*, 55, 444-445.

Van Rijn J. M., Schneeberger K., Wiegerinck C. L., Nieuwenhuis E. E. & Middendorp S. 2016. Novel approaches: Tissue engineering and stem cells—*In vitro* modelling of the gut. *Best Practice & Research Clinical Gastroenterology*, 30, 281-293.

VanDussen K. L., Carulli A. J., Keeley T. M., Patel S. R., Puthoff B. J., Magness S. T., Tran I. T., Maillard I., Siebel C., Kolterud A., Grosse A. S., Gumucio D. L., Ernst S. A., Tsai Y. H., Dempsey P. J. & Samuelson L. C. 2012. Notch signaling modulates proliferation and differentiation of intestinal crypt base columnar stem cells. *Development*, 139, 488-497.

Vanuytsel, T., Senger, S., Fasano, A. & Shea-Donohue, T. 2013. Major signaling pathways in intestinal stem cells. *Biochimica et Biophysica Acta (BBA)-General Subjects*, 1830, 2410-2426.

Velcich A., Yang W., Heyer J., Fragale A., Nicholas C., Viani S., Kucherlapati R., Lipkin M., Yang K. & Augenlicht L. 2002. Colorectal cancer in mice genetically deficient in the mucin Muc2. *Science*, 295, 1726-1729.

Viney M., Bullock A., Day M. & MacNeil S. 2009. Co-culture of intestinal epithelial and stromal cells in 3D collagen-based environments. *Regenerative Medicine*, 4, 397-406.

Walczak A. P., Kramer E., Hendriksen P. J., Helsdingen R., Van der Zande M., Rietjens I. M. & Bouwmeester H. 2015. *In vitro* gastrointestinal digestion increases the translocation of polystyrene nanoparticles in an *in vitro* intestinal co-culture model. *Nanotoxicology*, 9, 886-894.

Walker M., Patel K. & Stappenbeck T. 2009. The stem cell niche. *The Journal of Pathology*, 217, 169-180.

Walker M. R. & Stappenbeck T. S. 2008. Deciphering the 'black box' of the intestinal stem cell niche: taking direction from other systems. *Current Opinion in Gastroenterology*, 24, 115-120.

Wallace K. L., Zheng L. B., Kanazawa Y. & Shih D. Q. 2014. Immunopathology of inflammatory bowel disease. *World Journal of Gastroenterology*, 20, 6-21.

Walter E., Janich S., Roessler B. J., Hilfinger J. M. & Amidon G. L. 1996. HT29-MTX/Caco-2 co-cultures as an *in vitro* model for the intestinal epithelium: *In vitro–in vivo* correlation with permeability data from rats and humans. *Journal of Pharmaceutical Sciences*, 85, 1070-1076.

Wan L. M., Allen K. J., Turner P. C. & El-Nezami H. 2014. Modulation of mucin mRNA (MUC5AC and MUC5B) expression and protein production and secretion in Caco-2/HT29-MTX co-cultures following exposure to individual and combined *Fusarium* mycotoxins. *Toxicological Sciences*, 139, 83-98.

Wang A. & Sander M. 2012. Generating cells of the gastrointestinal system: current approaches and applications for the differentiation of human pluripotent stem cells. *Journal of Molecular Medicine*, 90, 763-771.

Wang F., Scoville D., He X. C., Mahe M. M., Box A., Perry J. M., Smith N. R., Lei N. Y., Davies P. S. & Fuller M. K. 2013a. Isolation and characterization of intestinal stem cells based on surface marker combinations and colony-formation assay. *Gastroenterology*, 145, 383-395.

Wang F., Schwarz B. T., Graham W. V., Wang Y., Su L., Clayburgh D. R., Abraham C. & Turner J. R. 2006. IFN- γ -induced TNFR2 expression is required for TNF-dependent intestinal epithelial barrier dysfunction. *Gastroenterology*, 131, 1153-1163.

Wang L., Acosta M. A., Leach J. B. & Carrier R. L. 2013b. Spatially monitoring oxygen level in 3D microfabricated cell culture systems using optical oxygen sensing beads. *Lab on a Chip*, 13, 1586-1592.

Wang L., Murthy S. K., Fowle W. H., Barabino G. A. & Carrier R. L. 2009a. Influence of micro-well biomimetic topography on intestinal epithelial Caco-2 cell phenotype. *Biomaterials*, 30, 6825-6834.

Wang Y., Gunasekara D. B., Reed M. I., DiSalvo M., Bultman S. J., Sims C. E., Magness S. T. & Allbritton N. L. 2017. A microengineered collagen scaffold for

generating a polarized crypt-villus architecture of human small intestinal epithelium. *Biomaterials*, 128, 44-55.

Wang P., Chen C. L., Li M. & Wang F. J. 2009b. The role of myosin light chain kinase in intestinal epithelial barrier dysfunction due to hypoxia. *Zhonghua Shao Shang Za zhi*, 25, 57-60.

Watson C. L., Mahe M. M., Múnera J., Howell J. C., Sundaram N., Poling H. M., Schweitzer J. I., Vallance J. E., Mayhew C. N. & Sun Y. 2014. An *in vivo* model of human small intestine using pluripotent stem cells. *Nature Medicine*, 20, 1310-1314.

Wikman-Larhed A. & Artursson P. 1995. Co-cultures of human intestinal goblet (HT29-H) and absorptive (Caco-2) cells for studies of drug and peptide absorption. *European Journal of Pharmaceutical Sciences*, 3, 171-183.

Williams D. A. 2001. Inflammatory cytokines and mucosal injury. *Journal of the National Cancer Institute Monographs*, 29, 26-30.

Wirtz S. & Neurath M. F. 2007. Mouse models of inflammatory bowel disease. *Advanced Drug Delivery Reviews*, 59, 1073-1083.

Wolf S. E., Debroy M. A., Ikeda H., Jeschke M., Matin S., Rajaraman S., Ko T. C., Englander E. W., Norman J. G. & Thompson J. C. 2000. Increased small bowel epithelial turnover in interleukin-1 receptor knockout mice. *Annals of Surgery*, 232, 42-45.

Wong V. W., Stange D. E., Page M. E., Buczacki S., Wabik A., Itami S., Van De Wetering M., Poulosom R., Wright N. A. & Trotter M. W. 2012. Lrig1 controls intestinal stem-cell homeostasis by negative regulation of ErbB signalling. *Nature Cell Biology*, 14, 401-408.

Wong S. C., Macrae V. E., McGrogan P. & Ahmed S. F. 2006. The role of pro-inflammatory cytokines in inflammatory bowel disease growth retardation. *Journal of Pediatric Gastroenterology and Nutrition*, 43, 144-155.

Wu L. & Ding J. 2004. *In vitro* degradation of three-dimensional porous poly (D, L-lactide-co-glycolide) scaffolds for tissue engineering. *Biomaterials*, 25, 5821-5830.

Xinaris C., Brizi V. & Remuzzi G. 2015. Organoid models and applications in biomedical research. *Nephron*, 130, 191-199.

Yamashita S., Konishi K., Yamazaki Y., Taki Y., Sakane T., Sezaki H. & Furuyama Y. 2002. New and better protocols for a short-term Caco-2 cell culture system. *Journal of Pharmaceutical Sciences*, 91, 669-679.

Yeung T. M., Chia L. A., Kosinski C. M. & Kuo C. J. 2011. Regulation of self-renewal and differentiation by the intestinal stem cell niche. *Cellular and Molecular Life Sciences*, 68, 2513-2523.

Yi B., Shim K. Y., Ha S. K., Han J., Hoang H., Choi I., Park S. & Sung J. H. 2017. Three-dimensional *in vitro* gut model on a villi-shaped collagen scaffold. *BioChip Journal*, 11, 219-231.

Yin X., Farin H. F., Van Es J. H., Clevers H., Langer R. & Karp J. M. 2014. Niche-independent high-purity cultures of Lgr5 intestinal stem cells and their progeny. *Nature Methods*, 11, 106-112.

Yoshida A., Chitcholtan K., Evans J. J., Nock V. & Beasley S. W. 2012. *In vitro* tissue engineering of smooth muscle sheets with peristalsis using a murine induced pluripotent stem cell line. *Journal of Pediatric Surgery*, 47, 329-335.

Yoshihara K., Yajima T., Kubo C. & Yoshikai Y. 2006. Role of interleukin 15 in colitis induced by dextran sulphate sodium in mice. *Gut*, 55, 334-341.

Yoshikawa T., Hamada S., Otsuji E., Tsujimoto H. & Hagiwara A. 2011. Endocrine differentiation of rat enterocytes in long-term three-dimensional co-culture with intestinal myofibroblasts. *In Vitro Cellular & Developmental Biology-Animal*, 47, 707-715.

Yu J., Peng S., Luo D. & March J. C. 2012. *In vitro* 3D human small intestinal villous model for drug permeability determination. *Biotechnology and Bioengineering*, 109, 2173-2178.

Yui S., Nakamura T., Sato T., Nemoto Y., Mizutani T., Zheng X., Ichinose S., Nagaishi T., Okamoto R. & Tsuchiya K. 2012. Functional engraftment of colon epithelium expanded *in vitro* from a single adult Lgr5 stem cell. *Nature Medicine*, 18, 618-623.

Zachos N. C., Kovbasnjuk O., Foulke-Abel J., In J., Blutt S. E., de Jonge H. R., Estes M. K. & Donowitz M. 2016. Human Enteroids/colonoids and intestinal organoids functionally recapitulate normal intestinal physiology and pathophysiology. *The Journal of Biological Chemistry*, 291, 3759-3766.

Zeitouni N. E., Chotikatum S., Von Köckritz-Blickwede M. & Naim H. Y. 2016a. The impact of hypoxia on intestinal epithelial cell functions: consequences for invasion by bacterial pathogens. *Molecular and Cellular Pediatrics*, 3, 1-9.

Zeitouni N. E., Dersch P., Naim H. Y. & Von Köckritz-Blickwede M. 2016b. Hypoxia decreases invasin-mediated *Yersinia enterocolitica* internalization into Caco-2 cells. *PloS One*, 11, e0146103.

Zhang Z. & Huang J. 2013. Intestinal stem cells—types and markers. *Cell Biology International*, 37, 406-414.

Zheng L., Kelly C. J. & Colgan S. P. 2015. Physiologic hypoxia and oxygen homeostasis in the healthy intestine. A Review in the Theme: Cellular Responses to Hypoxia. *American Journal of Physiology. Cell physiology*, 309, C350-60.

Ziambaras T., Rubin D. C. & Perlmutter D. H. 1996. Regulation of sucrase-isomaltase gene expression in human intestinal epithelial cells by inflammatory cytokines. *The Journal of Biological Chemistry*, 271, 1237-1242.